מכון ויצמן למדע

WEIZMANN INSTITUTE OF SCIENCE

Thesis for the degree
Doctor of Philosophy

חבור לשם קבלת התואר
דוקטור לפילוסופיה

By
Vladislav Gladkikh

מאת
ולדיסלב גלדקיך

ריאקציות ספין סלקטיביות של מעבר אלקטרונים ללא מגע
Spin-selective reactions of non-contact electron transfer

Published papers format

Advisors:
Prof. A. Burshtein,
Prof. E. Pollak

מנחים:
פרופ' א. בורשטיין,
פרופ' א. פולק

June 2007

יוני 2007

Submitted to the Scientific Council of the
Weizmann Institute of Science
Rehovot, Israel

מוגש למועצה המדעית של
מכון ויצמן למדע
רחובות, ישראל

Abstract

The theories of photochemical ionization followed by geminate recombination and separation of ions are developed to give accurate explanation of recent experimental findings. The Differential Encounter Theory (DET) is applied to the analysis of ionization kinetics of Rhodamine 3B quenched by N.N-dimethyleaniline in seven solvents with different viscosities. We found that it was the neglect of non-stationary stage that used to lead to wrong extraction of reaction radii and tunneling lengths in previous analyses of experimental data. The Unified Theory (UT) of photochemical charge separation is employed to fit the data obtained for photo-excited perylene quenched by aromatic amines in dimethylsulfoxide-glycerol mixtures. An explanation is found for the non-monotonous dependence of recombination efficiency on the inter-ion diffusion. Fluorescence dynamics of perylene in the presence of tetracyanoethylene in acetonitrile as well as the data on the recombination dynamics of ion pairs generated upon electron transfer quenching in the same system are analyzed and the explanation of unexpectedly low yield of survived ions is proposed. The UT is extended to explicitly account for reaction coordinate dynamics and for a proper description of the radical ions with different spin states in arbitrary large external magnetic fields. The limits of applicability of previously known incoherent models of spin conversion are specified. Analyzing a number of experiments, it is shown that electron transfer, both forward and backward, is essentially non-contact reaction. It's proper description is possible only with distance dependent rates. The spatial dependence of the transfer rate at arbitrary large electron coupling is studied for both resonance and highly exergonic electron transfer.

Contents

I. INTRODUCTION AND THEORETICAL BACKGROUND

Photochemical ionization and charge separation in liquid solutions is a promising way for conservation and utilization of light energy. As ions are created by primary photo-excitation, they may be separated by diffusion if they escape geminate recombination to either excited or ground states of the reactants. To involve more free ions in the subsequent reactions of photosynthesis or in electric current, one has to optimize the charge separation quantum yield. This may be done by the proper choice of reactants and solutions.

One of the simplest bimolecular reactions in liquid solutions is the impurity quenching of excited donor D^* by charge transfer to electron acceptors A. The competition of the excitation decay with the diffusion assisted electron transfer is represented by the following reaction scheme:

$$\begin{array}{l} D^* + A \longrightarrow D^+ + A^- \,, \\ \downarrow \tau \end{array} \tag{1}$$

where τ is the donor excited state lifetime in the absence of acceptors.

A. Differential Encounter Theory

In frames of the Differential Encounter Theory (DET), the energy dissipation is described by the following equation for the excitation density:

$$\dot{N}^* = -k(t)\, c\, N^*(t) - \frac{N^*}{\tau} \,. \tag{2}$$

Here $N^*(t) = [D^*]$ is the survival probability of excitation and $c = [A]$ is the concentration of quenchers. The latter is constant if the quenchers are in great excess. Immediately after the δ-pulse excitation there are 100% excitations, so that $N^*(0) = 1$. The relative quantum yield of fluorescence quenching is[1]:

$$\eta \;=\; \frac{\int_0^\infty N^*(c,t)dt}{\int_0^\infty N^*(0,t)dt} \;=\; \frac{1}{1 + c\kappa\tau} \,. \tag{3}$$

In the last expression, η is presented as the Stern-Volmer law. The quantity κ is called the Stern-Volmer constant. In reality, it is a constant only at small concentration of acceptors, c, while at larger concentration, κ increases approaching the kinetic constant $k_0 = k(0)$ at $c \to \infty$ (Ref.[2]).

The reaction constant $k(t)$ is found from the following DET equations for the pair distribution function of the reactants $n(r,t)$:

$$k(t) \,=\, \int W(r) n(r,t) d^3 r\,, \qquad \dot{n} \,=\, -W(r) n(r,t) \,+\, D\Delta n\,, \qquad \left.\frac{\partial n}{\partial r}\right|_{r=\sigma} \,=\, 0\,, \tag{4}$$

where $n(r,0) = 1$. The input data are only the diffusion coefficient D, the contact radius σ and the transfer rate $W(r)$ at the distance r between the reactants. The reaction always starts with the maximal reaction rate constant

$$k(0) = k_0 \,=\, \int W(r)\, d^3 r\ . \tag{5}$$

and then slows down gradually, approaching at $t \gg R_Q^2/D$ the stationary value, $k \,=\, k(\infty)$. The latter can be expressed via the stationary reactant distribution, n_s:

$$k \,=\, \int W(r) n_s(r) d^3 r \,=\, 4\pi R_Q D\,. \tag{6}$$

The stationary equation for n_s, which follows from Eq. (4), takes the form

$$W n_s \,=\, \frac{D}{r^2}\frac{\partial}{\partial r} r^2 \frac{\partial n_s}{\partial r}\,, \tag{7}$$

and should be solved with the same boundary condition. The last equality in Eq. (6) is actually a definition of the effective reaction radius R_Q that can be larger or smaller than the contact radius σ. The effective quenching radius is a liquid analog of the reaction cross-section in gas phase kinetics. The specification of the diffusional dependence of $R_Q(D)$ is the main achievement of DET. This dependence plays an important role in chemical kinetics of liquid state reactions, the same role as the energy (velocity) dependence of the gas phase reaction cross-section.

There are two regimes of a transfer reaction: kinetic and diffusional. The reaction is kinetic if the main factor that controls it, is the magnitude of the kinetic constant. This happens at small viscosity of the solvent (fast diffusion of the reactants). The opposite — diffusional regime occurs if the solvent viscosity is large (slow diffusion of the reactants). In other words, the reaction is in the kinetic regime if $k_0 \ll k_D$, and in the diffusional regime if $k_0 \gg k_D$, where $k_D = 4\pi\sigma D$ — the so called diffusional constant.

The reaction constant $k(t)$ is really a constant in the kinetic regime, that is $k(t) \approx k_0 \approx k$. The pair distribution function also changes little with time: $n(r,t) \approx n(r,0)$. On the contrary, the diffusional regime is characterized by a big temporal changes in both $k(t)$ and $n(r,t)$. We also have $R_Q \leq \sigma$ in the kinetic regime, while in the diffusional regime, R_Q increases monotonously with the solvent viscosity[3].

Since the real shape of the transfer rate is rather complex a few simple approximations were proposed to model them. For instance, the dipole-dipole energy transfer proceeds with the rate

$$W(r) = \frac{C}{r^6}.$$

In the case of single-channel electron transfer (without excitation of reaction products) the rate obtained with the perturbation theory by Marcus is given by the formula:[3,4]

$$W(r) \;=\; \frac{V_0^2}{\hbar}\exp\left(-\frac{2(r-\sigma)}{L}\right)\frac{\sqrt{\pi}}{\sqrt{\lambda k_B T}}\exp\left(-\frac{(\Delta G+\lambda)^2}{4\lambda k_B T}\right)\;, \tag{8}$$

where V_0 is the matrix element of the transfer, ΔG — its free energy, L is the tunneling length, k_B is the Boltzmann constant, and T is the temperature.

Here, it is assumed that the electron transfer assisted by the classical intra-molecular mode and polar media requires the reorganization energy

$$\lambda(r) \;=\; \lambda_i + \lambda_0(r), \tag{9}$$

where $\lambda_i = const$ is a contribution of an intra-molecular mode, while the second term, $\lambda_0(r)$, accounts for the polar solvent reorganization. The latter is given by the well known formula:

$$\lambda_0 = \frac{e^2}{8\pi\epsilon_0}\left(\frac{1}{\epsilon_{op}}-\frac{1}{\epsilon}\right)\left(\frac{1}{r_d}+\frac{1}{r_a}-\frac{2}{r}\right)\;, \tag{10}$$

where $\epsilon_{op} = 1/n^2$ and ϵ are the optical and static dielectric constants, and ϵ_0 is the permittivity of free space. r_d, and r_a are the donor and acceptor radii, $r_d + r_a = \sigma$.

In the normal Marcus region ($\Delta G < \lambda$) the rate (8) is often approximated with exponential model:[3]

$$W(r) \;=\; W_c e^{-2(r-\sigma)/l} \tag{11}$$

or contact model applicable for atom or proton transfer:

$$W(r) \;=\; \frac{k_0}{4\pi\sigma^2}\,\delta(r-\sigma)\;. \tag{12}$$

In contact approximation Eqs. (4) reduce to the following form:[5]

$$k(t) \;=\; k_0 n(\sigma,t)\,, \qquad \dot{n} \;=\; D\Delta n\,, \qquad 4\pi D r^2\,\frac{\partial n}{\partial r}\bigg|_{r=\sigma} \;=\; k_0\; n(\sigma,t)\;, \tag{13}$$

which gives the well known Collins-Kimball formula for the reaction rate:

$$k(t) \;=\; \frac{k_0 k_D}{k_0+k_D}\left(1 \;+\; \frac{k_0}{k_D}e^x \mathrm{erfc}\sqrt{x}\right)\;, \tag{14}$$

where $x = (1+k_0/k_D)^2 Dt/\sigma^2$.

The transfer rate in the inverted Marcus region (when $\Delta G > \lambda$) has the form very different from exponential. It can be approximated by the following bell-shaped function which allows analytical solution of the Equation (4) (see Ref.[6]):

$$W(r) = \frac{W_0}{\cosh^2\left(\frac{r-R}{\Delta}\right)}$$

B. Unified Theory of photochemical charge separation

The Unified Theory of photochemical charge separation[11,12] gives the unified description of both bimolecular ionization and geminate recombination reactions. The reaction scheme is as follows:

$$\begin{array}{ccccccc} D^* & + & A & \longrightarrow & [D^+ \ldots A^-] & \xrightarrow{\phi} & D^+ + A^-, \\ \downarrow \tau & & & & \downarrow W_R & & \\ & & & & D \ldots A & & \end{array}$$

The first stage of the process is bimolecular ionization considered in the previous subsection. As the ions are born, they may either approach each other and recombine to the ground state with the recombination rate W_R or be separated and go free to the solvent. The quantum yield of the free ions is denoted as ϕ on the above scheme.

The time evolution of the distribution of radical ion pairs $m(r,t)$ is described by the following equation:

$$\dot{m}(r,t) = W_I(r) n(r,t) N^*(t) + \frac{1}{r^2}\frac{\partial}{\partial r}\tilde{D} r^2 e^{r_c/r}\frac{\partial}{\partial r} e^{-r_c/r} m - W_R(r) m \tag{15}$$

The first term on the right hand site of the equation is the source term of the ions created by bimolecular ionization. The quantities W_I, $n(r,t)$, and $N(t)$ are defined in Eqs. (2) and (4). The second term is the diffusional motion of the ions with the diffusion coefficient $\tilde{D}$ which can be different from the diffusion coefficient of neutral reactants, D. r_c is the Onsager radius of the Coulomb attraction. The third term describes geminate recombination of ions with the recombination rate W_R.

The initial and boundary conditions are:

$$m(r,0) = m(\infty,t) = 0\,, \qquad \left.\frac{\partial}{\partial r} m(r,t)\right|_{r=\sigma} = 0.$$

The total ion density $P(t)$, and the free-ion quantum yield ϕ are defined respectively as:

$$P(t) = c\int m(r,t) d^3 r\,, \qquad \phi = P(\infty).$$

C. Spin multiplicity

It was recognized long ago that in the pairs of radicals or ion-radicals the recombination is affected by spin conversion between initially populated and other spin states. The pair of radicals created in either of its singlet or triplet states can recombine from there in the singlet or triplet products or be separated with the quantum yield ϕ, so the recombination scheme becomes:

$$\phi_t \qquad D + {}^3A^* \overset{W_R^T}{\longleftarrow} {}^3[\dot{D} \ldots \dot{A}] \longrightarrow \dot{D} + \dot{A} \tag{16a}$$

$$T_{tr}^{-1} \updownarrow \Omega \qquad\qquad \phi$$

$$\phi_s \qquad D + A \underset{W_R^S}{\longleftarrow} {}^1[\dot{D} \ldots \dot{A}] \longrightarrow \dot{D} + \dot{A} \; . \tag{16b}$$

Here, ϕ_s, and ϕ_t are the yields of the singlet and triplet recombination products respectively. T_{tr} is the transversal relaxation time assumed to be the same in both radicals and Ω is the rate of transitions between the spin states. In case of Δg mechanism of spin conversion in pairs of radicals having different g factors, the Ω is given by:

$$\Omega \; = \; \frac{1}{2} \Delta g \beta_0 H \; . \tag{17}$$

Here β_0 is the Bohr magneton, $\Delta g = g_+ - g_-$ where g_+ and g_- are g-factors of radical ions in a pair and H is the external magnetic field.

For a proper analisys of the photochemical transfer processes that include spin transitions, the Eq. (15) is substituted by a system of similar equations, each for separate spin component. If we collect all the spin components into a density matrix ρ of the radical pair, the most general form of the system of UT equations will be:

$$\frac{\partial \rho(r,t)}{\partial t} = \hat{s}(r,t) + \hat{L}\rho(r,t) + \hat{\mathcal{L}}\rho(r,t) - \hat{W}(r)\rho(r,t) \; , \tag{18}$$

with a reflective boundary condition at the contact of radicals $r = \sigma$:

$$\hat{j}\rho(r,t)|_{r=\sigma} = 0 \; . \tag{19}$$

Here, $\hat{s}$ is the sourse term of ions, $\hat{L}$ is the operator diagonal in the Liouville space which describes the relative stochastic motion of the radicals, while $\hat{j}$ is a flux operator. As to $\hat{\mathcal{L}}$, this is the Liouville operator which consists of the rates of the paramagnetic relaxation and the spin transitions induced by the magnetic field. The rate operator $\hat{W}(r)$ represents the radical recombination depending on distance between the radicals, r. The explicit form of the operators depend on the particular model of spin transitions.

The yields are usually represented as follows:[14,15]

$$\phi = \frac{\tilde{D}}{\tilde{D} + Z} \; , \qquad \phi_t = \frac{Z_t}{\tilde{D} + Z} \; , \qquad \phi_s = \frac{Z_s}{\tilde{D} + Z} \; , \tag{20}$$

where Z_s and Z_t are the efficiencies of recombination through singlet and triplet channels,respectively, while

$$Z = Z_s + Z_t$$

is the total efficiency of geminate recombination.

The magnetic field effect (MFE) is the dependence of the quantum yield of free ions on the external magnetic field H. It is defined as:

$$M(H) = \frac{\phi(H) - \phi(0)}{\phi(0)}$$

II. MAIN GOALS

Although the bases of both the Differential Encounter Theory (DET) and the Unified Theory of photochemical charge separation (UT) had been established, the theories did not get necessary experimental verification. There were two reasons for that:

- Old experimental equipment did not allow thorough study of forward and backward electron transfer. Lack of devices for time resolved measurements impeded accurate extraction of microscopic parameters of the reacting systems. This led to incorrect interpretation of the results and even to paradoxes. One of the examples is the paradox of unphysically large value of the tunneling length resulted form underestimation of the non-stationary stage in the kinetics of fluorescence quenching.[16,17] This paradox has been resolved in our published work[17].

- DET and UT themselves were not developed enough to deal with real complex photochemically reacting systems. The transfer rate was modeled as either contact or exponentially decaying with inter-particle distance. The dynamics along the reaction coordinate was not incorporated into the theories. Spin conversion was described as a stochastic process with a certain rate of transitions between the spin states.

Recent progress in experimental technology permitted more detailed study of electron transfer reactions. Such techniques as single photon counting and fluorescence up-conversion allowed the analysis of kinetic data in nano-second and even in sub-picosecond scales. Old simplified approaches proved to be too rough to describe the newly obtained data.

The main goal of our recent works was the development of the encounter theories and their implication for the fitting to real experimental data. Our research involved collaboration with experimental groups from the USA (Prof. Fayer Group, Stanford University, Switzerland (Vauthey Research Group, the University of Geneva) and Austria (ESR & Photochemistry Group, Graz University of Technology), and theoretical groups from Russia (Prof. A. I. Ivanov Group, Volgograd State University, Prof N. Lukzen, International Tomography Center, Novosibirsk), and Israel (Prof. Ilya Rips, Holon Institute of Technology).

Together with Fayer group we applied DET to the analysis of ionization kinetics of Rhodamine 3B quenched by N.N-dimethyleaniline in seven solvents with different viscosities. Our work showed why previous analyses of experimental data with DET have yielded distance dependences of electron transfer that are much too long range. We found that it was the neglect of non-stationary stage that used to lead to wrong extraction of reaction radii and tunneling length from the experiment.

In our joint works with ESR & Photochemistry Group from Graz University of Technology (Austria) we used the UT to fit the data obtained for photo-excited perylene quenched by

aromatic amines in dimethylsulfoxide-glycerol mixtures. Our goal was the explanation of the Angulo Effect[18] — the non-monotonous dependence of recombination efficiency on the inter-ion diffusion.

Our works with Vauthey Research Group, (the University of Geneva) were devoted to the analysis of their data on the fluorescence dynamics of perylene in the presence of tetracyanoethylene in acetonitrile as well as the data on the recombination dynamics of ion pairs generated upon electron transfer quenching in the same system. Our goal was the explanation of unexpectedly low yield of survived ions. Our work has called for detailed study of the energetic scheme of the system and we had to extend the UT to explicitly account for reaction coordinate dynamics.

The other goals of our research were:

- Further development of UT for a proper description of the radical ions with different spin states in arbitrary large external magnetic fields. In particular, we wanted to specify the limits of applicability of previously known incoherent and rate theories[3,14,20–24]
- The determination of the spatial dependence of the transfer rate $W(r)$ (see Eq.8) for arbitrary large matrix element V of the transfer, and for both normal and inverted Marcus regions.

The results are discussed in the subsequent sections.

III. LUMINESCENCE QUENCHING BY ELECTRON TRANSFER

A. Transient effect

As far as we know, the first experimental inspection of the $R_Q(D)$ dependence launched by a joint team of experimentalists and theoreticians was presented in Ref[16]. The fluorescence quenching of pheophytin$a$ by toluquinone was studied in a number of different pure solvents having viscosities that were either known or measured. The effective quenching radius was found assuming that only steady state quenching could be detected experimentally. However, the best fit of the theoretical dependence of $R_Q(D)$ to the data gave the unsatisfying results. It gave the abnormally large value of the tunneling length, $l = 5.4\mathring{A}$ — much larger than any reasonable value that should be 1 to $2\,\mathring{A}$. Two other attempts were undertaken to correct this result by changing the form of the transfer rate's spatial dependence.[6,25] Only in the last of them[6], a reasonable reduction of l was obtained by assuming that $W(r)$ has a bell shape with its maximum shifted far from contact. This is possible, but only in the inverted Marcus region. In the normal region, where the exponential approximation (11) works well, the problem of physically unreasonably large tunnelling lengths remained unsolved.

In our work[17], where we studied photoinduced intermolecular electron transfer between Rhodamine $3B$ and N,N-dimethylaniline in a series of seven liquids, we solved the paradox. We found that a systematic mistake was made when the quenching kinetics were considered to be exponential, that is the rate of the decay is constant. However, in reality, this is never the case.

Fig. 2 in the Ref.[17] demonstrates the fit of non-stationary electron transfer kinetics to the experimental data obtained in propylene glycol, the most viscous solution studied in Ref.[19]. The kinetics was fitted for a few different concentrations by the following formula:

$$-\ln P(t) = -\ln N/\ln N|_{c=0} = 4\pi c R_Q D t + 8 c R_Q^2 \sqrt{\pi D t}\ , \tag{21}$$

which is actually $\int_0^t k_I(t')dt'$ under diffusional control. This relationship allowed us to find R_Q, and the tunneling length L. It is easy to see from the Fig. 2 in the Ref.[17] that the fitting, which accounts for the non-stationary quenching, is much better than the estimate of the steady state rate from the tangent to kinetic curve as it used to be done in previous works. Even at the end of the available interval, the data are steeper than the line, $\ln P = -c4\pi R_Q D t$, the slope of which is the true stationary rate ck.

The fitting gave us reasonable value of the tunnelling length $L = 1.65\mathring{A}$, which does not exceed earlier reports.[26] In rigid structures, tunnelling over long distances was sometimes attributed to the super-exchange, through molecular intermediates (like in molecular wires).[27] However, in liquid solutions the inter-molecular electron transfer is expected to be shorter

than intra-molecular transfer. When the intermediates are mobile solvent molecules, the coherence of transfer is broken, and super-exchange becomes ineffective.[28]

In our work[17], we fit the non-Markovian quenching theory to nonstationary experimental kinetics to find a single quenching radius R_Q for each of the solvents. For fast diffusion, the viscosity dependence of R_Q obeys the Collins-Kimball equation (see Eq (3.3)), permitting the determination of the CK parameters: the kinetic rate constant k_0 and the phenomenological reaction radius R. However, the CK model does not describe the $R_Q(D)$ dependence over the full range of viscosities studied. The more general dependence obtained by means of DET for exponential $W_I(r)$ covers a much larger range of viscosity variation. From the fitting of this dependence to the experimental one, more reasonable parameters of the exponential rate and the tunnelling length $l = 0.85\mathring{A}$ are obtained. The latter can be easily related to the true tunnelling length L of the Marcus formula for $W_I(r)$, which is not exactly exponential. The true tunnelling length is found to be only twice as large as l which is reliable and compatible with others obtained earlier for intramolecular electron transfer. Thus, the theoretical results presented in Ref.[17] resolve the problem of unphysical long-range tunnelling that came from the analysis of an earlier experimental study of electron transfer in liquids.

B. Kinetics in the picosecond regime

The system studied in our previous article was recently subjected to a new investigation by Fayer experimental group but with another technique and in a few new solvents[29]. The main difference was that instead of a single-photon counting used earlier, now the fluorescence up-conversion was employed allowing more accurate study of the first 450 ps of the quenching kinetics. Contrary to the previous investigation which was based on the long time asymptotic behavior (up to 4 ns), now only the short time initial quenching was available for study but with a much better accuracy and shorter excitation pulse.

First of all it made absolutely inapplicable the previously used methodology. Therefore, in our next work[30], we had to change our strategy: instead of the long time asymptotic behavior (21) we turned our attention to the alternative, short time quenching. From the initial quenching rate we extracted the kinetic constant (Fig. 1 in the Ref.[30]) as a convolution of the Marcus electron transfer rate and the equilibrium pair distribution of reactants:

$$k_I(t) = \int W_I(r) n(r,t) d^3r \longrightarrow_{t\to 0} \int W_I(r) g(r) d^3r = k_c \tag{22}$$

From the best fit of the experimental data, the absolute value of the space dependent Marcus rate was specified, as well as its contact value in solvents of different viscosity.

Employing the well defined Marcus rate, we fitted the whole kinetics of energy quenching by electron transfer varying only the diffusion coefficient and tunneling length (Fig. 4 in

the Ref[30]). Comparing the results with the popular contact approximation[5], we found it inapplicable to the system under consideration (Fig. 8 in the Ref[30]). On the contrary, the encounter theory of remote electron transfer allowed not only to reproduce all the experimental findings but also to predict the fluorescence yield concentration dependence, as well as that of the Stern-Volmer constant.

Moreover, we found that k_c, as well as V_0 was not a constant but increased with D being inversely proportional to viscosity. This was a surprise. The electron coupling, V_0, is just a static property of the contacting reactants that should not be affected by their motion. Such a paradox could be qualitatively resolved only by taking into account the chemical anisotropy of the reaction. This factor used to be ignored in the UT and IET of electron transfer[3,14] but had exhaustively been studied earlier by means of DET though in contact approximation.[16] The averaging of the spherical anisotropy of the reaction by rotational diffusion, can explain the increasing of the reaction rate in less viscous solvents where rotation is faster (Fig. 10 in the Ref[30]). The same is true for the corresponding effective value of V_0.

IV. SPIN-LESS THEORY OF BIMOLECULAR IONIZATION FOLLOWED BY HOT RECOMBINATION

A. Double channel highly exergonic ionization

In our work[31] the fluorescence dynamics of perylene in the presence of tetracyanoethylene (TCNE) in acetonitrile was studied experimentally and theoretically, taking into consideration that the quenching is carried out by remote electron transfer in the Marcus inverted region. It is well known that, TCNE allowed Rehm and Weller to get the most exergonic points of their famous plot, though with other fluorophores.[33] The quenching of perylene also occurs deeply in the inverted Marcus region where $|\Delta G_I| > \lambda$. At so high exergonicity, the distance dependent transfer rate passes through the maximum shifted out of contact[3], so that even in the kinetic limit the reaction is remote, not to mention the diffusion controlled ionization.

We presented a successful fitting of the entire kinetics of fluorescence quenching which starts from the initial accumulation of excitations during the action of the light pulse (Fig. 5 in the Ref.[31]), extends to a kinetic electron transfer and ends by the final quasi-stationary quenching (Fig. 8 in the Ref.[31]).

We found that the simplest single-channel Marcus rate, as well as its multiphonon analogs, do not allow fitting satisfactorily both the initial and the final stages of quenching (Fig. 7 in the Ref.[31]). This can be done only if additional near contact quenching is added. The origin of such an additional quenching may be attributed to parallel electron transfer to the excited state of a cation radical as suggested in Ref.[33] For our analysis we had to extend the Differential Encounter Theory (DET) to the reactions of competing channels of electron transfer of different energetic and space extent.

We also accounted for saturation of the ionization rate at short distances, where the tunnelling can be so fast that the limiting stage becomes the diffusional motion along the reaction coordinate to the crossing point.[34,35] In polar solvents this is the so called "dynamical solvent effect" limited by the longitudinal relaxation of polarization.[36] Taking into account this effect the single channel rate takes the following form:[37,38]

$$W_I(r) \;=\; \frac{U(r)}{1+U(r)\tau} e^{-\frac{(\Delta G_I+\lambda)^2}{4\lambda T}} \;=\; W_0 e^{-\frac{(\Delta G_I+\lambda)^2}{4\lambda T}} \;, \tag{23}$$

where

$$U(r) \;=\; \frac{V_0^2}{\hbar}\frac{\sqrt{\pi}}{\sqrt{\lambda k_B T}} \exp\left(-\frac{2(r-\sigma)}{L}\right) . \tag{24}$$

The upper limit of the rate, τ^{-1}, is different for activationless ($\Delta G_I = 0$)[34] and highly activated reactions ($\Delta G_I \gg T$)[36], but we used the interpolation, which was reasonable between these two limits where most of our experimental data falled:[?]

$$\frac{1}{\tau} = \frac{1}{4\tau_L}\sqrt{\frac{\lambda}{\pi T}} \ . \tag{25}$$

Here τ_L is the longitudinal relaxation time of the solvent polarization which assists the electron transfer.

Taking into account the saturation of the tunnelling due to the dynamical solvent effect and having in hand an additional fitting parameter (the relative strength of the two channels), we fitted satisfactorily the whole kinetics of quenching (Fig. 8 in the Ref.[31]).

Besides, the experimentally found concentration dependence of the Stern-Volmer constant was well fitted with the same very parameters as the kinetic data. The contact approximation applied to the same data was shown to be inadequate (Fig. 13 in the Ref.[31]).

Our results are in conflict with what was found when Tachiya and Murata fitted the free energy Rehm-Weller dependence of the Stern-Volmer constant that they identified with the stationary rate constant k_i.[39] According to their Fig. 2 the transfer in the most exergonic systems is kinetic, that is $k_i \approx k_0$ (kinetic rate constant) at any time. Since our system is one of those it should be expected that k_0 is much less than the diffusional rate constant, which is not the case. Being free in choosing the fitting parameters the authors made their conclusion assuming that the matrix element of the transfer $V_0 = 12.4\, meV$. Making this choice they greatly underestimate k_0 which is in their work $42\, \mathring{A}^3/ps$, that is almost an order of magnitude smaller than our value, $322.6\, \mathring{A}^3/ps$ obtained experimentally. Found $k_i = 31.6 \ll k_0$ which clearly indicates that the ionization is very close to the diffusional limit and rather far from the kinetic limit.

Thus, two important conclusions follow from this investigation:

- The energy quenching by TCNE in liquid solutions is controlled by diffusion.
- This is essentially distant, non-contact quenching.

These conclusions provide the unambiguous answer to the long standing question: why the TCNE Stern-Volmer constant is placed on the diffusional plateau of the famous free energy gap law of Rehm and Weller[33], instead of being far below it as was expected.

The true value of the TCNE Stern-Volmer constant is at least twice as large as obtained in the contact approximation and this difference increases with concentration (Fig. 14 in the Ref.[31]). These facts show that the contact approximation is just a convenient method of analytic calculations, but not a proper tool for fitting to the real experimental data on transfer kinetics, especially under diffusion control and at high concentrations of quenchers.

B. Hot recombination and separation of RIPs

In our subsequent work[40], we consider the geminate recombination of ion pairs produced by bimolecular photoinduced electron transfer (ionization) in the same system (Pe + TCNE). The experiment gave us very surprising data on RIP kinetics and yield. The fraction of survived ions was unusually small and this brought up a question, why ions recombine so fast.

The study of the energetic scheme of this system (Fig. 1 in the Ref.[40]) led us to a possible explanation of this effect via so called "hot recombination" which proceeds before thermalization. It can be responsible for such a small yield of free ions. Hot recombination is possible when the ions moving along the RIP-surface meet the intersection with ground state energetic surface of neutral products before they reach the bottom of the well. Because hot recombination does not need any thermal activation it is more efficient and much faster than the subsequent thermal recombination that conventional UT had been confined to.

Since the hot transitions cannot be discussed in terms of the rate constant, their appropriate description has called for an extension of existing theories of electron transfer quenching in solutions to explicitly account for reaction coordinate dynamics. In the theory we present, both the chemical dynamics and the mutual spatial diffusion of the reactants have been taken into account. It should be noted that the spatial motion of the reactants was not considered in previous investigations of hot transitions.[41–46] In particular, in Ref.[43] the average lifetime of the immobile ion pairs subjected to hot and thermal recombination was calculated. On the contrary, we have considered the competition between both hot and thermal recombination of the ion pairs and their diffusional separation.

With our theory we achieved a rather good fit of the RIP kinetics to the experimental data in the 80 — 500 ps time window (Fig. 5 in the Ref.[40]). It was shown that, in the present system, the vast majority of ion pairs have recombined through the hot channel before they are equilibrated and start to recombine with the usual thermal rates. Almost 90% of the ion pairs recombine before equilibrium is reached and the subsequent thermal recombination is accelerated by their encounter diffusion. As a result, no more than 6% of their initial population are finally separated (at the acceptor concentration = 0.32 M). Such a surprisingly fast back electron transfer proceeding through the hot channel was also detected in $Ru(II) - Co(III)$ mixed-valence complexes in butyronitrile.[47] In this case as well, less than 50% of the ion pairs generated by the excitation of the metal-to-metal charge-transfer band avoid this recombination and reach the equilibrium. These examples show that the study of any system should start from the inspection of its energy scheme to find out whether the hot transitions are possible in this system. If this is the case, one should care not only for thermal but first of all for the hot transfer as a dominant factor in the charge recombination.

Second new element of present consideration is connected with the fact that ionization and recombination of the Pe-TCNE donor acceptor pairs are considerably affected by a quantum high frequency mode. In the presence of such a mode the hot transitions proceed in a number of vibrational repetitions of the term crossings. It was shown a quantum mode to vastly enhance the hot recombination efficiency. As a result only ion pairs born with large inter-ion distances have a chance to avoid hot recombination.

This is, to our knowledge, the first successful fit of a backward electron transfer kinetics taking into account the hot recombination of photo-generated ion pairs.

V. SPIN ASSISTED RIP RECOMBINATION

As it was recognized long ago in pairs of radicals or ion-radicals the recombination is affected by spin conversion between initially populated and other spin states. Such a conversion is carried out by the spin relaxation and/or some mechanisms acting in a magnetic field. These are the Δg-mechanism of spin-conversion in pairs of radicals having different g-factors and the mechanism of the hyperfine interaction (HFI) between the electron and nuclear spins.

A. Incoherent HFI-mechanism of spin-conversion

In Ref.[15] we studied the system where the spin-conversion is provided by HFI mechanism which is common for organic radical pairs. We developed the contact theory of geminate recombination to the ground and triplet states. It substitutes the inappropriate "exponential model" of such a reaction and differs from it by splitting the spin-forbidden transition into sequential spin-conversion and recombination stages. The efficiencies of contact geminate recombination to either ground or excited triplet state of neutral products were calculated for contact and remote starts of radical ion pair initially created in singlet state.

Considering the spin-conversion in this pair as a stochastic process with given rate, the diffusional dependence of recombination and charge separation yields and corresponding efficiencies were specified. The obtained diffusional dependence was compared with the experimental data obtained for photo-excited perylene quenched by aromatic amines in dimethylsulfoxide-glycerol mixtures, which allow for a wide variation of solvent viscosity with composition without changing the other parameters.

Actually, the description of the spin-assisted recombination we used for the fitting was still in a very simplified form. The spin-conversion was taken into account assuming stochastic transitions between the different spin states of RIPs. The averaging of quantum yields over the true initial distributions was also avoided. The unique starting distance r was assumed to remain constant although the average one shifts closer to contact with increasing diffusion.[56] Moreover, even the contact approximation itself is too rough to deal with the closest starts brought into narrow recombination layer (and leads to some unphysical results, which is discussed in the paper). In view of all these simplifications, agreement between the theory and experiment is surprisingly good indicating that the main features of the phenomenon were nevertheless taken into account. It confirms that the spin-forbidden recombination is composed of two sequential stages. Considering that the radical-ion pair is created in singlet state, the spin conversion should precede its recombination to the excited triplet product.

B. Account of remote nature of creation and recombination of radical-ions

In our subsequent paper[48] we improved the fitting of the experimental data discussed in previous subsection. First, we accounted for the initial space distribution of ions due to distant photo-ionization. Second, we used distance dependent recombination rates instead of simplified contact approximation.

Forward electron transfer proceeding with the space dependent ionization rate results in some distribution of radical ion pairs over inter-ion distances which is farther from contact the slower is the encounter diffusion of neutral reactants. The actual shape of the distribution can be obtained with Differential Encounter Theory for any space dependence of the transfer rate.[11,12]

The charge separation quantum yield $\bar{\varphi}$ is then calculated as an average of partial yields $\varphi(r)$ of ions born at the distance r and is therefore different from $\varphi(r_0)$ for any fixed r_0. There is a similar difference between the yields of singlet and triplet neutral products,$\varphi_s(r_0)$ and $\varphi_t(r_0)$, and their averaged values, $\bar{\varphi}_s$ and $\bar{\varphi}_t$. The same is true for the corresponding recombination efficiencies.

In particular, this means that the yield of photo-generated radical-ions is different from that of the neutral radicals that are created at contact being the products of monomolecular photo-dissociation.

Because the electron transfer either forward or backward is not contact, the ions are not only born far from contact, but they also recombine distantly. Therefore the contact reaction approximation widely used for heavy particles and proton transfer in liquids is too rough for electron transfer. The shape and width of the remote transfer rates strongly affect the yields of reaction products, changing essentially their diffusional dependence.

Using exponential reaction rates for both singlet and triplet channels we fitted the experimental data for recombination of ionized Perylene with aromatic amine counter-ions (Fig. 10 in the Ref.[48]). In particular, the diffusional deceleration of the recombination was explained. This unexpected effect obtained by Dr. Angulo was first given a proper interpretation in Ref.[18] using the rectangular model of the recombination rate, or its Marcus analog in the deeply inverted region. This effect was attributed to the escape from the extended recombination layer when the start is taken from inside it.[18,51,52]

Although the fitting was rather good there is still room for improvement. The exponential models for the ionization and recombination rates should be substituted by the Marcus formulae for these rates, which relate them to the true free energies of the reactions, as well as to the reorganization energy in a particular solvent. The true hyperfine interaction mechanism of spin-conversion should be substituted for the phenomenological rate model of spin transitions in the RIP. The difference in size and encounter diffusion coefficients of ions and their neutral precursors should be taken into account especially in polar solvents.

Hopefully these improvements will enable the theory to correspond better with the fast diffusion experiments and relate the spin-conversion rate to the true values of the hyperfine interaction in particular radicals.

C. Incoherent Δg-mechanism of spin-conversion

In our next article[49] we turn to another conversion mechanism , assuming that it is assisted by incoherent spin conversion executed by spin relaxation and the Δg mechanism. We studied the recombination and separation of the radical pair from its singlet and triplet state. The spin conversion in a pair was considered as a stochastic (incoherent) process, assuming that the recombination of both singlet and triplet radical pairs is contact. The quantum yields of recombination products and free radical production were calculated for any initial separation of radicals in a pair.

We presented a general solution for the problem of singlet radical pair recombination at contact through one or two parallel channels. It reproduces all the efficiencies of contact recombination obtained earlier within the rate description of spin conversion as well as their diffusional and field dependencies. It was shown that the exact and rate treatment of the problem lead to the results which are identical in the lowest order approximation in the magnetic field. Our general results, valid at any initial separation of radicals in a pair, r_0, can be averaged over the initial distribution of these distances $f(r_0)$ if it is known.

The main restriction of our results is the stochastic (rate) description of spin conversion in a non-zero magnetic field. It is justified if spin relaxation in compexes is much faster than the difference between their resonance frequencies. This condition is met in a number of transition metal complexes with strong spin-orbital coupling[20,53,54], where $T_2 \approx T_1 \sim 10$ ps. Quite the opposite is the situation with organic radicals whose spin relaxation is about a few μs while the frequency of the hyperfine interaction responsible for spin conversion is higher than the relaxation rates. This is the coherent conversion that was widely studied[3,53,54,14], as well as the magnetic field effects resulting from it. However, to the best of our knowledge all these studies were confined to single channel recombination. The problem of double-channel recombination assisted by coherent HFI-mechanism of spin-conversion has been done in Ref.[55] Coherent conversion assisted by Δg-mechanism has been successfully solved in our next work[50] which is discussed in the next subsection.

D. Coherent Δg-mechanism of spin-conversion

In Ref.[50] we continue the study of the contact recombination from both singlet and triplet states of a radical pair, assuming that the spin conversion is carried out by the fast transversal

relaxation and Δg-mechanism. Here we did not confine to small external magnetic field but consider an arbitrary large field, allowing the spin conversion to be coherent. The alternative HFI mechanism was neglected as being much weaker.

The magnetic field dependent quantum yields of the singlet and triplet recombination products, as well as of the free radical production were calculated for any initial spin state and arbitrary separation of radicals in a pair. The Magnetic Field Effect (MFE) was traced and its diffusional (viscosity) dependence was specified.

The best analytical solution of this problem valid at any magnetic field was obtained by Mints and Pukhov[57], but only for a single channel recombination of a radical pair (RP)- just from its singlet state to the ground state of the product. Unfortunately the authors did not present the evaluation of their results and to generalize them for the double-channel recombination we have to derive everything from the very beginning.

The results were compared to previously known incoherent and rate theories (See Ref.[3,20,14,21–24]) which can be viewed as particular cases of our more general theory (Fig. 4 in the Ref.[50]). The main weakness of the rate theories is that they first reduce the coherent spin conversion to incoherent with the motion of radicals switched off, and only then account for the encounter diffusion and recombination of radicals. When afterwards the motion of radicals is accounted for, their recombination is affected by the spin conversion, but the recombination itself no longer affects the spin conversion.

Instead, we did quite the opposite: we first solved the problem with simultaneously taking into account the relative motion and conversion and only then turned to the particular case where the latter is incoherent. In particular, we proved that the rate model of spin conversion is not appropriate at any field. It becomes exact only in zero field, provided the spin relaxation times are equal. In this particular case, the diffusional dependence of all the yields coincides with the exact one and may be used for discrimination between the channels.

The only limitation of our theory is the contact approximation for distant recombination rates. It can be overcome by numerical calculations provided that the distance dependence of the rate is known.

VI. SPACE DEPENDENCE OF THE TRANSFER RATE

The electron transfer rate is a fundamental property used in the theories of intramolecular and inter-molecular reactions in dense media.[3,14,58,61] It is known to obey the Arrhenius equation:

$$W \;=\; k(V,\gamma)\, e^{-(U-V)/k_B T}\;, \qquad\qquad U = \frac{(\Delta G+\lambda)^2}{4\lambda}\;,$$

where V is the rate of resonant tunnelling and γ is the friction along the reaction coordinate. The main problem is the evaluation of the pre-exponential factor, $k(V,\gamma)$. It can not be solved universally within a single theory. A number of theories have been proposed[35,62–64]. Each of them describes k in a particular subregion of the two-dimensional domain (V,γ), separately for normal and inverted Marcus regions . In each subregion the expressions for k differ from one another. However, the variation of $V(r)$ with interparticle distance can be very large, changing from one subregion to another. This, requires that the bridges between all these theories should be established and interpolating formulas for $k(V,\gamma)$ should be found and used for the fitting of experimental data.

The r-dependence of $V(r)$ is

$$V(r) = V_0 e^{-\frac{r-\sigma}{L}}\;,$$

where L is the tunnelling length. The tunneling determines the level splitting $2V$ at the crossing point of the diabatic energy levels. The transfer is non-adiabatic at large distances where the splitting is small but becomes adiabatic at contact if the coupling there is strong enough. In between it passes through the so called Dynamic Solvent Effect (DSE), when the transfer is limited by diffusion along the reaction coordinate to the crossing point.[65,66] Zusman proposed the formula that sewed together the perturbation theory and DSE.[65] The latter becomes the upper limit of the transfer rate achieved at the largest $Max\, V = V_0$.

The DSE was obtained and studied a lot of times in the intramolecular transfer and in the solid state.[67–74] However, it was common until recently to use mainly the perturbation theory in the theories of electron transfer in liquids presuming that V_0 is small enough.[3,14] However, the precise fitting of transfer kinetics showed us that the true V_0 is rather large (57 meV) and would have to take the DSE into account.[31,40] Now we think that this isn't enough.

A. Normal Marcus region

In our work[59] two competing theories were used for bridging the gap between the non-adiabatic and deeply adiabatic electron transfer between symmetric parabolic wells. For the high friction limit a simple analytic interpolation was proposed as a reasonable alternative to

them, well fitted to the results of numerical simulations. It provided a continuous description of the electron transfer rate in the whole range of variation of the non-adiabatic coupling between the diabatic states. With an increase in coupling the cusped barrier transforms into the parabolic one. Correspondingly, the pre-exponent of the Arhenius transfer rate first increases with coupling, then levels off approaching the "dynamic solvent effect" plateau but finally reduces reaching the limit of the adiabatic Kramers theory for the parabolic barrier. These changes proceeding with a reduction in the particle separation, affect significantly the spatial dependence of the total transfer rate. If V_0 is large then, as the exact rate approaches the contact distance, it becomes smaller than in the theory of dynamical solvent effects and much smaller than predicted by perturbation theory (golden rule), conventionally used in photochemistry and electrochemistry.

The necessity to match the Fermi Golden Rule and Kramers high friction theory, including DSE which separates them, was recognized long ago. At first it was realized by Zusman[36], then it appeared in the well known Calef and Wolynes work[75] and then by means of the Eli Pollak's "Variational Transition State Theory" (VTST).[76–79] We rely upon these approaches to the problem at hand.

On a particular example of the resonant electron transfer, we have demonstrated that the Zusman account for the dynamical solvent effect is insufficient for determination of the transfer rate if electron coupling at contact is too strong. Zusman's expression was generalized using the original interpolation between DSE and the adiabatic Kramers limit for high friction. The same was done for moderate values of the friction using two theories of diffusion controlled electron transfer.[75,78] The model we proposed allows specifying the continuous distance dependence of the transfer rate from the infinite reactant separation and up to their closest approach where the maximal electron coupling is reached.

Although our analysis is quantitative only for the resonant transfer (with energy gap $\Delta G = 0$) it is qualitatively valid in the normal region ($-\Delta G < \lambda$) provided the transfer barrier

$$U = \frac{(\Delta G + \lambda)^2}{4\lambda}$$

does not differ significantly from $\lambda/4$.

B. Inverted Marcus region

In Ref.[60] the space dependence of electron transfer rate in deeply inverted Marcus region was calculated taking into account the adiabaticity of the process at strong coupling near the contact. The result is qualitatively similar from that obtained earlier for resonant electron transfer.[59] The transfer rate is non-monotonous, bell-shaped with a maximum shifted far from the contact.

Taking a few competing theories of activated electron transfer in inverted Marcus region[80] we bridged the non-adiabatic, solvent controlled and deeply adiabatic transfer. We proposed a simple analytical interpolation between these theories which provides a continuous description of the electron transfer rate at any non-adiabatic coupling between the diabatic states. When coupling increases with shortening of inter-particle distance the pre-exponent of the Arrhenius transfer rate first increases being quadratic in coupling, then levels off approaching the "dynamic solvent effect" (DSE) region and finally is cut off exponentially due to adiabaticity of the transfer.

These changes affect significantly the spatial dependence of the transfer rate near the contact provided the coupling there is strong. The rate reduces when the distance between the reactants decreases being strongly suppressed adiabatically near the contact. It is much smaller then the perturbation (golden rule) and even DSE results. The latter is actually unattainable anywhere if contact tunneling is really strong. The transfer rate is a bell-shaped curve adiabatic and non-adiabatic on the opposite sides and sensitive to the friction (DSE damping) only in between, near the maximum.

VII. CONCLUSIONS

As it follows from previous sections of this report, most of the problems announced in my PhD proposal and interim report has been successfully solved. Some of these results were presented at the Workshops on Diffusion Assisted Reactions in Graz University of Technology (August, 2004), and in Novosibirsk Tomography Centre (August 2006), at the Spin Chemistry Meeting 2005 in St. Johns College, Oxford, UK (September 2005), and at the Israel Chemical Society meeting in Tel-Aviv (February 2006).

There are a few important conclusions:

- The kinetics of ionization quenching should be studied taking into account its non-stationary nature even at long times. Neglecting the non-stationary stage leads to overestimation of the effective reaction radius and tunneling length.

- The contact approximation of the reaction rate is just a convenient method of analytic calculations, but not a proper tool for fitting the real experimental data on transfer kinetics and quantum yields of its products, especially under diffusion control, at high free energies of the transfer.

- The study of the recombination of radical-ion pairs should start from the inspection of its energy scheme to find out whether the hot transitions are possible in this system. If this is the case, one should care not only for thermal but first of all for the hot transfer as a dominant factor in the charge recombination.

- The popular model that considers the spin conversion as an incoherent rate process is exact only at zero magnetic field, provided the spin relaxation times are equal. This model is not appropriate at high fields where coherent description of spin dynamics should be used instead.

- The transfer rates employed in Encounter Theories should take into account the effects of reaction coordinate dynamics especially when tunneling is so fast that the diffusional motion along the reaction coordinate to the crossing point of the energy levels becomes the limiting factor.

Currently we are working on fitting the new experimental data on kinetics of ionization and recombination of photo-induced ions in the system studied earlier by us and Fayer group[19,17]. We are employing Encounter Theory that accounts for the motion along both spatial and reaction coordinates. This is going to yield more detailed description of photochemical transfer reactions in liquid solutions, and provide methods of accurate extraction of basic physical quantities associated with the transfer processes.

[1] Stern, O.; Volmer, M. *Physik. Z.*, **20**, 183, (1919).

[2] Popov, A. V.; Gladkikh, V. S.; and Burshtein, A. I. *J.Phys.Chem. A*, **107**, 8177, (2003).

[3] Burshtein, A. I. *Adv. Chem. Phys.*, **114**, 419 (2000).

[4] Marcus, R. A., *J.Chem.Phys.* **24**, 966, (1956); *idem* **43**, 679, (1965).

[5] F. C. Collins, G. E. Kimball, J. Colloid. Sci., **4**, 425, (1949).

[6] Burshtein, A. I.; Frantsuzov, P. A. *J. Luminesc.*, **51**, 215, (1992).

[7] Sakun, V. P., *Physica, A*, **80**, 128, (1975).

[8] Doktorov, A. B., *Physica, A*, **90**, 109, (1975).

[9] Kiprianov, A. A.; Doktorov, A. B.; Burshtein, A. I. *Chem. Phys.*, **76**, 149, (1983).

[10] Burshtein, A. I., *J. Lumin.*, **93**, 229, (2001).

[11] Burshtein, A. I. *Chem. Phys. Lett.*, **194**, 247, (1992).

[12] Dorfman, R. C.; Fayer, M. D. *J.Chem.Phys.*, **96**, 7410, (1992).

[13] M. V. Smoluchowski, *Z. Phys. Chem.*, **92**, 129, (1917).

[14] Burshtein, A. I. *Adv. Chem. Phys.*, **129**, 105, (2004).

[15] V. Gladkikh, A. I. Burshtein, G. Angulo, G. Grampp, *Phys.Chem.Chem.Phys.* **5**, 2581, (2003).

[16] Burshtein, A. I.; Kapinus, E. I.; Kucherova, I. Yu.; Morozov, V. A.; *J. Luminescence*, **43**, 291, (1989).

[17] V. S. Gladkikh, A. I. Burshtein, H. L. Tavernier, M. D. Fayer, *J.Phys.Chem.*, **A 106**, 6982, (2002).

[18] Burshtein A. I., Neufeld A. A. *J.Phys.Chem.*, **105**, 12364 (2001).

[19] H. L. Tavernier, M. M. Kalashnikov, M. D. Fayer, *J.Chem.Phys.*, **113**, 10191, (2000).

[20] U. E. Steiner, Th. Ulrich, Chem. Rev., **89**, 51, (1989).

[21] Tomkiewicz, M.; Cocivera, M. *Chem. Phys. Lett.*, **8**, 595, (1971).

[22] Bube, W.; Haberkorn, R.; Michel-Beyerle, M. E. *J. Am. Chem. Soc.*, **100**, 5993, (1978).

[23] Sterna, L.; Ronis, D.; Wolfe, S.; Pines, A. *J.Chem.Phys.*, **73**, 5493 (1980).

[24] Hayashi, H.; Nagakura, S. *Bull. Chem. Soc. Jpn.*, **57** 322 (1984).

[25] Burshtein, A. I.; Morozov V. A. *Chem. Phys. Lett.* **1990165**, 432.

[26] Wasielewski, M. R. *Chem. Phys. Rev.*, **92**, 435, **1992**.

[27] Davis, W. B.; Svec, W. A.; Ratner, M. A.; Wasielewski, M. R., *Nature*, **396**, 60, (1998).

[28] Kroon, J.; Oliver, A. M.; Verhoeven, J. W.; Paddon-Row, M. N., *J. Am. Chem. Soc.*, **112**, 4868, (1990).

[29] A. Goun, K. Glusak, M. D. Fayer *J.Chem.Phys.*, **124**, 084504, (2006).

[30] V. Gladkikh, A. I. Burshtein, *J.Chem.Phys.*, **126**, 014506, (2007).

[31] V. Gladkikh, A. I. Burshtein, G. Angulo, S. Pagès, B. Lang, E. Vauthey, *J.Phys.Chem. A*, **108**, 6667, (2004).

[32] S. Pagès, B. Lang, and E. Vauthey, *J.Phys.Chem. A*, **108**, 549 (2004).

[33] Rehm, D.; Weller, A. *Israel J. Chem.*, **8**, 259, (1970).

[34] Burshtein, A. I.; Kofman, A. G. *Chem. Phys.*, **40**, 289, (1979).

[35] Yakobson, B. I.; Burshtein, A. I. *Chem. Phys.*, **49**, 385, (1980).

[36] Zusman, L. D. *Chem. Phys.*, **49**, 295, (1980).

[37] Burshtein, A. I.; Morozov V. A. *Chem. Phys. Lett.* , **165**, 432, (1990).

[38] Zharikov, A. A.; Burshtein, A. I. *J.Chem.Phys.*, **93**, 5573, (1990).

[39] Tachiya, M.; Murata, S. *J.Phys.Chem.*, **96**, 8441, (1992).

[40] V. Gladkikh, A. I. Burshtein, S.V. Feskov, A. I. Ivanov, E. Vauthey, *J.Chem.Phys.*, **123**, 244510, (2005).

[41] G. C. Walker, E. Akesson, A. E. Johnson, N. E. Levinger, P. F. Barbara, *J.Phys.Chem.*, **96**, 3728, (1992).

[42] J. Najbar, R. C. Dorfman, and M. D. Fayer, *J.Chem.Phys.*, **94**, 1081, (1991).

[43] M. Tachiya and S. Murata, *J. Am. Chem. Soc.*, **116**, 2434, (1994).

[44] R. D. Coalson, D. G. Evans, and A. Nitzan, *J.Chem.Phys.*, **101**, 436, (1994).

[45] M. Cho, R. J. Silbey, *J.Chem.Phys.*, **103**, 595, (1995).

[46] A. I. Ivanov and V. V. Potovoi, *Chem. Phys.*, **247**, 245, (1999).

[47] H. Torieda, K. Nozaki, A. Yoshimura, and T. Ohno, *J.Phys.Chem. A*, **108**, 4819, (2004).

[48] V. Gladkikh, G. Angulo, A. I. Burshtein, *J.Phys.Chem. A*, **111**, 3458, (2007).

[49] V. Gladkikh, A.I. Burshtein, *Chem. Phys.*, **323**, 351, (2006).

[50] V. Gladkikh, A.I. Burshtein, *J.Phys.Chem. A*, **110**, 3364, (2006).

[51] Neufeld A. A., Burshtein A. I., Angulo G., Grampp G. *J.Chem.Phys.*, **116**, 2472, (2002).

[52] G. Angulo, G. Grampp, A. Neifeld, A. I. Burshtein *J.Phys.Chem.* A, **107**, 6913, (2003).

[53] E. B. Krissinel, A. I. Burshtein, N. N. Lukzen, U. E. Steiner, Mol. Phys., **96**, 1083, (1999).

[54] A. I. Burshtein, E. Krissinel and U. E. Steiner, Phys. Chem. Chem. Phys., **3**, 198, (2001).

[55] N. N. Lukzen, J. B. Pedersen, A. I. Burshtein, *J.Phys.Chem. A*, **109**, 11914, (2005).

[56] A. I. Burshtein, A. A. Neufeld *J. Phys. Chem. B*, **105**, 12364, (2001).

[57] Mints, R. G.; Pukhov, A. A. *Chem. Phys.*, **87**, 467, (1984).

[58] Kuznetsov, A. M. *Charge Transfer in Physics, Chemistry and Biology* Gordon & Breach, Amsterdam, 1995.

[59] V. Gladkikh, A. I. Burshtein, I. Rips, *J.Phys.Chem. A*, **109**, 4983, (2005).

[60] V. Gladkikh, A. I. Burshtein, *Chem. Phys.*, **325**, 359, (2006).

[61] May, V.; Kühn, O. *Charge and Energy Transfer Dynamics in Molecular Systems.* Wiley-VCH, Berlin, 2000.

[62] A. I. Burshtein, A. A. Zharikov Chem. Phys., **152**, 23 (1991).

[63] A. I. Burshtein, Yu. Georgievskii *J.Chem.Phys.*, **100**, 7319, (1994).

[64] Yu. Georgievskii, A. I. Burshtein, B. M. Chernobrod *J.Chem.Phys.*, **105**, 1, (1996).

[65] Zusman, L. D. *Chem. Phys.*, **49**, 295, (1980).

[66] Yakobson, B. I.; Burshtein, A. I. *Chem. Phys.*, **49**, 385, (1980).

[67] Sumi H., Marcus R. A *J.Chem.Phys.*, **84**, 4894 (1986).

[68] Grampp G., Jaenicke W., Harrer W. *J. Electroanal. Chem.*, **209**, 223 (1986).

[69] Nielson R. M., McManis G. E., Golovin M. N. Weaver M. J. *J.Phys.Chem.*, **92**, 3441, (1988).

[70] Rempel U. von Maltzan B. von Borczyskowski C. *Zeitschrift für Physikalische Chemie*, **d.170**, 107, (1991).

[71] Zusman, L. D. *Zeitschrift für Physikalische Chemie*, **Bd. 186**, 1, (1994).

[72] Evans D. G., Nitzan A. Ratner M. A. *J.Chem.Phys.*, **108**, 6387, (1998).

[73] Frantsuzov P. A. *J.Chem.Phys.*, **111**, 2075, (1999).

[74] Rips I. *J.Chem.Phys.*, **121**, 5356, (2004).

[75] Calef D. F.; Wolynes P. G. *J.Phys.Chem.*, **87**, 3387, (1983).

[76] Pollak, E. *J.Chem.Phys.*, **93**, 1116, (1990).

[77] Rips I.; Pollak, E. *J.Chem.Phys.*, **103**, 7912, (1995).

[78] Starobinets, A.; Rips, I.; Pollak, E. *J.Chem.Phys.*, **104**, 6547, (1996).

[79] Pollak, E. in *Theoretical Methods in Condensed Phase Chemistry;* Schwartz, S. D., Ed.; Kluwer Acad. Publ.: Dordrecht, 2000; pp. 1-46.

[80] Georgievskii, Yu.; Burshtein, A. I.; Chernobrod, B. *J.Chem.Phys.*, **105**, 3108, (1996).

VIII. MY CONTRIBUTION TO EACH PAPER INCLUDED IN THE THESIS

1. Influence of diffusion on the kinetics of donor-acceptor electron transfer monitored by the quenching of donor fluorescence, V. S. Gladkikh, A. I. Burshtein, H. L. Tavernier, and M. D. Fayer, J. Phys. Chem. A 2002, 106, 6982

   In this work I did the fitting of the non-Markovian quenching theory to non-stationary energy quenching by electron transfer for 3 quencher concentrations in 7 solvents. From these kinetic data I extracted the values of the reaction radii R_Q and the stationary reaction rate constants k_i. Plotting the viscosity dependence of the inverse rate constant $1/k_i$ (Fig. 3 in this paper), I found the value of the kinetic constant k_0. I did analytical calculation for the parameter μ for the exponential transfer rate, and numerical calculations for the Marcus rate. Employing the obtained slope parameters I found the correspondence between the effective tunneling length l and the true tunneling length L.

2. Photoionization affected by chemical anisotropy, V. S. Gladkikh and A. I. Burshtein, J. Chem. Phys. 2007, 126, 014506

   My contribution to this work was the fitting of the Differential Encounter Theory to the experimental kinetics at small, moderate and long time intervals. Analysing the initial stage of the quenching, I extracted from the experimental data the values of the kinetic constants for all the solvents studied. I also studied the influence of the equilibrium radial distribution function on the quenching kinetics, and rotational averaging of chemical anysotropy.

3. Kinetics and yields of electron transfer in the inverted region, V. S. Gladkikh, A. I. Burshtein, Angulo, Stephane Pages, Bernard Lang, and Eric Vauthey, J. Phys. Chem. A 2004, 108, 6667

   In this article I did the fitting of the kinetic data at short, moderate and long times with the single-channel, the double-channel, and the multi-phonon models. Employing the energetic scheme of the reaction, I studied the contributions of the transfers to different excited $(per^+)^* + TCNE^-$ states to the overall kinetic constant k_0. I analyzed the concentration dependence of the relative quantum yield of the fluorescence and the Stern-Volmer constant, using both stationary and time-resolved experimental data. In case of the time-resolved data, I did numerical integration to find the values of the yields. Fitting the data, I made a comparison between the remote and the contact models of transfer.

4. Hot recombination of photogenerated ion pairs, V. S. Gladkikh, A. I. Burshtein, S. V. Feskov, A. I. Ivanov, Eric Vauthey, J. Chem. Phys. 2005, 123, 244510

   Here, I participated in fitting of both ionization and recombination kinetics. I also studied the influence of the spatial dispersion of the diffusion coefficient and dielectric permittivity on the ion-pair dynamics.

5. Quantum yields of singlet and triplet recombination products of singlet radical ion pairs, V. S. Gladkikh, A. I. Burshtein, G. Angulo, and G. Grampp, Phys. Chem. Chem. Phys. 2003, 5, 2581

   In this work I did the fitting of theoretical quantum yields and recombination efficiencies to the experimental data. I also studied the behaviour of the yields and the recombination efficiencies in the limit of slow diffusion.

6. Production of free radicals and triplets from contact radical pairs and from photochemically generated radical-ions, V. S. Gladkikh, G. Angulo, A. I. Burshtein, J. Phys. Chem. A 2007, 111, 3458

   In this paper I studied the initial distributions of the radical ion pairs (RIP) originated by photo-ionization. I made numerical calculations to obtain the dependence of the average initial RIP separation on diffusion. Having these results, I made a comparison of the recombination efficiencies for radical pairs generated in contact and those initially distributed according to the DET predictions for bimolecular ionization.

7. Double-channel recombination of the radical pairs via incoherent delta-g-mechanism of spin-conversion, V. S. Gladkikh and A. I. Burshtein, Chem. Phys. 2006, 323, 351

   In this work I performed the exact analytical solution of the main system of differential equations (Eq. (2.1) in the article). I obtained analytic expressions for the populations of the singlet and triplet states, quantum yields of recombination to the ground state, and to the excited triplet state as well as the quantum yield of free ions. I also calculated the corresponding recombination efficiencies, the formula for the magnetic field effects and the expressions for their small field limit.

8. Double-channel contact recombination of radical pairs subjected to spin conversion via the delta-g mechanism, V. S. Gladkikh and A. I. Burshtein, J. Phys. Chem. A 2006, 110, 3364

In this article I performed the exact analytical solution of the main equations (Eq. (2.1) in the article). I obtained analytic expressions for the populations of the singlet and triplet states, quantum yields of recombination to the ground state, to the excited triplet state and the quantum yield of free ions as well as the corresponding recombination efficiencies. I found that the efficiencies of recombination from either the singlet or equilibrated triplet state can be represented uniformly in a nice and very compact form (see Eq. (7.12) and (7.13) in the article). This form gives the same formulas for both coherent and rate models of spin conversion, and includes all the differences between them into a single parameter α - the efficiency of the spin conversion. I also obtained the explicit form of α for the case of double-channel recombination for the coherent model of spin conversion.

9. Variation of the resonant transfer rate when passing from nonadiabatic to adiabatic electron transfer, V. S. Gladkikh and A. I. Burshtein, I. Rips, J. Phys. Chem. A 2005, 109, 4983

   In this work I made numerical calculation of the correction factor for a cusp barrier rate, J_0, as a function of the reorganization energy, and all calculations in the formulas that contain this factor.

10. Near-contact adiabatic suppression of electron transfer in the inverted region, V. S. Gladkikh and A. I. Burshtein, Chem. Phys. 2006, 325, 359

    In this work I made numerical calculation of thermally averaged pre-factor A for moderate (intermediate) friction region, and all calculations in the formulas that contain this factor.

During my studies at the Weizmann Institute, I also participated in the following publications not included in this thesis:

1. Quantum yields of singlet and triplet recombination products of singlet radical ion pairs, V. S. Gladkikh, A. I. Burshtein, G. Angulo, and G. Grampp, Phys. Chem. Chem. Phys. 2003, 5, 2581

2. Inhomogeneous electrochemiluminescence. I: Integral encounter theory of kinetics and yield, V. S. Gladkikh, A.I. Burshtein, Chem. Phys. 2005, 317, 16

3. Inhomogeneous electrochemiluminescence. II Markovian encounter theory of the phenomenon, V. S. Gladkikh, A.I. Burshtein, Chem. Phys. 2005, 317, 27

Influence of Diffusion on the Kinetics of Donor−Acceptor Electron Transfer Monitored by the Quenching of Donor Fluorescence

V. S. Gladkikh,[†] A. I. Burshtein,[†] H. L. Tavernier,[‡] and M. D. Fayer*[,‡]

Department of Chemical Physics, Weizmann Institute of Science, 76100 Rehovot, Israel, and Department of Chemistry, Stanford University, Stanford, California 94305

Received: March 14, 2002; In Final Form: May 8, 2002

The problem of photoinduced donor−acceptor electron transfer in liquid solution is analyzed to obtain an understanding of the relationship between approximate treatments of the role of diffusion in electron transfer, that is, the Collins−Kimball approach, and a detailed analysis of the problem. It is shown why previous analyses of experimental data have yielded distance dependences of electron transfer that are much too long range. From an appropriate fitting of the nonstationary kinetics of donor fluorescence quenching by diffusion-assisted electron transfer, the effective radii and the steady-state constants associated with electron transfer are found for a donor−acceptor system studied experimentally in seven solvents with different viscosities. The dependence of diffusion agrees with the one predicted theoretically for electron transfer having a distance-dependent transfer rate initially taken to be exponential with distance. In the fast-diffusion limit, the dependence on the rate of diffusion is well approximated by the Collins−Kimball relationship, which permits the kinetic rate constant and the effective radius associated with diffusion-induced quenching to be extracted from the experimental data. The effective radius is then related to the electron transfer rate with arbitrary distance dependence. From this relationship, the tunnelling length for both exponential and Marcus-type rates is obtained from the data analysis, and it is demonstrated that the latter is almost twice as long as the former. For the Marcus transfer rate, it is found that the Marcus parameter $\beta = 1.2$ Å^{-1} ($\beta = 2$/tunnelling length), which is in accord with previous measurements on a variety of systems. The theoretical analysis presented here resolves the apparent discrepancies between early measurements of very long tunnelling lengths in liquid systems and physically reasonable values of $\beta \approx 1$ Å^{-1}.

I. Introduction

One of the simplest bimolecular reactions in liquid solutions is the impurity quenching of an excited donor D^* by charge transfer to electron acceptors A. The competition of the excitation decay with the diffusion-assisted electron transfer is represented by the following reaction scheme

$$\begin{array}{l} D^* + A \rightarrow D^+ + A^- \\ \downarrow \tau \end{array} \qquad (1.1)$$

where τ is the donor excited-state lifetime in the absence of acceptors. The energy dissipation is often described by conventional (Markovian) chemical kinetics, represented by a single equation for the excitation density $N = [D^*]$

$$\dot{N} = -k_i c N \qquad (1.2)$$

where $c = [A]$ remains constant if acceptors are present in great excess. Under this condition, the quenching proceeds exponentially with the time-independent rate ck_i and the rate constant

$$k_i = 4\pi R_Q D \qquad (1.3)$$

where $D = D_D + D_A$ is the coefficient of encounter diffusion and R_Q is the effective radius of the reaction.

In the classical theory of bimolecular reactions,[1,2] the transfer proceeds with a kinetic rate constant k_0 in a thin layer adjacent to the contact sphere of radius σ. In this case, the effective radius is related to the external radius of the reaction layer, R, according to the Collins−Kimball (CK) relationship:

$$R_Q = R\frac{k_0}{k_0 + 4\pi RD} \qquad (1.4)$$

R_Q increases with viscosity but cannot exceed R. In the original CK theory, the reaction layer was assumed to be infinitely thin; therefore, $R \equiv \sigma$. This is actually a contact model of transfer reactions. Later, R came to be regarded as a fitting parameter, partially accounting for the remote nature of transfer, but only for $R - \sigma \ll \sigma$.

Evidently, both the contact and generalized CK models of electron tunnelling are simplifications that are too rough to describe real transfer that is governed by the distance-dependent tunnelling rate, $W_I(r)$. Much better, though not perfect, is an exponential model of this dependence:

$$W_I(r) = W_c e^{-2(r-\sigma)/l} \qquad (1.5)$$

It is often assumed that the rate decreases exponentially with a characteristic tunnelling length, l. It is possible to obtain l in some circumstances from experimental studies of intramolecular electron transfer.[3,4] In the case of intermolecular transfer assisted by diffusion, l can be obtained only indirectly from experiments

* Corresponding author. E-mail: fayer@stanford.edu.
[†] Weizmann Institute of Science.
[‡] Stanford University.

10.1021/jp0207228 CCC: $22.00
Published on Web 07/02/2002

through the rate constants related to $W_I(r)$ by the theory of distance-dependent electron transfer in liquid solution.

Early theoretical treatments, presented almost simultaneously, were developed intuitively[5] but were justified in terms of a binary approximation in ref 6. Not only the rate processes but also the dynamic transfer governed by the Hamiltonian were studied using the approach called encounter theory (ET).[7] At present, the method is better known as differential encounter theory (DET), which can be deduced, in some limits, from the more general integral encounter theory.[8] DET permitted calculation of the $R_Q(D)$ dependence for the exponential rate[5] and proved that the CK model, with $R \approx \sigma$, is valid in the fast-diffusion limit.[7] However, for slower diffusion (higher viscosity), the steady-state constant $k_i = 4\pi R_s D$, where $R_s > R$. The dependence on diffusion for R_Q was given in a number of papers:[7,9,10]

$$R_Q = R_s \approx \sigma + \frac{l}{2}\ln\left(\frac{\gamma^2 W_c l^2}{4D}\right) \qquad \text{at } R_s \gg R \qquad (1.6)$$

where $\gamma = \exp(C)$ and C is the Euler constant.

The effective quenching radius, R_Q, is a liquid analogue of the reaction cross section in gas-phase kinetics. The specification of the dependence on the diffusion of $R_Q(D)$ is the main achievement of DET. This dependence plays an important role in chemical kinetics of liquid-state reactions, which is the same role as the energy (velocity) dependence of the gas-phase reaction cross section. The gas-phase reaction cross section is the subject of numerous theoretical studies and related cross-beam experiments. However, the variation of molecular velocities in the beams is more readily accomplished than is changing the mobility (diffusion) of particles in liquid solutions. Changing the diffusion can be done in a very limited range by varying the solvents or their compositions or by using external pressure, which changes the viscosity of the solution. However, any of these methods can affect not only diffusion but also other properties of the media (solvation, polarity, refractive index, etc.).[11] Whenever the experimental difficulties were overcome, new and very important results were obtained.[12−14]

As far as we know, the first experimental inspection of the $R_Q(D)$ dependence[6] launched by a joint team of experimentalists and theoreticians was presented in ref 13. The fluorescence quenching of pheophytin a by toluquinone was studied in a number of different pure solvents having viscosities that were either known or measured. The diffusion coefficients obtained from the Stokes−Einstein relationship vary in the series of solvents studied by 2 orders of magnitude. The effective quenching radius, $R_Q = k_i/4\pi D$, was found by assuming that only steady-state quenching could be detected experimentally. However, the best fit of the theoretical dependence of $R_Q(D)$ to the data gave the following unsatisfying results:[13] $W_c = 1.8 \times 10^{10}$ s^{-1}, $\sigma = 4$ Å, and $l = 5.4$ Å. The last number is much larger than any reasonable value for the tunnelling length, which should be 1 to 2 Å. Two other attempts were undertaken to correct this result by changing the form of the transfer rate's spatial dependence.[15,16] Only in the last attempt[16] was a reasonable reduction of l obtained by assuming that $W_I(r)$ has a bell shape with its maximum shifted far from contact. This reduction is possible, but only in the inverted Marcus region. In the normal region, where the exponential approximation[5] works well, the problem of unreasonably large physical tunnelling lengths remained unsolved.

Unfortunately, until now no other attempts to resolve this problem theoretically or experimentally were made. Only recently, electron transfer in the normal Marcus region was studied again in another system and in seven different solvents.[17] However, the quenching kinetics that were measured much more accurately were found to be nonstationary, that is, the evolution of $N(t)$ is not exponential; the rate depends on the time when it is measured. The preliminary analysis of these results showed that l is overestimated if the experiments are analyzed in the same way as in ref 13. This overestimation stimulated the critical analysis of the way in which R_Q should be extracted from the experimentally studied kinetics. Here, we prove that a systematic mistake is made when the quenching kinetics are considered to be exponential, even at the very end of the available time interval.

In our present study, we fit the non-Markovian quenching theory to nonstationary experimental kinetics to find a single quenching radius R_Q for each of the solvents. For fast diffusion, the viscosity dependence of R_Q obeys the Collins−Kimball equation (3.3), permitting the determination of the CK parameters: the kinetic rate constant k_0 and the phenomenological reaction radius R. However, the CK model does not describe the $R_Q(D)$ dependence over the full range of viscosities studied. The more general dependence obtained by means of DET[7] for exponential $W_I(r)$ covers a much larger range of viscosity variation. From the fitting of this dependence to the experimental one, more reasonable parameters of the exponential rate (1.5) and the tunnelling length $l = 0.85$ Å are obtained. The latter can be easily related to the true tunnelling length L of the Marcus formula for $W_I(r)$, which is not exactly exponential. The true tunnelling length is found to be only twice as large as l and gives the Marcus parameter $\beta = 1.2$ Å^{-1}. This result is reliable and compatible with others obtained earlier for intramolecular electron transfer.[3] Thus, the theoretical results presented below resolve the problem of unphysical long-range tunnelling that came from the analysis of an earlier experimental study of electron transfer in liquids.

II. Nonstationary Energy Quenching

It is remarkable that in the theory of contact reactions first developed by Smoluchowski,[1] the limitations of the Markovian approach were removed from the very beginning. The "time-dependent" rate constant, $k_I(t)$, was substituted for k_i in the kinetic equation (1.2). In the Collins−Kimball theory, $k_I(t)$ is defined as follows:[2]

$$k_I(t) = k_i\left(1 + \frac{k_0}{k_D}\, e^x \mathrm{erfc}\sqrt{x}\right) \qquad (2.1)$$

where $k_D = 4\pi RD$ is the diffusional rate constant and $x = (1 + k_0/k_D)^2 Dt/R^2$. As a result, the survival probability of excitation vanishes nonexponentially:

$$N(t) = \exp(-c\int_0^t k_I(t')\,dt' - t/\tau) \qquad (2.2)$$

This effect is especially pronounced when $k_0 \gg k_D$ so that the reaction is under diffusion control. The quenching always starts with the maximal reaction rate constant k_0 and then slows down gradually, approaching a much smaller diffusional value, k_D:

$$k_I(t) = \begin{cases} k_0 & \text{at } t = 0 \\ k_D\left(1 + \dfrac{R}{\sqrt{\pi Dt}}\right) & \text{at } t \to \infty \end{cases} \qquad (2.3)$$

From Figure 1, which demonstrates the evolution of the

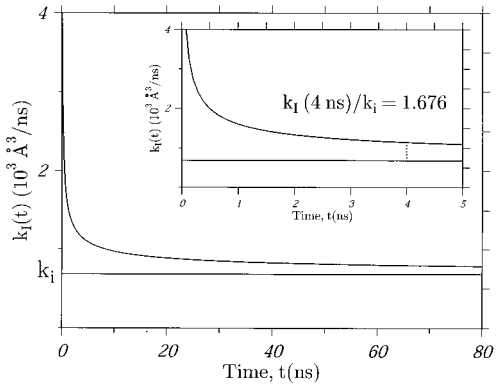

Figure 1. Time dependence of the instantaneous rate constant $k_I(t)$ compared to its asymptotic (steady-state) value k_i in the contact theory of diffusion-assisted electron transfer. Two parameters of the theory, k_0 and σ, are taken to be the same as in Figure 3. The vertical dotted line in the inset indicates the upper bound of the time interval, which was available experimentally, where the instantaneous rate constant is still almost 70% larger than the steady state value.

Collins−Kimball rate constant (2.1) in the full time domain, it is easy to see that the CK rate constant is larger than the steady state constant, k_i, at any finite time, and the difference is more pronounced the earlier they are compared.

From work done in the last decade, there is growing evidence that fluorescence quenching by electron transfer is actually nonexponential.[18] In this and other studies[19], the non-Markovian Collins−Kimball theory[2] was used to fit the experimental kinetics from very short times to long times. However, this manner of extracting quenching parameters from nonstationary kinetics was deservedly criticized in ref 20 because there are too many parameters to obtain reliable results. It should be added that the electron transfer in the inverted region studied in ref 19 does not occur at contact at all, which makes the Collins−Kimball theory inapplicable, at least at short times. Instead of fitting all of the kinetics, the authors of ref 20 analyzed only the long-time asymptotic behavior of the survival probability, which is given by the well-known two term expression[23]

$$\ln P = \ln[N \exp(t/\tau)] = -c[4\pi RDt + 8R^2\sqrt{\pi Dt}] \qquad (2.4)$$

This expression accounts for the nonstationary diffusional transfer for any free energy of reaction. Varying the solvent viscosity by changing the external pressure, the authors provided an example of how to obtain the kinetic constant k_0 from the Collins−Kimball model of the $R_Q(D)$ dependence. This constant was found to be an order of magnitude smaller than that reported in ref 19.

The kinetics at the shortest times can be somewhat smoothed by excitation with a light pulse of finite duration.[24,25] However, the subsequent nonstationary quenching is not actually perturbed by excitation and is worthy of quantitative investigation. The first term in eq 2.4 represents the steady-state quenching with a diffusional rate constant of $4\pi RD$, whereas the second term accounts for the initial nonstationary quenching, which is faster. Because of the second term, the long-time asymptote of this process never becomes exponential in a strict sense. There is the pseudo-Markovian asymptotic expression

$$P(t) \rightarrow A\mathrm{e}^{-ck_i t}$$

but the pre-exponent permanently decreases with time: $A = \exp(-8R^2c\sqrt{\pi Dt})$. For this reason, one cannot obtain an accurate estimate of k_i by setting it equal to d ln P/dt at the latest available time. If this derivative $ck_I(t)$ is identified with the steady-state rate of quenching, ck_i, the rate constant $k_i = 4\pi R_Q D$ and the effective quenching radius R_Q are overestimated. This naive method of specifying R_Q was a source of systematic error that led to abnormally large values of the tunnelling parameter that was obtained in ref 13.

At even higher viscosities, when the electron transfer is already under diffusional control, a noticeable difference appears between encounter theory and the primitive contact model of Collins−Kimball. This difference is usually attributed to the remote nature of electron transfer described by either the rectangular model of $W(r)$ proposed by Szabo[26] or the exponential approximation of $W(r)$ (eq 1.5).[27,28] However, the best alternative to any model is the true Marcus-type rate of transfer, which is a product of both the tunnelling and Arrhenius factors:[29]

$$W_I(r) = V_0^2 \exp\left(-\frac{2(r-\sigma)}{L}\right)\frac{\sqrt{\pi}}{\sqrt{\lambda T}}\exp\left(-\frac{(\Delta G_i + \lambda)^2}{4\lambda T}\right) \qquad (2.5)$$

Here, V_0 is the tunnelling matrix element, L is the true tunnelling distance, and ΔG_i is the free-energy change associated with electron transfer. The advantage of employing the true transfer rate compared to using the CK model has been recognized in ref 24, but an attempt to fit the nonstationary quenching kinetics using eq 2.5 was launched by this group later.[25] Unfortunately, their choice of ethylene glycol as a more viscous solvent was inappropriate for the reasons that were presented in ref 30 and are confirmed here (see below). Other authors also appealed to the Marcus $W_I(r)$,[28,31,32] though in the vast majority of earlier works, the exponential approximation of this dependence was used.[7,29,33,34]

In the next section, we show how the effective radius R_Q can be properly found from the nonstationary kinetics of electron transfer causing fluorescence quenching. Then the diffusional dependence of this radius, $R_Q(D)$, will be used to specify the main parameters of the CK model: the external radius of the reaction zone, R, and the kinetic rate constant, k_0. The method for the extraction of R_Q is similar to the one proposed in ref 20, but its utilization here is different, and it is used to investigate not only the CK model but also the results obtained for the exponential transfer rate.

III. Extraction and Fitting of $R_Q(D)$

The long-time diffusional asymptote of quenching (eq 2.4) is actually a universal kinetic law, provided that the effective radius R_Q is substituted for R:

$$\ln P = -c[4\pi R_Q Dt + 8R_Q^2\sqrt{\pi Dt}] \qquad \text{at } t \gg R_Q^2/D \qquad (3.1)$$

When the concentration of quenchers in solution and the viscosity are known (as well as D, which is given by the Stokes−Einstein relationship $D = k_B T/6\pi\sigma\eta$), R_Q is the only fitting parameter in eq 3.1. It is expected that for fast diffusion R_Q coincides with the Collins−Kimball radius (eq 1.4) but that for slow diffusion R_Q becomes identical to R_s from eq 1.6.

In Figure 2, we demonstrate how R_Q can be obtained from the best fit of the two-term expression (eq 3.1) to the experimentally measured ln $P(t)$. $P(t) = N(t)\exp(t/\tau) = N/N|_{c=0}$ is obtained from the measured kinetics of energy dissipation, $N(t)$, which is related to the same kinetics in the absence of acceptors, $N(t)|_{c=0}$. The initial discrepancy between these kinetic parameters is natural and should be ignored.[24,25] The convolution of the excitation pulse with system response makes the top of a signal smoother whereas the long-time asymptote (eq 3.1)

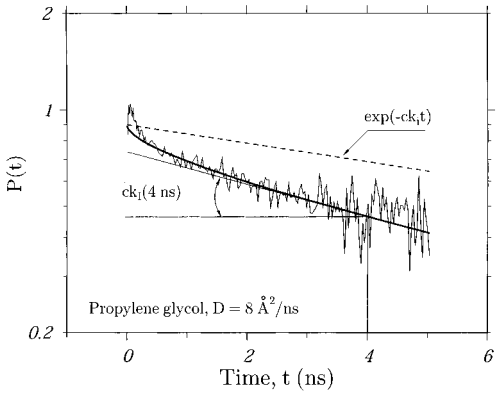

Figure 2. Fit of nonstationary electron-transfer kinetics (thick curve) to the experimental data obtained in propylene glycol, the most viscous solution studied in ref 17. The thin line represents the tangent to the kinetic curve at the longest time within the available interval. The dashed, straight line is the purely exponential decay, with the steady-state rate constant $k_i = 4\pi R_Q D$ obtained from the best R_Q value.

TABLE 1

	solvent	c (M)	τ (ns)	D (Å^2/ns)	R_Q (Å)	k_i (Å^3/ns)
		0.033			4.000	21 991
1	acetonitrile	0.067	1.45	438	4.110	22 622
		0.100			4.110	22 622
		0.025			4.545	13 823
2	ethanol	0.050	2.07	242	4.545	13 823
		0.075			4.545	13 823
		0.050			7.000	3985
3	eth gly/ethanol	0.100	2.21	45.3	7.000	3985
		0.150			7.000	3985
		0.050			7.470	3078
4	glycerol/butanol	0.100	2.60	32.8	6.402	2638
		0.150			6.646	2739
		0.050			6.597	2388
5	pr gly/butanol	0.100	2.66	28.8	6.597	2388
		0.150			6.597	2388
		0.050			7.624	2702
6	glycerol/ethanol	0.100	2.34	28.2	7.624	2702
		0.150			7.624	2702
		0.050			8.125	819
7	propylene glycol	0.100	2.80	8.0	7.500	754
		0.150			7.375	741
		0.050			10.067	1885
	ethylene glycol	0.100	2.38	14.9	10.067	1885
		0.150			10.067	1885

extrapolated into this region is sharper than the true $P(t)$. The time interval of fitting is also restricted from above by noise, whose relative value increases with time. However, even in a limited time interval, the fitting, which accounts for the nonstationary quenching, is much better than the estimate of the steady-state rate from the tangent to the kinetic curve. Even at the end of the available interval, the data are steeper than the line $\ln P = -c4\pi R_Q D t$, the slope of which is the true stationary rate ck_i.

In ref 20, reliable values of both R_Q and D were obtained using an iterative nonlinear least-squares method with sophisticated optimization of the fitted function. The time-zero shift parameter was also adjusted in the analysis. Knowing D from the separate measurements, we can do the same thing in a much simpler manner by varying only R_Q and using the vertical shift of the whole curve as an adjustable parameter. An example of such a fit is shown by the thick line in Figure 2. This procedure was used to find reaction radii as well as the corresponding

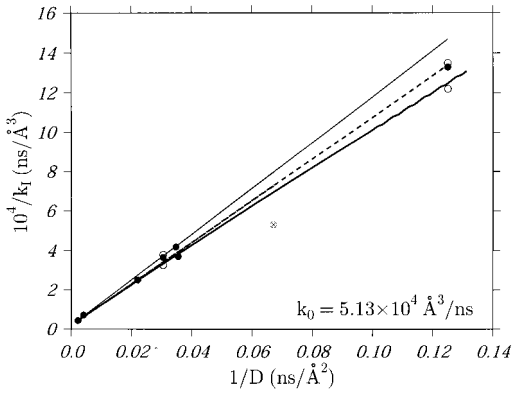

Figure 3. Dependence of the steady-state rate constant on diffusion. The points taken from Table 1 are interpolated by a thick line representing the theoretical dependence for the exponential transfer rate with $l = 0.85$ Å. The thin, straight line plots a contact approximation with $k_0 = 5.13 \times 10^4$ Å^3/ns and $\sigma = 6.87$ Å, whereas the dashed line represents the Collins−Kimball result with $\mu = 0.91$. The higher and lower values of the rate constants related to the same system but with different concentrations are depicted here and in successive Figures by empty circles.

steady-state rate constants

$$k_i = 4\pi R_Q D \tag{3.2}$$

Some authors[21,22] prefer to deal with k_i instead of R_Q. For a fixed value of D, it does not matter which of these is taken as the primary fitting parameter. However, R_Q is a more fundamental property of the transfer. The relationship of the value of R_Q to the contact distance σ and the tunneling length l contains a good deal of information about the transfer mechanism. In addition, there are analytical estimates of R_Q for high viscosities, for example, the one given in eq 1.6. For all of the systems studied here experimentally, the results for both R_Q and k_i are summarized in Table 1.

It is common and convenient to represent the CK equation (eq 1.4) as a linear relationship between inverse k_i and viscosity:

$$\frac{1}{k_i} = \frac{1}{k_0} + \frac{1}{4\pi RD} \tag{3.3}$$

This relationship is expected to hold, at least in the low-viscosity region where the contact approximation ($R \approx \sigma$) is the most reasonable. There is no contradiction in the fact that at small D some of our tabulated data deviate from the straight line (eq 3.3). The data need only approach the line as $D \rightarrow \infty$. There, $1/k_i \rightarrow 1/k_0$, so the kinetic rate constant can be unambiguously found from the intersection of the extrapolated straight line with the ordinate (Figure 3). For the system under study, k_0 was found in this way:

$$k_0 = 5.13 \times 10^4 \text{ Å}^3/\text{ns} \tag{3.4}$$

With this value for k_0 and $R = \sigma = 6.87$ Å taken from ref 17, we plotted the corresponding CK straight line, but its slope is somewhat too large to fit the experimental data well.

To improve agreement, the CK radius is often taken to be an adjustable parameter:[19,20,24]

$$R = \sigma/\mu \tag{3.5}$$

By changing μ, one changes the slope of the line representing the Collins−Kimball relationship. Selecting the proper value of μ permits the experimental data at low viscosities (in the fast-diffusion limit) to be fit very well because the electron

transfer in this limit is really a quasi-contact, provided the thin reaction layer is included in the reaction sphere of radius $R \gtrsim \sigma$.[28] The CK approximation works better the smaller the width of the actual reaction layer, $R - \sigma$.

In the case of the exponential transfer rate (eq 1.5), this width is approximately $l/2$. More accurately, it can be determined if the predictions of the CK model are compared with the exact solution obtained by means of encounter theory. In fact, the exponential transfer rate has the privilege of being one of the few models of $W_I(r)$ that enables a rigorous solution of the DET equations to be obtained. The solution results in the following dependence on diffusion of the effective radius:[7,29]

$$R_Q = \sigma + \frac{l}{2}\left[\ln(\gamma^2\beta_m) + 2\theta\left(\beta_m, \frac{2\sigma}{l}\right)\right] \qquad (3.6)$$

Here

$$\theta(x, y) = \frac{K_0(2\sqrt{x}) - y\sqrt{x}K_1(2\sqrt{x})}{I_0(2\sqrt{x}) + y\sqrt{x}I_1(2\sqrt{x})} \qquad \beta_m = \frac{W_c l^2}{4D}$$

$$\gamma = e^C \approx 1.781$$

where C is the Euler constant and $K(x)$ and $I(x)$ are modified Bessel functions. By substituting eq 3.6 into eq 1.3, one can easily deduce that

$$k_i = 4\pi\sigma D + 2\pi l D\left[\ln(\gamma^2\beta_m) + 2\theta\left(\beta_m, \frac{2\sigma}{l}\right)\right] \qquad (3.7)$$

where

$$\beta_m = \frac{k_0\rho}{8\pi\sigma D(1 + \rho + \rho^2/2)} \qquad \rho = l/\sigma$$

and

$$k_0 = \int_\sigma^\infty W_I(r)4\pi r^2\,dr = 2\pi W_c\sigma^2 l(1 + l/\sigma + l^2/2\sigma^2) \qquad (3.8)$$

Because k_0 and σ are fixed, there is only a single free parameter, l, that can be used for fitting.

In the data presented in Figure 3 (as well as in Figures 6 and 7), there are a few points in which somewhat different rate constants were obtained for the three concentrations studied. In such cases, we have plotted all of them with the higher and lower values depicted by empty circles. Almost all points fall on the theoretical curve (thick line) representing the exact solution (eq 3.7) with W_c fixed by the known kinetic constant and the tunnelling length found from the best fit,

$$l = 0.85\text{Å} \qquad (3.9)$$

Only a single point for ethylene glycol marked by the crossed circle is too low, but this system was recognized as exceptional by experimentalists themselves. The reasons that it is so different were discussed in a separate article.[30] For the same reasons, we excluded it from our fitting as well.

The exact result for exponential $W_I(r)$ was reduced in ref 7 to the standard CK relationship with $R = \sigma$ ($\mu = 1$), which appears in the zero-order approximation with respect to ρ. If the higher-order corrections were included, then $\mu < 1$ would be obtained. With the true value of μ, the CK straight line fits the data in the fast-diffusion region almost as well as the exact curve (see Figure 3) does. To specify the slope of this line theoretically, we have to find the general $\mu(\rho)$ dependence by means of DET. Therefore, in the next section, the CK relationship will be rederived for an arbitrary functional form of the transfer rate. Then $\mu(\rho)$ will be found not only for the exponential rate but also for the Marcus rate of electron transfer. From the analysis with the Marcus rate, the true tunnelling distance in liquids emerges.

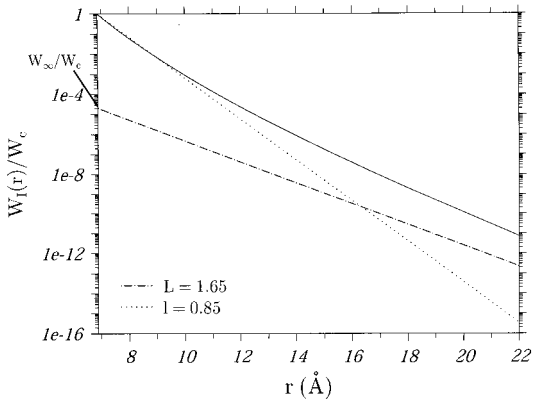

Figure 4. Distance dependence of the Marcus transfer rate (eq 2.5) in the normal region ($\Delta G_i = -0.59$ eV) with $L = 1.65$ Å and $\lambda_c = 1.3$ eV (thick line) in comparison to its exponential approximations for short (dotted line) and long (dashed−dotted line) distances.

IV. CK Approximation for Remote Electron Transfer

Although we obtained rather good agreement between the experiment and theory on the basis of the exponential transfer rate model (eq 1.5), this is not firm evidence that the distance dependence is actually exponential. In the Marcus theory of outer-sphere (solvent-assisted) electron transfer, the rate (eq 2.5) contains the Arrhenius factor that depends on the distance. In highly polar solvents, the free energy of transfer $\Delta G_i \approx$ a constant, but the reorganization energy $\lambda(r)$ slowly increases with distance, approaching twice the contact value, $2\lambda_c$:[29]

$$\lambda(r) = \lambda_c(2 - \sigma/r) \qquad (4.1)$$

In the normal Marcus region ($\Delta G_i < \lambda_c$), this effect significantly reduces the Arrhenius factor near the contact, though at large distances this factor approaches a constant. As a result, $W_I(r)$ can be approximated by exponential functions, but near contact and far from it, they have different decrements. The former ($2/l$) is larger then the latter ($2/L$), which is expressed through the true tunnelling length L:

$$W = \begin{cases} W_c e^{-2(r-\sigma)/l} & \text{at } r \approx \sigma \\ W_\infty e^{-2(r-\sigma)/L} & \text{at } r \gg \sigma \end{cases} \qquad (4.2)$$

Here, we have

$$W_c = \frac{V_0^2\sqrt{\pi}}{\sqrt{\lambda_c T}}\exp\left(-\frac{(\Delta G_i + \lambda_c)^2}{4\lambda_c T}\right)$$

$$W_\infty = \frac{V_0^2\sqrt{\pi}}{\sqrt{2\lambda_c T}}\exp\left(-\frac{(\Delta G_i + 2\lambda_c)^2}{8\lambda_c T}\right)$$

In Figure 4, the functions given in (eq 4.2) are compared with the true nonexponential Marcus rate in the normal region ($\Delta G_i = -0.59$ eV, $\lambda_c = 1.3$ eV). As was expected, the Marcus rate near the contact decreases much faster than does its exponential asymptote at large distance. The long-distance asymptote contains the true tunnelling parameter L, which is almost twice as large as the l value used above to obtain the best fit to the

experimental results. A more accurate relationship between l and L will be established below.

Moreover, the effective width of the reaction layer can be attributed to a nonexponential transfer rate provided that the CK reaction constant's dependence on diffusion (eq 3.3) can be approximately identified with that derived by DET for arbitrary $W_I(r)$. The derivation starts with the general definition of the steady-state constant in DET:

$$k_i = \int W_I(r) n_s(r)\, d^3r = 4\pi R_Q D \tag{4.3}$$

This expression relates k_i to the arbitrary rate of transfer and the steady-state pair distribution of reactants

$$n_s(r) = \lim_{t\to\infty} n(r, t) = \lim_{s\to 0} s\tilde{n}(r, s) \tag{4.4}$$

where $\tilde{n}(r, s) = \int e^{-st} n(r, t)\, dt$. The nonstationary distribution $n(r, t)$ is the solution of the diffusion equation:

$$\dot{n} = -W_I(r) n + \hat{L} n \qquad \left.\frac{\partial n}{\partial r}\right|_{r=\sigma} = 0 \qquad n(r, 0) = g(r) \tag{4.5}$$

Here, $\hat{L}$ is the diffusion operator for nonreacting particles, and $g(r) = e^{-U(r)}$ is the initial equilibrium distribution for a pair of reactants. The distribution is not homogeneous if there are electrostatic or other interactions, which are represented by the interparticle potential $U(r)$, but for $U = 0$, we have $\hat{L} = \frac{D}{r^2}\frac{\partial}{\partial r} r^2 \frac{\partial}{\partial r}$ and $g = 1$.

The general solution of eq 4.5 can be expressed through its Green function

$$n(r, t) = \int G(r, r_0, t)\, g(r_0)\, d^3r_0 \tag{4.6}$$

that has a Laplace transform that obeys the known integral equation[35]

$$\tilde{G}(r, r_0, s) = \tilde{G}_0(r, r_0, s) - \int \tilde{G}_0(r, r' s)\, W_I(r')\, \tilde{G}(r', r_0, s)\, d^3r' \tag{4.7}$$

Here, $G_0(r, r_0, t)$ is the Green function for diffusive motion without reaction, which obeys the much simpler differential equation

$$\dot{G}_0 = \hat{L} G_0 \qquad \left.\frac{\partial G_0}{\partial r}\right|_{r=\sigma} = 0 \qquad G_0(r, 0) = \frac{\delta(r - r_0)}{4\pi r^2} \tag{4.8}$$

It has the following general property following from the stationary nature of $g(r) = \int G(r, r_0, t)\, g(r_0)\, d^3r_0$:

$$\int \tilde{G}_0(r, r_0, s)\, g(r_0)\, d^3r_0 = \frac{g(r)}{s} \tag{4.9}$$

Using this property after the integration of eq 4.7 over r_0 with the weight $g(r_0)$, we obtain

$$\tilde{n}(r, s) = \frac{g(r)}{s} - \int \tilde{G}_0(r, r', s)\, W_I(r')\, \tilde{n}(r', s)\, d^3r' \tag{4.10}$$

After inserting this result into eq 4.4, we get the final integral equation for the desired stationary distribution:

$$n_s(r) = g(r) - \int W_I(r')\, \tilde{G}_0(r, r', 0)\, n_s(r')\, d^3r' \tag{4.11}$$

Equation 4.11 can be further simplified using the well-known Green function for free diffusion of charged reactants:[35]

$$\tilde{G}_0(r, r', 0) = \begin{cases} \dfrac{\exp(r_c/r)[1 - \exp(-r_c/r')]}{4\pi r_c D} & \text{at } r < r' \\ \dfrac{\exp(r_c/r) - 1}{4\pi r_c D} & \text{at } r > r' \end{cases} \tag{4.12}$$

$r_c = q^2/\epsilon k_B T$ is the Onsager radius.

For neutral reactants ($q = 0$) or highly polar solvents ($\epsilon \gg 1$), one can take $r_c = 0$ and $g(r) = 1$. Inserting the simplified Green function into the general equation (4.11) reduces eq 4.11 to

$$n_s(r) = 1 - \frac{1}{rD}\int_\sigma^r W_I(r_0)\, n_s(r_0)\, r_0^2\, dr_0 - \frac{1}{D}\int_r^\infty W_I(r_0)\, n_s(r_0)\, r_0\, dr_0 \tag{4.13}$$

The first integral in this expression describes the large distance asymptote, whereas the second integral determines the contact reduction of the particle density:

$$n_s(r) = \begin{cases} 1 - \dfrac{k_i}{4\pi D r} = 1 - \dfrac{R_Q}{r} & \text{at } r \to \infty \\ 1 - \alpha/D & \text{at } r = \sigma \end{cases}$$

$\alpha = \int_0^\infty W_I(r_0)\, n_s(r_0)\, r_0\, dr_0$. The asymptote at large r is very general and is well-established[7], whereas the contact reduction depends on the model of the transfer rate $W_I(r)$ and is more pronounced the slower the diffusion.

However, we need to use the whole distribution $n(r)$ in the calculation of the steady-state rate constant (eq 4.3). Near the kinetic limit, $n(r)$ can be readily obtained from eq 4.13. For fast diffusion, both corrections to 1 (the first term) in eq 4.13 are small and can be estimated by iteration. The first one gives us the following:

$$n_s(x) = 1 - \frac{1}{\sigma D}\left[\frac{1}{x}\int_1^x W_I(y)\, y^2\, dy + \int_x^\infty W_I(y)\, y\, dy\right] \qquad \text{for } k_0 \ll 4\pi\sigma D \tag{4.14}$$

$x = r/\sigma$ and $W_I(x) = W_I(r)\sigma^3$. Substituting this approximate result into the general definition of the rate constant, eq 4.3, we obtain

$$k_i = k_0\left[1 - \frac{k_0}{4\pi\sigma D}\mu(\rho)\right] \tag{4.15}$$

This is, in fact, the CK eq 3.3 expanded in terms of $k_0/4\pi RD \ll 1$, where $R = \sigma/\mu$ according to the definition in eq 3.5. However, μ is no longer a phenomenological parameter. Rather, it acquires the proper definition in terms of the arbitrary transfer rate:

$$\mu = \frac{\int_1^\infty \frac{W_I(x)}{x}\, d^3x \int_1^x W_I(y)\, d^3y + \int_1^\infty W_I(x)\, d^3x \int_x^\infty \frac{W_I(y)}{y}\, d^3y}{\left(\int_1^\infty W_I(x)\, d^3x\right)^2} \tag{4.16}$$

After substituting $W_I(x) = \frac{k_0}{4\pi}\delta(x - 1)$ into this equation, we obtain $\mu = 1$, which reduces eq 4.15 to the original Collins–Kimball expression for the contact reaction. However, for the exponential rate (eq 1.5), which accounts for the finite size of the reaction zone l, it follows that after integration (4.16)

$$\mu(\rho) = \frac{1 + 5\rho/4 + 5\rho^2/8 + 5\rho^3/32}{1 + 2\rho + 2\rho^2 + \rho^3 + \rho^4/4} \leq 1 \qquad (4.17)$$

This expression is identical to one that can be obtained from eq 54 of ref 21. That work used a different method (EDA), which implies the complete solution of the kinetic equation for electron transfer. In contrast, our general result, eq 4.16, does not depend on reactant dynamics and is applicable to an arbitrary $W_l(r)$. In particular, we will use it below to find $\mu(\rho)$ for a Marcus rate $W_l(r)$, eq 2.5.

As seen from Figure 3, the difference between the dashed line representing the CK result and the solid curve that is considered to be exact is rather small within the available range of viscosity variation. However, the difference increases at higher viscosity, indicating that the electron transfer when diffusion is slow is neither contact ($R = \sigma$) nor quasi-contact ($R \approx \sigma$) as in the Collins−Kimball approximation.

To illustrate the nature of this approximation, let us insert eq 4.11 into the definition (eq 4.3) and use only the zero iteration under the integral ($n_s = 1$). The result can be presented as

$$k_i = k_0 - \frac{k_0^2}{k_D} \qquad (4.18)$$

where

$$1/k_D = \frac{\int\int W_l(r)\, \tilde{G}_0(r, r', 0)\, W_l(r')\, d^3r\, d^3r'}{[\int W_l(r)\, d^3r]^2} \qquad (4.19)$$

By substituting this k_D for $4\pi RD$ in a more general Collins−Kimball expression (eq 3.3), one obtains the result derived with a "closure approximation"[36] that is given in ref 37. Evidently, $\mu = 4\pi\sigma D/k_D$, which is obtained from eq 4.19, accounts for the difference between remote and contact transfer.

The slope of the CK line obtained using the exponential transfer rate is given by the factor μ from eq 4.17, which decreases with $\rho = l/\sigma$ as shown in Figure 5. But the same parameter can be calculated numerically from eq 4.16 for the Marcus-type rate as well. From the numerical calculations, we found how the corresponding μ depends on $\rho = L/\sigma$, that is, on the true tunnelling parameter L. By comparing these curves in Figure 5, we see that L is larger than l if μ is the same for both curves. In particular, the exponent with $l = 0.85$ Å is equivalent in the CK approximation to the Marcus rate with $L = 1.65$ Å. The latter value is very close to the L value found in ref 17. There, $\beta = 2/L = 1$ Å^{-1} was obtained from fitting the DET theory with the Marcus rate to the experimental kinetic curves reflecting the fluorescence quenching by electron transfer. The small difference between the value obtained here and that reported previously[17] may be attributable to the fact that we included neither the solvent radial distribution function $g(r)$ nor the distance dependence of the diffusion constant $D(r)$.

V. High-Viscosity Asymptote of the Quenching Radius

The analysis of the dependence of the rate constant on diffusion, which is shown in the curves in Figure 3, was proven to be very useful. A similar analysis of the quenching radii variation with the diffusion constant, which is displayed in Figure 6, is even more instructive. The curve that represents the transition from kinetic to diffusion control in the simplest contact approximation levels off at the value of the true contact radius σ, whereas the generalized Collins−Kimball approximation, which includes the reaction layer in the reaction sphere, magnifies this value to the size of R. However, the effective quenching radii R_Q in more viscous solvents exceed even this value and tend to increase as $R_s(D)$ does with further increases of the viscosity.

The model dependencies of the radii on diffusion can be seen better in Figure 7, where they are represented over a much larger range of viscosity variation than the range that was available experimentally. In the region of deep diffusion control of electron transfer, both the contact and the generalized Collins−

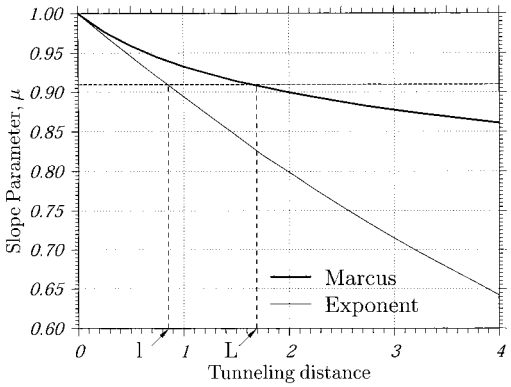

Figure 5. Slope parameter μ of the Collins−Kimball relationship for the Marcus transfer rate in the normal region (thick line) and for its exponential transfer rate equivalent (thin line). The difference between L and l related to the same μ is indicated by the vertical dashed lines.

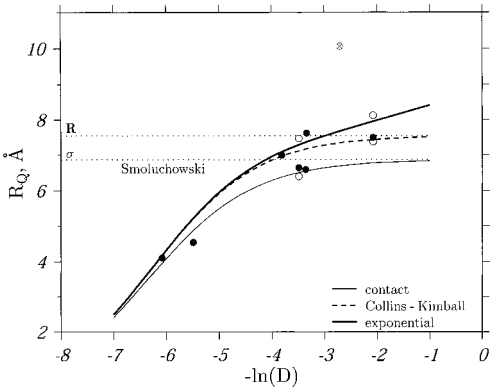

Figure 6. Dependence of the effective electron-transfer radius R_Q on diffusion. Experimental data, indicated by circles, are approximated by thin and dashed lines representing the contact and the Collins−Kimball relationships, respectively. The thick line depicts the same dependence, but for the exponential transfer rate with $l = 0.85$ Å and $W_c = 180$ ns^{-1} that is depicted by a dotted line in Figure 4.

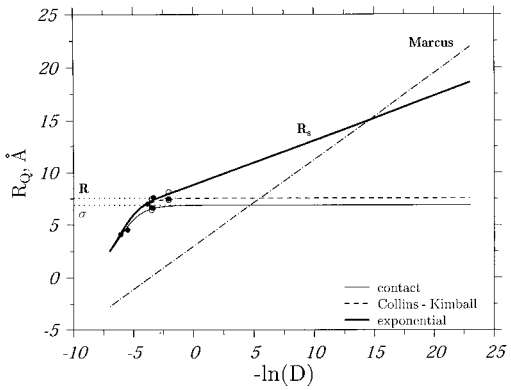

Figure 7. Same data as in Figure 6, but for a much larger range of viscosity variation. The dashed−dotted line represents the linear asymptote for the true Marcus rate, which is steeper than the asymptote for the exponential approximation of the transfer rate (the end of the thick line).

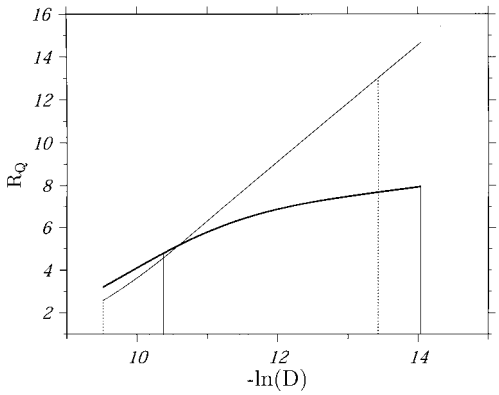

Figure 8. $R_Q(D)$ dependence for the exponential transfer rate for two different values of the tunnelling parameter. The thick line represents the short tunnelling length obtained in the present work ($l = 0.85$Å), whereas the thin line represents the overestimated $l = 5.4$ Å value found in ref 13. The vertical solid lines indicate the viscosity range used in the present study, whereas the dotted lines indicate the range studied in ref 13 in which the effective electron-transfer radii were substantially overestimated.

Kimball approximations are represented by horizontal lines. The heights of these plateaus indicate the sizes of the external radii of the reaction spheres. In contrast, the radius for remote quenching with the exponential transfer rate lies far above the plateaus and increases as the logarithm of inverse viscosity following eq 1.6. In fact, this relationship for $R_s(D)$ is the straight line with slope $^1/_2$ in the coordinates of Figure 7. This linear asymptote is common for reflecting[7] and absorbing[9,10] boundary conditions because under diffusional control it does not matter whether there is quenching at contact. The excitations never reach contact because, for slow diffusion, they are quenched by electron transfer farther apart, at $R_s \gg \sigma$.

However, it is important to remember that the largest R_Q results from the most remote electron transfer represented by the larger exponent of the Marcus transfer rate (eq 4.2) (see Figure 4). There, the asymptotic equation (eq 1.6) gives way to a similar equation but one with the true tunnelling length L:

$$R_Q = \sigma + \frac{L}{2}\ln\left(\frac{\gamma^2 W_\infty L^2}{4D}\right) \qquad (5.1)$$

Because in our case L is almost twice as large as l, the dashed−dotted line representing the final asymptotic behavior of $R_Q(\ln D)$ in Figure 7 is twice as steep as the heavy line calculated with the pure exponential rate. However, experiments at such a high viscosity seem unattainable. Even the initial change in the slope of the data is not definitive, which means that not only the kinetic but also the diffusional electron transfer remains near-contact in the available range of viscosities.

The opposite situation was expected in early work.[13] Owing to a strong overestimation of the effective radii, which were incorrectly extracted from the nonstationary quenching, the maximal values (about 15 Å) exceeded the contact radius (4 Å) by a factor of almost 4. The transfer reaction at such a large distance was attributed to diffusion control where $R_Q(D)$ has to obey the asymptotic relationship (eq 1.6), which is represented by the linear increase of $R_Q(\ln D)$ in Figure 8. Because the slope of this line can be greatly overestimated by the incorrect extraction of R_Q from the kinetic data, there is nothing surprising about the fact that the value of l found in ref 13 is also too large: $l = 5.4$ Å. When R_Q was found in the same way from the present data and was fit by the same linear asymptotic relation (eq 1.6), the result obtained was also incorrect: $l \approx 4$ Å. The real values of R_Q that we have obtained from the proper analysis of the same data are much smaller then their rough estimates that ignore nonstationary quenching. Therefore, fitting the data with the remote quenching equation (eq 1.6) is inappropriate, whereas the Collins−Kimball approximation of quasi-contact quenching holds in almost all situations.

VI. Conclusions

By fitting the differential encounter theory to the most accurate experimental data on electron-transfer kinetics observed by fluorescence quenching, we obtained excellent agreement between data and theory over the entire viscosity range used in the seven experimental systems. Reasonable values of the important parameters of electron transfer were obtained from the best fit of the predicted diffusion dependence of the transfer rate constant to the experimental value. A few important conclusions can be deduced from this work:

(1) The effective quenching radii should be extracted from the real quenching kinetics, taking into account its nonstationary nature.

(2) The linear relationship between the inverse rate constant and the inverse diffusion constant should be used to specify the kinetic rate constant, k_0, and the effective Collins−Kimball radius of the quenching sphere, R.

(3) For electron transfer in the Marcus normal region, the exponential approximation of the Marcus model is reasonable. Allowing an analytical solution of the problem, the exponential approximation gives a better fit to the experimental data than do contact or generalized Collins−Kimball models. The effective tunnelling length l is obtained from the appropriate fitting procedure.

(4) This length can be related to an actual length by equalizing the slopes of the Collins−Kimball lines corresponding to the Marcus transfer rate and its exponential approximation. The data can also be fit using the Marcus transfer rate with numerical methods.

The work presented here solves an important, long-standing problem—the overestimation of the tunnelling length L in liquid solutions.[13] Now it is clear that proper analysis will yield values similar to those obtained here, such as $L = 1.65$ Å, which corresponds to the Marcus value of $\beta = 2/L = 1.2$ Å^{-1} and does not exceed earlier reports.[3] In rigid structures, tunnelling over long distances was sometimes attributed to the super exchange through molecular intermediates (as occurs in molecular wires).[4] However, in liquid solutions, intermolecular electron transfer is expected to be shorter than intramolecular electron transfer. When the intermediates are mobile solvent molecules, the coherence of transfer is broken, and super exchange becomes ineffective.[38]

Acknowledgment. V.S.G. and A.I.B. are very grateful to the Israeli Science Foundation (Project No. 6863) for their support of this work. H.L.T. and M.D.F. thank the U.S. Department of Energy, Office of Basic Energy Science (DE-FG03-84ER13251), for their support of this research.

References and Notes

(1) Smoluchowski, M. V. *Z. Phys. Chem.* **1917**, *92*, 129.
(2) Collins, F. C.; Kimball, G. E. *J. Colloid Sci.* **1949**, *4*, 425.
(3) Wasielewski, M. R. *Chem. Phys. Rev.* **1992**, *92* 435.
(4) Davis, W. B.; Svec, W. A.; Ratner, M. A.; Wasielewski, M. R. *Nature (London)* **1998**, *396*, 60.
(5) Tunitskii, N. N.; Bagdasar'yan, Kh. S. *Opt. Spectra* **1963**, *15*, 303. Kilin, S. F.; Mikhelashvili, M. S.; Rozman, I. M. *Opt. Spectra* **1964**, *16*, 576. Vasil'ev, I. I.; Kirsanov, B. P.; Krongaus, V. A. *Kinet. Katal.* **1964**, *5*, 792.

(6) Steinberg, I. Z.; Katchalsky E. *J. Chem. Phys.* **1968**, *48*, 2404.
(7) Doktorov, A. B.; Burshtein, A. I. *Sov. Phys. JETP* **1975**, *41*, 671.
(8) Burshtein, A. I. *J. Lumin.* **2001**, *93*, 229.
(9) Pilling, M. J.; Rice, S. *J. Chem. Soc., Faraday Trans. 2*, **1975**, *71*, 1563.
(10) Berlin, Yu. A. *Dokl. Akad. Nauk. SSSR* **1975**, *223*, 625.
(11) Burshtein, A. I.; Neufeld, A. A. *J. Phys. Chem. B* **2001**, *105*, 12364.
(12) Burshtein, A. I.; Khudyakov, I. V.; Yakobson, B. I. *Prog. React. Kinet.* **1984**, *13*, 221.
(13) Burshtein, A. I.; Kapinus, E. I.; Kucherova, I. Yu.; Morozov, V. A. *J. Lumin.* **1989**, *43*, 291.
(14) Neufeld, A. A.; Burshtein, A. I.; Angulo, G.; Grampp, G. *J. Chem. Phys.*, submitted for publication.
(15) Burshtein, A. I.; Morozov, V. A. *Chem. Phys. Lett.* **1990**, *165*, 432.
(16) Burshtein, A. I.; Frantsuzov, P. A. *J. Lumin.* **1992**, *51*, 215.
(17) Tavernier, H. L.; Kalashnikov, M. M.; Fayer, M. D. *J. Chem. Phys.* **2000**, *113*, 10191.
(18) Angel, S. A.; Peters, K. S. *J. Phys. Chem.* **1991**, *95*, 3606.
(19) Nishikava, S.; Asahi, T.; Okada, T.; Mataga, N.; Kakitani, T. *Chem. Phys. Lett.* **1991**, *185*, 237.
(20) Scully, A. D.; Takeda, T.; Okamoto, M.; Hirayama, S. *Chem. Phys. Lett.* **1994**, *228*, 32.
(21) Zhou, H.; Szabo, A. *Biophys J.* **1996**, *71*, 2440.
(22) Doktorov, A. B.; Kipriyanov, A. A. *Mol. Phys.* **1996**, *88*, 453.
(23) Rice, S. A. *Compr. Chem. Kinet.* **1985**, *25*, 404.
(24) Murata, S.; Nishimura, M.; Matsuzaki, S. Y.; Tachiya, M. *Chem. Phys. Lett.* **1994**, *219*, 200.
(25) Murata, S.; Matsuzaki, S. Y.; Tachiya, M. *J. Phys. Chem.*, **1995**, *99*, 5354.
(26) Szabo, A. *J. Phys. Chem.* **1989**, *93*, 6929.
(27) Eads, D. D.; Dismer, B. G.; Fleming, G. R. *J. Chem. Phys.* **1990**, *93*, 1136.
(28) Kakitani, T.; Matsuda, N.; Yoshimori, A.; Mataga, N. *Prog. React. Kinet.* **1995**, *20*, 347.
(29) Burshtein, A. I. *Adv. Chem. Phys.* **2000**, *114*, 419.
(30) Tavernier, H. L.; Fayer, M. D. *J. Chem. Phys.* **2001**, *114*, 4552.
(31) Kakitani, T.; Yoshimori, A.; Mataga, N. *J. Phys. Chem.* **1992**, *96*, 5385.
(32) Yoshimori, A.; Watanabe, K.; Kakitani, T. *Chem. Phys.* **1995**, *201*, 35.
(33) Song, L.; Dorfman, R. C.; Swallen, S. F.; Fayer, M. D. *J. Phys. Chem.* **1995**, *95*, 3453.
(34) Song, L.; Swallen, S. F.; Dorfman, R. C.; Weidemaier, K.; Fayer, M. D. *J. Phys. Chem.* **1993**, *97*, 1374.
(35) Burshtein, A. I.; Zharikov, A. A.; Shokhirev, N. V.; Spirina, O. B.; Krissinel, E. B. *J. Chem. Phys.* **1991**, *95*, 8013.
(36) Wilemski, G.; Fixman, M. *J. Chem. Phys.* **1973**, *58*, 4009.
(37) Tachiya, M.; Hilczer, M. *AIP Conf. Proc.* **1994**, *298*, 447.
(38) Kroon, J.; Oliver, A. M.; Verhoeven, J. W.; Paddon-Row, M. N. *J. Am. Chem. Soc.* **1990**, *112*, 4868.

Photoionization affected by chemical anisotropy

V. S. Gladkikh and A. I. Burshtein
Weizmann Institute of Science, Rehovot 76100, Israel

(Received 27 July 2006; accepted 22 November 2006; published online 4 January 2007)

The kinetic constants of rhodamine 3B quenching by *N*,*N*-dimethyl aniline were extracted from the very beginning of the quenching kinetics, recently studied in a few solvents of different viscosities. They were well fitted with the conventional kinetic constant definition, provided the radial distribution function of simple liquids was ascribed to the reactant pair distribution and the contact electron transfer rate was different in all the cases. This difference was attributed to the chemical anisotropy averaging by the rotation of reactants, which is the faster in solvents of lower viscosity. With the proper choice of a space dependent encounter diffusion, the whole quenching kinetics was well fitted with an encounter theory, using the Marcus [J. Chem. Phys. **24**, 966 (1956); **43**, 679 (1965)] transfer rate instead of the contact Collins-Kimball [J. Colloid. Sci. **4**, 425 (1949)] approximation. Not only the beginning and middle part of the quenching were equally well fitted, but the long time (Markovian) rate constant was also found to be the same as previously obtained. Moreover, the concentration dependencies of the fluorescence quantum yield and the Stern-Volmer constant were specified and await their experimental verification. © *2007 American Institute of Physics*. [DOI: 10.1063/1.2423027]

I. INTRODUCTION

Energy quenching of A^* (excited rhodamine 3B) by electron transfer from donor D (*N*,*N*-dimethylaniline) obeys the typical reaction scheme

$$\begin{matrix} A^* \\ \downarrow \tau_A \end{matrix} + D \xrightarrow{W_I} \left[D^+ \cdots \underset{\Downarrow}{A^-} \right] \xrightarrow{\bar{\varphi}} D^+ + A^-. \tag{1.1}$$

Here we are interested only in the first stage of this reaction which is the irreversible bimolecular ionization with space dependent rate $W_I(r)$. In differential encounter theory (DET) the survival probability of excitation $N(t)$ is given by the expression:[1,2]

$$N = \exp\left[-\frac{t}{\tau_A} - c\int_0^t k_I(t')dt' \right] = e^{-t/\tau_A} P(t), \tag{1.2}$$

where the first exponent is the natural decay with the lifetime of the luminophore, τ_A, while $P(t)$ represents the kinetics of quenching by impurities whose concentration $c=[D]$. The time dependent ionization rate "constant" $k_I(t)$ is actually a convolution of $W_I(r)$ and the pair distribution of reacting particles, $n(r,t)$, but the particular expressions for the shortest and longest time limits are very special,

$$k_I(t) = \int W_I(r) n(r,t) d^3r = \begin{cases} \int W_I(r) g(r) d^3r = k_c & \text{at } t \to 0 \\ 4\pi R_Q D \left[1 + \sqrt{\dfrac{R_Q^2}{\pi D t}} \right] & \text{at } t \to \infty. \end{cases} \tag{1.3}$$

The equilibrium radial distribution function $g(r)$, together with $W_I(r)$, specifies the initial rate constant $k_c=k_I(0)$, while the encounter diffusion coefficient D and the effective reaction radius $R_Q(D)$ determine the final (Markovian) quenching rate $k_i=k_I(\infty)=4\pi R_Q D$.

In a very popular exponential model of tunneling the ionization rate exponentially decreases with separation of reactants,

$$W_I = W_c e^{-2(r-\sigma)/l}, \tag{1.4}$$

where l is an effective length of electron tunneling near the closest approach distance σ. For this model the quenching reaction radius was calculated exactly with DET long ago,[3] assuming that $g(r)=1$. Though very complex, this expression takes the especially simple form under diffusional control,

$$R_Q = \sigma + \tfrac{l}{2}[\ln(W_c l^2/4D) + 2C], \tag{1.5}$$

where C is the Euler constant. Since the long time quenching is always under diffusional control, the last formula is all one needs to study the longest time kinetics. This is what was done at the very first attempt to apply DET to a real experiment (quenching of pheophytin *a* by toluquinone).[4] Assuming that at the times studied the quenching is already stationary, the experimentally found diffusional dependence of its rate constant $k_i(D)$ was well fitted with the theoretically expected one [Eq. (1.5)]. Surprisingly, the value of l obtained from the best fit appeared to be too large (more than 5 Å). This confusion showed that the stationary quenching had not been reached in the restricted range of times studied. Unfortunately, the shorter times were not available for experimental study in the Ukraine of the late 1980s.[4]

The nonstationary diffusional quenching $P(t)$ was studied only recently: at moderate times and for a few different concentrations.[5] All of them gave the same result for a quantity

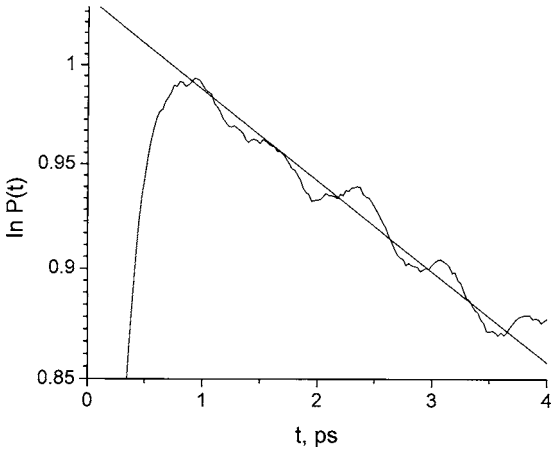

FIG. 1. The kinetics of energy accumulation and initial quenching (normalized to the maximum). Data for 0.27*M* solution of rhodamine 3B in acetonitrile borrowed from Ref. 6.

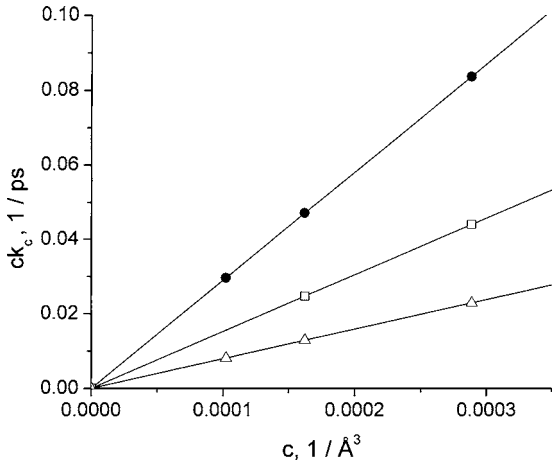

FIG. 2. The linear concentration dependence of the initial quenching rate in three different solvents: acetonitrile (●), butyronitrile (□), and benzonitrile (△).

$$-\ln P(t)/c = 4\pi R_Q D t + 8R_Q^2\sqrt{\pi D t}, \tag{1.6}$$

which is actually $\int_0^t k_I(t')dt'$ under diffusional control. This relationship allowed us to find R_Q, by fitting the nonstationary experimental data, and make sure that the extracted tunneling length l=0.85 Å had quite a reliable value.

However, the system thoroughly studied in Ref. 5 was recently subjected to a new investigation by the same experimental group but with another technique and a few new solvents.[6] The main difference is that instead of a single-photon counting used earlier, now the fluorescence upconversion was employed, allowing more accurate study of the first 450 ps of the quenching kinetics. Contrary to the previous investigation which was based on the long time asymptotic behavior (up to 4 ns), now only the short time initial quenching is available for study but with a much better accuracy and shorter excitation pulse, $f(t)$. In fact what is measured is

$$\int_0^t f(t)N(t-t')dt' \approx e^{-ck_c t} \quad \text{at } k_c > k_i \gg 1/\tau_A. \tag{1.7}$$

First of all it makes absolutely inapplicable the previously used methodology. The strategy should be completely changed: instead of the long time asymptotic behavior we have to turn our attention to the alternative, short time quenching, equally well defined in Eq. (1.3). From the initial quenching rate we extract the kinetic constant which is a convolution of the Marcus electron transfer rate and the equilibrium pair distribution of reactants. From the best fit of the experimental data, the absolute value of the space dependent Marcus rate can be specified, as well as its contact value in solvents of different viscosities. The dispersion of these values is related to the chemical anisotropy of the reaction, averaged by rotational diffusion. The latter accelerates the contact reactivity, making the kinetic constant viscosity dependent, as was predicted long ago.[7]

With the well defined Marcus rate, the whole kinetics of energy quenching by electron transfer is fitted here, varying only the diffusion coefficient and tunneling length. Comparing the results with the popular contact approximation,[8] we found it inapplicable to the system under consideration. On the contrary, the encounter theory of remote electron transfer allows us not only to reproduce all the experimental findings but also to predict the fluorescence yield concentration dependence, as well as that of the Stern-Volmer constant.

II. INITIAL RATES

The typical experimental equivalent of the quantity [Eq. (1.7)] is shown in Fig. 1. Ignoring the excitation accumulation, during the short light pulse represented by the ascending branch, one can find the rate of the initial quenching as a slope of the linear descending branch equal to ck_c. Doing the same for other concentrations, we confirm the linear concentration dependence of this rate for any of the solvents studied in Ref. 6 (Fig. 2). As a result, we have three k_c values, for acetonitrile (Ac), butyronitrile (Bu), and benzonitrile (Be) listed in Table I.

The initial kinetic rate constants found experimentally have to be compared with the theoretical ones. These constants should be calculated, not with a model but with the Marcus electron transfer rate obtained in the lowest order perturbation theory (regarding the coupling V_0 between the donor and acceptor states),[1,9]

$$W_M(r) = \frac{V_0^2}{\hbar}\sqrt{\frac{\pi}{\lambda T}}\exp\left(-\frac{2(r-\sigma)}{L}\right)\exp\left(-\frac{(\Delta G_I+\lambda)^2}{4\lambda T}\right)$$
$$= U(r)e^{-(\Delta G_I+\lambda)^2/4\lambda T}. \tag{2.1}$$

Here the Boltzmann constant k_B=1, while the free and reorganization energies are

TABLE I. Kinetic constants at different viscosities.

SOLVENTS	Ac	Bu	Be
k_c (Å^3/ps)	289	161	80
η (cP)	0.34	0.62	1.27

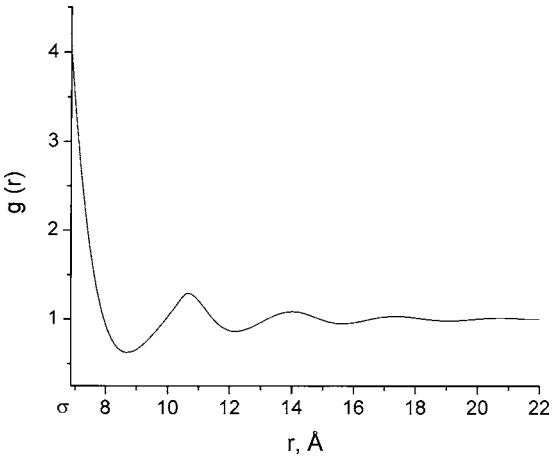

FIG. 3. The equilibrium radial distribution function kindly placed at our disposal by the authors of Ref. 6.

$$\Delta G_I = \Delta G_i + T\left(\frac{r_c}{\sigma} - \frac{r_c}{r}\right) \quad \text{and } \lambda(r) = \lambda_i + \lambda_0(r), \tag{2.2}$$

where $\Delta G_i = \Delta G_I(\sigma)$ and $\lambda_c = \lambda(\sigma)$ are the contact values of the free and reorganization energies, $r_c = e^2/T\epsilon$ is the Onsager radius of the Coulomb attraction, and $\sigma = r_d + r_a$ is the sum of the donor and acceptor radii. At a large static dielectric constant $\epsilon \to \infty$, one can take $r_c = 0$ and $\Delta G_I \equiv \Delta G_i$, as we did earlier.[5] The reorganization energy is composed of the space independent internal part, λ_i, and the external one, $\lambda_0(r)$, accounting for the polar solvent reorganization. The latter is given by the well known formula

$$\lambda_0 = \frac{e^2}{8\pi\epsilon_0}\left(\frac{1}{\epsilon_{\text{op}}} - \frac{1}{\epsilon}\right)\left(\frac{1}{r_d} + \frac{1}{r_a} - \frac{2}{r}\right), \tag{2.3}$$

where $\epsilon_{\text{op}} = 1/n^2$ is the optical dielectric constant.

Calculating the true ionization rate one has to account not only for the electron tunneling but also for the dynamical solvent effect (DSE) that can control the transfer at the shortest distances.[11] Doing it as in Ref. 12, we have

$$W_I(r) = \frac{U(r)}{1 + U(r)\tau} e^{-(\Delta G_I + \lambda)^2/4\lambda T} \quad \text{and } \frac{1}{\tau} = \frac{1}{4\tau_L}\sqrt{\frac{\lambda}{\pi T}}, \tag{2.4}$$

where τ_L is the longitudinal relaxation time of the solvent polarization which assists the electron transfer.

Knowing k_c, ΔG_I, λ, τ_L, and the true tunneling length L, it is easy to find

$$k_c = \int \frac{U(r)g(r)}{1 + U(r)\tau} \exp\left(-\frac{(\Delta G_I + \lambda)^2}{4\lambda T}\right) d^3r, \tag{2.5}$$

provided $g(r)$ is also known. The preceding analysis of the long time kinetics in the same system was made, assuming $g(r) = 1$.[5] The last assumption is reasonable for the diffusional quenching which occurs mainly at $r \sim R_Q > \sigma$ where $g(r)$ really tends to 1 (Fig. 3).

On the contrary, looking for the initial rate constant k_c, defined in Eq. (2.5), we cannot ignore the space modulation of $g(r)$ because the reaction proceeds everywhere. It is especially fast near the contact where maximal $g \sim 4$ (Fig. 3), but using the hard sphere model $g(r)$ in Eq. (2.5) the result after integration appears to be only twice as much as obtained with $g = 1$. As a matter of fact the g factor was accounted for only in the works of Tavernier *et al.* using the hard sphere model for $g(r)$. All the necessary information can be obtained from Ref. 10 and other works cited herein. Of course, the hard sphere model usually applied to the quasisimple liquids is the simpler but not the best choice. However, k_c resulting from the integration over r in Eq. (2.5) is expected to be weakly affected by substituting the real $g(r)$ for the model one. Anyhow, revising here the Fayer work we have to take $g(r)$ exactly like it is there, neither worse nor better.

The main fitting parameter of the transfer rate [Eq. (2.1)] is actually the electron coupling, V_0. Unfortunately, it cannot be uniquely determined from a single constant k_c that was determined here and listed in Table I. The complex expression obtained for it in Eq. (2.5) depends not only on V_0, but also on some other fitting parameters: τ_L and L. To specify them we have to fit the quenching kinetics at longer times which are affected by translational diffusion that can be either measured or extracted from the known viscosity η. This will be done in the next section to get the entire reliable information about the real transfer rate $W_I(r)$ and its contact value,

$$W_c = \frac{U_c}{1 + U_c\tau} e^{-(\Delta G_i + \lambda_c)^2/4\lambda_c T}, \tag{2.6}$$

where $U_c = V_0^2/\hbar\sqrt{\pi/\lambda_c T}$.

III. DIFFUSIONAL ACCELERATION OF QUENCHING

To specify the nonexponential quenching kinetics succeeding the initial exponential decay, the general time dependent rate constant [Eq. (1.3)] should be calculated with $n(r,t)$ obtained from the solution of the equation,

$$\dot{n} = -W_I n + \hat{L}n, \tag{3.1}$$

where

$$\hat{L}n = \frac{1}{r^2}\frac{\partial}{\partial r} D(r) r^2 \left(\frac{\partial n}{\partial r} + \frac{\partial u(r)}{\partial r} n\right).$$

$\hat{L}$ is the operator of encounter diffusion with space dependent coefficient $D(r)$ in the pseudopotential

$$u(r) = -T \ln g(r),$$

furnishing the equilibrium distribution of reactants before excitation: $\hat{L}n|_{t<0} = \hat{L}g(r) = 0$. The initial and reflecting boundary conditions to Eq. (3.1) are

$$n(r,0) = g(r), \qquad \left(\frac{\partial n}{\partial r} + \frac{\partial u(r)}{\partial r} n\right)\bigg|_{\sigma} = 0.$$

They differ from those previously used in encounter theory, assuming $g(r) = 1$ and $u(r) = 0$. This simplification ignores the liquid structure turning $\hat{L}$ into a conventional diffusional operator for neutral particles, $\hat{L} = D(r)\Delta$. Courtesy of Fayer, the original experimental data published in Ref. 6 was given to us by the authors for independent fitting. Unlike them, we took for all the systems $L = 1.65$ Å instead of $L = 2$ Å chosen

TABLE II. Static and optical dielectric constants.

SOLVENTS	ϵ	ϵ_{op}
Acetonitrile	36.6	1.8
Butyronitrile	20.9	1.9
Benzonitrile	25.9	2.3

in their work. The main reason is that the smaller value is more reliable, and this particular one was firmly established earlier in our joint article with Gladkikh *et al.*[5] Here we repeat the long time analysis once again using the new data and new solvents studied in their last work[6] and keeping the same $\lambda(r)$ calculated there with the intramolecular $\lambda_i=0.053$ and the data: $r_d=4.12$ Å and $r_a=2.75$ Å (Table II).

The bulk diffusion coefficient D was obtained from η by the Stokes-Einstein relationship, while the space dependence of $D(r)$ was defined as recommended by Deutsch and Felderhof,[14]

$$D(r)=D\left[1-\frac{3r_d r_a}{r(r_d+r_a)}\right].$$

This dependence was considered also in Ref. 15 but the preference there, as well as in subsequent works, was given for an alternative formula for $D(r)$ developed by Northrup and Hynes.[16] However, the latter involves an additional parameter, and we found it empirically to be less flexible and rather ineffective in fitting the quenching kinetics.

Using $\Delta G_i=-582$ meV, calculated from Eq. (10) of Ref. 10, we just had to fit the kinetic curves for both moderate and long times, operating with only two variable parameters, V_0 and τ_L, and keeping k_c=const. This work was done for all concentrations of the three solvents available, and the example of the best fit is given in Fig. 4. The electron couplings V_0 obtained from such fitting for all the solvents are listed in Table III together with τ_L values which establish the upper limits for the contact reaction rates, W_c, caused by DSE. The literature values for τ_L presented in Ref. 6 are the longest ones if the longitudinal relaxation proceeds a few different times. As was pointed out in such a case, only the shortest time contributes strongly to the DSE.[18–20] Therefore, we were free to choose τ_L from the best fit, whatever it is.

As a matter of fact, the time dependent rate constant $k_I(t)$ reducing with time from $k_c=k_I(0)$ to $k_i=k_I(\infty)$ is the main result of our fitting, allowing us to reproduce the quenching kinetics at any desirable concentration. To compare the different solvents it is enough to relate them to the corresponding $k_I(t)$. This is done in Fig. 5 which indicates the diffusional acceleration of quenching in the solvents of lower viscosity.

This is natural for the final (stationary) constant which is known to increase with D. For instance, in the contact approximation

$$k_i=\frac{k_0 k_D}{k_0+k_D}, \tag{3.2}$$

where $k_D=4\pi\sigma D$ is the diffusional rate constant, while k_0 is the diffusion independent kinetic rate constant which is easily calculated from the obtained k_i and k_D. In the contact

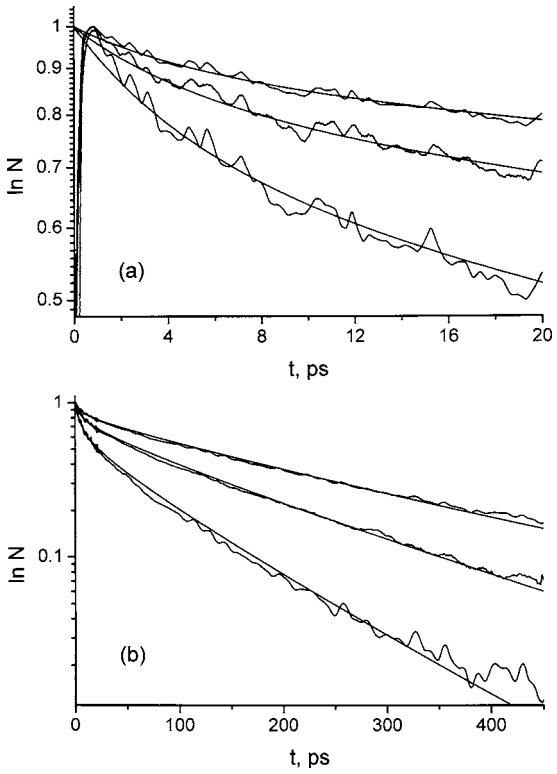

FIG. 4. The survival probability of excitation (in arbitrary units) at moderate (a) and long times (b). For $c=0.17M$, $0.27M$, and $0.48M$ (from top to bottom) in acetonitrile.

theory $k_I(0)\equiv k_0$ for any diffusion (viscosity).

However, our quenching is not contact and its rate constant is initially much larger k_0. Moreover, unlike k_0 the initial rate constant k_c is not a constant at all but increases with D being inverse proportional to viscosity (Table I). This is a surprise. According to Table III not only k_c and W_c, but also V_0, depend on the solvent viscosity although the latter controls only the reactant mobility. The electron coupling V_0 is just the static property of the contacting reactants that should not be affected by their motion.

This is the paradox resulting from the spherically isotropic model of reactants whose reactivity is implied to be independent of the mutual orientation. Such a paradox can be qualitatively resolved only by taking into account the chemical anisotropy of the reaction. Until now this factor was ignored in the unified theory (UT) and integral encounter theory (IET) of electron transfer[1,2] but was exhaustively studied earlier by means of DET though in contact

TABLE III. Fitting parameters.

SOLVENTS	Ac	Bu	Be
V_0 (meV)	44.32	18.32	27.72
τ_L (ps)	0.05	0.1	4
W_c (1/ns)	340	201	51.1
D (Å^2/ns)	440	240	120
k_i (Å^3/ps)	22.84	12.27	7.85
k_D (Å^3/ps)	37.99	20.72	10.36
k_0 (Å^3/ps)	57.26	30.12	12.63

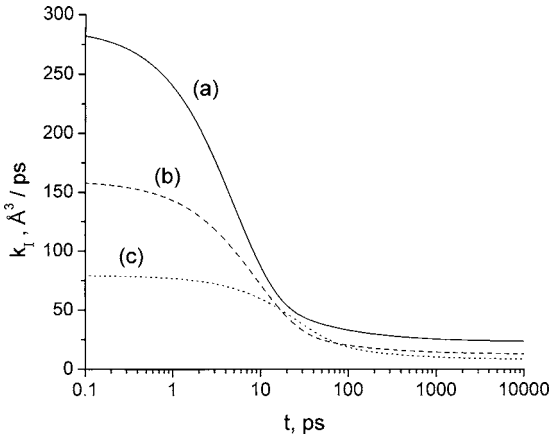

FIG. 5. The time dependent rate constants of quenching in acetonitrile (a), butyronitrile (b), and benzonitrile (c).

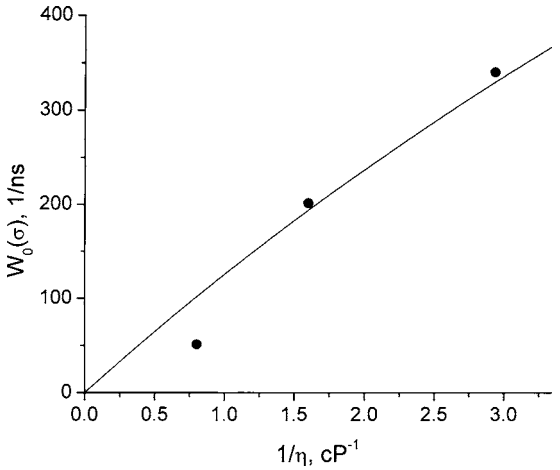

FIG. 6. The contact transfer rate (●) compared with the cage rate of the stereo-anisotropic reaction, accelerated by jumplike reorientations (solid line).

approximation.[4] The averaging of the spherical anisotropy of the reaction by rotational diffusion can explain the increasing of W_c in less viscous solvents where rotation is faster. The same is true for the corresponding effective value of V_0, if the relationship (2.6) between W_c and V_0 remains unchanged.

IV. SPHERICAL ANISOTROPY OF ELECTRON TRANSFER

The contact reaction is chemically anisotropic if the sphere of the contact radius σ is not equally active anywhere but only within the small spot on it of the area $\varsigma < 1$. Then the cage reaction is facilitated by rotation which averages the spherical anisotropy.

Such a reaction studied in Ref. 7 is sensitive to the kinematics of reorientation, modulating the reactivity of a pair. The survival probability of the reactants in a cage, $\bar{n}(t)$, decays nonexponentially with time, so that the effective reaction is actually the inverse lifetime of the reacting pair (Sec. V in Ref. 7):

$$W_0 = \left[\int_0^\infty \bar{n}(t)dt\right]^{-1}. \tag{4.1}$$

The orientationally averaged $\bar{n}(t)$ depends on the rate of rotation and its mechanism, not mentioning the particular anisotropy peculiar to a given reactant pair. Since nothing about this is known perfectly we will be concerned only with the simplest rotational model illustrating a main feature of the phenomenon: the acceleration of the reactivity by the jumpwise reorientation with frequency $1/\tau_0 \propto \eta$.[7] In the reactive spot model the rate of the reaction is w_c only within the spot and zero outside it. The reaction kinetics studied in Ref. 7 and used for calculating its hopping rate [Eq. (4.1)] furnishes the desired result,

$$W_0 = \frac{w_c\varsigma}{1 + w_c(1-\varsigma)\tau_0}\begin{cases} \dfrac{\varsigma}{1-\varsigma}\dfrac{1}{\tau_0} = \dfrac{\text{const}}{\eta} & \text{rotational control} \\ w_c\varsigma & \text{kinetic limit.} \end{cases} \tag{4.2}$$

As seen in Fig. 6, the effective contact rate W_c, which is the closest analog of W_0, quasilinearly depends on inverse viscosity, indicating that contact transfer is under rotational control. If $\varsigma \approx 0.2$ the latter is approximately the same as W_c in Table III, $W_0 = 0.25/\tau_0 = 250\ \text{ns}^{-1}$ provided $\tau_0 \sim 1$ ps and $w_c > 10^{13}$ which is necessary to maintain the true rotational control ($w_c\tau_0 \gg 1$). Under such conditions the spherical anisotropy of the reaction can be really averaged by reactant rotation. If the latter proceeds as a sequence of sudden turns, the reaction mechanism is hopping (jumping) provided the jump size θ is larger than the reaction spot and the hopping is faster than the orientational relaxation: $1/\tau_\theta \sim \theta^2/\tau_0$. Moreover, if the jumps are even smaller than the reactive spot then the system penetrates into it by rotational diffusion. The diffusional reaction in a cage which is an alternative to the hopping one was also studied in Ref. 7 and was used to describe the chemically anisotropic radical reactions considered as "pseudodiffusional."[13]

The continual diffusion in the angle space can also be originated not from sudden jumps but from the free inertial passes of finite length,[17] and the chemical activity is not necessary localized in the spot but can be distributed over the whole sphere.[7] The true mechanism of the anisotropic reaction is worthy of special consideration accounting for the real geometry of the reactants and the true mechanism of their rotation, available for independent (spectroscopical) investigation.[17] Unfortunately, all the theories of chemical anisotropy[7,13,21,22] addressed only the contact reactions. Neither of them spreads out to the remote electron transfer considered here. As long as such a transfer is spherically isotropic we can do no more than to recognize why its effective coupling is viscosity dependent.

V. FLUORESCENCE QUANTUM YIELD

With this effective coupling and other parameters obtained from the best fit, we got the reliable time dependence of $k_I(t)$ which monotonously reduces with time, approaching the final (stationary) rate constant $k_i = k_I(\infty)$. Being equalized to the well known expression (3.2) of the contact theory, it allows one to get two major parameters of the latter: k_0 and k_D. Using them in the famous Collins and Kimball formula,[8]

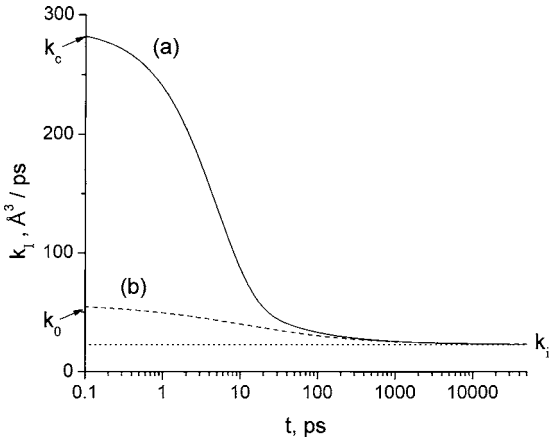

FIG. 7. The time dependent rate constant in acetonitrile, calculated by the encounter theory of remote electron transfer (a) and in the contact approximation of Collins and Kimball (b), provided the stationary rate constants $k_i=k_I(\infty)$ are the same. The dotted line represents the Markovian description of quenching: k_i=const at any time.

$$k_I(t) = k_i\left(1 + \frac{k_0}{k_D}e^x \operatorname{erfc}\sqrt{x}\right), \tag{5.1}$$

where $x=(1+k_0/k_D)^2Dt/\sigma^2$, we can restore the whole time dependent constant $k_I(t)$ of contact theory. In Fig. 7 we compared it with that found here for the remote transfer. Being almost the same at rather long times, they are quite different at the very beginning. The contact theory underestimates the initial quenching since $k_0 \ll k_c$. This defect is also seen in the kinetics of quenching which is very different in the contact and remote models of electron transfer. The remote energy quenching proceeds much faster than the contact one, especially at the beginning (Fig. 8).

As a result, the luminescence quantum yield appears to be quite different in these two cases. According to its general definition

$$\eta = \int_0^\infty N(t)dt/\tau_A = \frac{1}{1+c\kappa\tau_A}, \tag{5.2}$$

where κ is the constant of the Stern-Volmer law which is usually expected to be linear in coordinates $1/\eta$ vs c. Contrary to this expectation, the substitution into Eq. (5.2) of the general expression (1.2), with all parameters already known, leads to the nonlinear dependence of $1/\eta$ on c (Fig. 9). In other words the Stern-Volmer constant κ in Eq. (5.2) is concentration dependent. Only at the lowest quencher concentrations,

$$\eta \approx \int_0^\infty e^{-t/\tau_A}\left[1 - c\int_0^t k_I(t')dt'\right]\frac{dt}{\tau_A} = 1 - c\kappa_0\tau_A,$$

where the original Stern-Volmer constant

$$\kappa_0 = \int_0^\infty e^{-t/\tau_A}\left[\int_0^t \kappa_I(t')dt'\right]\frac{dt}{\tau_A} \tag{5.3}$$

is really concentration independent. For our system it appears to be a bit different in different solvents, as shown in Table IV.

However, the true constant from Eq. (5.2) increases at higher concentrations. This dependence, $\kappa(c)$, presented in Fig. 10 for all three solvents studied, can be subjected to a special experimental inspection for checking the self-consistency of the present theory and its validity limits.

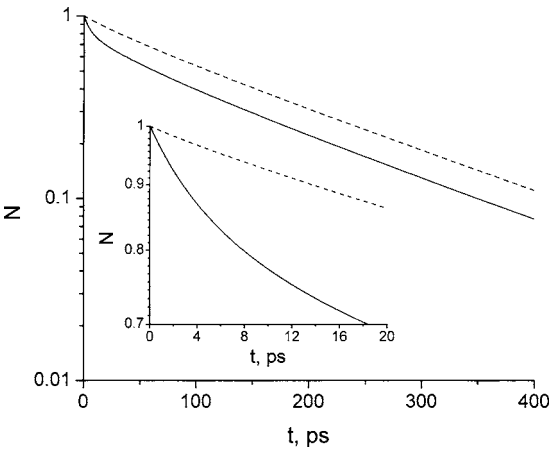

FIG. 8. The long time and short time (in the inset) decays of excitation in acetonitrile at quencher concentration $c=0.27M$. The dashed lines are obtained in contact approximation.

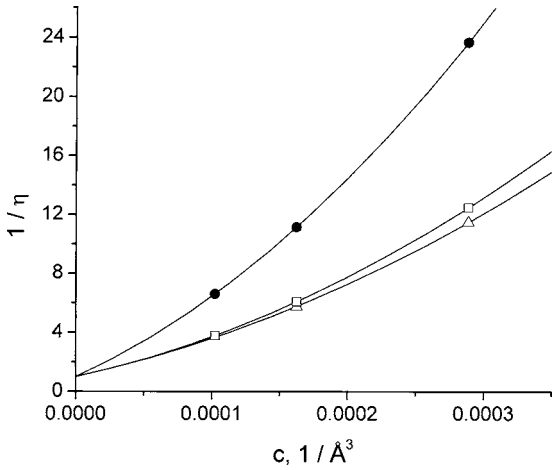

FIG. 9. The nonlinear Stern-Volmer law for the luminescence quantum yield in acetonitrile (●), butyronitrile (□), and benzonitrile (△).

VI. CONCLUSIONS

Although the most successful, this is not the first attempt to fit the different experimental data obtained for one and the same system in acetonitrile. Since all the data are compatible, one has to expect that the principal parameters of the transfer rate $W_I(r)$ obtained from the best fit in the present work must be comparable with those found earlier, from the fitting made in 2006 (Ref. 6) and 2002 (Ref. 5). The main ones listed in Table V indicate that there is nevertheless the wide scatter of the published results. There are reasonable explanations for such a discrepancy.

TABLE IV. Original Stern-Volmer constant.

SOLVENTS	Ac	Bu	Be
κ_0 (Å^3/ps)	27.8	16.7	12.0

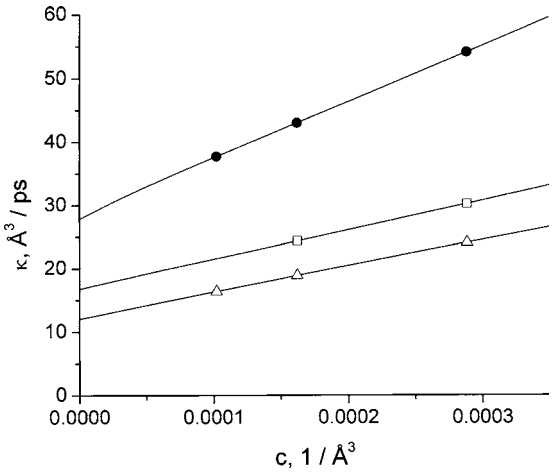

FIG. 10. The concentration dependence of the Stern-Volmer constants in acetonitrile (●), butyronitrile (□), and benzonitrile (△).

Making our first attempt in 2002 to fit the theory to the available experimental data, we had at our disposal only the long time kinetics of quenching and did not take into account the liquid structure represented by $g(r)$. It is not surprising that extrapolating too far to initial times and assuming $g(r)=1$ at any r, we underestimated the initial rate constant which appeared to be much closer to $k_0=57.26$ from Table III than to the actual $k_c=289.5$.

In 2006, the authors of Ref. 6 using the data for moderate times and accounting for a true $g(r)$ arrived at k_c which is almost twice as large as before but still much smaller than the actual one obtained from the initial quenching in the present work. However, taking *ad hoc* too large a $L=2$ Å they enhanced the quenching rate everywhere and had to reduce W_c, pushing down V_0 to keep k_c unchanged. In the present work we returned back to the earlier specified smaller $L=1.65$ Å and included $g(r)$ into consideration. Both these factors significantly enhance the initial quenching constant k_c which we bring into one-to-one correspondence with the value first obtained here from the original experimental data.

The W_c and V_0 values obtained here seem the most reliable. They are based on the analysis of both the initial and moderate quenching kinetics and account for the actual liquid structure and DSE. However, the spherically isotropic model of tunneling ignores the real chemical anisotropy of transfer. Therefore, we relate to these data as to the effective parameters of the model which perfectly well describes the whole quenching kinetics, allowing us to predict the fluorescence quantum yield and the concentration dependence of the Stern-Volmer constant. Moreover, the estimate of the most important tunneling parameters is rather reliable and does not depend too much on the choice of model. They are found in the admissible interval of possible values,

$$20 \text{ meV} < V_0 < 45 \text{ meV}, \quad 1.5 \text{ Å} \leqslant L \leqslant 2 \text{ Å}.$$

Most problems do not require better accuracy.

TABLE V. Comparison of the results.

WORKS	k_c (Å^3/ps)	W_c (1/ns)	V_0 (meV)	L (Å)
Present	289.5	340.38	44.32	1.65
Ref. 6	94.30	124.6	19.22	2
Ref. 5	51.33	203.8	25.23	1.65

ACKNOWLEDGMENTS

The authors are very grateful to Professor Michael Fayer and Dr. Alexei Goun for friendly communication and the original data kindly provided for their disposal.

[1] A. I. Burshtein, Adv. Chem. Phys. **114**, 419 (2000).
[2] A. I. Burshtein, Adv. Chem. Phys. **129**, 105 (2004).
[3] A. B. Doktorov and A. I. Burshtein, Sov. Phys. JETP **41**, 671 (1975).
[4] A. I. Burshtein, E. I. Kapinus, I. Yu. Kucherova, and V. A. Morozov, J. Lumin. **43**, 291 (1989).
[5] V. S. Gladkikh, A. I. Burshtein, H. L. Tavernier, and M. D. Fayer, J. Phys. Chem. A **106**, 6982 (2002).
[6] A. Goun, K. Glusak, and M. D. Fayer, J. Chem. Phys. **124**, 084504 (2006).
[7] A. I. Burshtein and B. I. Yakobson, Chem. Phys. **28**, 415 (1978).
[8] F. C. Collins and G. E. Kimball, J. Colloid Sci. **4**, 425 (1949).
[9] R. A. Marcus, J. Chem. Phys. **24**, 966 (1956); **43**, 679 (1965).
[10] H. L. Tavernier, M. M. Kalashnikov, and M. D. Fayer, J. Chem. Phys. **113**, 10191 (2000).
[11] L. D. Zusman, Chem. Phys. **49**, 295 (1980).
[12] V. Gladkikh, A. I. Burshtein, G. Angulo, S. Pagés, B. Lang, and E. Vauthey, J. Phys. Chem. A **108**, 6667 (2004).
[13] A. I. Burshtein, I. V. Khudyakov, and B. I. Yakobson, Prog. React. Kinet. **13**, 221 (1984).
[14] J. M. Deutsch and B. U. Felderhof, J. Chem. Phys. **59**, 1669 (1973).
[15] H. L. Tavernier and M. D. Fayer, J. Chem. Phys. **114**, 4552 (2001).
[16] S. H. Northrup and J. T. Hynes, J. Chem. Phys. **71**, 871 (1979).
[17] A. I. Burshtein and S. I. Temkin, *Spectroscopy of Molecular Rotation in Gases and Liquids* (Cambridge University Press, London, 1994), p. 300.
[18] L. D. Zusman, Z. Phys. Chem. **186**, 1 (1994).
[19] J. T. Hynes, J. Phys. Chem. **90**, 3701 (1986).
[20] L. D. Zusman, Theor. Exp. Chem. **19**, 381 (1984).
[21] S. I. Temkin and B. I. Yakobson, J. Phys. Chem. **88**, 2679 (1984).
[22] A. I. Shushin, Chem. Phys. Lett. **130**, 452 (1986).

Kinetics and Yields of Electron Transfer in the Inverted Region

V. Gladkikh and A. I. Burshtein*

Weizmann Institute of Science, Rehovot 76100, Israel

G. Angulo

Graz University of Technology, Graz, Austria

Stéphane Pagès, Bernard Lang, and Eric Vauthey

Department Physical Chemistry, University of Geneva, Geneva, Switzerland

Received: February 18, 2004; In Final Form: May 21, 2004

The fluorescence dynamics of perylene in the presence of tetracyanoethylene in acetonitrile was studied experimentally and theoretically, taking into consideration that the quenching is carried out by remote electron transfer in the Marcus inverted region. The initial stage was understood as a convolution of the pumping pulse with the system response accounting for the fastest (kinetic) electron transfer accompanied by vibrational relaxation. The subsequent development of the process was analyzed with differential encounter theory using different models of transfer rates distinguished by their mean square values. The single channel transfer having a bell-shaped rate with a maximum shifted far from the contact produces the ground state ion pair. It was recognized as inappropriate for fitting the quenching kinetics at moderate and long times equally well. A good fit was reached when an additional near contact quenching is switched on, to account for the parallel electron transfer to the electronically excited state of the same pair. The concentration dependence of the fluorescence quantum yield is well fitted using the same rates of distant transfer as for quenching kinetics while the contact approximation applied to the same data was shown to be inadequate.

I. Introduction

Fluorescence quenching in solutions is often considered within the classical theory of Smoluchowski[1] and Collins & Kimball,[2] assuming that the reaction is carried out at the closest approach distance between excited energy donor D* and acceptor A. This popular contact model applied to numerous systems[3] is reasonable for proton transfer[4] but bad for the long-range energy transfer governed by multipole interactions.[5−7] The electron transfer is intermediate between these two extremes. If the reaction occurs in the normal Marcus region, it can be considered as contact at fast diffusion, but at slow diffusion the effective quenching radius significantly exceeds the contact distance.[3,8,9] In the inverted region, the electron transfer is remote at any diffusion because the maximum of the Marcus rate is shifted out of contact.[3,10,11] In general, the ionization carried out by the position dependent rate $W_I(r)$ is represented by the following reaction scheme:[8]

$$\begin{array}{l} \mathrm{D}^* + \mathrm{A} \xrightarrow{W_I} \mathrm{D}^+ + \mathrm{A}^- \\ \downarrow \tau_D \end{array} \qquad (1.1)$$

The remote transfer in liquids assisted by the encounter diffusion of partners is well described by the differential encounter theory (DET)[12−17] recently reviewed in ref 3. However, for a long time the attempts to describe the reaction kinetics with either contact theory or DET were either unsuccessful or led to the nonphysical values of the electron-transfer parameters.

For instance, Fleming et al. studied the diffusion-influenced quenching reaction between rhodamine B and ferrocyanide and came to the conclusion that the Collins and Kimball contact model cannot consistently explain both the rapid initial decay (upconversion data) and the slower decay investigated with time-correlated single photon counting.[18] The fitting parameters of the model which are good for short times are poor for long-time decay and vice versa. This deficiency is inherent in the contact approximation which completely ignores the static quenching, preceding the diffusional one. Finally, it was widely recognized that "as long as we adopt realistic values of diffusion coefficients, the experimentally obtained decay curves...cannot be satisfactorily reproduced by the Collins and Kimball model, whatever values of the parameters are assumed".[19]

Calculations of this sort were also done with the rectangular[20,24] and exponential[21−23] models of the electron-transfer rate $W_I(r)$. In the normal Marcus region, the rectangular model with varying parameters is a bit better than the contact one, as well as the exponential model,

$$W_I(r) = W_c \exp\left(-\frac{2(r-\sigma)}{l}\right) \qquad (1.2)$$

which is the rough simplification of the single channel Marcus rate:

$$W_I(r) = \frac{V_0^2}{\hbar}\exp\left(-\frac{2(r-\sigma)}{L}\right)\frac{\sqrt{\pi}}{\sqrt{\lambda T}}\exp\left(-\frac{(\Delta G_I+\lambda)^2}{4\lambda T}\right)$$
$$= U(r)\mathrm{e}^{-(\Delta G_I+\lambda)^2/4\lambda T} \qquad (1.3)$$

Here V_0 and L are the contact matrix element and the length of the electron tunneling, while $\lambda(r)$ and $\Delta G_I(r)$ are the reorganiza-

10.1021/jp0492669 CCC: $27.50
Published on Web 07/10/2004

tion and free energies of ionization, T is the temperature in energy units ($k_B = 1$), and σ is the closest approach distance. Unfortunately, the very first fitting of the exponential model to the transfer kinetics also led to confusion. It was done by studying the quenching of excited pheophytin *a* by toluquinone in solvents of different viscosity.[25] The best fit for these data was obtained at $W_c = 1.8 \times 10^{10}$ s^{-1}, $\sigma = 4$ Å, and $l = 5.4$ Å. This value of l is abnormally large, not to mention L that should be even twice as large.[8]

The Marcus rate (1.3) was also used for fitting the entire quenching kinetics, but the authors failed to find the unique values of two fitting parameters, V_0 and L, in low viscosity solvents.[19] Only for high viscosity ethylene glycol they were able to fix reasonable values, but the choice of ethylene glycol was inappropriate for the reasons presented in ref 26 and confirmed later.[8] To reduce the number of parameters, L was arbitrarily put as 2 Å in ref 27 since this is "a value usually admitted in the literature". Such a choice allowed the authors to fit closely the transient quenching kinetics with rather small $V_0 = 6 \div 7$ meV.

However, the first successful attempt to estimate l from an unconditional fitting of the theory with an exponential rate to the real data was accomplished only recently.[8] The progress in experimental techniques made possible much more accurate investigation of the electron transfer between excited rhodamine 3B in the excited state and *N*,*N*-dimethylaniline in the normal Marcus region. It was studied in seven solvents of different viscosities.[28] The theoretical interpretation of the results was based on the analysis of quenching kinetics that obeys the universal asymptotic law:

$$\ln P = -c[4\pi R_Q D t + 8 R_Q{}^2 \sqrt{\pi D t}] \quad \text{at } t \to \infty \qquad (1.4)$$

where D is the coefficient of encounter diffusion, R_Q is the effective quenching radius, and

$$P(t) = N(t, c)/N(t, 0) = R(t) \exp(t/\tau_D) \qquad (1.5)$$

is the ratio of excitation populations with and without quenchers: $N(t, c)$ and $N(t, 0) = N(0) \exp(-t/\tau_D)$. The last term in eq 1.4 contributes to the nonstationary (transient) kinetics, which is not negligible over all times studied experimentally. The significant overestimation of R_Q as well as l in ref 25 resulted from ignoring this very term in the course of the fitting.

The proper extraction of R_Q from the experimental data, made in ref 8, allowed authors to fit the quasicontact and exponential models to the diffusional dependence $R_Q(D)$ getting from it a reasonable value of $l = 0.85$ Å.[8] Later a similar asymptotic analysis of transfer kinetics was employed to perylene quenched by *N*,*N*′-dimethyl-aniline in a dimethyl sulfoxide (DMSO)−glycerol mixture whose viscosity changes with composition.[29] Varying only l it was found from the best fit: $l = 0.81$ Å, $W_c = 29.12$ ns^{-1}. The transfer in this system also proceeds at relatively small $\Delta G_I < \lambda$, that is in the normal Marcus region. There $W_I(r)$ monotonically decreases with distance and can be modeled with the exponential function of eq 1.2.[3]

Here we at first turn to a reaction in the inverted region carried out by a strong electron acceptor, tetracyanoethylene (TCNE). The latter allowed Rehm and Weller to get the most exergonic points of their famous plot, although with other fluorophores.[30] The quenching of perylene (the lifetime τ_D measured after argon bubbling is 4.34 ns in our experiments) also occurs deeply in the inverted Marcus region where $\Delta G_I(\sigma) > \lambda(\sigma)$. At so high an exergonicity, $W_I(r)$ given by eq 1.3 passes through the maximum shifted out of contact,[3] so that even in the kinetic limit the reaction is remote, not to mention the diffusion-controlled ionization. However, we will demonstrate that the fitting of the experimental data with only this bell-shaped rate is impossible but becomes plausible if additional near contact quenching is added.

The origin of such an additional quenching may be attributed to parallel electron transfer to the excited state of a cation radical as suggested in ref 30. This transfer is much less exergonic and therefore occurs in the normal Marcus region, near the contact:

$$D^* + A \begin{matrix} \nearrow (\dot{D}^+)^* + \dot{A}^- \\ \searrow \dot{D}^+ + \dot{A}^- \end{matrix} \qquad (1.6)$$

Alternatively, one can consider the multichannel transfer to numerous vibronic sublevels of the ground electronic state of the ion radicals. The total rate of their production through all the vibronic channels is broader and located closer to the contact than the rate (1.3):[3,31,32]

$$W_I(r) = U(r) \sum_0^\infty e^{-S} \frac{S^n}{n!} \exp\left[-\frac{(\Delta G_I + \lambda + \hbar\omega n)^2}{4\lambda T}\right] \qquad (1.7)$$

where $S = \lambda_q/\hbar\omega$, while ω is the frequency and λ_q is the reorganization energy of the quantum vibration. Since there is no straight evidence in favor of one of these two possibilities we will sequentially consider both of them.

In fitting the real data, provision should be made for saturation of the ionization rate at short distances. There the tunneling can be so fast that the limiting stage becomes the diffusional motion along the reaction coordinate to the crossing point.[33,34] In polar solvents, this is the so-called "dynamical solvent effect" limited by the longitudinal relaxation of polarization.[35] Taking into account this effect the single channel rate takes the following form:[36,37]

$$W_I(r) = \frac{U(r)}{1 + U(r)\tau} e^{-(\Delta G_I + \lambda)^2/4\lambda T} = W_0 e^{-(\Delta G_I + \lambda)^2/4\lambda T} \qquad (1.8)$$

The upper limit of the rate, τ^{-1}, is different for activationless ($\Delta G_I = 0$)[33] and highly activated reactions ($\Delta G_I \gg T$),[35] but we will use the interpolation, which is reasonable between these two limits where most of our experimental data falls:[38]

$$\frac{1}{\tau} = \frac{1}{4\tau_L}\sqrt{\frac{\lambda}{\pi T}} \qquad (1.9)$$

Here τ_L is the longitudinal relaxation time of the solvent polarization, which assists the electron transfer. For the multiphonon rate (1.7), the generalization is straightforward:

$$W_I(r) = \sum_0^\infty \frac{U(r) e^{-S} S^n}{n! + U(r)\tau e^{-S} S^n} \exp\left[-\frac{(\Delta G_I + \lambda + \hbar\omega n)^2}{4\lambda T}\right] \qquad (1.10)$$

The saturation effect establishes the upper limit for the Arrhenius pre-exponent W_0, which is lower, the slower the dielectric relaxation. In Figure 1 we demonstrate how this limit is reached for a few solvents whose $1/\tau_L$ values were tabulated in ref 39. At the shortest interparticle distances all the curves are significantly lower than the tunneling rate, $U(r)$, especially those with long τ_L. This difference strongly reduces the total rate of

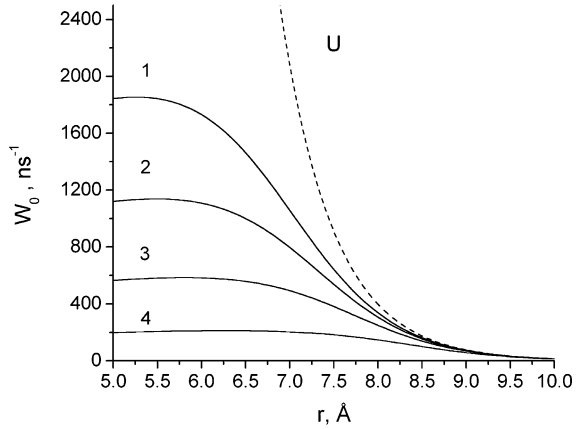

Figure 1. The Arrhenius pre-exponent as a function of distance for four solvents with different $1/\tau_L$ values: (1) acetonitrile (2.0 ps^{-1}), (2) acetone (1.2 ps^{-1}), (3) methyl acetate (0.6 ps^{-1}), (4) benzonitrile (0.21 ps^{-1}). Other parameters: $\lambda_0 = 1.15$ eV; $V_0 = 62$ meV; $\sigma = 5$ Å.

activated electron transfer $W_I(r)$, which is monotonic in the normal Marcus region (Figure 2A) and has the bell shape in the inverted one (Figure 2B).

The outline of this article is as follows. In the next section, the general formalism of DET will be briefly outlined. In section III the short, moderate, and long-time kinetics will be fitted sequentially with single-channel, double-channel, and multichannel models. In section IV, the experimental dependencies of the product quantum yields on quencher concentration will be compared with the theoretical ones specified with the transfer parameters obtained from the best fit to the kinetic data. In section V, we calculate with the same parameters the concentration dependence of the quantum yields of all the products of ionization. The results obtained are summarized in Conclusions.

II. Differential Encounter Theory of the Phenomenon

In the DET developed in refs 12−17 and reviewed in ref 3 the quenching kinetics is given by the general expression

$$R(t) = \exp(-t/\tau_D - c\int_0^t k_I(t')\,dt') \qquad (2.1)$$

where the time dependent rate constant is

$$k_I(t) = \int W_I(r) n(r, t)\, d^3r \qquad (2.2)$$

The pair correlation function $n(r, t)$ takes into account that the remote transfer running with the rate $W_I(r)$ is accelerated by the encounter diffusion represented by operator $\hat{L}$:

$$\dot{n} = -W_I(r)n + \hat{L}n \qquad (2.3)$$

If there is no inter-reactant interaction then the diffusional operator $\hat{L} = D\Delta$, while the initial and the boundary conditions to eq 2.3 take the following form:

$$n(r, 0) = 1 \quad \text{and} \quad \frac{\partial n}{\partial r}|_{r=\sigma} = 0 \qquad (2.4)$$

Over rather long times, the quenching is accelerated by diffusion and the corresponding asymptotic expression for the ionization rate constant acquires the following general form:

$$k_I(t) = 4\pi R_Q D\left[1 + \sqrt{\frac{R_Q^2}{\pi D t}}\right] \quad \text{at } t \to \infty \qquad (2.5)$$

By substituting expression (2.1) with this $k_I(t)$ into eq 1.5 one reproduces the asymptotic formula (1.4) successfully fitted to the long time kinetics. But at shorter times this asymptote is preceded by the static quenching with the rate constant followed from eqs 2.2 and 2.3 at $\hat{L} = D = 0$:

$$k_I(t) = \int W_I(r)\, e^{-W_I(r)t}\, d^3r = k_0 - \langle W_I^2 \rangle\, t + \cdots \qquad (2.6)$$

The quenching always starts with the maximal (kinetic) rate constant

$$k_0 = k_I(0) = \int W_I(r)\, d^3r = \langle W_I \rangle \qquad (2.7)$$

but then develops with retardation, which is the sharper, the higher is the mean square value

$$\langle W_I^2 \rangle = \int W_I^2(r)\, d^3r \qquad (2.8)$$

The asymptotic analysis based on eq 2.5 or (1.4) is determined by the universal parameter R_Q defined by the far periphery of $W_I(r)$ exponentially decreasing with distance. It can be approximately found from the equation:[40]

$$W_I(R_Q)l^2/D = 1$$

which is not sensitive to that part of $W_I(r)$ which is deeply inside the quenching sphere of radius R_Q. On the contrary, the static quenching starts from the maximal values of $W_I(r)$ and lasts until all the interior of the quenching sphere is burned. To discriminate between the different models of $W_I(r)$ the strategy of fitting employed in refs 8 and 29 should be changed. Here we will start by analyzing the static quenching and only after that the late diffusional quenching, as well as the total effect represented by the fluorescence and products quantum yields.

III. Experimental

The excited-state dynamics of perylene (Pe) has been measured by fluorescence upconversion (FU), using a setup already described in ref 41. Excitation was performed at 400 nm using the frequency-doubled output of a Kerr lens mode-locked Ti:sapphire laser (Tsunami, Spectra-Physics). The full width at half-maximum of the instrument response function was 210 fs.

Pe was recrystallized from benzene before use. TCNE was recrystallized from chlorobenzene and sublimed twice. Acetonitrile (acetonitrile, UV grade) was used as received. All the chemicals were from Fluka. The sample solutions were placed in a spinning cell with an optical path length of 0.4 mm. The absorbance of the sample at 400 nm was around 0.1, corresponding to a Pe concentration of the order of 10^{-4} M. All sample solutions were bubbled with Ar for 15−20 min before use. After the measurements, no significant sample degradation was observed.

The fluorescence dynamics of Pe in acetonitrile was measured with various TCNE concentrations: 0, 0.01, 0.08, 0.16, 0.32, and 0.64 M. The fluorescence dynamics of each solution was measured of five different time windows: 6, 35, 120, 300, and 1200 ps. To correct for any misalignment of the optical delay line and to have a signal intensity proportional to $P(t)$ from eq 1.5, the fluorescence time profiles at [TCNE] ≠ 0 were divided by the corresponding time profile at [TCNE] = 0. This procedure was performed with the data acquired in all time windows except the shortest one. The fluorescence dynamics

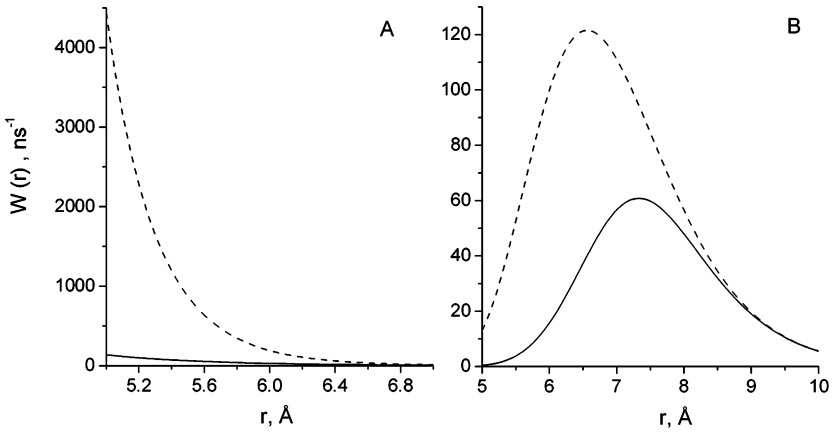

Figure 2. The ionization rates in acetonitrile with and without taking account for the transfer saturation (solid and dashed lines correspondingly). (A) Transfer in the normal Marcus region, $\Delta G_I = -0.6$ eV. (B) Transfer in the inverted Marcus region, $\Delta G_I = -2.14$ eV. The rest of the parameters are the same as in the previous figure.

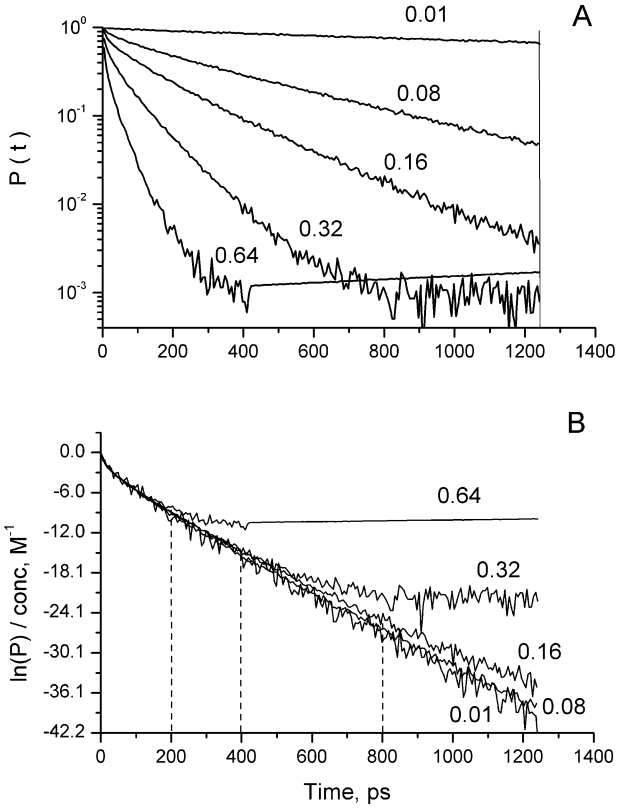

Figure 3. (A) The quenching kinetics at different concentrations of electron acceptors given in molar (numbers above curves). (B) The same but in an anamorphosis, extracting the universal time dependence of $\int_0^t k_I(t')\,dt'$. The vertical dashed lines indicate the upper borders of the credibility intervals for the highest concentrations.

was measured at 495 nm, where the effect of vibrational relaxation is the smallest, as discussed in refs 42 and 43.

IV. Fitting Kinetics of Quenching after Pulse Excitation

From the system response to the short pulse excitation in the presence and absence of quenchers, one can measure the quenching kinetics $P(t)$ given by eq 1.5. It is sharper the higher the quencher concentration used (Figure 3A), but according to the DET eq 2.1 the quantity

$$\frac{\ln P(t)}{c} = -\int_0^t k_I(t')\,dt' \tag{4.1}$$

should be the same for all concentrations. In fact, when these quantities are plotted against time all of them are practically the same for any concentrations, until they decrease (Figure 3B). However, each of them levels off approaching the level of noise. The border time between the descending branch and horizontal tail establishes the upper border of the credibility interval where the data fit the theoretical dependence (4.1). These intervals restricted by the vertical dashed lines are longer the smaller the quencher concentration. At the lowest concentrations such intervals are larger than that available for experimental study, but the depth of the reaction within the latter is small. The most suitable for fitting is the curve for $c = 0.16$ M. It reaches the same reaction depth at higher concentrations, but the integral $\int_0^t k_I(t')\,dt'$ is already as large as it is at lower concentrations. Besides, it has the lowest noise-to-signal ratio.

A. Accumulation and Dissipation of Energy at the Shortest Times. The pulse excitation to some vibrational sublevel of the upper electronic state gives way to the fast vibrational relaxation, simultaneous with the initial electron transfer. The latter proceeds with the highest (kinetic) rate constant (2.7) that allows it to compete with the vibrational relaxation. This competition can be represented by the set of model kinetic equations:

$$\dot{N}_1 = -\frac{1}{\tau_v}N_1 \quad N_1(0) = N_0 \tag{4.2a}$$

$$\dot{N} = \frac{1}{\tau_v}N_1 - ck_0N \quad N(0) = 0 \tag{4.2b}$$

where N_1 and N are the populations of initial and final (fluorescent) vibronic states, and τ_v is the vibrational relaxation time in the sub-picosecond scale. As a result, we have the following single equation for accumulation and dissipation of fluorescent particles:

$$\dot{N} = \frac{N_0}{\tau_v}\,e^{-t/\tau_v} - ck_0N \tag{4.3}$$

The solution to this equation,

$$N = \frac{N_0}{1 - ck_0\tau_v}[e^{-t/\tau_v} - e^{-ck_0t}] \tag{4.4}$$

describes both the ascending and descending branches of the initial kinetics locating the maximum between them.

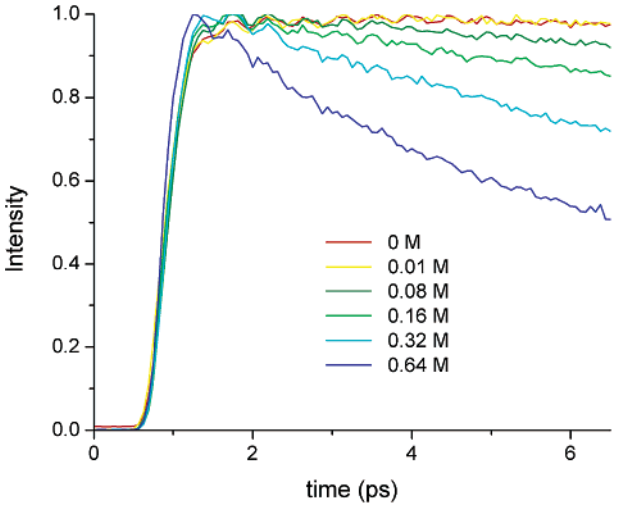

Figure 4. The FU time profiles measured with the time increment 0.062 ps at the same quencher concentrations as in the previous figure.

TABLE 1

	without convolution		with convolution	
c/M	τ_v/ps	k_0/M^{-1} ps^{-1}	τ_v/ps	k_0/M^{-1} ps^{-1}
0.08	0.282	0.20	0.215	0.25
0.16	0.257	0.20	0.200	0.22
0.32	0.255	0.20	0.186	0.23
0.64	0.183	0.20	0.119	0.21

In fact, the vibrational relaxation is not completely damped, as seen from Figure 4 which shows the fluorescence decay measured by the FU. Using the aperiodic model of vibrational relaxation (4.4) for fitting to very short data (up to 6 ps) we are looking mainly for the quenching parameter k_0 and will return back to the coherent vibrations afterward. The fitting was done in two ways: with and without convolution with the instrumental response function (IRF). They both gave similar results as shown in Table 1.

An example of the fit to the highest concentration of quenchers, $c = 0.64$ M, is given in Figure 5. It is better to include IRF in the fitting procedure, but the final values of k_0 are not affected too much. Since the further fitting of the longer time behavior will be done without convolution we set for it

$$k_0 = 0.2\ \mathrm{M}^{-1}\ \mathrm{ps}^{-1} = 322.6\ \text{Å}^3/\mathrm{ps} \qquad (4.5)$$

There is an approximately linear increase in the vibrational relaxation rate $1/\tau_v$ with quencher concentration that could be attributed to the intermolecular contribution to this rate. It can be ascribed to the vibrational energy transfer from Pe to TCNE (see Supporting Information).

B. Fitting the Moderate and Long Times with a Single-Channel Rate. If there is only the single channel of electron transfer (to the ground state of the ion pair), then in highly polar solutions the r-dependence of the ionization free energy is insignificant and according to the energy scheme of Figure 6 we have:

$$\Delta G_\mathrm{I}(r) \approx \Delta G_\mathrm{I}(\sigma) = \Delta G_i = -2.14\ \mathrm{eV}$$

The "outer-sphere" reorganization energy at contact is half at infinite separation:[3]

$$\lambda(r) = \lambda_0(2 - \sigma/r) \qquad (4.6)$$

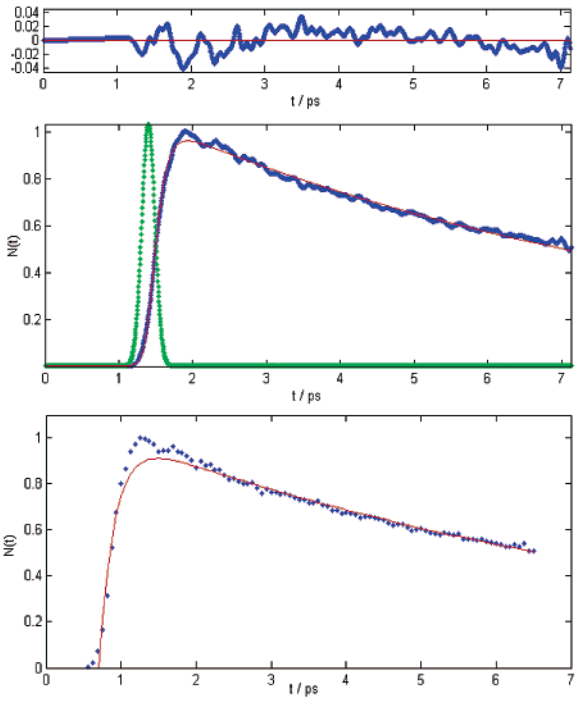

Figure 5. Fitting the very fast kinetics of accumulation and dissipation of the excited electronic state with (middle) and without (bottom) convolution with IRF. The residual of the former is shown at the top.

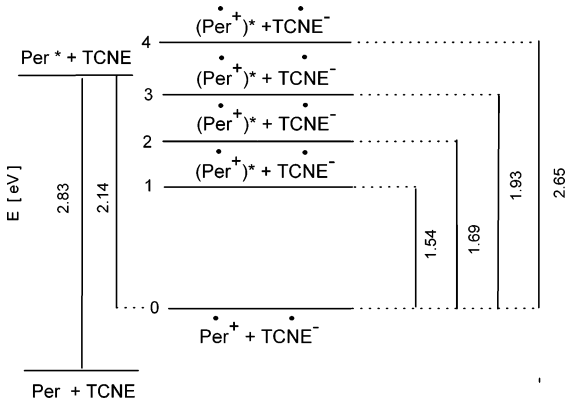

Figure 6. The energy diagram for the pair perylene + TCNE before (left) and after (right) the electron transfer.

It depends on the interparticle distance at contact σ and contact reorganization energy $\lambda_0 = \lambda(\sigma)$. In acetonitrile

$$\lambda_0 = 1.15\ \mathrm{eV}, \text{ and } \sigma = 5\ \text{Å} \qquad (4.7)$$

is an average distance between the contacting Pe and TCNE. In fact, it varies between 3.5 and 6.8 Å, depending on their coordination, but the effects of chemical anisotropy will be ignored here. Assuming a reasonable value for

$$L = 1.24\ \text{Å} \qquad (4.8)$$

we can find the remaining fitting parameter V_0 from the kinetic reaction constant (2.7), whose value is already fixed in eq 4.5. In the case of a single channel and weak transfer proceeding with the rate eq 1.3, V_0^2 is directly proportional to k_0:

$$V_0^2 = \hbar k_0 / \int \exp\left(-\frac{2(r-\sigma)}{L}\right) \frac{\sqrt{\pi}}{\sqrt{\lambda(r)T}} \exp\left(-\frac{[\Delta G_i + \lambda(r)]^2}{4\lambda(r)T}\right) \mathrm{d}^3 r$$

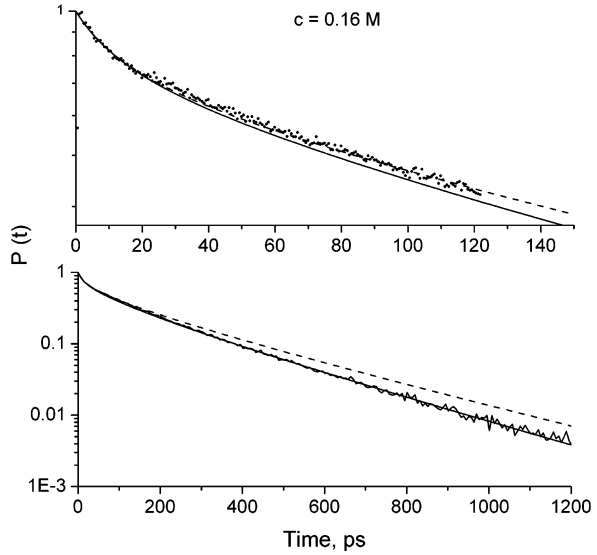

Figure 7. Fitting of single channel model to moderate (top) and long time (bottom) quenching kinetics at $c = 0.16$ M. Dashed lines obtained choosing $D = 2.45 \times 10^{-5}$ cm^2/s; solid lines represent the best fit with $D = 2.95 \times 10^{-5}$ cm^2/s ($\sigma = 5$ Å).

It follows from this relationship that

$$V_0 = 89.8 \text{ meV} \quad \text{and} \quad U_0 = \frac{V_0^2}{\hbar}\frac{\sqrt{\pi}}{\sqrt{\lambda_0 T}} = 127 \text{ ps}^{-1}$$

This value of $U_0 = U(\sigma)$ greatly exceeds the upper limit of the transfer rate established by

$$\frac{1}{\tau(\sigma)} = \frac{1}{4\tau_L}\sqrt{\frac{\lambda_0}{\pi T}} = 1.9 \text{ ps}^{-1} \tag{4.9}$$

where $\tau_L = 500$ fs (for acetonitrile). The inequality, $U\tau|_{r=\sigma} \gg 1$, clearly indicates that the saturation of electron transfer near the contact cannot be ignored.

Using the cropped transfer rate (1.8) instead of (1.3) in eq 2.7 one can find by a few iterations the appropriate V_0^2 and U_0. They appear to be larger than the previous ones to provide the same value of k_0:

$$V_0 = 138 \text{ meV} \quad \text{and} \quad U_0 = 300 \text{ ps}^{-1} \tag{4.10}$$

Using this parametrization, we tried to fit the kinetic data at moderate and long times having for our disposal only one fitting parameter: the diffusional constant D. The best results obtained for the solution with the smallest noise-to-signal ratio are shown in Figure 7. At small D, the quenching at moderate times is fitted well, but at long times is greatly underestimated. At large D, everything is quite the reverse: the quenching at long times is well approximated, but overestimated at moderate times. This is an alternative consistent with the conclusion made by Fleming et al.[18]

However, it follows unambiguously from the comparison of the short and long time results that the initial kinetic rate constant $k_0 = 322.6$ Å^3/ps is significantly larger than the final stationary rate constant

$$k_i = k_I(\infty) = 4\pi R_Q D \tag{4.11}$$

which is approximately 31.4 Å^3/ps. Such a nonstationarity of transfer is the direct indication that the quenching is under diffusion control and $k_i \approx 4\pi\sigma D \ll k_0$. This finding is in conflict with what was found when Tachiya and Murata fitted the free energy Rehm−Weller dependence of the Stern−Volmer constant that they identified with k_i.[44] According to their Figure 2, the transfer in the most exergonic systems is kinetic, that is $k_i \approx k_0$ at any time. Since our system is one of those it should be expected that $k_0 \ll k_D$ which is not the case. Being free in choosing the fitting parameters the authors made their conclusion assuming that

$$V_0 = 12.4 \text{ meV}$$

Making this choice they greatly underestimate the kinetic rate constant k_0 which is in their work 42 Å^3/ps, that is almost an order of magnitude smaller than that in eq 4.5 obtained experimentally.

Another possible cause of the discrepancy is the "closure approximation" used in this work. It is not much better than the primitive contact approximation and is especially bad in the inverted region where the transfer is essentially remote. Fortunately, this approximation is not obligatory and had been ignored in the preceding work of Marcus and Siders,[45] who applied to the similar data analysis the regular encounter theory.[15−17] They also demonstrated in their Figure 1 that at $V_0 = 4.5$ meV and $\lambda_0 = 0.56$ eV the reaction falls under kinetic control when the exergonicity of the transfer exceeds 1.5 eV. However, according to their Figure 2 the reaction remains diffusional up to $\Delta G_i = -2.2$ eV if

$$V_0 = 23 \text{ meV} \quad \text{and} \quad \lambda_0 = 0.86 \text{ eV}$$

This choice is much closer to our own although it is made for another system studied in refs 46 and 47. Marcus and Siders proposed also another way to make highly exergonic reactions diffusional, by taking into consideration the parallel transfer to the excited electronic state of the product. Until now this was a dominant idea for how to explain the too wide diffusional plateau obtained by Rehm and Weller.[3] However, it will be shown in the next subsection that the electronic excitation which occurs near the contact is much less helpful if one accounts for electron-transfer saturation which was ignored by Marcus and Siders[45] as well as by Tachiya and Murata.[44]

C. Fitting the Double-Channel Model. Looking for all possible interpretations of our data, we should take into account that the perylene cation has a number of low lying excited electronic states and at least three of them are energetically accessible from the excited reactant (Figure 6). Therefore, the formation of the cation in one of these states can compete with creation of the ground-state cation.[48−50] There are also some indications of excited ion generation in the course of highly exergonic fluorescence quenching studied in other systems: cyanoanthracene (A) and aromatic amines or aminobenzenes (D).[51,52] In all such cases there are parallel channels of ionization, to the ground state ($i = 0$) and to the excited charged products ($i = 1, 2, ...$). In our system, the transfer is exergonic to only three states. Taking them into account, one should represent the total transfer rate as a sum over parallel channels:

$$W_I(r) = \sum_{i=0}^{3} W_i(r) \tag{4.12}$$

All partial rates have the same form (1.3), but different $\Delta G_I \equiv \Delta G_i$ and tunneling matrix elements V_i. All of them contribute to the kinetic rate constant

$$k_0 = \sum_{i=0}^{3} \int W_i(r)\, \mathrm{d}^3 r = \sum_{i=0}^{3} K_i(\Delta G_i) \qquad (4.13)$$

Borrowing ΔG_i from the energetic scheme of Figure 6 we reproduced the k_0 value (4.5) with

$$V_0 = 123 \text{ meV} \quad \text{and} \quad V_i = 138 \text{ meV} \quad i = 1, 2, 3 \qquad (4.14)$$

Although tunneling to all the excited states was assumed to be equally strong their contributions to k_0 are different because of the different exergonicity of transfer.

As seen from Table 2 even at relatively high V_i the contributions from the two upper states does not exceed 3%. Therefore, they can be ignored in further investigation. Leaving only the lowest excited-state, we arrive at the double-channel model with the total rate

$$W_\mathrm{I}(r) = W_0(r) + W_1(r) \qquad (4.15)$$

where

$$W_0 = W(\Delta G_0, V_0, L) \quad \text{and} \quad W_1 = W(\Delta G_1, V_1, L)$$

are given by the general Marcus formula (1.3) but with partial arguments:

$$\Delta G_0 = -2.14 \text{ eV} \quad \text{and} \quad \Delta G_1 = -0.60 \text{ eV}$$

ΔG_1 is the free energy of transfer to the lowest excited level of perylene cation (Figure 6).[53]

In the double-channel model only V_0 and V_1 should be considered as fitting parameters. In fact, we have only a single new parameter, V_1/V_0, provided

$$k_0 = \int [W_0(r) + W_1(r)]\, \mathrm{d}^3 r \qquad (4.16)$$

is kept equal to that in eq 4.5. After finding this ratio from the best fit to the intermediate times, we adjusted also D to get the right slope of the longest quenching. The last procedure does not affect too much either the short or intermediate time behaviors which are kinetic and quasistatic in nature, that is, weakly sensitive to particle motion. At the same time, an inclusion of the excited-state production facilitates the near contact quenching, making the fitting much better, provided

$$V_0 = 123 \text{ meV} \quad V_1/V_0 = 1.12 \quad D = 3.05 \times 10^5 \text{ cm}^2/\text{s} \qquad (4.17)$$

The results shown in Figure 8 are actually much better than those achieved in Figure 7 with a single channel model.

The results of such a successful fitting allow specifying the time development of $k_\mathrm{I}(t)$ at all times, from its kinetic value, k_0, up to the stationary one, k_i (Figure 9). The slope of the $k_\mathrm{I}(t)$ dependence at $t = 0$ is the quantitative characteristic of the ln $P(t)$ curvature. It is given by the mean square rate (2.8), which is very sensitive to the shape of the particular $W_\mathrm{I}(r)$ dependence. For any remote transfer, it is finite but turns to ∞ for the contact $k_\mathrm{I}(t)$ of Collins and Kimball:

$$k_\mathrm{I}(t) = k_i^{\mathrm{con}} \left[1 + \frac{k_0}{k_\mathrm{D}} \mathrm{e}^{\alpha^2 t} \mathrm{erfc}(\alpha\sqrt{t}) \right] \qquad (4.18)$$

where $k_\mathrm{D} = 4\pi\sigma D$ is the diffusional rate constant, $\alpha = \sqrt{(D/\sigma^2)(1 + (k_0/k_\mathrm{D}))}$ and

TABLE 2

channels	0	1	2	3
K_i [Å^3/ps]	273	42.3	7.21	0.211
K_i/k_0 [%]	84.6	13.1	2.23	0.07

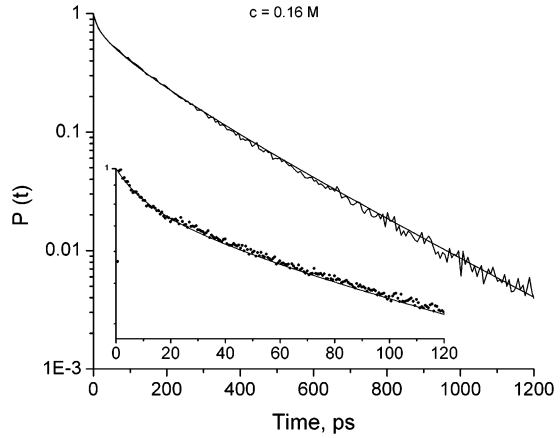

Figure 8. The fitting of the double-channel model to the quenching kinetics at $c = 0.16$ with the parameters given in eq 4.17.

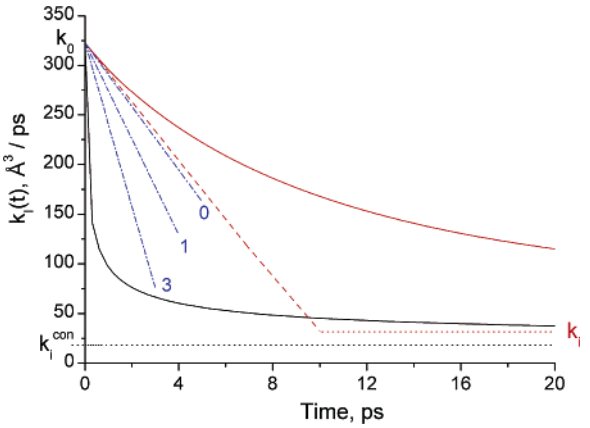

Figure 9. The double-channel "rate constant" $k_\mathrm{I}(t)$ (red line) approaching its stationary value, k_i, shown by the dotted red line. The red dashed line indicates the tangent to this curve at $t = 0$ whose absolute value is $-\dot{k}_\mathrm{I}(0) = \langle W_\mathrm{I}^2(r) \rangle$. This value for the multiphonon transfer (dashed−dotted blue lines) increases with $S = 0$, 1, 3, and turns to ∞ in the contact approximation. The latter is shown by the black line approaching its stationary value, k_i^{con} (dotted line).

$$k_i^{\mathrm{con}} = \frac{k_0 k_\mathrm{D}}{k_0 + k_\mathrm{D}} \qquad (4.19)$$

As seen from Table 3 for the double-channel model the value $|\dot{k}_\mathrm{I}(0)| = \langle W_\mathrm{I}^2 \rangle$ is a bit smaller than for the single-channel model that we failed to fit well. The latter can be considered as the "zero-phonon" model ($S = 0$). In the next subsection, we will demonstrate that for the multiphonon rates ($S = 1, 2, 3, \ldots$) this quantity even increases with S, to say nothing about the contact model ($\langle W_\mathrm{I}^2 \rangle = \infty$). This hierarchy is marked in Figure 9.

The double-channel rate (4.15) is composed from two components (Figure 10). The transfer saturation by the dynamic solvent effect reduces mainly the near contact one, which is responsible for the transfer to the excited state. The relative contribution of this component into $\langle W_\mathrm{I}^2 \rangle$ is even smaller due to the statistical weight $4\pi r^2$. Conversely, the role of another component responsible for the transfer to the ground state is dominant and more the further it is from the contact. At relatively slow diffusion, the outer branch of this component

TABLE 3

$c = 0.16$ M	double-channel	single-channel
V_0 (meV)	123	138
V_1/V_0	1.12	0
$\langle W_I^2 \rangle$ (Å^3/ps^2)	29.6	32
$D \times 10^5$ (cm^2/s)	3.05	2.45 ÷ 2.95
R_Q (Å)	8.25	
$k_i = 4\pi R_Q D$ (Å^3/ps)	31.6	
$k_D = 4\pi\sigma D$ (Å^3/ps)	19.2	

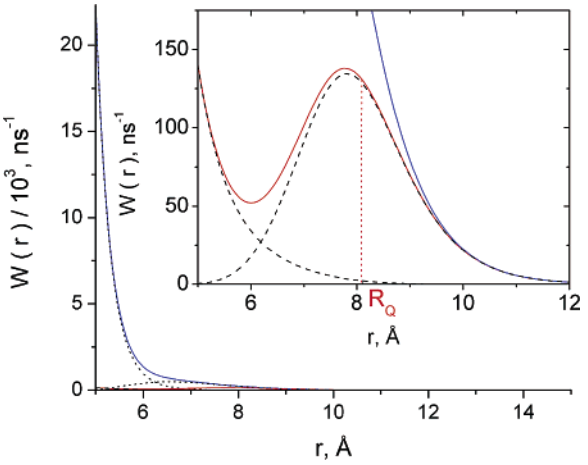

Figure 10. The rates of double-channel electron transfer with (red) and without (blue) tunneling saturation ("dynamic solvent effect"). Their components (the rates of tunneling to the ground and excited ion states) are shown by the dashed lines. The vertical dotted line indicates the quenching radii, R_Q.

determines the quenching radius R_Q, as well as the long-time asymptote of the rate constant (2.5) expressed through it.

It is of interest to compare the true value of $k_i = k_I(\infty)$ with its contact estimate (4.19). Using k_D from Table 3 we have

$$k_i^{con} = 18.1 \text{ Å}^3/\text{ps} = 0.94\, k_D = 0.056\, k_0 \qquad (4.20)$$

These results clearly indicate that the ionization is very close to the diffusional limit and rather far from the kinetic limit. In the latter case, $k(t) \equiv k_0$ should be the horizontal line shown in the same plot. The deep reduction of the rate constant with time is the clear manifestation of diffusional control over ionization. On the other hand, under diffusional control one always has $R_Q > \sigma$ and $k_i > k_i^{con}$. According to Table 3, R_Q and k_i are almost twice as much as σ and k_i^{con}.

D. Fitting the Multiphonon Model. There are at least four candidates for assistance of the electron transfer: two modes of Pe: 800 and 3100 cm^{-1}, and two of TCNE: 1100 and 2200 cm^{-1} (see Figure 2S, Supporting Information). Choosing the low-frequency ones, we compared in Figure 11 their shapes at different electron−phonon interaction measured by parameter S of the multiphonon rate (1.10). All of them are normalized to $k_0 = \int W_I(r)\, d^3r$. This value is fixed by eq. 4.5 while the rest of characteristics change with S. The general conclusion is that with growing S the rate maximum increases and shifts toward the contact. Approaching the contact is faster at a larger frequency of the assisting mode. At $\omega = 1100$ cm^{-1} the rate maximum disappears at $S = 3$ and the quenching, proceeding with quasiexponential $W_I(r)$, is maximal at the contact. Figure 12 demonstrates that $\langle W_I^2 \rangle$ monotonically increases with S and the sharper, the higher the frequency of the assisting mode. For the lowest two modes $\langle W_I^2 \rangle$ grows almost linearly with S.

At $S = 0$ any multiphonon rate reduces to a single-channel one which has the minimal $\langle W_I^2 \rangle = 32$ Å^3/ps^2. At larger S the multiphonon rates are placed between the latter and the contact one which has $\langle W_I^2 \rangle = \infty$ (see Figure 9). Therefore, in fitting our data all multiphonon models are worse than the single-channel one, let alone the double-channel model whose $\langle W_I^2 \rangle = 29.6$ Å^3/ps^2 due to the most uniform rate distribution between σ and R_Q. Judging from this criterion, we conclude that the double-channel model provides the ultimate explanation of the transient kinetics obtained in our system.

Nonetheless, it is worthy of notice that the first experimental evidence of the diffusional transfer at high exergonicity was obtained by direct study of transient effects[54] fitted with the multiphonon model. The obtained kinetic rate constants $k_0 \approx 10^{11}-10^{12}$ M^{-1}s^{-1} were shown to be much larger than diffusional ones (2×10^{10} M^{-1} s^{-1}) all over the Rehm−Weller plateau, up to $\Delta G_i = -2.2$ eV. The attempts to explain this fact theoretically were undertaken using the Collins and Kimball contact approximation.[54,55] Since $\langle W_I^2 \rangle = \infty$ in this approximation, the transient kinetics could not be well reproduced. This was not recognized as a significant drawback because the measurements on the nanosecond time scale did not allow one to study the kinetics in all the details, as we did. The disadvantage of the contact approximation manifested itself only in the diffusion control limit. There the stationary rate constants calculated with eq 4.19 were systematically smaller than the real ones: $k_D = 4\pi\sigma D < 4\pi R_Q D$.

Although both the transfer kinetics and the stationary rate constant k_i were fitted in refs 54 and 55 with the classical contact model, the single parameter of this model, k_0, was calculated using in eq 2.7 an essentially noncontact $W_I(r)$.[55] In this way, the authors carefully accounted for not only multiphonon transfer, but also for the dynamic solvent effect taking

$$\frac{1}{\tau} = 5 \text{ ps}^{-1} \quad \omega = 800 \text{ cm}^{-1} \quad S = 3$$

The upper limit for the rate ($1/\tau$) as well as ω are almost the same as ours while S is surprisingly large. Since the authors did not care about the $\langle W_I^2 \rangle$ values they admitted this choice.

But the most important difference results from the intention to stretch the region where k_0 is larger than k_D, up to the highest exergonicity of transfer. To do this Kakitani et al. revised the common definition of the reorganization energy space dependence, presenting it in the following form:

$$\lambda(r) = \Lambda(2 - \Sigma/r) \quad \text{at } r > \sigma = 4.4 \text{ Å} \qquad (4.21)$$

Considering Λ and Σ as fitting parameters they found for them the following values:

$$\Lambda = 1.35 \text{ eV} \quad \text{and} \quad \Sigma = 7.2 \text{ Å} \qquad (4.22)$$

Both of them are noticeably larger than their analogues (4.7) obtained from the available experimental data. Especially surprising is that $\Sigma > \sigma$. This relationship allows $\lambda(r)$ to vary from 0.49 eV at contact, to 2.7 eV at infinite separation, while the conventional formula (4.6) allows one only to double the minimal value.

Such an unphysical stretching of $\lambda(r)$ was taken but not for the best fit of the high exergonicity transfer. As we ensured, it can be done without any variation of the conventional space dependence of λ, eq 4.6. The stretching was necessary to fit with the same theory, the ascending branch of the Rehm−Weller free energy dependence, where the transfer is endergonic ($\Delta G_i > 0$). In fact, the same objective was also pursued by other authors cited above.[44,45] Unfortunately, it is unattainable. DET used by all of them does not hold at $\Delta G_i \gtrsim 0$. DET is good for

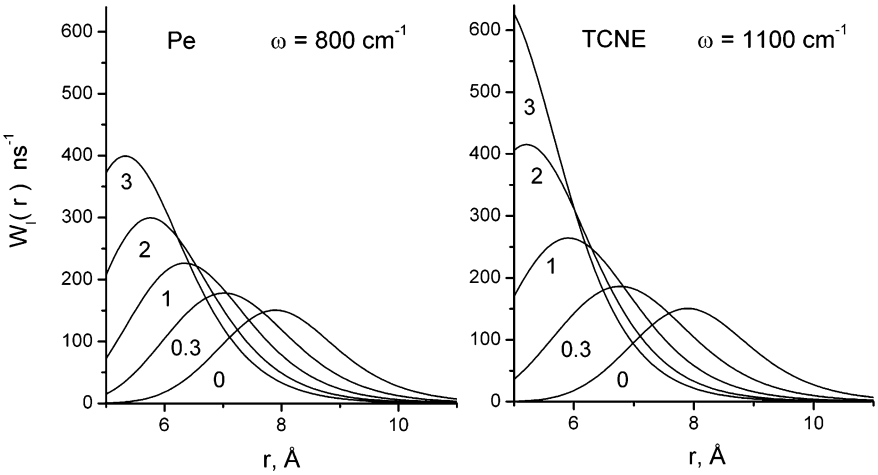

Figure 11. The rates of transfer accompanied by the vibrational excitation of Pe (left) or TCNE (right) at different $S = 0$, 0.3, 1, 2, 3 in comparison with single channel rate ($S = 0$).

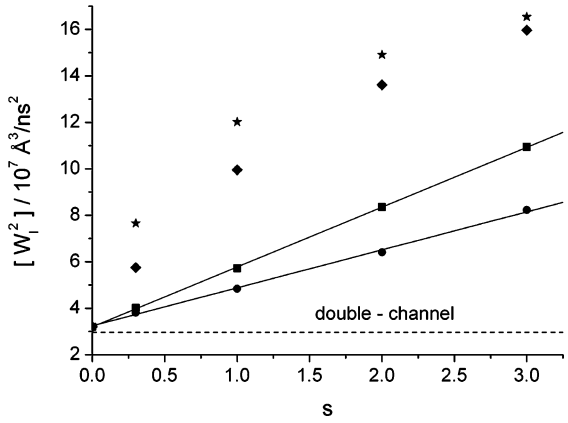

Figure 12. The S-dependence of $\langle W_l^2 \rangle$ for the quantum modes of Pe (●, 800 cm^{-1} and ★, 3100 cm^{-1}), and TCNE, (■, 1100 cm^{-1} and ◆, 2200 cm^{-1}).

high exergonicity ($-\Delta G_i \gg T$) when the backward transfer from ion pair to initial excited state is negligible, but DET is incapable of accounting for the reversible electron transfer between the excited reactants.[56] Accounting for the backward transfer requires a fundamentally different technique known as integral encounter theory (IET). It was employed for the ascending (endergonic) branch of Rehm−Weller dependence in a few recent works.[57,58] As was shown, not only the shape but the very position of the ascending branch depends on the relative strength of the radical ion pair recombination (after spin conversion in the cage or in the bulk) to either the starting excitation or excited triplet product. The rate of the latter determines the position of the ascending branch which is different for different families of the reactants. This was called the "multiple Rehm−Weller plot" in ref 59 where it was observed experimentally. At least "two different plots were clearly observed corresponding to the aromatic and olefinic compounds". This proves that fitting the data for particular systems, endergonic or exergonic, is preferable to trying to find a unique explanation for all of them together.

V. Concentration Dependence of the Stern−Volmer Constant. The relative quantum yield of the fluorescence is generally defined through the system response to instantaneous excitation (1.5) and presented in the form of the Stern−Volmer law:[3]

$$\eta = \frac{\int_0^\infty N(t, c)\,\mathrm{d}t}{\int_0^\infty N(t, 0)\,\mathrm{d}t} = \frac{1}{\tau_D}\int_0^\infty P(t)\,\mathrm{e}^{-t/\tau_D}\,\mathrm{d}t = \frac{\tilde{R}(0)}{\tau_D} = \frac{1}{1 + c\kappa\tau_D} \tag{5.1}$$

Its "constant" is in fact the concentration-dependent function $\kappa(c)$, but in the limit of small concentration it follows from the concentration expansion of eq 5.1 with $R(t)$ from eq 2.1 that

$$\eta \approx 1 - c\kappa_0\tau_D$$

where

$$\kappa_0 = \frac{1}{\tau_D}\int_0^\infty \mathrm{e}^{-t/\tau_D}\,k(t)\,\mathrm{d}t \tag{5.2}$$

is an "ideal" Stern−Volmer constant. As long as $\kappa = \kappa_0 = \text{const}$ the original Stern−Volmer law

$$1/\eta = 1 + c\kappa\tau_D \tag{5.3}$$

is linear in concentration of quenchers.

However, the factual nonlinearity of eq 5.3 resulting from the $\kappa(c)$ dependence was many times demonstrated experimentally.[60−64] We also illustrate it by Figure 13. To get η one can either use the Laplace transformation of the experimental quenching kinetics $R(t)$ in eq 5.1, or employ the conventional stationary methods for the straightforward measuring of this quantity. Using both these ways, we obtained the results which are in conformity with each other and with those resulting from the best theoretical $P(t)$ obtained with the double-channel model and integrated in eq 5.1.

Unfortunately, such a conformity is just an illusion: the presentation of data in these coordinates masks the problem. It is visualized if κ is extracted from η and plotted as a function of c. As seen from Figure 14 there is a pronounced difference between the data obtained from the time-resolved (●) and the stationary (★) experiments, not to mention the accuracy of the latter which leaves much to be desired at small c. The coincidence is satisfactory only at the highest concentration where the quenching is accomplished within the credibility time interval and conversely it is the worst at the lowest concentration when the long tail remains out of the interval available experimentally (see Figure 3A). The integration within such a limited time interval is equivalent to the sudden quenching of all donors survived to the end of it. Therefore, the quenching

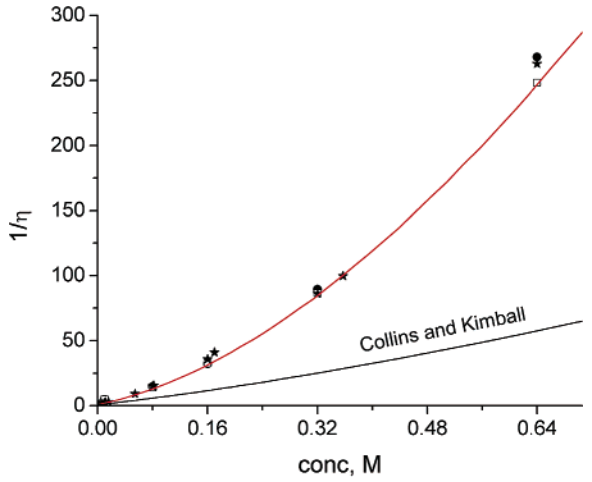

Figure 13. The nonlinear Stern−Volmer law for the quantum yield obtained by integration of the experimental quenching kinetics within the credibility intervals (●) and from the stationary measurements of the quantum yield (★). The theoretical approximation of this law with the double-channel (red line) and contact (black line) models.

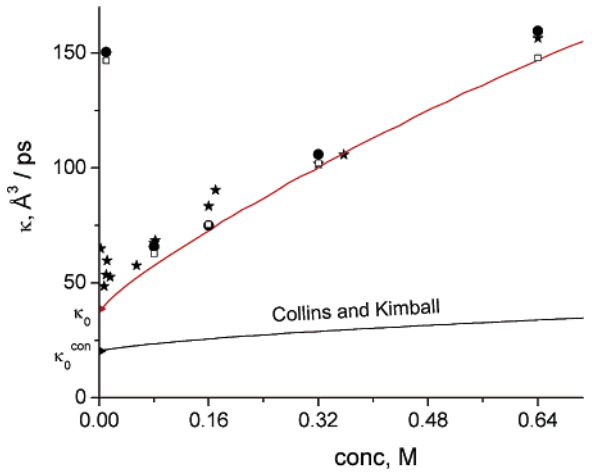

Figure 14. The Stern−Volmer constants obtained from the stationary (★) and time-resolved data (●) in comparison with the theoretical predictions, following from the double-channel quenching kinetics integrated over the credibility intervals (□) and up to infinite time (red line). Black line: the similar result but for the contact kinetics integrated over all times. Triangles (red and black): the ideal Stern−Volmer constants for the double-channel and contact models.

constant at low concentrations is greatly overestimated if $P(t)$ measured in an experimentally restricted time interval is integrated in eq 5.1.

The same is true for the theoretical κ if the integration of the model $P(t)$ in eq 5.1 is performed within the credibility time intervals (□). The coincidence of theoretical and experimental results is good for low concentration and a bit worse for the higher ones where the data are more noisy. However, it is in the range of the low concentration that the overestimation of κ takes place due to incomplete quenching within limited time interval. Fortunately, the integration of the theoretical $P(t)$ in eq 5.1 can be extended to infinity and this provides the most reliable estimate of the quantity under study (red line in Figure 14). We see that this estimate made with the double-channel model is in rather good agreement with the experimental results, unlike the contact estimate of κ (black line) obtained in the same way with the Collins-Kimball $k_I(t)$ from eq 4.18. As has been already demonstrated with Stevens data (see Figure 4 in ref 65), the contact approximation greatly underestimates the Stern−Volmer constant, and this effect increases with growing concentration. In fact, the popular contact approximation is inapplicable to electron-transfer reactions especially in the inverted region.

The main tendency established in ref 65 and seen in Figure 14 is an increase of $\kappa(c)$ from its "ideal" value $\kappa_0 = \kappa(0)$ to the maximal one: $\kappa(\infty) = k_0$. This conclusion is sustained by a number of different theoretical methods compared in ref 65. All of them except DET deal with the contact approximation ($L \rightarrow 0$). In this approximation, the ideal Stern−Volmer constant was shown to be given by the following analytic expression:[66,68]

$$\kappa_0^{con} = \frac{k_0 k_D}{k_D + k_0/(1 + \sqrt{\sigma^2/D\tau_D})} \tag{5.4}$$

Substituting into this relationship the corresponding k_0 and D values we obtain:

$$\kappa_0^{con} = 20.4\ \text{Å}^3/\text{ps} = 0.527\ \kappa_0 \tag{5.5}$$

where

$$\kappa_0 = 38.8\ \text{Å}^3/\text{ps}$$

was found from Figure 14 by extrapolation of the theoretical curve to $c = 0$. It was known for very long that in some systems even the ideal Stern−Volmer constant measured experimentally can be twice as large as its contact estimate.[67] Admitting the quenching radius R to be twice σ, the discrepancy could be understood in the framework of the extended contact theory.[67] The latter differs from the original Collins−Kimball model only by substitution of $R = \sigma/\mu$ for σ, where the numerical parameter μ can be rigorously defined through $W_I(r)$, but only near the kinetic limit ($1 - \mu \ll \mu$).[8] However, such a phenomenological extension of the contact model completely ignores the static quenching and is not applicable to true diffusional quenching ($R - \sigma \gtrsim \sigma$), especially at high concentrations.

On the contrary, the present theory accounts for remote transfer as it is. Some uncertainty is left only for the value of the tunneling length L. It may be a bit larger or smaller than $L = 1.24$ Å yet employed. The best way to eliminate such an uncertainty is to repeat the investigation in a number of solvents of different viscosities as has been done already a few times.[8,29] Varying the encounter diffusion coefficient D one can specify the $R_Q(D)$ dependence which is sensitive to the model of the transfer rate and especially to the L value.

As follows from comparison of eqs 5.4 and 4.19 $\kappa_0^{con} > k_i^{con}$ in the diffusional limit, because the Stern−Volmer constant accounts for nonstationary quenching while k_i does not. The same is true for the noncontact values of the same constants: $\kappa_0 > k_i$ (compare eqs 5.2 and 4.11). Since $\kappa(c) > \kappa_0 > k_i > k_i^{con}$ the fitting of the Rehm−Weller $\kappa(\Delta G_i)$, with the theoretically calculated $k_i(\Delta G_i)$ and especially with $k_i^{con}(\Delta G_i)$ dependence is inconsistent. Although performed in almost all published works it is incorrect in principle, but especially bad in the region of the diffusional plateau. On the other hand, the values of $\kappa(\Delta G_i)$ obtained and plotted without experimental control on quencher concentrations can differ noticeably from what they are expected to be, that is, from the ideal $\kappa_0(\Delta G_i)$ dependence.

VI. Conclusions

We present the first successful fitting of the entire kinetics of fluorescence quenching carried out by remote electron transfer

in the inverted region. Our study covers three different time scales studied with the appropriate techniques. It starts from the initial accumulation of excitations during the action of the light pulse, extends to a quasistatic electron transfer, and ends by the final quasistationary quenching.

We proved that the simplest single-channel Marcus rate, as well as its multiphonon analogues, do not allow fitting satisfactorily both the initial and the final stages of quenching. This can be done only with the double-channel model of transfer (to the ground and excited electronic state of charged products). Taking into account the saturation of the tunneling due to the dynamical solvent effect and having in hand an additional fitting parameter (the relative strength of the two channels), we fitted satisfactorily the whole kinetics of quenching. Besides, the experimentally found concentration dependence of the Stern−Volmer constant was well fitted with the same double-channel model and the same fitting parameters. Using this model, the quantum yields of the ground and excited-state products of transfer were also specified.

Two important conclusions follow from this investigation:

(i) The energy quenching by TCNE in liquid solutions is controlled by diffusion.

(ii) This is essentially distant, noncontact quenching.

These conclusions provide the unambiguous answer to the long standing question: Why is the TCNE Stern−Volmer constant placed on the diffusional plateau of the famous free energy gap law of Rehm and Weller,[30] instead of being far below it as was expected? In addition, the true value of the TCNE Stern−Volmer constant is at least twice as large as obtained in the contact approximation and this difference increases with concentration. These facts show that the contact approximation is just a convenient method of analytic calculations, but not a proper tool for fitting to the real experimental data on transfer kinetics, especially under diffusion control and at high concentrations of quenchers.

Acknowledgment. The authors are very grateful to Dr. Krissinel for the necessary perfection of the SSDP2 software package[70] and kind assistance in usage of this efficient program in our calculations. We are also grateful to Drs. D. Kattnig and A. Rosspeintner from the TU Graz for the usage of their software.

Supporting Information Available: Details of vibrational spectra and relaxation accompanied the electron transfer are presented. This material is available free of charge via the Internet at http://pubs.acs.org.

References and Notes

(1) Smoluchowski, M. V. *Z. Phys. Chem.* **1918**, *92*, 129.
(2) Collins, F. C.; Kimball, G. E. *J. Colloid Sci.* **1949**, *4*, 425.
(3) Burshtein, A. I. *Adv. Chem. Phys.* **2000**, *114*, 419.
(4) Cohen, B.; Huppert, D.; Agmon, N. *J. Phys. Chem.* **2001**, *A105*, 7165.
(5) Sveshnikov, B. Ya.; Shirokov, V. I. *Opt. Spectrosc. (USSR)* **1962**, *12*, 320.
(6) Tunitskii, N. N.; Bagdasar'yan, Kh. S. *Opt. Spectrosc. (USSR)* **1963**, *15*, 303.
(7) Yokoto, M.; Tonimoto, O. *J. Phys. Soc. Jpn.* **1967**, *22*, 779.
(8) Gladkikh, V. S.; Burshtein, A. I.; Tavernier, H. L.; Fayer, M. D. *J. Phys. Chem. A* **2002**, *106*, 6982.
(9) Neufeld, A. A.; Burshtein, A. I.; Angulo, G.; Grampp, G. *J. Chem. Phys.* **2002**, *116*, 2472.
(10) Brunchwig, B. S.; Ehrenson, S.; Sutin, N. *J. Am. Chem. Soc.* **1984**, *106*, 6859.
(11) Burshtein, A. I.; Frantsuzov, P. A.; Zharikov, A. A. *Chem. Phys.* **1991**, *155*, 91.
(12) Tunitskii, N. N.; Bagdasar'yan, Kh. S. *Opt. Spectrosc.* **1963**, *15*, 303.
(13) Kilin, S. F.; Mikhelashvili, M. S.; Rozman, I. M. *Opt. Spectrosc.* **1964**, *16*, 576.
(14) Vasil'ev, I. I.; Kirsanov, B. P.; Krongaus, V. A. *Kinet. Katal.* **1964**, *5*, 792.
(15) Steinberg I. Z.; Katchalsky, E. *J. Chem. Phys.* **1968**, *48*, 2404.
(16) Doktorov, A. B.; Burshtein, A. I. *Sov. Phys. JETP* **1975**, *41*, 671.
(17) Wilemski, G.; Fixman, M. *J. Chem. Phys.* **1973**, *58*, 4009.
(18) Eads, D. E.; Dismer, B. G.; Fleming, G. R. *J. Chem. Phys.* **1990**, *93*, 1136.
(19) Murata, S.; Matsuzaki, S. Y.; Tachiya, M. *J. Phys. Chem.* **1995**, *95*, 5354.
(20) Szabo, A. *J. Phys. Chem.* **1989**, *93*, 6929.
(21) Dorfman, R. C.; Lin, Y.; Fayer, M. D. *J. Phys. Chem.* **1990**, *94*, 8007.
(22) Song, L.; Dorfman, R. C.; Swallen, S. F.; Fayer, M. D. *J. Phys. Chem.* **1991**, *95*, 3454.
(23) Song, L.; Swallen, S. F.; Dorfman, R. C.; Weidemaier K.; Fayer M. D. *J. Phys. Chem.* **1992**, *97*, 1374.
(24) Kakitani, K.; Matsuda, N.; Denda, T.; Mataga, N.; Enomoto, Y. *Ultrafast Reaction Dynamics and Solvent Effects*; AIP Conference Proceedings 298; Gauduel, Y., Rossky, P. J, Eds., New York, 1993.
(25) Burshtein, A. I.; Kapinus, E. I.;. Kucherova, I. Yu; Morozov, V. A. *J. Luminesc.* **1989**, *43*, 291.
(26) Tavernier, H. L.; Fayer, M. D. *J. Chem. Phys.* **2001**, *114*, 4552.
(27) Allonas, X.; Jacques, P.; Accary, A.; Kessler, M.; Heisel, F. *J. Fluoresc.* **2000**, *10*, 237.
(28) Tavernier, H. L.; Kalashnikov, M. M.; Fayer, M. D. *J. Chem. Phys.* **2000**, *113*, 10191.
(29) Angulo, G.; Grampp, G.; Neufeld, A. A.; Burshtein, A. I. *J. Phys. Chem. A* **2003**, *107*, 6913.
(30) Rehm, D.; Weller, A. *Isr. J. Chem.* **1970**, *8*, 259.
(31) Efrima, S.; Bixon, M. *Chem. Phys. Lett.* **1974**, *25*, 34.
(32) Jortner, J.; Bixon, M. *J. Chem. Phys.* **1988**, *88*, 167.
(33) Burshtein, A. I.; Kofman, A. G. *Chem. Phys.* **1979**, *40*, 289.
(34) Yakobson, B. I.; Burshtein, A. I. *Chem. Phys.* **1980**, *49*, 385.
(35) Zusman, L. D. *Chem. Phys.* **1980**, *49*, 295.
(36) Burshtein, A. I.; Morozov V. A. *Chem. Phys. Lett.* **1990**, *165*, 432.
(37) Zharikov, A. A.; Burshtein, A. I. *J. Chem. Phys.* **1990**, *93*, 5573.
(38) Rips, I.; Jortner, J. *J. Chem. Phys.* **1987**, *87*, 6513.
(39) Walker, G. C.; Akesson, E.; Johnson, A. E.; Levinger, N. E.; Barbara, P. F. *J. Phys. Chem.* **1992**, *96*, 3728.
(40) Burshtein, A. I.; Doktorov, A. B.; Kipriyanov, A. A.; Morozov, V. A.; Fedorenko, S. G. *Sov. Phys. JETP* **1985**, *61*, 516.
(41) Morandeira, A.; Engeli, L.; Vauthey, E. *J. Phys. Chem. A* **2002**, *106*, 4833.
(42) Morandeira, A.; Furstenberg, A.; Gumy, J. C.; Vauthey, E. *J. Phys. Chem. A* **2003**, *107*, 5375.
(43) Pigliucci, A.; Vauthey, E. *Chimia* **2003**, *57*, 200.
(44) Tachiya, M.; Murata, S. *J. Phys. Chem.* **1992**, *96*, 8441.
(45) Marcus, R. A.; Siders, P. *J. Phys. Chem.* **1982**, *86*, 622.
(46) Creutz, C.; Sutin, N. *J. Am. Chem. Soc.* **1977**, *99*, 241.
(47) Brunschwig, B.; Sutin, N. *J. Am. Chem. Soc.* **1978**, *100*, 7568.
(48) Marcus, R. A. *J. Chem. Phys.* **1956**, *24*, 966; idem., **1965**, *43*, 679.
(49) Mataga, N.; Kanda, J.; Okada, T. *J. Phys. Chem.* **1986**, *90*, 3880.
(50) Mataga, N.; Kanda, Y.; Asahi, T.; Miyasaka, H.; Okada, T.; Kakitani, T. *Chem. Phys.* **1988**, *127*, 239.
(51) Kikuchi, K.; Katagiri, T.; Niwa, T.; Takahashi, Y.; Suzuki, T.; Ikeda, H.; Miyashi, T. *Chem. Phys. Lett.* **1992**, *193*, 155.
(52) Kikuchi, K.; Niwa, T.; Takahashi, Y.; Ikeda, H.; Miyashi, T. *J. Phys. Chem.* **1993**, *97*, 5070.
(53) Hirata, S.; Lee, T. J.; Head-Gordon M. G. *J. Chem. Phys.* **1999**, *111*, 8904.
(54) Nishikava, S.; Asahi, T.; Okada, T.; Mataga, N.; Kakitani, N. *Chem. Phys. Lett.* **1991**, *185*, 237.
(55) Kakitani, T.; Yoshimori, A.; Mataga, N. *J. Phys. Chem.* **1992**, *96*, 5385.
(56) Burshtein, A. I. *J. Lumin.* **2001**, *93*, 229.
(57) Burshtein, A. I.; Ivanov, K. L. *J. Phys. Chem. A* **2001**, *105*, 3158.
(58) Burshtein, A. I.; Ivanov, K. L. *Phys. Chem. Chem. Phys.* **2002**, *4*, 4115.
(59) Jacques, P.; Allonas, X. *J. Photochem, Photobiol. A: Chem.***1994**, *78*, 1.
(60) Nemzek, Th. L.; Ware, W. R. *J. Chem. Phys.* **1975**, *62* 479.
(61) Eftink, M. R.; Ghiron, C. R. *J. Phys. Chem.* **1975**, *80*, 486.
(62) Stevens, B.; McKeithan, D. N. *J. Photochem. Photobiol. A: Chem.* **1989**, *47*, 131.
(63) Stevens, B.; Biver, C. J., III; McKeithan, D. N. *Chem. Phys. Lett.* **1991**, *187*, 590.
(64) Stevens, B.; Biver, C. J., III *Chem. Phys. Lett.* **1994**, *226*, 268.

(65) Popov, A. V.; Gladkikh, V. S.; Burshtein, A. I. *J. Phys. Chem. A* **2003**, *107*, 8177.
(66) Lukzen, N. N.; Doktorov, A. B.; Burshtein, A. I. *Chem. Phys.* **1986**, *102*, 289.
(67) Chol, H. T.; Lipsky, S. *J. Phys. Chem.* **1981**, *85*, 4089.
(68) Burshtein, A. I.; Sivachenko, A. Y. *J. Photochem. Photobiol. A* **1997**, *109*, 1.
(69) Burshtein, A. I. *Chem. Phys. Lett.* **1992**, *194*, 247.
(70) Krissinel, E. B.; Agmon, N. *J. Comput. Chem.* **1996**, *17*, 1085.

Hot recombination of photogenerated ion pairs

Vladislav Gladkikh and Anatoly I. Burshtein[a)]
Weizmann Institute of Science, Rehovot 76100, Israel

Serguei V. Feskov and Anatoly I. Ivanov[b)]
Department of Physics, Volgograd State University, University Avenue 100, Volgograd 400062, Russia

Eric Vauthey[c)]
Department of Physical Chemistry, University of Geneva, 1211 Geneva, Switzerland

(Received 7 July 2005; accepted 27 October 2005; published online 30 December 2005)

The recombination dynamics of ion pairs generated upon electron transfer quenching of perylene in the first singlet excited state by tetracyanoethylene in acetonitrile is quantitatively described by the extended unified theory of photoionization/recombination. The extension incorporates the hot recombination of the ion pair passing through the level-crossing point during its diffusive motion along the reaction coordinate down to the equilibrium state. The ultrafast hot recombination vastly reduces the yield of equilibrated ion pairs subjected to subsequent thermal charge recombination and separation into free ions. The relatively successful fit of the theory to the experimentally measured kinetics of ion accumulation/recombination and free ion yield represents a firm justification of hot recombination of about 90% of primary generated ion pairs. © *2005 American Institute of Physics*. [DOI: 10.1063/1.2140279]

I. INTRODUCTION

Most theories of electron transfer reactions in condensed media, reviewed in Refs. 1,2, incorporate as input data the thermal transfer rates between reactants separated by a distance r. These rates are controlled either by the tunneling near the intersection point of reactant and product levels or the system delivery to this point from the equilibrium position. It is usually assumed that the system motion along the reaction coordinate q proceeds faster than the modulation of the interparticle distance r by encounter diffusion and that the transfer always starts from the equilibrium position in the reactant well. If one of these conditions is violated, the encounter theory has to account for the occurrence of the process along $\mathbf{r}$ and q simultaneously. This has been done once for a diffusion-controlled thermal ionization competing with the diffusion along the reaction coordinate.[3] In the present work, we consider the geminate recombination of ion pairs produced by bimolecular photoinduced electron transfer (ionization). The backward electron transfer proceeding before thermalization, known as "hot recombination," does not need any thermal activation and is therefore more efficient and much faster than the subsequent thermal recombination that conventional theories are confined to.

The chemical system investigated here consists of perylene (Pe) in the first singlet excited state as electron donor in the presence of tetracyanoethylene (TCNE) in acetonitrile. The fluorescence quenching dynamics of Pe after excitation by an ultrashort optical pulse was recently studied both experimentally and theoretically.[4] It was concluded that the electron transfer quenching results to both the ground and the excited state of the ion pair with the rates W and W^*, respectively,

$$\mathrm{Pe^+TCNE^-} \overset{W_I}{\leftarrow} \mathrm{Pe^*} + \mathrm{TCNE} \overset{W_I^*}{\rightarrow} \mathrm{Pe^{+*}TCNE^-}.$$

Using the abbreviations, D for Pe and A for TCNE, we consider a four-level energy scheme (Fig. 1) including vibrational sublevels ($n=0, 1, 2, \ldots$) of the DA and D^+A^- states. According to this scheme, both the excited and the ground channels of ionization-recombination include hot transitions. These two ionization channels are depicted separately in Fig. 2. It is useful to introduce the probabilities α and α^* to produce equilibrated ion pairs through the ground and the excited channels, respectively. These pairs recombine thermally to the neutral ground state.

The overall reaction scheme includes the recombination of charged products assisted by vibrational and solvent relaxation. After the forward electron transfer generating the ion pair in the ground state, the population moves down diffusively and crosses a number of vibronic sublevels of neutral products before reaching the equilibrium. A fraction $1-\alpha$ of the ion-pair population recombines during this stage, i.e., prior to thermalization, which is approximately equal to the time scale of the longitudinal solvent relaxation τ_L. The remaining fraction of the ion-pair population (α) reaches equilibrium and recombines thermally with a rate W_R [see Figs. 1 and 2]. The fate of the excited ion-pair population is more complex [see Fig. 2]. These ion pairs are born near contact,[4] at a distance where electron transfer (either forward or backward) is essentially limited by the solvent relaxation ($1/\tau_L$). These ion pairs undergo charge recombination to one of the vibrational states of the neutral products (dotted levels in Fig. 1) with approximately this rate. This is followed by the

[a)]Electronic mail: cfbursh@wisemail.weizmann.ac.il
[b)]Electronic mail: physic@vlink.ru
[c)]Electronic mail: eric.vauthey@chiphy.unige.ch

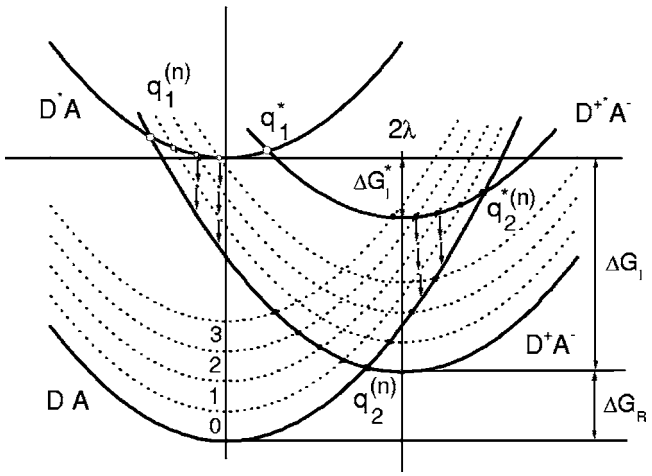

FIG. 1. Ground and excited electronic states of the reactants, DA and D^*A, and charged products, D^+A^- and $D^{+*}A^-$, at contact distance. The dotted lines represent vibrational excited states ($n=1, 2, 3$); the crossing points for forward transfer are marked by circles (○) and for backward transfer by bullets (•). The arrows show the direction of the intramolecular vibrational relaxation.

even faster intramolecular vibrational relaxation to the neutral ground state. Afterwards, this neutral population passes diffusively through the lowest crossing point with the charge-transfer states where a fraction α^* converts back to the ion pair in the ground state. This ion-pair population undergoes equilibration and thermal recombination with a rate W_R. Therefore, the equilibrated ion-pair population, which recombines thermally, consists of the fractions α and α^* of the primary ion-pair populations generated by the parallel pathways [(A) and (B) in Fig. 2], with hot recombination taking place earlier.

The dynamics of hot-electron transfer at a fixed interparticle distance has been extensively studied with the nonequilibrium generalization of the golden rule formula.[5,6] As the transfer was assumed to be limited by weak electronic coupling, the hot transfer yield was very small. In the limit of weak transfer, almost all the neutral ground-state population originating from the recombination of excited ion pairs undergoes complete equilibration, i.e., $\alpha^* \ll 1$. Similarly, the hot charge recombination of the ion pairs formed in the ground state D^+A^- is almost insignificant, i.e., $\alpha \approx 1$. As a result, this equilibrated ion-pair population is the product of forward electron transfer with the rate W_I and should represent 89%–96% of the total quenching product. However, the opposite result was found experimentally:[7] Only 10% of the quenching product ends up as equilibrated ion pairs. This indicates that hot recombination is efficient and should thus be better described with a stochastic approach[8,9] than with perturbation theory. When the reaction is limited by the diffusion to the crossing point rather than by the electronic coupling, this approach allows $\alpha \ll 1$ to be obtained. This is the so-called dynamic solvent effect (DSE) regime realizing at the highest friction. It was first studied in the Marcus normal region[8,10–15] and opposed to the other regimes (of moderate and low friction) in a few reviews.[16,17] Later on the same analysis was done also for the Marcus inverted region where DSE takes place as well.[18]

The simplest version of a stochastic theory accounting for the DSE was first developed in Ref. 19. It neglects the reversibility of the transfer in the crossing point, because of the instantaneous decay of the transfer product and thus reduces the problem to a single level with a sink. A similar approach to the problem was applied in Ref. 20 and then in Ref. 21. There is, however, no necessity for such a simplification. Using the most general stochastic approach to the problem, the reversible transfer between three intersecting levels, D^*A, D^+A^-, and DA, has been studied in Ref. 22. The arrangement of the energy levels in the case E of Fig. 4(a) in Ref. 22 is exactly the same as in Fig. 1. In the case of fast transfer, the kinetics of ion-pair decay consists of a fast hot recombination and a subsequent much slower thermal recombination.[22] Perturbation theory holds only in the opposite limit of the weak transfer where the hot stage is almost eliminated [Fig. 4(b) of the same work]. The relationship between stochastic and perturbation theories has been investigated in more detail in Ref. 23. In this work, the analytically estimated α value was shown to change from 0 to 1 when the transfer in the intersection point becomes more efficient.

In the following, only the results of the last two papers[22,23] will be used. They will be incorporated in the unified theory (UT) of irreversible photoionization and recombination, which accounts for the r dependence of all electron transfer rates and the encounter diffusion of the counterions in a Coulomb well.[1] As the original UT (Refs. 24,25) deals with thermal electron transfer only, it will be generalized to account for hot recombination prior to equilibration.

II. EXTENDED UNIFIED THEORY

Using a general approach, we consider a set of energy levels accounting for the electronic states and their vibra-

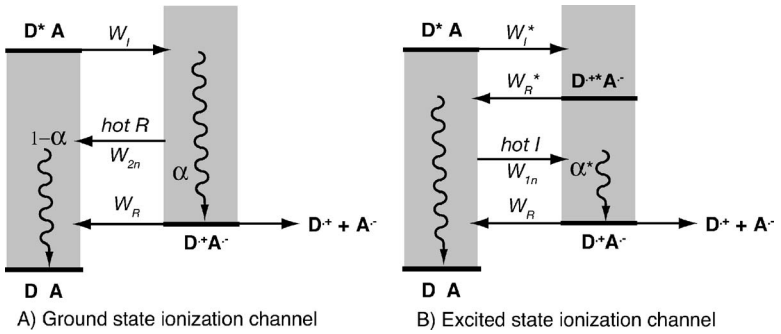

FIG. 2. Energy-level schemes illustrating the two channels to the thermalized ion pairs. The grey areas stand for the nonthermalized levels while the wavy arrows represent vibrational and/or solvent relaxation.

tional sublevels[26] involved in the overall reaction scheme [Figs. 2]. All energies are assumed to have a quadratic dependence on the solvent coordinate q,

$$U_{D^*A} = \frac{q^2}{4\lambda}, \quad U^{(n)}_{D^+A^-} = \frac{(q-2\lambda)^2}{4\lambda} + \Delta G_I + n\hbar\Omega,$$

$$U_{D^{+*}A^-} = \frac{(q-2\lambda)^2}{4\lambda} + \Delta G^*_I, \tag{1}$$

$$U^{(n)}_{DA} = \frac{q^2}{4\lambda} + \Delta G_I + \Delta G_R + n\hbar\Omega,$$

where $\Delta G_I < 0$ and $\Delta G_R < 0$ are the free energies of the primary ionization and of the subsequent charge recombination to the ground state, respectively, ΔG^*_I is the free energy of electron transfer to the excited ion pair (Fig. 1), λ is the solvent reorganization energy, Ω is the frequency of intramolecular vibrational mode, and $\hbar$ is the Planck constant. The index n stands for the nth vibrational sublevel of the appropriate electronic state.

As the relaxation of the high-frequency modes of the excited reactant is assumed to be much faster than all the electron transfer reactions considered, and as $\hbar\Omega \gg k_B T$, the vibrational excited states are not included in U_{D^*A}. Moreover, since the transition between U_{D^*A} and $U_{D^{+*}A^-}$ proceeds in the Marcus normal region, the vibrational excited sublevels of the latter are not considered as well.

The reaction scheme [Figs. 2] shows the two pathways associated with the forward electron transfer to the ion-pair ground state D^+A^- and to the ion pair in the excited state $D^{+*}A^-$. These processes occur at the term crossing points $q^{(n)}_1$ and q^*_1, where $U_{D^*A}(q^{(n)}_1) = U^{(n)}_{D^+A^-}(q^{(n)}_1)$ and $U_{D^*A}(q^*_1) = U_{D^{+*}A^-}(q^*_1)$ (Fig. 1), that is, at

$$q^{(n)}_1 = \lambda + \Delta G_I + n\hbar\Omega, \quad q^*_1 = \lambda + \Delta G^*_I. \tag{2}$$

Similarly, charge recombination from the ground and excited ion states takes place at the crossing points $q^{(n)}_2$ and $q^{*(n)}_2$ (Fig. 1), where the energies of the D^+A^- and $D^{+*}A^-$ states are equal to those of the DA state, respectively, that is, at

$$q^{(n)}_2 = \lambda - \Delta G_R - n\hbar\Omega,$$
$$q^{*(n)}_2 = \lambda + \Delta G^*_I - \Delta G_I - \Delta G_R - n\hbar\Omega. \tag{3}$$

It is also seen from Fig. 1 that the crossing points $q^{(n)}_2$ lie to both the left and the right of $q^{(0)}_2$, so the index n in the equation for $q^{(n)}_2$ may be either positive or negative.

The positions of all crossing points depend implicitly on r because

$$\lambda(r) = \lambda_0(2 - \sigma/r) \tag{4}$$

depends on the inter-reactant distance. In acetonitrile the contact reorganization energy is taken as

$$\lambda_0 = 1.15 \text{ eV}, \tag{5}$$

and the average contact distance between Pe and TCNE is $\sigma = 5$ Å.[4]

The bimolecular forward electron transfer (ionization) is universally described by the differential encounter theory (DET) equations,[1,24,25]

$$\dot{N} = -ck_I(t)N(t) - N(t)/\tau_D, \tag{6}$$

where $c = [A] = \text{const}$ and $N(t) = [D^*]$ is the survival probability of the excited donor, provided that initially $N(0) = 1$, $k_I(t)$ is the time-dependent rate constant of ionization, and τ_D is the lifetime of the excited donor in the absence of quencher.

In the original formulation of DET, $k_I(t)$ is the average product of the thermal ionization rate $W_I(r)$ and the pair distribution function of the reactants $n(r,t)$.[1] To account for dynamic solvent effects, we extend the coordinate space to include the solvent coordinate q as follows.[3]

$$k_I(t) = \int w_I(r,q)\nu(r,q,t)dq\, d^3r, \tag{7}$$

where w_I is the r- and q-dependent rate of ionization and $\nu(r,q,t)$ is the distribution function of the D^*A pairs in the extended coordinate space. The latter obeys the following equation:[3]

$$\frac{\partial \nu(r,q,t)}{\partial t} = -w_I(r,q)\nu(r,q,t) + (\hat{\mathbf{D}} + \hat{\mathbf{L}})\nu(r,q,t), \tag{8}$$

where the operator of encounter diffusion of the neutral reactants is

$$\hat{\mathbf{D}} = \frac{D}{r^2}\frac{\partial}{\partial r}r^2\frac{\partial}{\partial r}, \tag{9}$$

D being the encounter diffusion coefficient, and

$$\hat{\mathbf{L}} = \frac{1}{\tau_L}\left[1 + q\frac{\partial}{\partial q} + 2\lambda k_B T\frac{\partial^2}{\partial q^2}\right] \tag{10}$$

is the diffusion operator in the solvent coordinate q. τ_L is the longitudinal dielectric relaxation time of the solvent.

Since there are several parallel channels of ionization at the points $q^{(n)}_1$ and q^*_1, the total rate $w_I(r,q)$ is

$$w_I(r,q) = \sum_n w^{(n)}_I(r,q) + w^*_I(r,q)$$
$$= \sum_n \frac{2\pi V^2_{In}(r)}{\hbar}\delta(q - q^{(n)}_1(r))$$
$$+ \frac{2\pi V^{*2}_I(r)}{\hbar}\delta(q - q^*_1(r)), \tag{11}$$

where $V_I(r)$ and $V^*_I(r)$ are the electronic coupling constants between the D^*A and D^+A^- states and between the D^*A and $D^{+*}A^-$ states, respectively. The quantity $V^2_{In}(r)$ includes the Franck-Condon factor for the vibrational transition $0 \to n$,

$$V^2_{In}(r) = V^2_I(r)\frac{e^{-S_I}S^n_I}{n!}, \tag{12}$$

where $S_I = \lambda_{iI}/\hbar\Omega$, λ_{iI} being the reorganization energy of intramolecular vibrational mode for the electron transfer processes from D^*A. The electronic coupling constants $V_I(r)$

and $V_I^*(r)$ are assumed to decrease exponentially in r space with the characteristic decay length L_I,

$$V_I(r) = V_I e^{-(r-\sigma)/L_I}, \quad V_I^*(r) = V_I^* e^{-(r-\sigma)/L_I}. \tag{13}$$

The accumulation and decay of the ion pairs produced by ionization can be studied within UT (Ref. 1) after its proper generalization. We first introduce the distribution functions in the extended coordinate space $\mu(r,q,t)$ and $\mu^*(r,q,t)$ for the ion pairs in the ground and excited states, and $\pi(r,q,t)$ for the neutral pairs in the ground state DA. The time evolution of these functions obeys the following diffusion equations:

$$\frac{\partial \mu}{\partial t} = \sum_n w_I^{(n)} N(t)\nu + \sum_{n\leqslant 0} w_R^{(n)}\pi - \sum_{n\geqslant 0} w_R^{(n)}\mu + (\hat{\mathbf{D}}_{\mathbf{cs}} + \hat{\mathbf{L}}_{\mathbf{cs}})\mu, \tag{14a}$$

$$\frac{\partial \mu^*}{\partial t} = w_I^* N(t)\nu + w_R^{*(0)}\pi - \sum_{n\geqslant 0} w_R^{*(n)}\mu^* + (\hat{\mathbf{D}}_{\mathbf{cs}} + \hat{\mathbf{L}}_{\mathbf{cs}})\mu^*, \tag{14b}$$

$$\frac{\partial \pi}{\partial t} = -w_R^{*(0)}\pi + \sum_{n\geqslant 0} w_R^{(n)}\mu - \sum_{n\leqslant 0} w_R^{(n)}\pi + \sum_{n\geqslant 0} w_R^{*(n)}\mu^* + (\hat{\mathbf{D}} + \hat{\mathbf{L}})\pi, \tag{14c}$$

with

$$\hat{\mathbf{D}}_{\mathbf{cs}} = \frac{D}{r^2}\frac{\partial}{\partial r} r^2 e^{-U_c/k_B T}\frac{\partial}{\partial r} e^{U_c/k_B T}, \tag{15}$$

$$\hat{\mathbf{L}}_{\mathbf{cs}} = \frac{1}{\tau_L}\left[1 + (q-2\lambda)\frac{\partial}{\partial q} + 2\lambda k_B T \frac{\partial^2}{\partial q^2}\right], \tag{16}$$

where $U_c(r) = -e^2/\varepsilon(r)r$ is the Coulomb potential accounting for the spatial dispersion of the dielectric constant.

In Eqs. (14), the recombination rates $w_R^{(n)}(r,q)$ and $w_R^{*(n)}(r,q)$ through the ground and excited channels are

$$w_R^{(n)} = \frac{2\pi V_{Rn}^2(r)}{\hbar}\delta(q - q_2^{(n)}(r)), \tag{17}$$

$$w_R^{*(n)} = \frac{2\pi V_{Rn}^{*2}(r)}{\hbar}\delta(q - q_2^{*(n)}(r)), \tag{18}$$

with

$$V_{Rn}^2(r) = V_R^2(r)\frac{e^{-S_R}S_R^n}{n!}, \tag{19}$$

where $S_R = \lambda_{iR}/\hbar\Omega$, λ_{iR} being the reorganization energy of the intramolecular vibrational modes for the charge recombination processes to the neutral ground state. The r dependencies of the electronic coupling constant for charge recombination are

$$V_R(r) = V_R e^{-(r-\sigma)/L_R}, \quad V_R^*(r) = V_R^* e^{-(r-\sigma)/L_R}. \tag{20}$$

Equations (8) and (14) should fulfill the boundary conditions[1]

$$\left.\frac{\partial \nu(r,q,t)}{\partial r}\right|_{r=\sigma} = 0, \quad \lim_{q\to\pm\infty}\nu(r,q,t) = 0, \tag{21a}$$

$$\left.\frac{\partial \mu(r,q,t)}{\partial r}\right|_{r=\sigma} = 0, \quad \lim_{q\to\pm\infty}\mu(r,q,t) = 0, \tag{21b}$$

$$\left.\frac{\partial \mu^*(r,q,t)}{\partial r}\right|_{r=\sigma} = 0, \quad \lim_{q\to\pm\infty}\mu^*(r,q,t) = 0, \tag{21c}$$

$$\left.\frac{\partial \pi(r,q,t)}{\partial r}\right|_{r=\sigma} = 0, \quad \lim_{q\to\pm\infty}\pi(r,q,t) = 0, \tag{21d}$$

and the initial conditions

$$\nu(r,q,0) = \varphi_1(q) = (4\pi\lambda T)^{-1/2}\exp(-q^2/4\lambda T), \tag{22}$$

$$\mu(r,q,0) = \mu^*(r,q,0) = \pi(r,q,0) = 0. \tag{23}$$

The total amount of ion pairs surviving at time t is calculated as a sum

$$P_t(t) = P(t) + P^*(t), \tag{24}$$

where

$$P(t) = c\int d^3r \int \mu(r,q,t)dq,$$

$$P^*(t) = c\int d^3r \int \mu^*(r,q,t)dq \tag{25}$$

are the populations of the ground and excited ion pairs, respectively.

It is also useful to introduce the r distributions of D^+A^- and $D^{+*}A^-$ pairs initially produced through the ground- and the excited-state channels $m(r)$ and $m^*(r)$,

$$m(r) = \int_0^\infty dt\, N(t)\int dq \sum_n w_I^{(n)}(r,q)\nu(r,q,t), \tag{26a}$$

$$m^*(r) = \int_0^\infty dt\, N(t)\int dq\, w_I^*(r,q)\nu(r,q,t), \tag{26b}$$

where $\nu(r,q,t)$ and $N(t)$ obey Eqs. (6) and (8).

Equations (6)–(24) provide a formal basis for the theory of ionization and geminate recombination accounting explicitly for hot transitions. This model was investigated numerically using a simulation algorithm given in the Appendix. The results of the simulation are presented in the next section.

III. REPRODUCING THE KINETICS OF QUENCHING AND CHARGE RECOMBINATION

Two independent sets of experimental data have to be reproduced: (1) the time dependence of the excited-state population $N(t)$ and (2) the time dependence of the ground-state-ion pair population $P(t)$.[7] Since the parameters for charge recombination do not affect the ionization dynamics in Eq. (8), we will follow Ref. 4 and start with the fitting of $N(t)$. Below we present the results for $c = 0.32\ M$ only, though analogous results are obtained for $c = 0.16\ M$ as well.

The following fixed parameters were used:[4] $\Delta G_I = -2.14$ eV, $\Delta G_I^* = -0.6$ eV, $\Delta G_R = -0.69$ eV, $\Omega = 0.1$ eV, $L_I = 1.24$ Å, and $\tau_D = 4.34$ ns. On the other hand, the parameters V_I, V_I^*, S_I, and D were adjusted.

A remark concerning the choice of the solvent relaxation time τ_L should be added. Like the other solvents, acetonitrile exhibits non-Markovian polarization relaxation dynamics, which is usually described in terms of several solvent modes with different relaxation times. Acetonitrile is characterized by at least two modes with an ultrafast inertial mode having a relaxation time $\tau_1 \approx 0.2$ ps and a slower Debye-type mode with $\tau_2 \approx 0.5$ ps.[27] Only the latter mode was taken into account because, with the energetic parameters adopted here, the hot transitions predominantly occur when the relaxation of the fastest mode is over and before the slowest mode has started. Of course, the Markovian approach used in this paper can only yield a limited precision of the description.

The strategy for choosing the best-fit parameters was the following. In the ionization kinetics, several regimes, which are controlled by different parameters, can be distinguished. The quenching at early time proceeds at the kinetic regime and can be well described with a rate constant $k_0 = k_I(t=0)$.[4] At this stage, the initial equilibrium distribution of reactants in both q and r spaces is assumed not to be perturbed. This quantity can be calculated using Eq. (7) with $\nu(r,q,0)$ determined by Eq. (22). Its value $k_0 = 322.6$ Å^3/ps was found earlier from the best fit of the short-time kinetics in the 0–6.5 ps interval.[4] The V_I, V_I^*, and S_I parameters able to reproduce this k_0 value were then chosen. This allowed the reduction of the number of independent parameters. At longer times, the quenching is controlled by the diffusive delivery of the reactants to the ionization zone. In this regime, the role of D is dominant, and its value can be determined rather precisely from the analysis of the dynamics of the excited-state population $N(t)$ in the 0.2–1.2 ns interval (see Fig. 3 of Ref. 4). The excited-state population dynamics measured in an intermediate time interval (1–300 ps) was used for the determination of the other parameters.

A. Double-channel ionization model

A few sets of parameters, which can be considered as candidates for the best fit of quenching kinetics, were found. At least two of them reproduce the experimental data of Ref. 4 quite well.

The first set of parameters is the same as that found in Ref. 4 within the framework of the DET. These parameters are

$$V_I = 0.123 \text{ eV}, \quad V_I^* = 0.138 \text{ eV}, \quad S_I = 0, \quad D = 3.05 \times 10^{-5} \text{ cm}^2/\text{s}. \tag{27}$$

Figure 3(a) shows that the excited-state dynamics $N(t)$, calculated earlier in Ref. 4, can be well reproduced with these parameters.

This close agreement between our results and those obtained within the original DET is not surprising. Because ionization through the ground channel occurs in the far Marcus inverted region, the ion pairs should be predominantly formed at relatively large inter-ionic distances. This is illustrated by the $m(r)$ dependence shown in Fig. 4(a). Since the electronic coupling at such distances is very weak, ionization proceeds mostly as a nonadiabatic reaction and does not violate the thermal distribution over the reaction coordinate q.

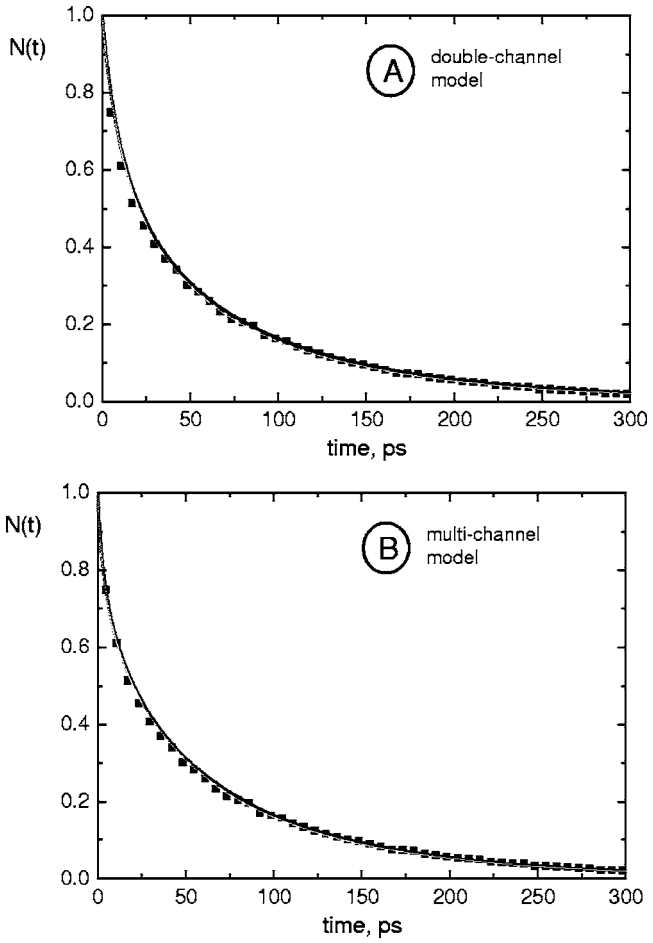

FIG. 3. Best fit of the ionization kinetics at $c = 0.32M$ and reported in Ref. 7 (dots) using the double-channel model (A) and the multichannel model (B). The best-fit parameters are given by Eqs. (27) and (28), respectively.

B. Multichannel ionization model

A rather good fit of the ionization kinetics $N(t)$ to the experimental data [see Fig. 3(b)] was achieved with the following parameters:

$$V_I = 0.048 \text{ eV}, \quad V_I^* = 0.057 \text{ eV}, \quad S_I = 2, \quad D = 3.95 \times 10^{-5} \text{ cm}^2/\text{s}. \tag{28}$$

Since $S_I = 2$, the forward electron transfer proceeds through several vibrational channels at $q_1^{(n)}$. This changes considerably the energetics of ionization and decreases the electronic coupling constants V_I and V_I^*. The vibrational sublevels lower the effective activation barrier of ionization, shifting the reaction closer to the contact distance $r = \sigma$. The distance distribution of the ion pairs produced by ionization is presented in Fig. 4(b). In this case, a somewhat larger value of the diffusion coefficient D was used to reproduce the observed dynamics at long time scale.

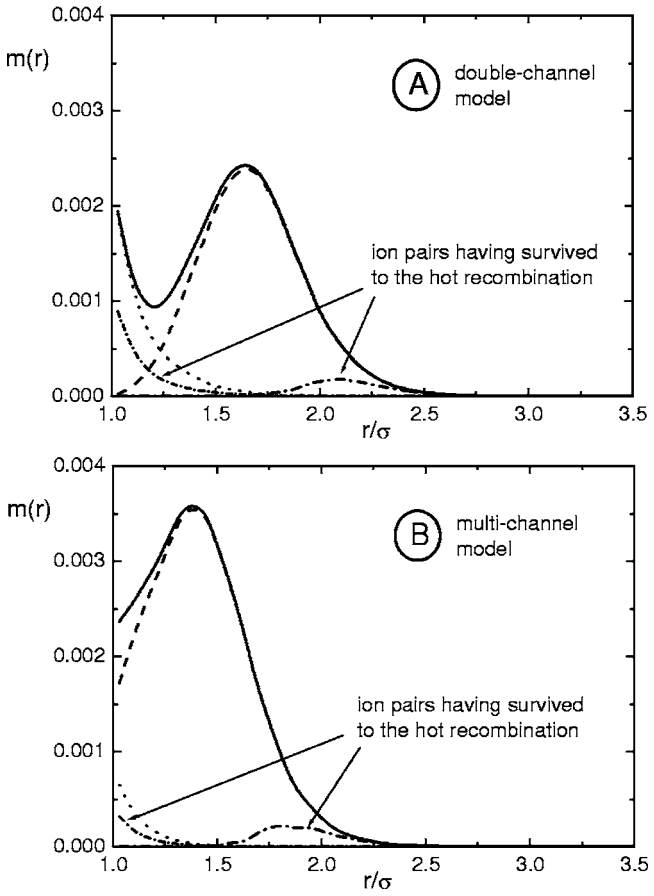

FIG. 4. Distributions of ion pairs generated in the ground state D^+A^- (dashed lines) and the excited state $D^{+*}A^-$ (dotted lines) as a function of the separation distance $m(r)$ and $m^*(r)$: (A) double-channel model with parameters given by Eq. (27) and (B) multichannel model [Eq. (28)]. The solid lines are the overall ion-pair distributions.

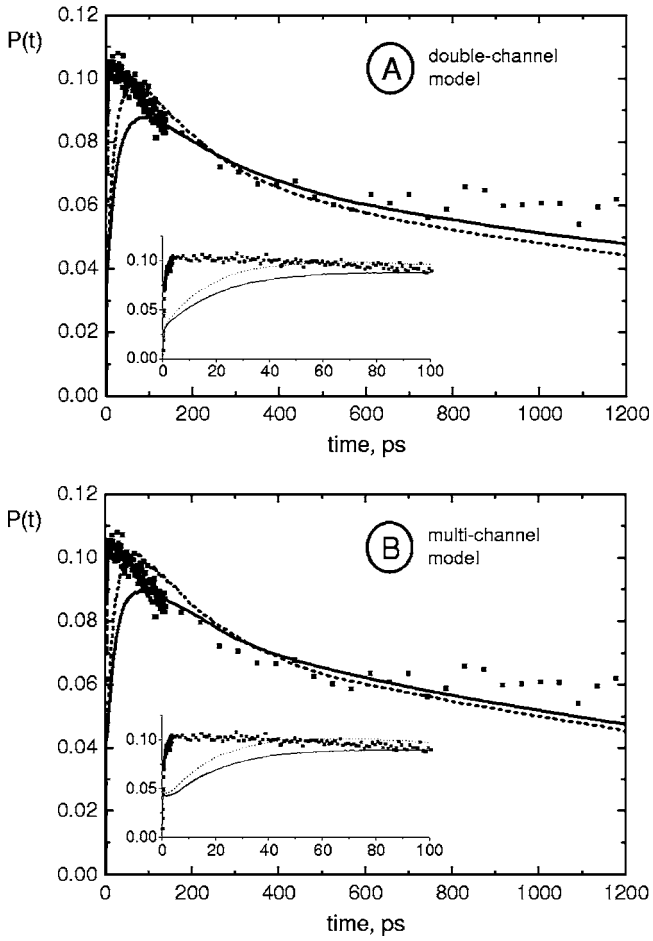

FIG. 5. Best fit of the ion-pair accumulation/recombination kinetics measured with $c=0.32M$ and reported in Ref. 7 (dots) using the double-channel model (A) and the multichannel model (B). The solid lines are the numerical results obtained within the original model [parameters of the fits are given by Eqs. (29) and (30)], while the dashed lines are the same results but accounting for $D(r)$ and $\epsilon(r)$ dependencies with $\Lambda=1.6$ Å ($V_R=V_R^*=0.15$ eV, for the double-channel model, and $V_R=V_R^*=0.075$ eV for the multichannel model).

One remark concerning the sensitivity of the numerical curve $N(t)$ to a particular choice of the fitting parameters needs to be added. Since the efficiency of the excited-state ionization channel is considerably lower than that of the ground-state one, the ionization kinetics is weakly sensitive to the magnitude of V_I^*, and therefore the uncertainty on this value obtained from the fit is rather large. On the other hand, a variation of the other fitting parameters within 5% leads to a noticeable degradation of the fit.

C. Ion-pair accumulation-recombination kinetics

For the fitting of the ion-pair kinetics $P(t)$ to the experimental data, the best-fit parameters in Eq. (27) or alternatively in Eq. (28) were used as input data and only the quantities V_R, V_R^*, L_R, and S_R were adjusted.

With the parameters from Eq. (27), a rather good fit of $P(t)$ to the experimental data in the 80–500 ps time window was achieved [Fig. 5(a)]. It shows that the equilibrated ion-pair population never exceeds 11% of the primary quenching product population $P_t(t)$. The reason is that most of the initially produced ion-pair population undergo ultrafast hot recombination after their birth at the q_1 point. This conclusion will be confirmed in the next section by the direct estimation of hot transition probability.

The free ion yield $P(\infty)$ measured independently by photoconductivity is even smaller and amounts to 6%.[7] This number was used to relate the experimental time profiles of the transient absorption, given in the same work in arbitrary units, to the absolute ion yield. A good fit of the double-channel model [Eq. (27)] at long times was obtained with the following set of parameters:

$$V_R = 0.165 \text{ eV}, \quad V_R^* = 0.165 \text{ eV}, \quad S_R = 3, \quad L_R = 2.2 \text{ Å}. \tag{29}$$

These values are in relatively good agreement with those found in the literature. In particular, the contact values of the electronic coupling constant V_R and V_R^* are comparable with those found in a few independent studies on exciplexes (contact ion pairs). Values between 0.11 and 0.13 eV and between 0.15 and 0.4 eV are reported in Refs. 28 and 29, respectively.

The fit of the multichannel model to the ion-pair kinetics $P(t)$ using the ionization parameters given in Eq. (28) is presented in Fig. 5(b). The best fit was obtained with the following set of parameters:

$$V_R = 0.093 \text{ eV}, \quad V_R^* = 0.093 \text{ eV}, \quad S_R = 3, \quad L_R = 2.2 \text{ Å}. \tag{30}$$

Since the ion pairs are produced at closer distance than in the double-channel model, efficient hot recombination can be achieved with smaller electronic coupling constants V_R and V_R^*.

It should be noted that the recombination dynamics at relatively short times $t<80$ ps could not be reproduced. However, a rather good fit was obtained at moderate times 80 ps$<t<500$ ps. Finally, the simulations at long times $t>500$ ps predict a slow decay of the ion-pair population due to the diffusion-assisted geminate recombination, while the experimentally observed population remains constant.

The ion-pair population dynamics is determined by the competition between production and recombination. The discrepancy at short times can be due to either an underestimation of the ion production or an overestimation of the ion recombination.

The approach used here is only applicable if the electronic transitions are essentially nonadiabatic. It implies that the single crossing of the nonadiabatic transition region results in a small transition probability hence electronic coupling V must be sufficiently small. The DSE regime is a consequence of multiple crossings of the nonadiabatic region. A thorough discussion of the physical mechanisms of the friction influence on the criteria for nonadiabaticity was given in Refs. 16,17. The applicability domain of the stochastic approach for the parameters obtained in this paper may be roughly estimated as $V \lesssim k_B T$.[30] Too large electronic coupling were obtained with the double-channel model ($S_I=0$) as shown by Eqs. (27) and (29). In this case, the adiabatic corrections can be considerable. However, much smaller values have been obtained with the multichannel theory ($S_I=2$): $V=0.048-0.093$ eV [Eqs. (28) and (30)]. The effective electronic coupling between vibrational sublevels is even smaller than these values by the square root of the Franck-Condon factor as indicated by Eqs. (12) and (19). Therefore, the short-time discrepancy cannot be ascribed to a nonapplicability of the model.

As noted above, acetonitrile exhibits a non-Markovian polarization relaxation dynamics. The presence of several relaxation components can affect the ion-pair population dynamics especially at short times.[31] This requires further investigation.

The fit to the experimental data at short times could also be improved by taking into account a nonuniform distribution of inter-reactant distances. This is reasonable if D and A form weak complexes with a coupling energy of the order of $k_B T$. In this case, the number of excited donors with a quencher at contact distance is increased, and the electron transfer rate at early time becomes substantially faster.

The influence of the spatial dispersion on the ion-pair accumulation-recombination kinetics is considered in the next section.

D. Influence of the spatial dispersion of diffusion coefficient and dielectric permittivity on the ion-pair dynamics

The encounter diffusion at large separation differs from that at the closest approach distance where the structure of the few first solvent shells should be taken into account. This can be done phenomenologically by assuming that the diffusion coefficient is r dependent and becomes smaller at shorter distances,[32]

$$D(r) = D\left[1 - \frac{1}{2}\exp\left(\frac{\sigma - r}{\sigma_s}\right)\right], \tag{31}$$

where σ_s is the diameter of a solvent molecule, which amounts to 3.62 Å for acetonitrile, and D is the conventional Fick diffusion coefficient at infinite separation. The actual diffusion coefficient at contact distance is predicted to be about twice as small. The probability for the charge recombination of ion pairs born out of the recombination layer is reduced because their penetration into this layer is slower. A similar effect can be obtained in more viscous solutions by decreasing the Fick diffusion coefficient. In such a diffusion-controlled recombination, observed a few times experimentally,[1,33] the rate decreases with increasing viscosity.[34]

If the spatial dependence of $D(r)$ is taken into account, the spatial dispersion of the dielectric constant $\epsilon(r)$, which affects recombination in the opposite direction, should not be ignored. The spatial dependence of the dielectric constant results from the nonlocal screening of the Coulomb potential.[35,36] The simplest model accounting for the absence of screening at short distances is[35]

$$\epsilon(r) = \frac{\epsilon}{1 + (\epsilon/\epsilon_0 - 1)\gamma \exp(-r/\Lambda)}, \tag{32}$$

where $\epsilon_0=2$ is the optical dielectric constant, ϵ is its static value in the continuum, Λ is a fitting parameter, and $\gamma = 2(\Lambda^2/\sigma^2)(\cosh(\sigma/\Lambda)-1)$ is the correction for the excluded volume of finite-size particles. If this effect is included in $U_c(r)$ appearing in Eq. (15), the Coulomb well becomes deeper,

$$U_c(r) = \frac{e^2}{\epsilon(r) r}. \tag{33}$$

This potential is characterized by a sharp feature near contact, which looks like an additional narrow and rather deep well. It originates from the same Coulomb attraction but is not screened by intercalated solvent molecules. The deepening of the Coulomb well accelerates the drift of ions toward the region of maximum recombination rate, and thus this latter process is enhanced. The depth of this well can be adjusted by the independent parameter Λ.

Accounting for the spatial dispersion of both $\epsilon(r)$ and $D(r)$ improves the fitting of the kinetics $P(t)$ in the interval 30 ps$<t<80$ ps (dashed lines in Fig. 5), but at long time scale the ion state population is still underestimated. For a further improvement of the theory, the chemical anisotropy

of the reaction, which makes all the rates angular dependent and affected by the rotational diffusion,[37] should be taken into account.

E. Internal conversion of the excited ion pairs and free ion yield

In the simple scheme shown in Fig. 1, the potential of the excited ion pair is not displaced horizontally relative to that of the ground state. Since these two potentials do not cross, the electron-vibration interactions are actually absent. Thus, the straightforward transformation of electronic energy of the ion pairs into vibrational energy, followed by vibrational relaxation, is totally ignored. In reality, the two potentials are displaced, and internal conversion can efficiently compete with the above-considered mechanism of double electron transfer, namely, charge recombination of the excited ion pair to the neutral products, followed by hot ionization to the ion pair in the ground state [Fig. 2]. If internal conversion dominates, then all ion pairs are deactivated with 100% efficiency and consequently $\alpha^*=1$.

This alternative has been considered using a time constant of internal conversion of $\tau_{ic}=3$ ps.[7] However, this did not bring any significant change. Although this mechanism produces more ion pairs in the ground state, all of them are born in or near the charge recombination layer and thus recombine much faster than they separate. Therefore their contribution to the free ion yield is negligible. It can thus be concluded that the free ion yield is only weakly sensitive to a particular value of α^*.

IV. HOT RECOMBINATION

The results of the fit indicate a significant role of hot transitions in the recombination dynamics. The effect of hot recombination on the formation of ions depends strongly on the quenching channel. Let us start with the electron transfer to the excited ion pair [Fig. 1], which proceeds in the Marcus normal region (at q_1^*) and is followed by downward diffusion to the bottom of the $D^{+*}A^-$ well. Since the most effective sinks at the $q_2^{*(n)}$ points lie in the Marcus inverted region (Fig. 1), the bottom is reached before the crossing points and the subsequent recombination is mainly thermal, that is, it goes "up and down" from this well to the neutral product potentials.

On the contrary, the charge recombination following the forward electron transfer to the ion pair in the ground state D^+A^- [see Fig. 1] is in the Marcus normal region and includes "down-down" hot transition (Fig. 1). Indeed, starting from a crossing point $q_1^{(n)}$, the system moves down to the intersection points $q_2^{(n)}$ and further down to the bottom of the well. Therefore, the ions pair undergoes first a charge recombination to the neutral product at the points $q_2^{(n)}$ and thermalize afterward. In other words, hot recombination at $q_2^{(n)}$ precedes thermalization, taking away a $(1-\alpha)$ fraction of the ion-pair population and leaving only an α fraction that will recombine thermally ("up-down") afterwards.

On the other hand, the neutral product generated by thermal charge recombination of the excited ion pair also experiences a hot ionization at $q_2^{(n)}(n\leqslant 0)$ before reaching the bottom of the DA state. This is the secondary ionization proceeding with efficiency α^* to the ion-pair state D^+A^- [Fig. 2].

The distributions of ionization products were calculated from Eqs. (26) with the parameters obtained from the best fit of the ionization kinetics Eqs. (27) and (28). As mentioned above, excited ion pairs are produced near contact distance, while those in the ground state are produced in a larger amount and larger distance (see Fig. 4). If we neglect the encounter diffusion of the ions during the motion from q_1 to q_2 and from q_2^* to q_2, the fractions of ions reaching equilibrium by the two parallel pathways can then be estimated as $\alpha(r)m(r)$ and $\alpha^*(r)m^*(r)$. The r distributions of these equilibrated ion pairs are shown by the dash-dotted lines in Fig. 4. These distributions are significantly altered and reduced compared to $m(r)$ and $m^*(r)$ because of hot recombination. These changes arise from $\alpha(r)$ and $\alpha^*(r)$ whose values and space dispersions are calculated below.

The value of α for a system subjected to a single crossing during relaxation has been determined in Refs. 23 and 38. However, the present situation is more complex. Indeed, immediately after the transition to the D^+A^- well near $q_1^{(n)}$, the system almost instantaneously reaches the lowest vibrational level $(n=0)$ because of the ultrafast intramolecular vibrational redistribution and crosses a number of vibrational sublevels of DA while moving toward the bottom of the D^+A^- well (Fig. 1). If these vibrations participate in the charge recombination, i.e., are being Franck-Condon active, the survival probability of the ion pair reduces upon each crossing. Similarly, hot transitions reduce by a factor $1-\alpha^*$ the survival probability of neutral product, which moves down from $q_2^{*(n)}$ toward the bottom of the DA well and crosses several vibrational sublevels of the D^+A^- state.

Following Ref. 26, we consider a sequence of hot electronic transitions to the sublevels $U_{DA}^{(n)}$. The probability of a transition generating n vibrational quanta W_{2n} can be calculated using the method developed in Ref. 23 In the present notation it is given by

$$W_{2n}=\frac{2\pi V_{Rn}^2(r)}{|A_{1n}|}\left[1+2\pi V_{Rn}^2(r)\left(\frac{1}{|A_{1n}|}+\frac{1}{|A_{2n}|}\right)\right]^{-1}, \quad (34)$$

where

$$A_{1n}=\frac{2\lambda}{\tau_L}\frac{\partial U_{D^+A^-}^{(n)}}{\partial q}\bigg|_{q=q_2^{(n)}}=\frac{q_2^{(n)}-2\lambda}{\tau_L},$$
$$A_{2n}=\frac{2\lambda}{\tau_L}\frac{\partial U_{DA}^{(n)}}{\partial q}\bigg|_{q=q_2^{(n)}}=\frac{q_2^{(n)}}{\tau_L} \quad (35)$$

are the slopes of the potential intersecting at $q_2^{(n)}$. Only those points, which are to the right of $q_1^{(0)}$ and whose number is $n_{\max}$, need to be considered.

If $\hbar\Omega\gg k_BT$, the mutual influence of the nearest crossing points is negligible. Under this condition, the survival

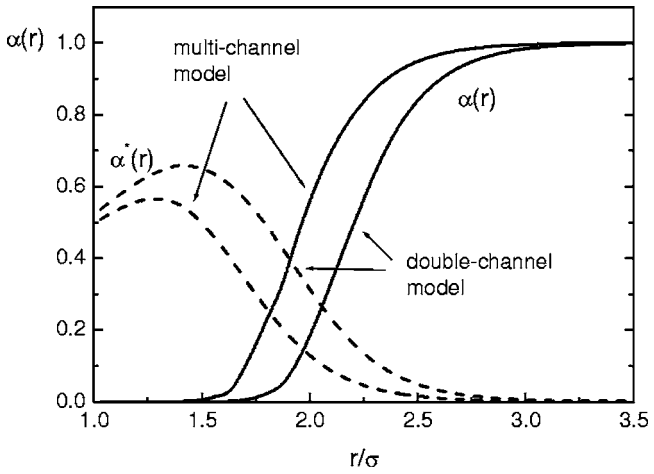

FIG. 6. Fractions of ion pairs having escaped hot recombination to the neutral products α (solid lines) and thermalized fraction of excited ion pairs α^* (dashed lines) as a function of interionic distance r calculated using the double-channel model [Eq. (29)] and the multi-channel model [Eq. (30)].

probability of the ion-pair population is the product of the partial survival probabilities considered as independent events,

$$\alpha(r) = \prod_{n=0}^{n_{\max}} (1 - W_{2n}). \tag{36}$$

The r dependence of α originating from the r dependence of both $V_R(r)$ and $\lambda(r)$ is depicted in Fig. 6.

A similar reasoning can be used to estimate the ground-state ion population generated via the excited-state channel. The value of α^* is

$$\alpha^*(r) = 1 - \prod_{n=0}^{n_{\max}} (1 - W_{1n}), \tag{37}$$

where

$$W_{1n} = \frac{2\pi V_{Rn}^2(r)}{|A_{2n}^*|}\left[1 + 2\pi V_{Rn}^2(r)\left(\frac{1}{|A_{2n}^*|} + \frac{1}{|A_{1n}^*|}\right)\right]^{-1}, \tag{38}$$

$$A_{1n}^* = \frac{q^{*(n)} - 2\lambda}{\tau_L}, \quad A_{2n}^* = \frac{q^{*(n)}}{\tau_L}, \tag{39}$$

where $q^{*(n)} = \lambda - \Delta G_R + n\hbar\Omega$, and $n_{\max}$ is determined from the condition $q^{*(n)} = 2\lambda$. The difference between $\alpha^*(r)$ and $\alpha(r)$ shown in Fig. 6 is most pronounced at large separation where $\alpha^* \to 0$, because hot ionization is switched off, and $\alpha \to 1$, because hot recombination is no longer efficient. Because of the hot transfer processes, the population of thermalized ion pairs is significantly reduced compared to those of their primary generated precursors.

The calculated $\alpha(r)$ and $\alpha^*(r)$ dependencies, along with the initial r distribution of ion pairs $m(r)$ and $m^*(r)$ (Fig. 4), allow the efficiency of hot transitions in both channels to be estimated. Introducing the efficiencies of ion-pair production through the ground and excited channels,

$$P_0 = c \int m(r) d^3 r, \tag{40a}$$

$$P_0^* = c \int m^*(r) d^3 r, \tag{40b}$$

the amounts of thermalized pairs P_{th} and P_{th}^* participating in the subsequent thermal recombination are then calculated as

$$P_{\text{th}} = c \int \alpha(r) m(r) d^3 r, \tag{41a}$$

$$P_{\text{th}}^* = c \int \alpha^*(r) m^*(r) d^3 r. \tag{41b}$$

These parameters, calculated for the double-channel model, are

$$P_0 = 0.89, \quad P_0^* = 0.10, \quad P_{\text{th}} = 0.08, \quad P_{\text{th}}^* = 0.04, \tag{42}$$

and those for the multichannel model are

$$P_0 = 0.96, \quad P_0^* = 0.03, \quad P_{\text{th}} = 0.08, \quad P_{\text{th}}^* = 0.02. \tag{43}$$

Because of the hot transfer, the total amount of thermalized pairs $P_{\text{th}} + P_{\text{th}}^*$ is equal to only 10%–12% of that of the initially generated pairs, $P_0 + P_0^*$. Therefore, for the system considered here, about 90% of the initially created radical ion pairs undergo hot transitions, 4% of them dissociate into free ions, and only 6% recombine through thermal channels.

V. CONCLUSIONS

This is, to our knowledge, the first relatively successful fit of a backward electron transfer kinetics which takes into account the hot recombination of photogenerated ion pairs. The information obtained earlier from the best fit of the forward electron transfer with the same system has been used.[4] This study indicates the presence of two parallel channels of ionization, to the ground and excited states of ion pairs, whose products are located rather far and close to the contact, respectively. Since the backward transfer occurs essentially near contact, the closely spaced excited ion pairs disappear almost completely upon geminate recombination while those in the ground state have a high probability to escape it and thus provide the main contribution into the free ion yield.

The hot recombination of ion pairs is a decisive factor. It is shown that, in the present system, the vast majority of ion pairs have recombined through the hot channel before they are equilibrated and start to recombine with the usual thermal rates. Almost 90% of the ion pairs recombine before equilibrium is reached and the subsequent thermal recombination is accelerated by their encounter diffusion. As a result, no more than 6% of their initial population are finally separated (at $c = 0.32\ M$). Such a surprisingly fast back electron transfer proceeding through the hot channel was also detected in Ru(II)–Co(III) mixed-valence complexes in butyronitrile.[39] In this case as well, less than 50% of the ion pairs generated by the excitation of the metal-to-metal charge-transfer band avoid this recombination and reach equilibrium. These examples show that the study of any system should start from

the inspection of the energy scheme as presented in Fig. 1. This has to be done to find out whether the quenching product has to pass a crossing point (like q_2) on its way to the bottom of the well. If this is the case, one should care not only for thermal but first of all for the hot transfer as a dominant factor in the charge recombination.

Since hot transitions cannot be discussed in terms of rate constant, their appropriate description has called for an extension of existing theories of electron transfer quenching in solutions to explicitly account for reaction coordinate dynamics. In the theory presented here, both the chemical dynamics and the mutual spatial diffusion of the reactants have been taken into account. It should be noted that the spatial motion of the reactants was not considered in previous investigations of hot transitions.[5,6,20–23] In particular, in Ref. 21 the average lifetime of the immobile ion pairs subjected to hot and thermal recombination was calculated. On the contrary, we have considered here the competition between the recombination of thermalized ion pairs and their diffusional separation.

A second new element of the present investigation is connected to the fact that both the ionization and recombination of the Pe-TCNE pairs are considerably affected by the introduction of a high-frequency quantum mode. With such a mode, many term crossings with different values of the vibrational quantum number are available for hot transition. Therefore, the hot recombination efficiency is greatly enhanced. As a result, only the pairs created with a relatively large inter-ionic distance have a finite probability to avoid hot recombination. This allows the unusually small free ion yield of this donor-acceptor pair to be explained.

ACKNOWLEDGMENT

Two of the authors (S.V.F. and A.I.I.) acknowledge the Russian Foundation for Basic Researches for support (Grant No. 05-03-32680).

APPENDIX: SIMULATION METHOD

In the numerical simulations, the Brownian simulation method in the form proposed before in Refs. 38 and 40 was used. Here we outline some features of the program implementation specific to the model considered. The software is available on the web (http://physics.volsu.ru/feskov).

The first step in the simulations is the time propagation of an ensemble of N ($N=10^6-10^7$) Brownian quasiparticles representing the initial distribution of the excited donor-acceptor pairs in extended coordinate space according to the diffusion equations [(8) and (14)] and the reflective boundary conditions at contact radius (21). The important points of the algorithm are as follows.

(1) The initial distribution of quasiparticles obeys Eq. (22).
(2) The unreactive Brownian trajectory of quasiparticle is a Markovian random process in $\{r,q\}$ space.
(3) The electronic transitions in donor-acceptor pairs are modeled by hops of quasiparticles between the potential surfaces (1) at the crossing points $q_i^{(n)}$, $q_i^{*(n)}$ $(i=1,2)$.
(4) The internal conversion of the excited ion pairs is accounted for as an irreversible decay $D^{*+}A^- \rightarrow D^+A^-$ with the characteristic time constant τ_{ic}.

An unreactive trajectory of the kth quasiparticle is calculated as a set of coordinates $\{r_k^{(i)}, q_k^{(i)}\}$ at consecutive time intervals Δt_i. Using well-known Green's functions for the diffusion operators $\hat{\mathbf{D}}$ and $\hat{\mathbf{L}}$ as the probability distributions of random walks at r and q subspaces, one obtains the following simulation rules:

$$q_k^{(i)} = q_k^{(i-1)} e^{-\Delta t_i/\tau_L} + X_i \sqrt{2\lambda(r_k^{(i-1)}) k_B T (1 - e^{-2\Delta t_i/\tau_L})},$$

$$r_k^{(i)} = r_k^{(i-1)} + Y_i \sqrt{2D(r_k^{(i-1)})\Delta t_i} + \frac{2}{r_k^{(i-1)}} D(r_k^{(i-1)}) \Delta t_i,$$

for trajectory on the neutral state surface, and

$$q_k^{(i)} = 2\lambda(r_k^{(i-1)}) + (q_k^{(i-1)} - 2\lambda(r_k^{(i-1)})) e^{-\Delta t_i/\tau_L} + X_i \sqrt{2\lambda(r_k^{(i-1)}) k_B T (1 - e^{-2\Delta t_i/\tau_L})},$$

$$r_k^{(i)} = r_k^{(i-1)} + Y_i \sqrt{2D(r_k^{(i-1)})\Delta t_i} + \left(2 - \frac{r_c}{r_k^{(i-1)}}\right) \frac{1}{r_k^{(i-1)}} D(r_k^{(i-1)}) \Delta t_i,$$

for that on the ion state surface. Here X_i and Y_i are the Gaussian random numbers with zero mean value and unit dispersion. The above equations are exact for unreactive diffusion along q and are approximate for the spatial diffusion along r, valid for small-time steps.

Each particle is assumed to occupy the volume $\Delta\Gamma$ in the configuration space $\{r,q\}$. This quantity appears naturally when one relates the initial normalized probability distribution function [Eq. (22)] and the finite number N of Brownian quasiparticles. Since the diffusion along r results in an alteration of $\Delta\Gamma$, an additional weight factor $v_k^{(i)}$ is introduced and calculated at each time step as follows:

$$v_k^{(i)} = v_k^{(i-1)} \left(\frac{r_k^{(i-1)}}{r_k^{(i)}}\right)^2, \quad (v_k^{(0)} = 1). \tag{A1}$$

This guarantees the conservation of the distribution function normalization in the absence of reactions

$$\sum_k 4\pi (r_k^{(i)})^2 \Delta\Gamma_k^{(i)} = \Delta\Gamma \sum_k 4\pi (r^{(i)})^2 v_k^{(i)} = \text{const}. \tag{A2}$$

The surface-hopping algorithm[38,41] is applied to simulate electronic transitions between the diabatic surfaces at the crossing points $q_i(r)$. The probability of survival at the same surface is

$$p_k^{(i)} = \exp\left(-\frac{2\pi V_{\text{el}}^2(r_k^{(i-1)})\Delta t_i}{\hbar \Delta U_k^{(i)}}\right), \tag{A3}$$

which is the well-known result of perturbation theory. Here $\Delta U_k^{(i)} = U(r_k^{(i)}, q_k^{(i)}) - U(r_k^{(i-1)}, q_k^{(i-1)})$ and $V_{\text{el}}(r_k^{(i-1)})$ is the corresponding electronic coupling element.

The reaction flux $j(t_i)$ between two free-energy surfaces can be easily calculated through the total configuration volume transferred from one surface to another during the time

interval Δt_i. Since each hop of a quasiparticle generates the elementary flux $\Delta j_k^{(i)} = 4\pi (r_k^{(i)})^2 \Delta\Gamma_k^{(i)} / \Delta t_i$, the total flux is

$$j(t_i) = \sum_k \Delta j_k^{(i)} = \Delta\Gamma / \Delta t_i \sum_k 4\pi (r_k^{(i)})^2 v_k^{(i)}, \tag{A4}$$

where the summation is taken over particles having transferred between the given surfaces.

The time-dependent survival probabilities of the excited donors $N(t)$ and radical-ion pairs $P(t)$ are then directly determined by the reaction fluxes $j_I(t)$ and $j_R(t)$ for ionization and recombination, respectively. Since the ionization proceeds through two parallel channels the flux $j_I(t)$ is a sum

$$j_I(t) + j_I^*(t) = k_I(t) = \int d^3 r \int dq\ w_I(r,q) \nu(r,q,t). \tag{A5}$$

Similarly the recombination fluxes through the ground and excited channels are

$$j_R(t) = \int d^3 r \int dq\ w_R(r,q) \mu(r,q,t), \tag{A6a}$$

$$j_R^*(t) = \int d^3 r \int dq\ w_R^*(r,q) \mu^*(r,q,t). \tag{A6b}$$

Using these quantities, the survival probability of the excited donor state is calculated as

$$N(t) = \exp\left\{ - c \int_0^t j_I(t') dt' - t/\tau_D \right\} \tag{A7}$$

and the kinetics of the ground- and excited-state ion pairs,

$$P(t) = c \int_0^t [j_I(t') N(t') - j_R(t')] dt', \tag{A8}$$

$$P^*(t) = c \int_0^t [j_I^*(t') N(t') - j_R^*(t')] dt'. \tag{A9}$$

The numerical integration in Eqs. (A7) and (A8) is performed by the standard finite-difference methods.

[1] A. I. Burshtein, Adv. Chem. Phys. **114**, 419 (2000).
[2] A. I. Burshtein, J. Lumin. **93**, 229 (2001).
[3] A. A. Zharikov and A. I. Burshtein, J. Chem. Phys. **93**, 5573 (1990).
[4] V. Gladkikh, A. I. Burshtein, G. Angulo, S. Pagès, B. Lang, and E. Vauthey, J. Phys. Chem. A **108**, 6667 (2004).
[5] R. D. Coalson, D. G. Evans, and A. Nitzan, J. Chem. Phys. **101**, 436 (1994).
[6] M. Cho and R. J. Silbey, J. Chem. Phys. **103**, 595 (1995).
[7] S. Pagès, B. Lang, and E. Vauthey, J. Phys. Chem. A **108**, 549 (2004).
[8] L. D. Zusman, Chem. Phys. **49**, 295 (1980).
[9] A. I. Burshtein and B. I. Yakobson, Chem. Phys. **49**, 385 (1980).
[10] A. B. Helman, Chem. Phys. **65**, 271 (1982).
[11] J. N. Onuchic, J. Chem. Phys. **86**, 3925 (1986).
[12] I. Rips and J. Jortner, J. Chem. Phys. **87**, 6513 (1987).
[13] H. Sumi and R. A. Marcus, J. Chem. Phys. **84**, 4272 (1986); **84**, 4894 (1986).
[14] W. Nadler and R. A. Marcus, J. Chem. Phys. **86**, 3906 (1987).
[15] L. D. Zusman, Chem. Phys. **119**, 1988 (51).
[16] A. I. Burshtein and B. I. Yakobson, High Energy Chem. **14**, 211 (1981).
[17] H. Frauenfelder and P. G. Wolynes, Science **229**, 337 (1985).
[18] Y. Georgievski, A. I. Burshtein, and B. M. Chernobrod, J. Chem. Phys. **105**, 3108 (1996).
[19] A. I. Burshtein and A. G. Kofman, Chem. Phys. **40**, 289 (1979).
[20] G. C. Walker, E. Akesson, A. E. Johnson, N. E. Levinger, and P. F. Barbara, J. Phys. Chem. **96**, 3728 (1992).
[21] M. Tachiya and S. Murata, J. Am. Chem. Soc. **116**, 2434 (1994).
[22] J. Najbar, R. C. Dorfman, and M. D. Fayer, J. Chem. Phys. **94**, 1081 (1991).
[23] A. I. Ivanov and V. V. Potovoi, Chem. Phys. **247**, 1999 (245).
[24] A. I. Burshtein, Chem. Phys. Lett. **194**, 247 (1992).
[25] R. C. Dorfman and M. D. Fayer, J. Chem. Phys. **96**, 7410 (1992).
[26] J. Jortner and M. Bixon, J. Chem. Phys. **88**, 167 (1988).
[27] S. A. Passino, Y. Nagasawa, and G. R. Fleming, J. Phys. Chem. A **101**, 725 (1997).
[28] F. Schael and H.-G. Löhmansröben, J. Photochem. Photobiol., A **105**, 317 (1997).
[29] M. G. Kuzmin, I. V. Soboleva, E. V. Dolotova, and D. N. Dogadkin, Photochem. Photobiol. Sci. **2**, 967 (2003).
[30] A. V. Barzykin, P. A. Frantsuzov, K. Seki, and M. Tachiya, Adv. Chem. Phys. **123**, 511 (2002).
[31] O. Nicolet and E. Vauthey, J. Phys. Chem. A **106**, 5553 (2002).
[32] S. F. Swallen, K. Weidemaier, and M. D. Fayer, J. Chem. Phys. **104**, 2976 (1996).
[33] A. I. Burshtein, Adv. Chem. Phys. **129**, 105 (2004).
[34] A. I. Burshtein, J. Chem. Phys. **103**, 7927 (1995).
[35] A. A. Kornyshev and J. Ulstrup, Chem. Phys. Lett. **126**, 74 (1986).
[36] M. A. Vorotyntsev and A. A. Kornyshev, *Electrostatics of a Medium with the Spatial Dispersion* (Nauka, Moscow, 1993).
[37] A. I. Burshtein, I. V. Khudiakov, and B. I. Yakobson, Prog. React. Kinet. **13**, 221 (1984).
[38] S. V. Feskov, A. I. Ivanov, and A. I. Burshtein, J. Chem. Phys. **122**, 124509 (2005).
[39] H. Torieda, K. Nozaki, A. Yoshimura, and T. Ohno, J. Phys. Chem. A **108**, 4819 (2004).
[40] D. J. Bicout and A. Szabo, J. Chem. Phys. **109**, 2325 (1997).
[41] R. G. Fedunov, S. V. Feskov, A. I. Ivanov, O. Nicolet, S. Pagès, and E. Vauthey, J. Chem. Phys. **121**, 3643 (2004).

PCCP

Quantum yields of singlet and triplet recombination products of singlet radical ion pairs

V. S. Gladkikh,[a] A. I. Burshtein,[a] G. Angulo[b] and G. Grampp[b]

[a] *Weizmann Institute of Science, Rehovot 76100, Israel*
[b] *Graz University of Technology, Institute of Physical and Theoretical Chemistry, Graz, Austria*

Received 24th January 2003, Accepted 7th April 2003
First published as an Advance Article on the web 23rd May 2003

The efficiencies of contact geminate recombination to either the ground or excited triplet state of neutral products are calculated for contact and remote starts of radical ion pairs initially created in the singlet state. Considering the spin-conversion in this pair as a stochastic process with given rate, the diffusional dependence of recombination and charge separation yields and corresponding efficiencies are specified. This is compared with the experimental data obtained for photo-excited perylene quenched by aromatic amines in dimethyl sulfoxide–glycerol mixtures, which allow for a wide variation of solvent viscosity with composition. The successful fitting of the theory to non-trivial viscosity dependences confirms that the spin-forbidden recombination is composed of two sequential stages. Considering that the radical-ion pair is created in the singlet state, the spin conversion should precede its recombination to the excited triplet product.

1 Introduction

Radical Ion Pairs (RIPs) are created in either the singlet or triplet state depending on the precursors which are excited singlet or triplet donor (^{1}D or ^{3}D) and charge acceptor A in the bulk. The ion pairs $[D^+\cdots A^-]$ can be either separated by diffusion producing free ions or recombine to give either the ground or excited triplet state of the neutral product. The ruthenium tris-bipyridine complex quenched by methylviologen (MV^{2+}) is so far is the most thoroughly studied reaction of this sort:[1–5]

$$\begin{array}{l}\left(^3Ru^{2+}\right)^* + MV^{2+} \xrightarrow{W_L} {}^3\left[\dot{R}u^{3+}\ldots\dot{M}V^{+}\right] \rightarrow {}^2\dot{R}u^{3+} + {}^2\dot{M}V^{+} \\ \qquad\qquad k_s \downarrow\uparrow 3k_s \\ \qquad\qquad {}^1\left[\dot{R}u^{3+}\ldots\dot{M}V^{+}\right] \rightarrow {}^2\dot{R}u^{3+} + {}^2\dot{M}V^{+} \\ \qquad\qquad \Downarrow W_S \\ \qquad\qquad {}^1\left[Ru^{2+}\ldots MV^{2+}\right]\end{array} \qquad (I)$$

This reaction scheme can be generalized and formalized as follows:

$$\begin{array}{l} \qquad\qquad\quad D^+ + A^- \\ \qquad\qquad\quad \nearrow\ \bar{\varphi}\ \nwarrow \\ {}^3D^* + A \xrightarrow{W_L} {}^3[D^+\ldots A^-] \underset{3k_s}{\overset{k_s}{\rightleftharpoons}} {}^1[D^+\ldots A^-] \\ \downarrow\tau \qquad\qquad\qquad\qquad \Downarrow W_S \\ D \qquad\qquad\qquad\qquad [D\ldots A]\end{array} \qquad (1.1)$$

There is a single channel of charge recombination: only to the ground state with the rate W_S. This competes with the diffusional separation of RIP from both the singlet and triplet states which has a yield $\bar{\varphi} = (1 + Z/\tilde{D})^{-1}$ expressed through the recombination efficiency Z and encounter diffusion coefficient $\tilde{D} = D_{D^+} + D_{A^-}$.[5–7]

The sum of the yields of the neutral and charged reaction products is evidently 1,

$$\bar{\varphi}_s + \bar{\varphi} = \frac{Z}{\tilde{D}+Z} + \frac{\tilde{D}}{\tilde{D}+Z} = 1, \qquad (1.2)$$

and $Z/\tilde{D}$ is a single parameter of the problem. It was studied as a function of the free energy of recombination, encounter diffusion and spin conversion responsible for the magnetic field effects.[4,6–8]

Much less study has been done for RIPs having a singlet precursor. Although this situation is more often studied than the case of RIPs with triplet precursors, it is rarely investigated as a function of viscosity. There are only a few studies where the forward transfer was investigated in solvents of different viscosities[9–11] and similarly only a few studies where backward transfer was also investigated.[12,13] The system studied in this work is perylene (Per) quenched by aromatic amines (D):

$$\begin{array}{l}Per^* + D \Rightarrow \ [\dot{P}er^- \ldots D^+] \ \rightarrow \dot{P}er^- + \dot{D}^+ \\ \qquad\qquad\quad \Downarrow \\ \qquad\qquad\quad [Per\ldots D]\end{array} \qquad (II)$$

This reaction can be represented by the following comprehensive scheme:

$$\begin{array}{lllll} & A^- & + & D^+ & \\ & \nearrow & \bar{\varphi} & \nwarrow & \\ {}^1A^* + D \xrightarrow{W_L} & {}^1[A^-\ldots D^+] & \underset{k_s}{\overset{3k_s}{\rightleftharpoons}} & {}^3[A^-\ldots D^+]. & \\ \downarrow\tau & \Downarrow W_S & & \Downarrow W_T & \\ A & [A\ldots D] & & [{}^3A^*\ldots D] & \end{array} \qquad (1.3)$$

Now we have two parallel channels of geminate recombination: to the singlet (ground) and triplet (excited) states and should discriminate between their efficiencies, Z_S and Z_T which contribute to the total

$$Z = Z_S + Z_T. \qquad (1.4)$$

Correspondingly, there are three terms in the quantum yield balance instead of only two as in eqn. (1.2):

$$\bar{\varphi}_t + \bar{\varphi}_s + \bar{\varphi} = \frac{Z_T}{\tilde{D}+Z} + \frac{Z_S}{\tilde{D}+Z} + \frac{\tilde{D}}{\tilde{D}+Z} = 1. \qquad (1.5)$$

The presence of the triplet channel of geminate recombination was first recognized by Weller *et al.* and the existence of the excited triplet products was experimentally proved.[14,15] The RIP recombination through a triplet channel assumed in ref. 16 allowed an explanation of the non-trivial charge accumulation and geminate recombination kinetics studied in ref. 17. Later on not only the value but also the viscosity dependence of $\bar{\varphi}_t$ became experimentally available.[13] Having at hand two independent components of eqn. (1.5), $\bar{\varphi}_t$ and $\bar{\varphi}$, one can easily obtain two corresponding recombination parameters,

$$Z_T = \tilde{D}\frac{\varphi_t}{\bar{\varphi}} \quad \text{and} \quad Z = \tilde{D}\left(\frac{1}{\bar{\varphi}} - 1\right), \tag{1.6}$$

as well as the third , $Z_S = Z - Z_T$. The main goal of the present article is to specify the diffusional dependence of all three of these.

In spin-less theory there is a single recombination parameter $Z(D)$ which was investigated in refs. 5 and 6. There it was shown that contact geminate reactions can be subdivided into kinetic and diffusion controlled reactions provided the initial separation of radical ions, r, essentially exceeds the contact distance σ where recombination takes place. At small $\tilde{D}$ the geminate recombination is under diffusion control and its efficiency increases linearly with $\tilde{D}$ but then saturates and approaches the kinetic limit $qz = \lim_{\tilde{D}\to\infty} Z$ which is viscosity independent. In highly polar solvents

$$q = \sigma/r, \quad \text{and} \quad z = k_{-et}\sigma^2/3 = k_c/4\pi\sigma, \tag{1.7}$$

where k_{-et} is the recombination rate of the so-called Exponential Model (EM) easily related to the kinetic rate constant of contact bimolecular recombination, k_c.[5] In the EM, $Z \equiv z =$ const. everywhere because the model assumes that ions not only recombine but that this also starts from contact (that is $r = \sigma$). For electron transfer this is rarely the case because ions can be created at larger distances especially when ionization is under diffusion control.[5,18,19]

There is also an extension of the EM for a two channel reaction (II).[20,21] The yields of triplets and separated ions are represented as follows:

$$\varphi_t = \frac{k_{isc}}{k_{sep} + k_{-et} + k_{isc}}, \quad \varphi = \frac{k_{sep}}{k_{sep} + k_{-et} + k_{isc}}, \tag{1.8}$$

where k_{sep} is the EM rate of ion separation. The only difference from a single-channel EM is the substitution of k_{-et} by the sum of the spin-allowed and spin-forbidden transfer rates $k_{-et} + k_{isc}$, to the ground and to the triplet state, respectively. Like k_{-et} the inter-system crossing rate k_{isc} does not depend on viscosity. Moreover, EM does not recognize two different steps of the forbidden transition: spin-conversion to the triplet RIP and subsequent allowed electron transfer into the triplet product.[20–24] However, it has been shown already that one should discriminate between spin conversion and subsequent recombination even in the case of a single channel but spin-forbidden reaction (I).[25] The simplest (stochastic) model of spin-conversion implies that it proceeds with the rate k_s from the triplet to singlet and with rate $3k_s$ from the singlet to triplet. Within this model implemented into unified theory not only the magnetic field effect was estimated[25] and compared with a real one,[4] but also exciplex formation and dissociation was studied[26–28] as well as chemiluminescence.[29] In most instances, the backward electron transfer was assumed to be contact:

$$W_S = \frac{k_c^S}{4\pi\sigma^2}\delta(r-\sigma), \quad W_T = \frac{k_c^T}{4\pi\sigma^2}\delta(r-\sigma). \tag{1.9}$$

The incoherent spin-conversion and contact recombination were also assumed when the two-channel reaction (II) was considered by means of Integral Encounter Theory (IET).[30,31] However, the goal of these studies was to determine the free energy dependence of the forward and backward electron transfer rather than the diffusional dependence of the quantum yields and recombination efficiencies which are of the most interest here. Using the conventional Green function formalism the efficiencies of singlet and triplet RIP recombination will be calculated and compared relative to each other. The qualitative difference between spin-allowed and spin-forbidden recombination will be established as well as the crucial dependence of both on the rate of spin conversion.

The outline of this paper is as follows. In the next section we will present the general expression for singlet and triplet recombination efficiencies, Z_S and Z_T. In section 3 they will be specified assuming contact creation of the radical-ion pair in addition to their contact recombination. In section 4 the results will be reconsidered allowing the distant production of RIP in the course of diffusion controlled ionization. In section 5 we present the fitting of real data with our model. The results will be summarized in Conclusions.

2 Recombination efficiencies of singlet and triplet channels

Rearranging eqn. (1.6) we can obtain the uniform definitions for the singlet and triplet efficiencies:

$$Z_T = \tilde{D}\frac{\bar{\varphi}_t}{\bar{\varphi}} \quad \text{and} \quad Z_S = \tilde{D}\frac{\bar{\varphi}_s}{\bar{\varphi}}, \tag{2.1}$$

where the relationships (1.4) and (1.5) hold as before and all quantum yields are averaged over the normalized initial distribution of RIPs produced by bimolecular ionization:[5–7]

$$\bar{\varphi} = \int \varphi(r) f_0(r) \mathrm{d}^3 r, \quad \bar{\varphi}_s = \int \varphi_s(r) f_0(r) \mathrm{d}^3 r,$$
$$\bar{\varphi}_t = \int \varphi_t(r) f_0(r) \mathrm{d}^3 r. \tag{2.2}$$

The general solution of the problem can be deduced from results obtained in refs. 5 and 25. There we considered the exciplex formation from RIPs experiencing recombination to triplet and ground states. In that case, the singlet channel of recombination was composed of two parallel sub-channels: to the singlet exciplex (with the rate constant K) and the ground state (with another constant k_c^S). If the former is switched off we reduce the problem to the present one. Thus setting $K = 0$ in the total rate constant of the singlet RIP recombination $K^{\ddagger} = K + k_c^S \to k_c^S$ we obtain instead of eqns. (9.56) and (9.57) of ref. 5 the following quantum yield for RIP recombination to the ground state:

$$\varphi_s(r) = k_c^S \tilde{p}_{SS}(\sigma, r, 0)$$
$$= \frac{k_c^S}{k_c^S + k_D}\left\{\frac{\sigma}{r} - \tilde{p}_{ST}(\sigma, r, 0)\left(k_c^T + k_D\right)\right\}, \tag{2.3}$$

where $k_D = 4\pi\sigma\tilde{D}$ is the diffusional rate constant for the contact transfer and

$$\tilde{p}_{ST}(\sigma, r, 0) = 3\frac{\mathscr{J}(\sigma, r, 0)\left[1 + k_c^S/k_D\right] - \mathscr{J}(\sigma, \sigma, 0)\left[k_c^S/4\pi r\tilde{D}\right]}{1 + k_c^S/k_D + 3\left[k_c^T - k_c^S\right]\mathscr{J}(\sigma, \sigma, 0)}. \tag{2.4}$$

Here the spin sensitive quantity is defined as:

$$\mathscr{J}(\sigma, r, 0) \equiv k_s J(r, 0) = \frac{1 + \alpha - \mathrm{e}^{-\alpha(r-\sigma)/\sigma}}{16\pi r\tilde{D}(1 + \alpha + k_c^T/k_D)}, \tag{2.5}$$

where $\alpha = \sqrt{4k_s\sigma^2/\tilde{D}}$ is a measure of the spin-conversion during the encounter time $\tau_d = \sigma^2/\tilde{D}$. Substituting eqn. (2.5) into (2.4) we obtain the final and most general expression for the

Green function of the singlet to triplet transition in RIP:

$$\tilde{p}_{ST}(\sigma,r,0)=\frac{3\sigma}{4r}\frac{\alpha k_D+\left[1-e^{-\alpha(r-\sigma)/\sigma}\right](k_D+k_c^S)}{[k_D(1+\alpha)+k_c^T](k_D+k_c^S)+\frac{3}{4}\alpha k_D(k_c^T-k_c^S)}. \quad (2.6)$$

As follows from eqn. (9.60) of ref. 5, the quantum yield of the triplet recombination products of RIPs started from distance r is

$$\varphi_t(r)=k_c^T\tilde{p}_{ST}(\sigma,\ r,\ 0). \quad (2.7)$$

Correspondingly, the charge separation quantum yield is:

$$\varphi(r)=1-\frac{k_c^S/4\pi r\tilde{D}+(k_c^T-k_c^S)\tilde{p}_{ST}(\sigma,r,0)}{1+k_c^S/k_D}. \quad (2.8)$$

When $k_s=\alpha=0$, there is no triplet production: $\varphi_t\equiv 0$. As a result the two other yields coincide with their conventional EM analogs:

$$\varphi_t=0,\quad \varphi_s(r)=\frac{\sigma}{r}\frac{k_c^S}{k_c^S+k_D}=1-\varphi(r). \quad (2.9)$$

In the alternative limit $k_s=\alpha=\infty$ the complete equilibration of the spin states in RIP is immediately achieved, as follows from eqns. (2.6) and (2.7), (2.3):

$$\varphi_t=\frac{3\sigma}{4r}\frac{k_c^T}{k_D+\frac{1}{4}k_c^S+\frac{3}{4}k_c^T},$$
$$\varphi_s=\frac{\sigma}{r}\frac{k_c^S}{k_c^S+k_D}\left\{1-\frac{3}{4}\frac{k_c^T+k_D}{k_D+\frac{1}{4}k_c^S+\frac{3}{4}k_c^T}\right\}. \quad (2.10)$$

These values of quantum yields are quite different if one of the recombination channels is switched off:

$$\varphi_t=0,\quad \varphi_s=\frac{\sigma}{r}\frac{\frac{1}{4}k_c^S}{k_D+\frac{1}{4}k_c^S}\quad \text{at}\quad k_c^T=0 \quad (2.11a)$$

$$\varphi_t=\frac{\sigma}{r}\frac{\frac{3}{4}k_c^T}{k_D+\frac{3}{4}k_c^T},\quad \varphi_s=0\quad \text{at } k_c^S=0. \quad (2.11b)$$

The results are self-evident.

3 Contact start

This is the simplest case related mainly to atom transfer which is contact in both directions. When not only backward transfer is contact but also the forward transfer then RIPs are created only at $r=\sigma$. Thus, all the above formulae are greatly simplified. In particular eqn. (2.6) becomes the following:

$$\tilde{p}_{ST}(\sigma,\sigma,0)=\frac{3\alpha}{4[k_D(1+\alpha)+k_c^T](1+k_c^S/k_D)+3\alpha[k_c^T-k_c^S]}. \quad (3.1)$$

Using this result in eqns. (2.3), (2.7) and (2.8) we obtain all quantum yields and from them the recombination efficiencies (2.1):

$$\frac{Z_T}{\tilde{D}}=\frac{3\alpha/4}{1+y^T(1+\alpha)},\quad \frac{Z_S}{\tilde{D}}=\frac{1}{y^S}\left[1-\frac{3\alpha/4}{1+y^T(1+\alpha)}y^T\right], \quad (3.2)$$

where $y^S=k_D/k_c^S$ and $y^T=k_D/k_c^T$.

If $k_s=0$ then we return back to a particular case (2.9) with zero triplet production and $Z/\tilde{D}=Z_S/\tilde{D}=k_c^S/k_D$. If the recombination to triplet product is not possible due to some other reason (*e.g.* unfavorable free energy balance making $k_c^T=0$) then, again, we have no triplet production but the recombination to the ground state is affected by spin-conversion:

$$Z_T=0,\quad \frac{Z_S}{\tilde{D}}=\frac{k_c^S}{k_D}\frac{1+\alpha/4}{1+\alpha}=\frac{Z}{\tilde{D}}\quad \text{at } k_c^T=0. \quad (3.3)$$

This case is identical to the previous one only at zero spin conversion ($k_s=0$). Otherwise, the transition from the singlet to triplet RIP makes the latter unable to recombine, thus favoring the charge separation. Therefore Z decreases with k_s to 1/4 of the initial value and correspondingly increases the quantum yield of separated radical ions. The similar difference between slow and fast spin mixing was obtained in ref. 32 using a coherent Δg mechanism of spin conversion.

Conversely, when the decay of the RIPs to the ground state is switched off, then the spin-conversion facilitates their recombination by opening the triplet channel:

$$\frac{Z_T}{\tilde{D}}=\alpha\frac{\frac{3}{4}k_c^T}{k_D(1+\alpha)+k_c^T}=\frac{Z}{\tilde{D}},\quad Z_S=0\quad \text{at } k_c^S=0. \quad (3.4)$$

At $k_s=\infty$ we have from the general formulae (3.3) and (3.4) correspondingly:

$$\text{(a)}\quad \frac{Z^{min}}{\tilde{D}}=\frac{1}{4}k_c^S/k_D,\quad \text{or (b)}\quad \frac{Z^{max}}{\tilde{D}}=\frac{3}{4}k_c^T\Big/k_D. \quad (3.5)$$

Here both the recombination rates appear with their equilibrium weights and in full accordance with eqn. (2.11). In Fig. 1 the recombination efficiencies for single channel recombination, be it a singlet (Z_S) or triplet one (Z_T), are shown as functions of k_s at a fixed diffusion constant k_D.

The situation is qualitatively different when the spin conversion efficiency $\alpha=\sqrt{4k_s\sigma^2/\tilde{D}}$ changes due to the diffusion (viscosity) variation instead of k_s variation. This is not a hypothetical situation like the previous one, but rather a feasible possibility that has been realized experimentally a number of times.[3,4,12,13] The principal difference lies in the fact that the diffusion changes not only α but $k_D=4\pi\sigma\tilde{D}$ as well. This does not affect

$$Z_S=z_s\frac{1+\alpha/4}{1+\alpha},\quad z_s=k_c^S/4\pi\sigma, \quad (3.6)$$

which is a universal function of α, but makes the shape of $Z_T(1/\sqrt{\tilde{D}})$ different from that of $Z_T(\sqrt{k_s})$ (Fig. 2). As a function of $\tilde{D}$, Z_T passes through a maximum being zero at

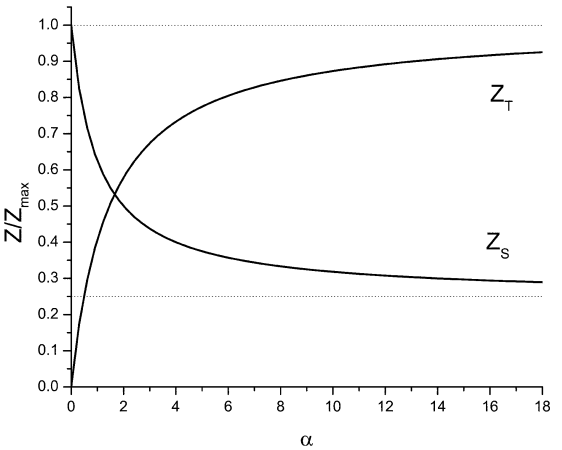

Fig. 1 The variation of the efficiencies of single channel recombination (normalized to their maxima) with spin-conversion rate given by $\alpha=\sqrt{4k_s\sigma^2/\tilde{D}}$ at $\sigma=7$ Å and fixed $\tilde{D}=20$ Å^2 ns^{-1}. The contact recombination constant $k_c=800$ Å^3 ns^{-1} is taken to be the same for both reaction channels.

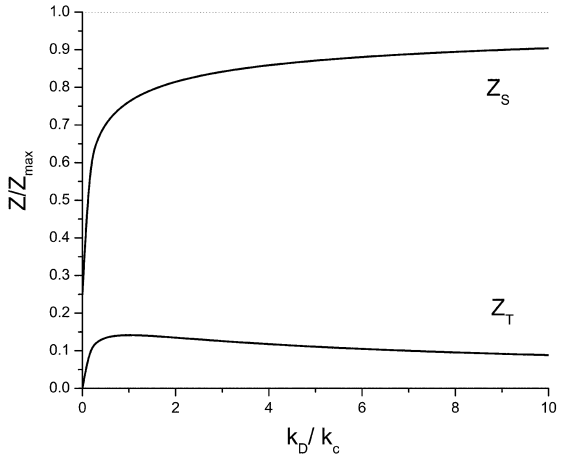

Fig. 2 Diffusional (viscosity) dependence of recombination efficiencies of single channel reactions which proceed through singlet (Z_S) or triplet (Z_T) transfer channels at fixed $k_s = 0.01$ ns^{-1}. Other parameters are as for Fig. 1.

$\tilde{D} \to 0$ as well as at $\tilde{D} \to \infty$:

$$Z_T = \frac{3}{4} z_t \frac{\sqrt{k_c^T \kappa k_D}}{k_c^T + \sqrt{k_c^T \kappa k_D} + k_D}, \quad z_t = k_c^T/4\pi\sigma, \tag{3.7}$$

where $\kappa = \alpha^2 k_D/k_c^T = 16\pi\sigma^3 k_s/k_c^T$. This is exactly the same formula as (8.38) in ref. 5 that was obtained for the recombination to the ground state of triplet born RIP,[5,25] except that k_c^T is substituted for k_c^S and the triplet statistical weight (3/4) is substituted for the singlet one (1/4). An exhaustive explanation of the non-trivial extremal behavior of Z with diffusion was given in Section VII F of the same review.[5] It originates from the extremal behavior of the survival time t_e of RIPs which limits the spin conversion but is not identical to the encounter time. For the contact born RIPs it turns to zero not only in the fast but also in the slow diffusion limit.[5,33] That is why $Z_T \to \frac{3}{4}\alpha\tilde{D} \to 0$ as $\tilde{D} \to 0$ while the quantum yield of triplets,

$$\varphi_t = \frac{Z_T}{Z_T + \tilde{D}} \to \frac{3\alpha}{3\alpha + 4} \to 1 \tag{3.8}$$

tends towards 1 as $\alpha \to \infty$ (Fig. 3).

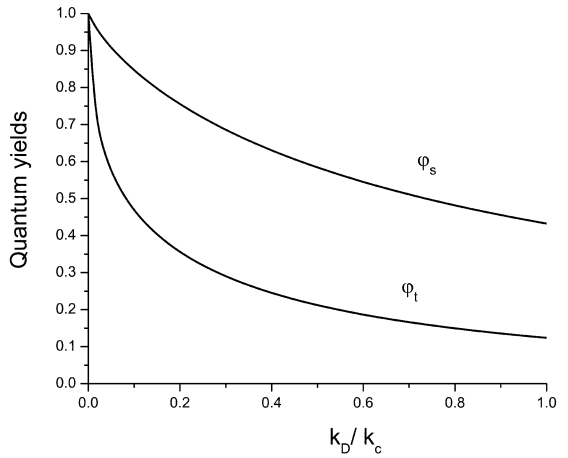

Fig. 3 Quantum yields of single-channel recombination through singlet (φ_s) or triplet (φ_t) RIPs. Other parameters are as for Fig. 1.

Much more complex is the two-channel reaction that is the situation when both recombination rates are non-zero. It is instructive to consider it when recombination through both reaction channels proceeds with the same transfer rate: $k_c^S = k_c^T = k_c$. In this case, which is halfway between the two previous cases, the spin conversion does not affect the total recombination rate but only the relationship between the singlet and triplet channels. Their recombination efficiencies obtained from eqn. (3.2) are different:

$$\frac{Z_T}{\tilde{D}} = \frac{3\alpha/4}{1 + y(1+\alpha)} = \frac{1}{y} - \frac{Z_S}{\tilde{D}}, \tag{3.9}$$

where $y = k_D/k_c$. This asymmetry is caused by the initial conditions promoting singlet RIPs. It has far reaching consequences for the viscosity dependence of both $Z_S(\tilde{D})$ and $Z_T(\tilde{D})$, but not

$$Z = Z_S(0) = k_c/4\pi\sigma = z. \tag{3.10}$$

Since not only $Z_S(0) = z$ but $Z_S(\infty) = z$ as well, the curve $Z_S(\tilde{D})$ has a minimum which appears exactly at the same argument $\tilde{D}_e = z$, where the maximum of $Z_T(\tilde{D})$ is located (Fig. 4). The height of the latter is higher the larger is k_s:

$$Z_T^{max} = \frac{3}{2} z \frac{\sqrt{k_s\sigma^2/z}}{1 + 2\sqrt{k_s\sigma^2/z}} \le \frac{3}{4} Z. \tag{3.11}$$

This quantity becomes equal to the minimal value of Z_S when the rate of spin-conversion equals the rate of recombination, $k_s = z/\sigma^2$, that is

$$Z_T = Z_S = Z/2, \quad \text{when} \quad k_s = k_c/4\pi\sigma^3 = k_{-et}/3. \tag{3.12}$$

It is also instructive to compare the diffusional dependence of the corresponding quantum yields shown in Fig. 5. This monotonously increases with diffusion, $\varphi = \tilde{D}/(\tilde{D} + Z)$, and has exactly the same shape as in the exponential model because according to eqn. (3.10) $Z = z = \text{const}$. The yield of recombination to the singlet products, $\varphi_s = Z_S/(\tilde{D} + Z)$, has quite the opposite dependence, because Z_S is approximately constant as far as it does not deviate essentially from Z. However, the yield of triplet products is non-monotonous. At high diffusion φ_t decreases as φ_s and for the same reason: the fast separation of radicals prevent them from recombining. However, at slow diffusion $Z_T \to (3\alpha/4)\tilde{D}$ and

$$\varphi_t = \frac{Z_T}{Z_T + Z_S + \tilde{D}} \to \frac{3\alpha\tilde{D}}{3\alpha\tilde{D} + 4Z + 4\tilde{D}} \to 0, \tag{3.13}$$

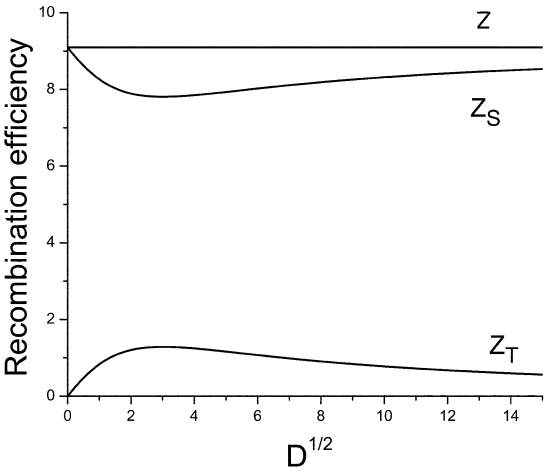

Fig. 4 Diffusional dependence of singlet and triplet recombination efficiencies at equal rates of parallel recombination channels ($k_c^S = k_c^T = k_c = 800$ Å^3 ns^{-1}, $k_s = 0.01$ ns^{-1}).

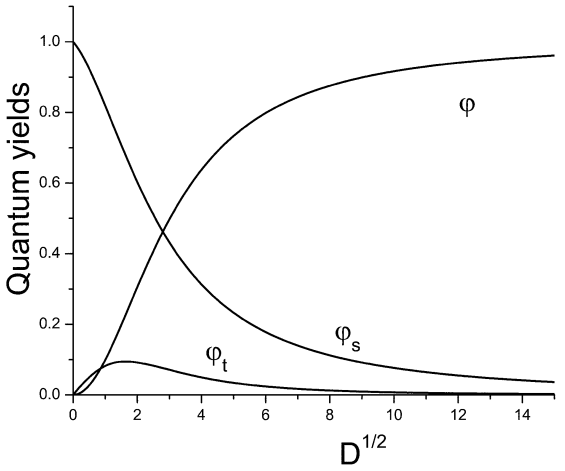

Fig. 5 Quantum yields corresponding to efficiencies shown in previous figures as functions of diffusion given in units $Å^2\ ns^{-1}$.

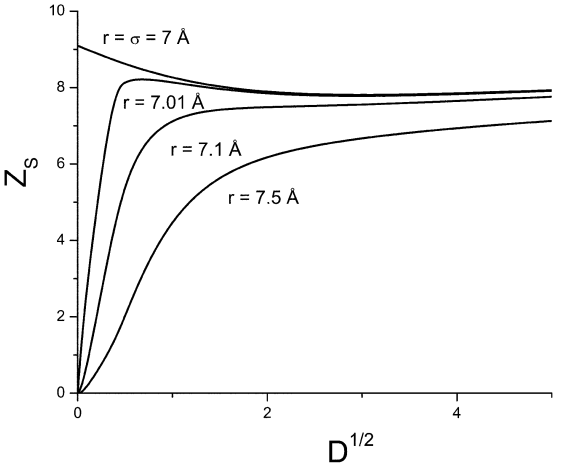

Fig. 6 The singlet efficiency of double-channel recombination for different initial separations of the RIP r ($\sigma = 7$ Å). Other parameters are as for Fig. 1

resembles the φ behavior. The extremal diffusional dependence of this yield was discovered by Schultens who solved the same problem (of "spin-independent recombination", $k_c^S = k_c^T$) assuming that coherent spin-conversion is separable from the inter-particle dynamics.[34] Their Fig. 5 is qualitatively similar to our Fig. 5 although the latter relates to incoherent spin conversion.

4 Non-contact start

When the ionization is due to remote electron transfer the radical ions in a pair can be created far from each other provided the reaction is under diffusion control. This is accounted for by setting the initial separation $r > \sigma$ in our general formulae (2.3), (2.4) and (2.5). However, the recombination carried out by the backward electron transfer is also remote especially as it is usually highly exergonic.

Nonetheless, the contact recombination must not be completely ruled out. Sometimes the backward charge transfer can be conducted by proton transfer resulting in production of two neutral radicals. Such recombinations were the subject of a few time-resolved investigations[35–37] and a theoretical study of neutral radical accumulation after photoionization.[38] Here we will concentrate only on the quantum yield of them which is $\varphi_s(r)$ because the radicals are the products of the contact recombination of the singlet RIP initially separated by distance r.

In such a case the geminate recombination is subdivided into either kinetic or diffusional. In the spin-less theory the latter appears from the general eqn. (2.9) at $\tilde{D} \to 0$:[5,6]

$$\lim_{\tilde{D}\to 0} \varphi_s(r) = \frac{\sigma}{r}, \quad Z = Z_S = \frac{\sigma}{r-\sigma}\tilde{D}. \tag{4.1}$$

Even if spin-conversion is present in the diffusional limit it is so strong that one can address the alternative eqns. (2.11) and (2.12). It follows from these equations that the result for Z is the same regardless of what recombination channel is working:

$$\lim_{\tilde{D}\to 0} \varphi_s(r) = \lim_{\tilde{D}\to 0} \varphi_t(r) = \frac{\sigma}{r} = 1 - \lim_{\tilde{D}\to 0} \varphi(r).$$

Due to complete equilibration of reactive and inactive states the result remains the same at any recombination rates as long as recombination is limited by diffusion and not by reaction. Nothing is changed even if both channels are working with equal rates ($k_c^S = k_c^T = k_c$):

$$\varphi_t + \varphi_s = 1 - \varphi = \frac{\sigma}{r}\frac{k_c}{k_D + k_c} \quad Z = \frac{qz}{1 + (1-q)z/\tilde{D}}, \tag{4.2}$$

where $q = \sigma/r$ and $z = k_c/k_D$. This is the straightforward extension of the spin-less result of eqn. (5.19) in ref. 5 to a double-channel reaction. The linear increase of Z_S with $\tilde{D}$ is a general feature of any reaction when diffusion is the slowest process: $\tilde{D} \ll (r/\sigma - 1)z$.

However, the presence of spin conversion makes the situation more complex. Diffusion not only facilitates the delivery of singlet pairs to the contact but also controls their conversion into triplets. At close starts these two opposite tendencies lead to the non-monotonic behavior of $Z_S(\tilde{D})$. Initially, the effect of a remote start dominates and Z_S increases with diffusion but then it turns down copying the behavior inherent to the contact start: it passes through the minimum and approaches the kinetic plateau $Z_S = Z$ (Fig. 6). With increasing starting distance the difference between the maximum and minimum decreases until it disappears completely.

Since the non-monotonous diffusional dependence $Z(\tilde{D})$ takes place at too short initial separations, smaller than the real tunnelling length $L \sim 1$ Å, it is only of heuristic interest. Contact approximation is hardly applicable to such a case and should be replaced by the theory of remote recombination. At faster diffusion and/or larger initial separations, Z_S increases monotonously with $\tilde{D}$, as well as in the spin-less theory.[5,6]

Not less dramatic changes happen to φ_t when the starting separation of RIP is too small (Fig. 7). In the case of double-channel recombination with equal rates we obtain from eqns. (2.6) and (2.7):

$$\varphi_t(r) = \frac{3\alpha}{4r}\frac{k_c}{k_c + (1+\alpha)k_D}\left[\frac{\alpha k_D}{k_D + k_c} + 1 - e^{-\alpha(r-\sigma)/\sigma}\right]. \tag{4.3}$$

This equation describes the rapid initial decrease of $\varphi_t(r)$ with diffusion from its maximal value $3\sigma/4r$. It is represented by descending branches of the curves depicted in Fig.7. The lowest of them passing through the minimum approach the lower bell shaped curve related to the contact start. The curves related to larger initial separations do the same but at faster diffusion.

When

$$\tilde{D} \gg \tilde{D}_0 = 4k_s(r-\sigma)^2, \tag{4.4}$$

then in the first order approximation in α it follows from eqns. (2.3), (2.7) and (2.8) that

$$\varphi_s(r) = \frac{k_c^S}{k_c^S + k_D}\left\{\frac{\sigma}{r} - \frac{3\alpha\left[1 + k_c^S/k_D - k_c^S/4\pi r\tilde{D}\right]}{4\left(1 + k_c^S/k_D\right)}\right\}, \tag{4.5}$$

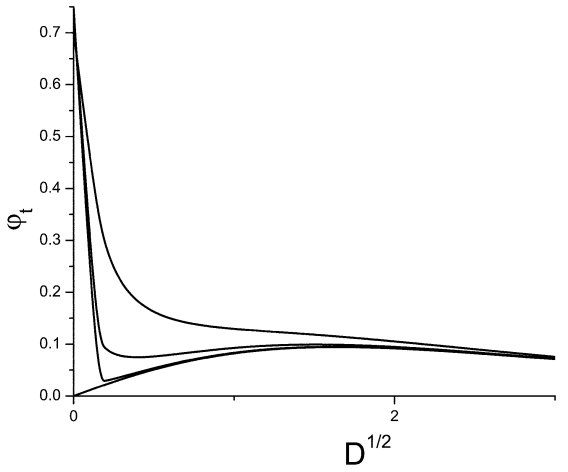

Fig. 7 The yield of triplet products for the same non-contact starts as in the previous figure: $r = 7$, 7.01, 7.1, 7.5 Å (from bottom to top).

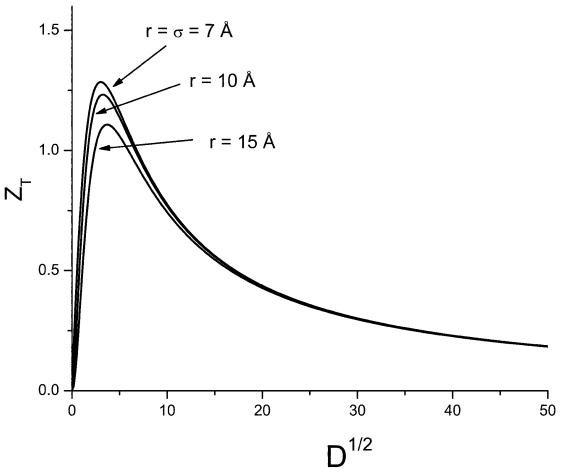

Fig. 8 The triplet efficiency of double-channel recombination with equal rates at non-contact starts.

$$\varphi_t(r) = k_c^T \frac{3\alpha\left[1 + k_c^S/k_D - k_c^S/4\pi r\tilde{D}\right]}{4\left(1 + \alpha + k_c^S/k_D\right)\left(k_D + k_c^T\right)}, \qquad (4.6)$$

and

$$\varphi(r) = 1 - \frac{1}{1 + k_c^S/k_D} \times \left\{ \frac{k_c^S}{4\pi r\tilde{D}} + \frac{3\alpha\left(k_c^T - k_c^S\right)\left[1 + k_c^S/k_D - k_c^S/4\pi r\tilde{D}\right]}{4\left(k_D + k_c^T\right)\left(1 + k_c^S/k_D\right)} \right\}. \qquad (4.7)$$

For the example of double-channel recombination with $k_c^S = k_c^T = k_c$ we have:

$$\varphi_t(r) = \frac{3\alpha}{4}\frac{z}{z + \tilde{D}(1+\alpha)}\varphi(r), \quad \varphi(r) = \frac{\tilde{D} + (1-q)z}{z + \tilde{D}}, \qquad (4.8)$$

where $z = k_c/4\pi\sigma$ and $q = \sigma/r$ as above. According to definitions (1.6)

$$Z_T = \frac{3\alpha}{4}\frac{z\tilde{D}}{z + \tilde{D}(1+\alpha)}, \quad Z = \frac{qz}{1 + (1-q)z/\tilde{D}}. \qquad (4.9)$$

The latter expression is exactly the same as in eqn. (4.2) while the former does not depend on $q = \sigma/r$ at all and coincides with that derived for the contact start in eqn. (3.2).

Moreover, the efficiency of triplet production for remote starts weakly depends on the initial conditions everywhere but especially when condition (4.4) is met (Fig. 8). When $\sqrt{\tilde{D}}$ is much larger then $\sqrt{\tilde{D}_0}$ the triplet efficiency for any starting distance approaches the contact one. Unlike Z_S which is saturated in this region, Z_T passes through the maximum and turns to zero as $\tilde{D} \to \infty$.

Although $Z = Z_S + Z_T$, it is not affected as much as both constituents when fast spin-conversion gives way to slow spin-conversion with an increase of $\tilde{D}$. The total Z simply grows monotonously within the diffusion controlled region and approaches the kinetic plateau qz as $\tilde{D} \to \infty$ (Fig. 9). The latter is lower the larger the initial separation of RIPs.

5 Fitting experimental data

Experimentally the quenching of perylene (Per) by dimethylaniline was studied in dimethyl sulfoxide–glycerol mixtures which allow for a wide variation of solvent viscosity with composition, without changing any other physical properties.[12]

The quantum yields, $\bar{\varphi}$ and $\bar{\varphi}_t$, were obtained through measured transient absorption of the Per radical anion and Per triplet state in solutions of different viscosity, η (Table 1). The efficiencies of recombination to the ground and triplet states of the products were calculated from eqn. (2.1) and were plotted as functions of the encounter diffusion coefficient of the radical ions (Fig. 10).

Assuming that ions have the same diffusion coefficients as the corresponding neutral particles, $D_+ = D_D$ and $D_- = D_A$ were estimated through the Stokes–Einstein relationship corrected by Spernol and Wirtz:[39]

$$D_X = \frac{k_B T}{f_X 6\pi\eta r_X}. \qquad (5.1)$$

Here X is either D or A, the solvent radius $r_s = 2.5$ Å and the correcting factor

$$f_X = \left[0.16 + 0.4\frac{r_X}{r_s}\right]\left(0.9 + 0.4\tilde{T}_X - 0.25\tilde{T}_s\right)$$

is expressed through the reduced temperature $\tilde{T} = \dfrac{T - T_f}{T_b - T_f}$, where T_f and T_b are the freezing and boiling temperatures, and $\tilde{T}_s$ is also the reduced temperature but for solvent. The calculated values of the encounter diffusion coefficient, $\tilde{D} = D_+ + D_-$, are listed in Table 1.

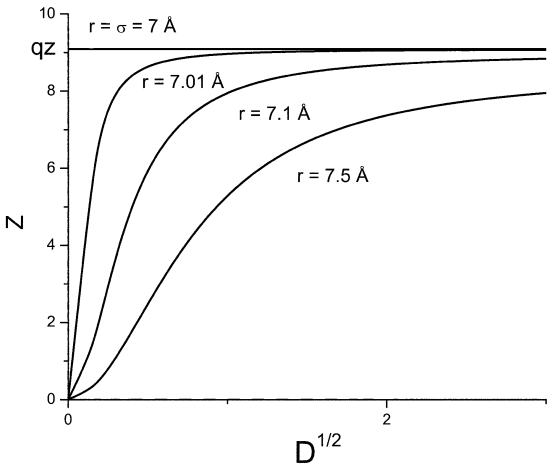

Fig. 9 The total efficiency of double-channel recombination with equal rates at contact (horizontal line) and remote starts.

Table 1 Experimental quantum yields and $\tilde{D}$ calculated from η

η/cP	$10^7\tilde{D}$/cm^2 s^{-1}	φ	φ_t
2.25	136	0.279	0.271
5.28	58.3	0.109	0.144
9.64	31.9	0.061	0.103
16.32	18.9	0.036	0.103
31.46	9.81	0.020	0.099
48.00	6.42	0.014	0.116
57.41	5.37	0.011	0.101
66.64	4.63	0.011	0.108
74.75	4.13	0.011	0.090
82.42	3.74	0.010	0.105
92.99	3.32	0.009	0.097
101.05	3.05	0.008	0.077
117.54	2.63	0.008	0.105
137.22	2.25	0.006	0.095

The theoretical curves shown in Fig. 10 were obtained in contact approximation, using initial RIP separation r as a fitting parameter in line with k_c^S, k_c^T and k_s. At such a rough fitting the agreement obtained is rather good except for the final points at the highest diffusion. This is not a surprise because the efficiency of recombination to the ground state in this system was studied earlier and recognized to be anomalous.[8,12] It passes through a maximum and decreases when diffusion accelerates. This effect was attributed to non-contact recombination. At fast diffusion ionization is under kinetic control so that ions are born near the contact, inside the reaction layer for recombination to the ground state. The latter is rather extended or even shifted out of contact when reaction occurs in the Marcus inverted region due to high exergonicity of recombination. As a result, the recombination efficiency is hindered by diffusion that helps ions to cross the reaction layer sooner. This effect was completely lost here because the recombination was assumed contact throughout.

This is even more true for the quantum yields shown in Fig. 11. Here again only the final points are essentially deviating from the theoretical curves. Only taking into account the non-contact character of recombination to the ground state can bend the upper curve and direct it to the lowest point. As soon as the last Z_S turns smaller, both $\varphi = \tilde{D}/[\tilde{D}+Z_T+Z_S]$ and $\varphi_t = Z_T/[\tilde{D}+Z^T+Z_S]$ have to increase correspondingly making the total agreement better.

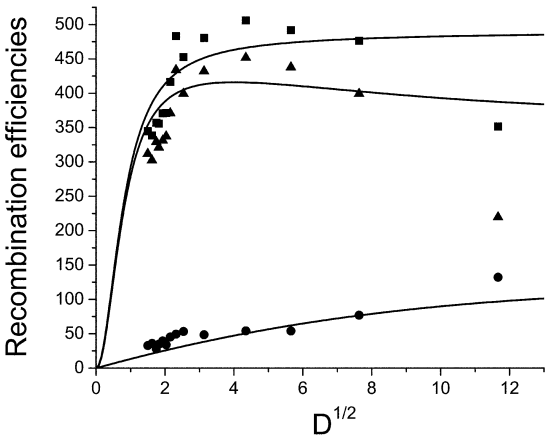

Fig. 10 Experimental efficiencies of recombination to ground (triangles) and triplet (circles) products as well as the total (squares), fitted with our theory of contact recombination from a remote start $r = 7.51$ Å, at $k_s = 1.5$ ns^{-1} and following recombination rates: $k_c^S = 4.5 \times 10^4$ Å^3 ns^{-1}, $k_c^T = 5\times 10^4$ Å^3 ns^{-1}, ($\sigma = 7.5$ Å).

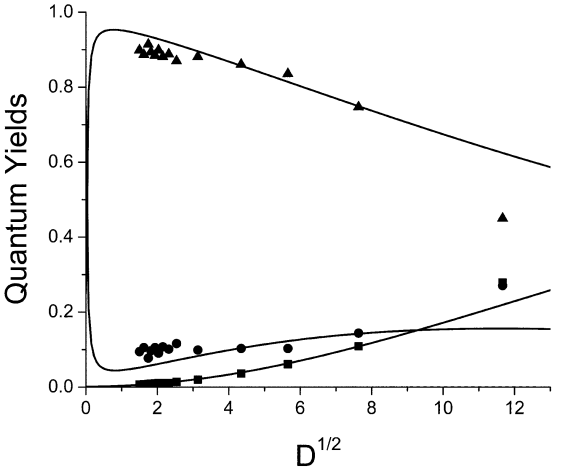

Fig. 11 The quantum yields of singlet (triangles) and triplet (circles) recombination products as well as the charge separation yield (squares). All the points and fitting curves are recalculated from Z data depicted in Fig. 10.

The last but not the least argument for such a revision is the value of initial separation found from the best fit being only 0.1 Å larger than the contact one. Even for proton transfer the contact approximation is hardly suitable for such a small separation and definitely inappropriate for electron transfer. The contact solutions are very unstable regarding the variation of small r as was demonstrated in Figs. 6 and 7. Insignificant changes in r strongly affect the results, making the fitting much less successful. From a physical point of view this is an artefact. Changing the starting position deeply inside the recombination layer of the width $L \approx 1$–2 Å, should not be as crucial. This is just an indication that contact approximation must be substituted for one which accounts for the remote recombination. This makes actual the solution of the present problem with the non-contact model of $W_S(r)$ that can better reproduce the extremal behavior of the two upper curves in Fig. 10.

6 Conclusions

The contact theory of geminate recombination to the ground and triplet states is developed. It substitutes the inappropriate "exponential model" of such a reaction and differs from it by splitting the spin-forbidden transition into sequential spin-conversion and recombination stages. However, the spin-conversion is taken into account in the simplest way by assuming a stochastic transition between the different spin states of RIPs. The averaging of quantum yields (2.2) over the true initial distributions $f_0(r)$ was also avoided. The unique starting distance r was assumed constant although the average distance shifts closer to contact with increasing diffusion.[8] Moreover, even the contact approximation itself is too rough to deal with the closest starts brought in to the narrow recombination layer. In view of all these simplifications, agreement between the theory and experiment is surprisingly good, indicating that the main features of the phenomenon are taken into account.

Acknowledgements

This work was supported by the Israeli Science Foundation.

References

1 U. E. Steiner and Th. Ulrich, *Chem. Rev.*, 1989, **89**, 51.

2 D. Bürßner, H.-J. Wolff and U. Steiner, *Z. Phys. Chem. Bd.*, 1993, **182**, 297; D. Bürßner, H.-J. Wolff and U. Steiner, *Angew. Chem., Int. Ed. Engl.*, 1994, **33**, 1772.

3 H.-J. Wolff, D. Bürßner and U. Steiner, *Pure Appl. Chem.*, 1995, **67**(1), 167.
4 E. Krissinel, A. I. Burshtein, N. Lukzen and U. Steiner, *Mol. Phys.*, 1999, **96**, 1083.
5 A. I. Burshtein, *Adv. Chem. Phys.*, 2000, **114**, 419.
6 A. I. Burshtein, *J. Chem. Phys.*, 1995, **103**, 7927.
7 A. I. Burshtein and E. Krissinel, *J. Phys. Chem.*, 1996, **100**, 3005.
8 A. I. Burshtein and A. A. Neufeld, *J. Phys. Chem. B*, 2001, **105**, 12364.
9 A. I. Burshtein, E. I. Kapinus, I. Yu. Kucherova and V. A. Morozov, *J. Lumin.*, 1989, **43**, 291.
10 H. L. Tavernier, M. M. Kalashnikov and M. D. Fayer, *J. Chem. Phys.*, 2000, **113**, 10191.
11 V. S. Gladkikh, A. I. Burshtein, H. L. Tavernier and M. D. Fayer, *J. Phys. Chem. A*, 2002, **106**, 6982.
12 A. A. Neufeld, A. I. Burshtein, G. Angulo and G. Grampp, *J. Chem. Phys.*, 2002, **116**, 2472.
13 G. Angulo, G. Grampp, A. Neufeld and A. I. Burshtein, *J. Phys. Chem.*, in press.
14 K. Schulten, H. Staerk, A. Weller, H.-J. Werner and B. Nickel, *Z. Phys. Chem. NF*, 1976, **101**, 371.
15 A. Weller, H. Staerk and R. Treichel Faradei, *Discuss. Chem. Soc.*, 1984, **78**, 217.
16 A. I. Burshtein and A. Yu. Sivachenko, *Chem. Phys.*, 1998, **235**, 257.
17 N. Mataga, T. Asahi, J. Kanda, T. Okada and T. Kakitani, *Chem. Phys.*, 1988, **127**, 249.
18 A. I. Burshtein, *Chem. Phys. Lett.*, 1992, **194**, 247.
19 A. I. Burshtein, E. Krissinel and M. S. Mikhelashvili, *J. Phys. Chem.*, 1994, **98**, 7319.
20 K. Kikuchi, M. Hoshi, T. Niwa, Y. Takahashi and T. Miyashi, *J. Phys. Chem.*, 1991, **95**, 38.
21 T. Niwa, K. Kikuchi, N. Matsusita, M. Hayashi, T. Katagiri, Y. Takahashi and T. Miyashi, *J. Phys. Chem.*, 1993, **97**, 11960.
22 M. Ottolenghi, *Charge-Transfer Complexes*, 1973, **6**, 153.
23 H. A. Montejano, J. J. Cosa, H. A. Garrera and C. M. Previtali, *J. Photochem. Photobiol. A: Chem.*, 1995, **86**, 115.
24 G. P. Zanini, H. A. Montejano and C. M. Previtali, *J. Photochem. Photobiol. A: Chem.*, 2000, **132**, 161.
25 A. I. Burshtein and E. B. Krissinel, *J. Phys. Chem. A*, 1998, **102**, 816.
26 A. I. Burshtein and E. B. Krissinel, *J. Phys. Chem. A*, 1998, **102**, 7541.
27 A. I. Burshtein, *Chem. Phys.*, 1999, **247**, 275.
28 A. I. Burshtein, *J. Chem. Phys.*, 2002, **117**, 7640.
29 A. I. Burshtein, *Chem. Phys.*, 2003, **289**, 251.
30 A. I. Burshtein and K. L. Ivanov, *J. Phys. Chem. A*, 2001, **105**, 3158.
31 A. I. Burshtein and K. L. Ivanov, *Phys. Chem. Chem. Phys.*, 2002, **4**, 4115.
32 R. G. Mints and A. A. Pukhov, *Chem. Phys.*, 1984, **87**, 467.
33 A. I. Burshtein, A. A. Zharikov, N. V. Shokhirev, O. B. Spirina and E. B. Krissinel, *J. Chem. Phys.*, 1991, **95**, 8013.
34 Z. Schulten and K. Schulten, *J. Chem. Phys.*, 1977, **66**, 4616.
35 D. Beckert, M. Plüschau and K. P. Dinse, *J. Phys. Chem.*, 1992, **96**, 3193.
36 M. Plüschau, G. Kroll, K. P. Dinse and D. Beckert, *J. Phys. Chem.*, 1992, **96**, 8820.
37 C. D. Borsareli, H. A. Montejano, J. J. Cosa and C. M. Previtali, *J. Photochem. Photobiol. A: Chem.*, 1995, **91**, 13.
38 A. I. Burshtein and P. A. Frantsuzov, *Chem. Phys. Lett.*, 1996, **263**, 513.
39 A. Spernol and K. Z. Wirtz, *Z. Naturforsch., Teil A*, 1953, **8**, 522.

ARTICLES

Production of Free Radicals and Triplets from Contact Radical Pairs and from Photochemically Generated Radical Ions

V. S. Gladkikh, G. Angulo, and A. I. Burshtein*

Weizmann Institute of Science, Rehovot 76100, Israel

Received: December 6, 2006; In Final Form: January 24, 2007

The quantum yields of triplets and free radicals (or radical ions) that escaped recombination in photochemically created primary radical pairs (or radical ion pairs) are calculated. As the products of monomolecular photodissociation, the neutral radicals appear at contact, while the ions are initially distributed over the space due to distant photoionization (bimolecular electron transfer) in the liquid solution. The diffusional dependence of the quantum yields is shown to be different when recombination starts from contact or from separated reactants. The experimental data for recombination of ionized perylene with aromatic amine counterions is well fitted with the noncontact initial distribution provided the recombination is also noncontact and even more distant than ionization.

I. Introduction

The formation of free ions and triplets due to recombination/separation of photochemically created radical ion pairs (RIPs) was the subject of the numerous investigations starting from the classical works of Weller and his co-workers.[1−7] The yields of recombination products are very specific functions of encounter diffusion, which were first given analytic interpretation in ref 8. This theory was reasonably well fitted to the experimental data assuming that the recombination is contact and the counterions are initially separated by a definite distance, r_0. The system studied is excited perylene (A*) quenched by electron transfer to some aromatic amines (D). The subsequent incoherent spin conversion proceeding with the rate k_s[9] makes possible the RIP recombination to both the singlet and triplet neutral products accompanied by RIP separation, according to the following comprehensive scheme:

$$\begin{array}{ccccc} & & A^- + D^+ & & \\ & \nearrow & \bar{\varphi} & \searrow & \\ {}^1A^* + D & \xrightarrow{W_I} & {}^1[A^- \ldots D^+] & \underset{k_s}{\overset{3k_s}{\rightleftarrows}} & {}^3[A^- \ldots D^+]\,. \\ \downarrow \tau & & \Downarrow W_S & & \Downarrow W_T \\ A & & [A \ldots D] & & [{}^3A^* \ldots D] \end{array} \qquad (1.1)$$

Here the rate of ionization, $W_I(r)$, as well as the rates of recombination through the singlet and triplets channels, $W_S(r)$ and $W_T(r)$, are space dependent. τ is the excitation life time and the charge separation yield, $\bar{\varphi}(r)$, is averaged over the initial distribution of charges, $f_0(r)$:

$$\bar{\varphi} = \int \varphi(r) f_0(r)\, \mathrm{d}^3 r \qquad (1.2)$$

Setting $f_0(r) = \delta(r - r_0)$, one can calculate the yield of the charge separation from any given starting point, $\varphi(r_0)$. It is very specific for any r_0 and quite different from $\bar{\varphi}$. The same is true for the partial yields of the singlet and triplet recombination and related to their efficiencies. For the averaged yields, these relationships are given by the following formulas:

$$\bar{\varphi} = \frac{\tilde{D}}{Z + \tilde{D}}; \quad \bar{\varphi}_S = \frac{Z_S}{Z + \tilde{D}}; \quad \bar{\varphi}_T = \frac{Z_T}{Z + \tilde{D}} \qquad (1.3)$$

where Z_S and Z_T are the efficiencies of recombination to the singlet and triplet products, whereas

$$Z = Z_S + Z_T$$

is the total one, and $\tilde{D}$ is the counterion diffusion coefficient. As is known,[10]

$$\bar{\varphi} + \bar{\varphi}_S + \bar{\varphi}_T = 1 \qquad (1.4)$$

This relationship holds also for any particular starting distance r_0, including the contact one.

The difference between the charge separation from contact, $\varphi(\sigma)$, and from the remote start, $\bar{\varphi}$, should be especially emphasized. The latter is averaged over the true distribution $f_0(r)$, prepared by preceding photoionization. There is a similar difference between the yields of singlet and triplet neutral products, $\varphi_s(\sigma)$ and $\varphi_t(\sigma)$, and their averaged values, $\bar{\varphi}_s$ and $\bar{\varphi}_t$. The same is true for the corresponding recombination efficiencies.

In principle, the contact yields, $\varphi_s(\sigma)$, $\varphi_t(\sigma)$, and $\varphi(\sigma)$, are worthy of study in their own right. They are the true yields of the photodissociation products provided the excited molecule separates into two contact born radicals: A + $h\nu$ → A* →

10.1021/jp068375f CCC: $37.00
Published on Web 04/18/2007

[$\dot{B}\cdots\dot{C}$]. However, the same description of the photoionization (eq 1.1) serves only as a useful model for understanding the problem. For the real fitting, all the yields should be averaged over the preliminary calculated initial distribution of the partners in the geminate pairs.

To calculate $\varphi(\sigma)$ and $\varphi_t(\sigma)$ or $\bar{\varphi}$ and $\bar{\varphi}_t$, we have to use the results obtained in ref 8 for the contact recombination in polar solvents (with Onsager radius $r_c = e^2/(\epsilon T) < \sigma$):

$$\varphi_t(r) = k_c^T \frac{3\sigma}{4r} \frac{\alpha k_D + [1 - e^{-\alpha(r-\sigma)/\sigma}](k_D + k_c^S)}{[k_D(1+\alpha) + k_c^T](k_D + k_c^S) + \frac{3}{4}\alpha k_D(k_c^T - k_c^S)} \quad (1.5a)$$

$$\varphi(r) = 1 - \frac{k_c^S/(4\pi r\tilde{D}) + (1 - k_c^S/k_c^T)\varphi_t(r)}{1 + k_c^S/k_D} \quad (1.5b)$$

Here $\alpha = \sqrt{4k_s\sigma^2/\tilde{D}}$ is a measure of the singlet−triplet conversion during encounter time $\sigma^2/\tilde{D}$, and $k_D = 4\pi\sigma\tilde{D}$ is the diffusional rate constant. The double-channel contact recombination, proceeding at only the closest approach distance σ, is represented by two rate constants,

$$k_c^S = \int W_S(r)\, d^3r \quad \text{and} \quad k_c^T = W_T(r)\, d^3r$$

They depend on the free energies of electron transfer to the singlet and triplet products and the electron coupling between the corresponding states.

Assuming recombination to be contact, eqs 1.5a,b were used to obtain the yields and recombination efficiencies at the contact (section II) start. For a remote start, the initial distributions of ions, $f_0(r,\tilde{D})$, have to be calculated for any $\tilde{D}$. This is done by means of differential encounter theory (DET)[10] in section III using the exponential model for the ionization rate:

$$W_I(r) = W_i \exp[-2(r - \sigma)/l_I] \quad (1.6)$$

In section IV, the distributions obtained for such a rate were used for averaging the yields according to recipe 1.2. At small $\tilde{D}$, the diffusional acceleration of the recombination due to a remote start was confirmed for fixed $r_0 \gg \sigma$, as well as for the distributed initial separation. In any case, the theory of contact recombination fits the experimental data only qualitatively, leaving unexplained the diffusional deceleration of recombination at the highest $\tilde{D}$.

The quantitative agreement is reached only in section V, where the exponential rate model is substituted for the contact one, also for recombination:

$$W_S(r) = W_s \exp[-2(r - \sigma)/l_R] \quad \text{and}$$
$$W_T(r) = W_t \exp[-2(r - \sigma)/l_R] \quad (1.7)$$

Then the diffusional deceleration of the recombination is naturally explained. This unexpected effect obtained by Dr. Angulo was first given a proper interpretation in ref 11 using the rectangular model of the recombination rate or its Marcus analog in the deeply inverted region. This effect was attributed to the escape from the extended recombination layer when the start is taken from inside it.[11−13] The spin conversion and recombination through the triplet channel were ignored in these works dealing with single channel recombination. Conversely, the treatment of spin effects in ref 8 was done using the contact model of recombination, which excludes the possibility of an inner start. Here we obtain the same effect once again employing the exponential approximation for both the ionization and recombination rates, eqs 1.6 and 1.7. This helps us to reach the best fit to the experimental data of the total efficiency of recombination, as well as of partial ones, to singlet and triplet recombination products.

II. Contact Start and Contact Recombination

Setting $r = \sigma$, we obtain from eq 1.5:

$$\varphi_t(\sigma) = \frac{3}{4}\alpha \frac{k_c^T k_D}{[k_D(1+\alpha) + k_c^T](k_D + k_c^S) + \frac{3}{4}\alpha k_D(k_c^T - k_c^S)} \quad (2.1a)$$

$$\varphi(\sigma) = \frac{1}{1 + k_c^S/k_D} - \frac{1 - k_c^S/k_c^T}{1 + k_c^S/k_D}\varphi_t(\sigma) \quad (2.1b)$$

If there is no spin conversion, $\varphi_t(\sigma) = \alpha = 0$ but

$$\varphi(\sigma) = \frac{1}{1 + k_c^S/k_D} = \frac{1}{1 + Z/D}, \quad \text{so that} \quad Z = \frac{k_c^S}{4\pi\sigma} = z_s \quad (2.2)$$

These are the conventional results of the spin-less theory,[10] and the same gains from eq 2.1 in the exceptional case $k_c^T = k_c^S$, though the triplet yield is not zero in such a case:

$$\varphi_t(\sigma) = \frac{3}{4}\alpha \frac{k_c k_D}{[k_D(1+\alpha) + k_c](k_D + k_c)} \quad \text{at} \quad k_c^T = k_c^S = k_c \quad (2.3)$$

From the general expression for Z_T and Z_S derived in ref 8 (eq 3.2), we can specify $Z = Z_T + Z_S$ as well:

$$\frac{Z_T}{\tilde{D}} = \frac{3\alpha}{4} \frac{k_c^T}{k_c^T + k_D(1+\alpha)} \quad (2.4a)$$

$$\frac{Z}{\tilde{D}} = \frac{k_c^S}{k_D}\left[1 + \frac{3\alpha}{4} \frac{k_D(1 - k_c^T/k_c^S)}{k_c^T + k_D(1+\alpha)}\right] \quad (2.4b)$$

It is remarkable that Z_T does not depend on the rate of the singlet recombination; it remains invariant at different k_c^S, unlike Z. The total efficiency changes with k_c^S at any $\tilde{D}$ except the borders (at $\tilde{D} = 0$ and $\tilde{D} = \infty$) where always $Z_T = 0$ and $Z = Z_S = z$ (Figure 1). In accordance with eq 2.4b, there is also constant $Z \equiv z$ at any $\tilde{D}$ if $k_c^S = k_c^T$ (horizontal line) and the curvature sign of $Z(\tilde{D})$ is the opposite for $k_c^S < k_c^T$ and $k_c^S > k_c^T$ (upper and lower curves).

For understanding better the physics that is behind the triplet efficiency (eq 2.4a), let us represent it like some "in-cage recombination constant" for the backward electron transfer, k_{bet}, keeping in mind that $\varphi = 1/(1 + Z/\tilde{D}) = 1/(1 + k_{bet}/k_D)$ while $k_{bet} = k_{bet}^T + k_{bet}^S$ and

$$k_{bet}^T = 4\pi\sigma Z_T = \frac{3}{4}\alpha \frac{k_c^T k_D}{k_c^T + k_D(1+\alpha)} = \begin{cases} \frac{3}{4}\alpha k_D & \text{at } k_D/k_c^T \ll 1/\kappa \\ \frac{3}{4}\frac{\alpha}{1+\alpha}k_c^T & \text{at } k_D/k_c^T \gg 1/\kappa \end{cases} \quad (2.5)$$

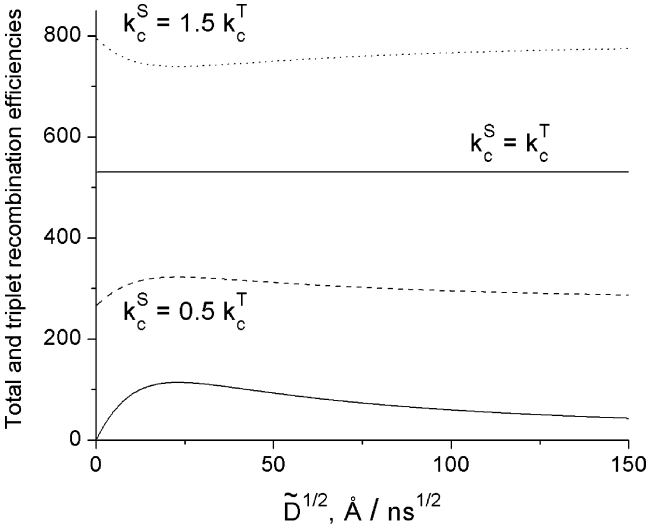

Figure 1. The total recombination efficiency, Z (upper curves), and the triplet one, Z_T (the lowest curve), shown for $k_c^S = k_c^T$ (—), $k_c^S = 0.5\ k_c^T$ (– – –), and $k_c^S = 1.5k_c^T$ (•••) at $k_c^T = 5 \times 10^4$ Å^3/ns.

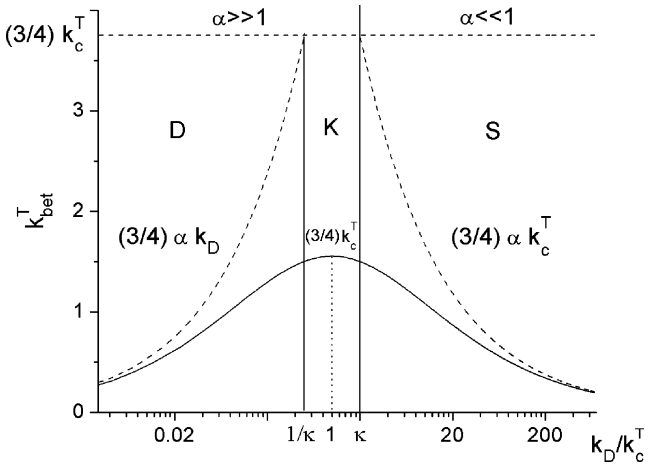

Figure 2. The diffusional dependence of the triplet "in-cage recombination constant" at fast spin conversion ($\kappa = 2$), shown by a solid curve, and the lowest order approximations to this dependence in diffusional (D), kinetic (K), and spin-conversion controlled (S) regions (dashed lines). The solid vertical lines mark the boundaries between these regions, while the dotted line indicates the position of the maximum.

where $\kappa = 16\pi\sigma^3 k_s/k_c^T$ is a measure of the relative spin-conversion strength.

In Figure 2, the diffusional dependence of k_{bet}^T is shown for the fast spin conversion ($\kappa > 1$). In this limit, there are three distinguishable regions: diffusional (D), kinetic (K) and spin-conversion controlled (S). In each of them, the approximate expressions for k_{bet}^T, deduced from eq 2.5, are exposed. Although the start is taken from contact, the radicals are immediately separated and do not recombine until the next recontact and the sequence of subsequent ones. The sooner they follow each other, the faster geminate recombination is accelerated by the diffusion:

$$k_{bet}^T = \frac{3}{4}\alpha k_D = 6\pi\sigma^2\sqrt{k_s\tilde{D}} \quad \text{diffusional limit:} \quad \frac{k_D}{k_c^T} \ll \frac{1}{\kappa} \ll 1 \tag{2.6}$$

When the diffusion becomes too fast, the diffusional control gives way to kinetic control with

$$k_{bet}^T = \frac{3}{4}k_c^T \quad \text{kinetic limit:} \quad \frac{1}{\kappa} \ll \frac{k_D}{k_c^T} \ll \kappa \quad \text{but} \quad \alpha \gg 1 \tag{2.7}$$

This constant value is an upper limit for k_{bet}^T, which is hardly attainable. When diffusion increases, the spin conversion becomes inefficient ($\alpha \ll 1$) and starts to control recombination:

$$k_{bet}^T = \frac{3}{4}\alpha k_c^T = \frac{3}{4}k_c^T\sqrt{\frac{4k_s\sigma^2}{\tilde{D}}} \quad \text{spin conversion control:} \quad \alpha \ll 1 \quad \text{at} \quad \frac{k_D}{k_c^T} \gg \kappa \tag{2.8}$$

Generally speaking the side regions of the diffusional and spin-conversion control extend toward each other, when k_s (as well as κ) reduces. At very slow spin conversion ($\kappa \ll 1$), the intermediate kinetic region is expelled entirely as shown in Figure 3. Simultaneously the maximal k_{bet}^T located at $k_D/k_c^T = 1$ decreases:

$$\max k_{bet}^T = \frac{3}{4}k_c^T\frac{\sqrt{\kappa}}{2+\sqrt{\kappa}} = \begin{cases} \frac{3}{4}k_c^T & \text{at } \kappa \gg 1 \\ \frac{3}{2}\sqrt{\pi\sigma^3 k_s k_c^T} & \text{at } \kappa \ll 1 \end{cases} \tag{2.9}$$

When $k_s \to 0$, the maximum turns to 0 and the whole curve disappears. Such a transformation qualitatively coincides with that studied previously in ref 14 and reviewed in ref 10 (Figure 66). The only distinction is that previously the RIP was created in the triplet state and recombined due to the spin conversion via the permitted singlet channel, while now the process is going back to front.

Another difference is in that here we consider the double channel recombination, looking for both the singlet and triplet channel efficiencies. It is true that the latter does not depend on how strong the former is but not vice versa. If one changes k_c^T, then not only Z_T but also Z_S as well as Z change simultaneously. This is demonstrated in Figure 4, where Z and Z_T are plotted as functions of $\sqrt{\tilde{D}}$ but contrary to Figure 1,

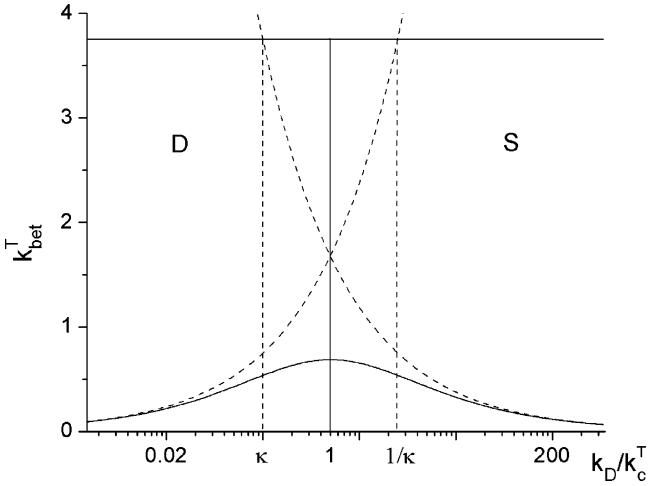

Figure 3. The diffusional dependence of the triplet "in-cage recombination constant" at ten times slower spin conversion than that in Figure 2 ($\kappa = 16\pi\sigma^3 k_s/k_c^T = 0.2$), shown by a solid curve, and the lowest order approximations to this dependence in diffusional (D) and spin-conversion controlled (S) regions (dashed lines). The solid vertical line marks the boundaries between these regions.

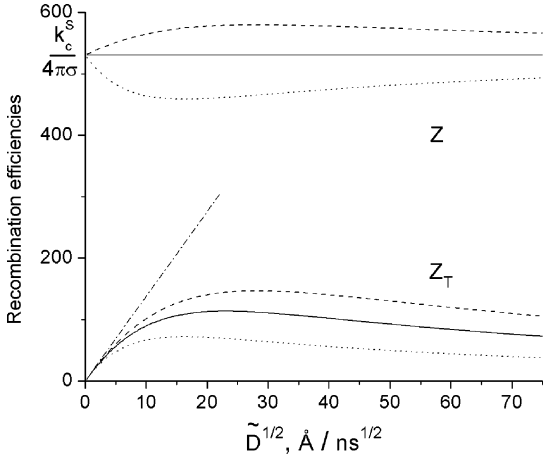

Figure 4. The total (above) and triplet (below) recombination efficiencies at fixed $k_c^S = 5 \times 10^4$ Å^3/ns but different $k_c^T = k_c^S$ (—) as well as for lower $k_c^T = 0.5k_c^S$ (···) and for the larger $k_c^T = 1.5k_c^S$ (— — —). The slope of all triplet curves at $\tilde{D} = 0$ is shown by the dashed-dotted (—·—) straight line.

now k_c^S is kept constant while k_c^T varies. It is remarkable that at these coordinates the linear asymptote of Z_T at $\sqrt{\tilde{D}} \rightarrow 0$, shown by the dashed-dotted line in Figure 4, has the same slope for any k_c^T:

$$Z_T \rightarrow \frac{3}{4}\alpha\tilde{D} = \theta\sqrt{\tilde{D}} \quad \text{where} \quad \theta = \frac{3}{2}\sigma\sqrt{k_s} \qquad (2.10)$$

If such a slow diffusion is attainable, it is easy to find from θ the rate of the spin conversion, k_s, while $Z(0)$ provides us with k_c^S and the argument for maximal Z_T with k_c^T. Having the latter, one can also extract κ from the height of the maximum (eq 2.9) and use it to find $k_s = \kappa k_c^T/(16\pi\sigma^3)$. The low diffusion region is not reachable.

The total recombination efficiency $Z =$ const if $k_c^S = k_c^T$ but has a positive curvature if $k_c^S < k_c^T$ and negative in the opposite case. Unlike Z_T, the total recombination efficiency Z is never zero as $\tilde{D} \rightarrow 0$, unless the radicals start from the contact.

III. Distribution of Initial Separations of Counterions

The diffusional dependence of Z is qualitatively different when the RIPs are the products of bimolecular plotoionization. The electron transfer proceeding with the space-dependent ionization rate, $W_I(r)$, results in some distribution of RIP over interion distances, $m_0(r)$, which is farther from contact the slower is the encounter diffusion of neutral reactants, D. The actual shape of it is given by DET:[15,16]

$$m_0(r) = W_I(r) \int_0^\infty n(r,t)N(t)\, dt \qquad (3.1)$$

In polar solvents, the distribution of reactants, $n(r,t)$, obeys the following equation[17,18]

$$\dot{n} = -W_I(r)n(r,t) + \frac{D}{r^2}\frac{\partial}{\partial r}r^2\frac{\partial n}{\partial r} \qquad (3.2)$$

with reflecting boundary condition

$$4\pi D r^2 \frac{\partial n}{\partial r}\bigg|_{r=\sigma} = 0 \quad \text{and initial one,} \quad n(r,0) = 1 \qquad (3.3)$$

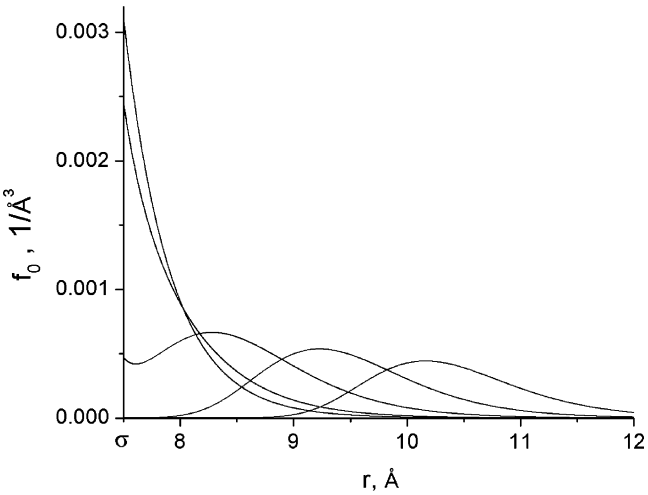

Figure 5. The initial RIP distributions resulting from the exponential ionization with $W_i = 29.12$ ns^{-1} and $l_I = 0.81$ Å at different encounter diffusions of neutral precursors: $D = 10^{-4}$, 10^{-6}, 10^{-7}, 10^{-8}, or 10^{-9} cm^2/s (from left to right).

whereas the quenching kinetics is given by the expression

$$N(t) = \exp\{-t/\tau - c\int d^3r\, W_I(r) \int_0^t n(r,t')\, dt'\} \qquad (3.4)$$

The normalized initial distributions

$$f_0(r) = \frac{m_0(r)}{\int m_0(r)\, d^3r} \qquad (3.5)$$

depend on diffusion and the shape of $W_I(r)$.[10,19] For ionization in the normal Marcus region, the exponential model (eq 1.6) is rather a good approximation. It was used in our calculations performed with the SSDP2 program.[20] The family of initial RIP distributions that are obtained is shown in Figure 5 and confirms once again that at faster diffusion the ions are born closer to the contact distance σ. As $D \rightarrow \infty$, the closest distribution takes the shape that $W_I(r)$ has.

The starting distance averaged over such distributions

$$\bar{r} = \int r f_0(r)\, d^3r \qquad (3.6)$$

decreases with D until ionization is diffusional, but with $D \rightarrow \infty$ it approaches $\bar{r}_{min}$ and remains constant being under kinetic control (Figure 6). Although in this limit $f_0(r)$ coincides in shape with $W_I(r)$, the minimal separation calculated from eq 1.6 is still larger than the contact distance: $\bar{r}_{min} \approx \sigma + l/2$.

IV. Remote Start and Contact Recombination

Since initially the photogenerated ions are always separated (at least by $l/2$), it takes them some time to reach the contact and recombine there. This time is shorter the faster is (at $D \rightarrow \infty$) diffusion of (at $D \rightarrow \infty$) ions, which facilitates the recombination from the remote start.[10,19] In such a case, the total recombination efficiency Z increases with small $\tilde{D}$, instead of being quasi-constant at the contact start considered in the previous section. In particular, at $k_c^S = k_c^T = k_c$, it is a true constant $Z = k_c/(4\pi\sigma)$, shown in Figure 7 by the horizontal dashed line, while Z obtained for the noncontact start (even from the minimal separation $\bar{r}_{min}$) is qualitatively different. It grows with $\tilde{D}$ until recombination is diffusional (region D) and approaches the constant but lower value $Z = k_c/(4\pi\bar{r}_{min})$, when it becomes kinetic (region K). The triplet efficiency Z_T does

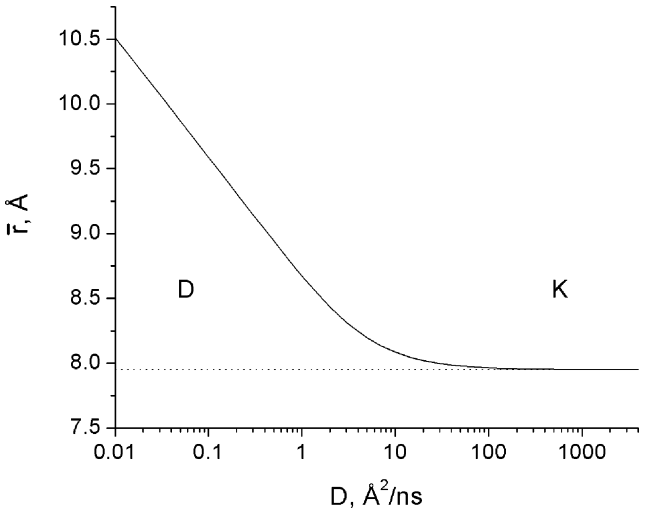

Figure 6. The average initial RIP separation at different encounter diffusion. In region D, where $\bar{r} > \bar{r}_{min}$, diffusion controls ionization, whereas in region K, where ionization is kinetic, the separation becomes minimal: $\bar{r} \approx \bar{r}_{min} = 7.95$ Å.

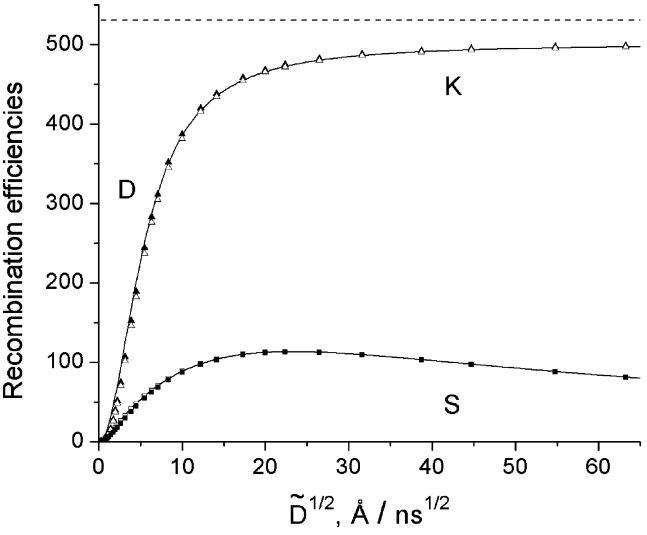

Figure 7. The efficiencies of recombination from different starts at $k_c^S = k_c^T = k_c = 5 \times 10^4$ Å^3/ns. Total recombination from the contact start $Z = k_c/(4\pi\sigma)$ (− − −) and from minimal separation (—, upper), as well as from remote start distributed with $f_0(D)$ (▲) and from the average initial separation, $\bar{r}(D)$ (△), is shown. The efficiency of the triplet recombination from minimal separation (—, lower), as well as from the distributed starts (■) and from $\bar{r}(D)$ (□), is also shown.

not experience such dramatic changes: the recombination accelerated at slow diffusion passes the maximum and slows down due to spin-conversion control (in region S).

So far we confined ourselves to recombination starting from a single initial separation (the same at any D) that was equalized to either σ or $\bar{r}_{min}$. The results were shown in Figure 7 by dashed and solid lines, respectively. Now we turn to the initial conditions changing with D and represent the results by either filled points when initial separations are distributed according to $f_0(r)$ or empty ones when the start is taken from a single distance $\bar{r}(D)$ (averaged over $f_0(r)$, which is different at any D).

Our calculations address the situation when

$$D = \tilde{D} = \frac{T}{6\pi\sigma\eta} \tag{4.1}$$

In fact, the ion diffusion in polar solvents is a bit slower than that of the neutral reactants and their relationship to viscosity

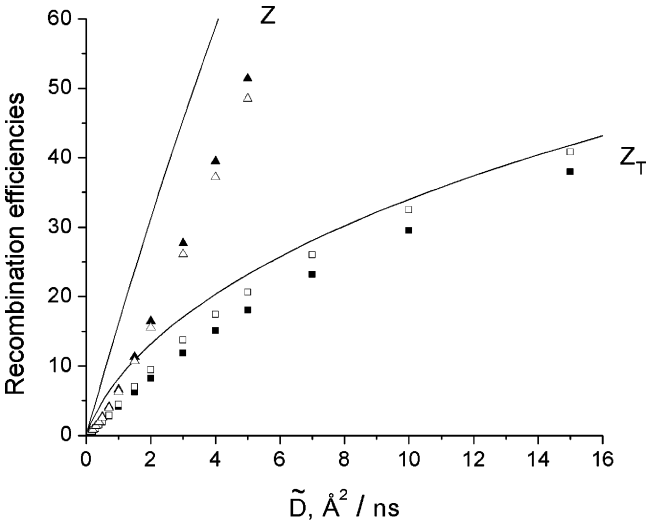

Figure 8. The efficiencies of recombination from different starts at $k_c^S = k_c^T = k_c = 5 \times 10^4$ Å^3/ns in slow diffusion domain. Total recombination from minimal separation (—, upper), as well as from remote start distributed with $f_0(D)$ (▲) and from the average initial separation, $\bar{r}(D)$ (△), is shown. The efficiency of the triplet recombination from minimal separation (—, lower), as well as from the distributed starts (■) and from $\bar{r}(D)$ (□), is also shown.

η, used actually and previously,[8] differs a bit from the Stokes−Einstein expression in eq 4.1. The latter has just to emphasize that D and $\tilde{D}$, changing with viscosity, affect simultaneously both the integrands in eq 1.2, $\varphi(\tilde{D})$ and $f_0(D)$. The results obtained are specific to particular $D = \tilde{D}$ changing with viscosity.

As was expected, the average yield, $\bar{\varphi}$, and the yield from the average separation, $\varphi(\bar{r})$, are not identical, as well as the corresponding efficiencies. However, the difference between Z calculated from the former (●) and from the latter (○) is not pronounced. Similarly Z_T calculated from the distributed starts (▲) and their average value (△) do not differ too much. Moreover, the points do not deviate significantly from the solid curves calculated for the fixed start from $\bar{r}_{min}$. However, this statement is only valid for the fast diffusion limit when recombination is under kinetic or spin-conversion control and $\bar{r}$ has already approached $\bar{r}_{min}$. Along with it, Z approaches its upper limit, which is the plateau of the height

$$\lim_{\tilde{D}\to\infty} Z = \frac{k_c}{4\pi\bar{r}_{min}}$$

This plateau is a bit lower than that shown by the dashed line, which is peculiar for the constant start ($k_c/(4\pi\sigma)$).

The situation is rather different in the opposite limit of slow diffusion, which is mainly studied experimentally. There the total efficiency of diffusional recombination from the fixed start should be linear in $\tilde{D}$, as it really is for $r_0 = \bar{r}_{min}$ (upper solid line in Figure 8). However, the true start at such diffusion is far away from the near contact region and moves toward it when diffusion increases. Therefore the points representing recombination from either distributed (●) or average (○) initial separation lie far below this line. Hence, the diffusional acceleration of total recombination is actually less efficient for remote starts, drawing near with diffusion, than for the fixed and the closest one. Qualitatively the same happens to triplet efficiency: all related points are below the lower solid line, though those calculated from average (△) initial separation are closer to it than those from distributed (▲) initial separation.

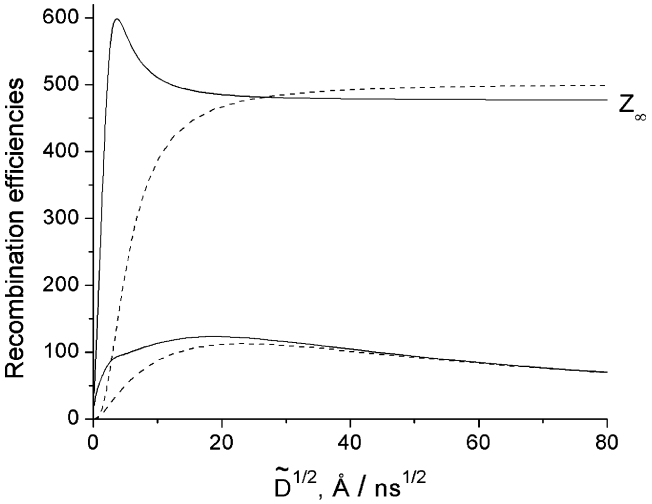

Figure 9. The total (above) and triplet (below) efficiencies of recombination obtained with contact (− − −) and exponential (—) approximations of the recombination layer.

V. Remote Start and Remote Recombination

As a matter of fact, there are no grounds to consider recombination as contact, except the simplicity of the yields calculation. There is the unified theory recipe given in ref 10 (section IX E) how to calculate the averaged yields,

$$\bar{\varphi}_S = \int \varphi_S(r') f_0(r')\, d^3r' \qquad \bar{\varphi}_T = \int \varphi_T(r') f_0(r')\, d^3r'$$
$$\bar{\varphi} = 1 - \bar{\varphi}_S - \bar{\varphi}_T \quad (5.1)$$

expressed via the partial yields of the singlet and triplet recombination products

$$\varphi_S(r') = \int W_S(r) \tilde{p}_{SS}(r,r',0)\, d^3r \quad \text{and}$$
$$\varphi_T(r') = \int W_T(r) \tilde{p}_{ST}(r,r',0)\, d^3r \quad (5.2)$$

that can be found at any $W_S(r)$ and $W_T(r)$. All that we need is the Laplace transformations of the Green functions $\tilde{p}_{SS}(r,r',s)$ and $\tilde{p}_{ST}(r,r',s)$, which obey the set of equations for RIPs subjected to spin conversion and remote double channel recombination (eqs 9.27 in ref 10):

$$-\delta(r-r')/(4\pi r^2) + s\tilde{p}_{SS} = k_s\tilde{p}_{ST} - 3k_s\tilde{p}_{SS} + \mathbf{L}\tilde{p}_{SS} - W_S(r)\tilde{p}_{SS} \quad (5.3a)$$

$$s\tilde{p}_{ST} = -k_s\tilde{p}_{ST} + 3k_s\tilde{p}_{SS} + \mathbf{L}\tilde{p}_{ST} - W_T(r)\tilde{p}_{ST} \quad (5.3b)$$

The encounter diffusion operator

$$\mathbf{L} = \tilde{D}\frac{1}{r^2}\frac{\partial}{\partial r} r^2\, e^{r_c/r}\frac{\partial}{\partial r} e^{-r_c/r}$$

should be used in eqs 5.3a,b together with the reflecting boundary conditions. Solving these equations for only highly polar solvents, we ignored the Coulomb interaction, setting to zero the Onsager radius r_c.

The results presented in Figure 9 were actually obtained using the program Qyield developed by Dr. Krissinel (see http://www.fh.huji.ac.il/ krissinel/software.html). It allows the straightforward calculation of the singlet and triplet pair densities, obeying the set:

$$\dot{m}_S = k_s m_T - 3k_s m_S + \tilde{D}\frac{1}{r^2}\frac{\partial}{\partial r} r^2\, e^{r_c/r}\frac{\partial}{\partial r} e^{-r_c/r}\, m_S - W_S(r)m_S + W_I^S n(r,t) N_S \quad (5.4a)$$

$$\dot{m}_T = -k_s m_T + 3k_s m_S + \tilde{D}\frac{1}{r^2}\frac{\partial}{\partial r} r^2\, e^{r_c/r}\frac{\partial}{\partial r} e^{-r_c/r}\, m_T - W_T(r)m_T \quad (5.4b)$$

identical to eqs 9.6 from ref 10 but with reflecting boundary conditions (and $m_S(0) = m_T(0) = 0$). Here n and N borrowed from eqs 3.2 and 3.4 determine also the initial RIP distributions eqs 3.1 or 3.5. Taking the integrals

$$\phi_S(r') = \int_0^\infty \int W_S(r) m_S(r,t)\, d^3r\, dt = \psi\bar{\varphi}_S,$$
$$\phi_T(r') = \int_0^\infty \int W_T(r) m_T(r,t)\, d^3r\, dt = \psi\bar{\varphi}_T$$

we get the photoionization yields of the singlet and triplet products. They differ from $\bar{\varphi}_S$ and $\phi_T(r')$ by only the multiplier

$$\psi = c\int m_0(r)\, d^3r = \frac{c\kappa\tau}{1 + c\kappa\tau} = 1 - \eta \quad (5.5)$$

which is the RIP yield related to the fluorescence yield η and Stern−Volmer constant as usual.[10]

The recombination rates are usually more extended than the ionization one due to the larger exergonicity of the backward electron transfer. To account for this feature using the exponential models (eq 1.7), we assumed that

$$l_R > l_I \quad (5.6)$$

Under this condition, the total efficiency of remote recombination is a non-monotonous function of diffusion (red line in Figure 9), contrary to what was obtained in the contact approximation (the blue line there). This is due to diffusional deceleration, following the diffusional acceleration of the recombination. At the greatest diffusion, the initial ion distribution coincides in shape with $W_I(r)$.[10] Under condition 5.6, it appears to be narrower than the recombination layer common for the singlet and triplet exponential rates (eq 1.7). Therefore the recombination is weaker the faster the ions get rid of this layer interior. Passing the maximum, the total recombination efficiency Z shown by the red line falls off with the further increase of $\tilde{D}$.

Finally it approaches the plateau, which is lower than the kinetic one reached in the contact approximation (blue line). This pseudo-kinetic value, Z_∞, can be found from the fast diffusion approximation for $\bar{\varphi}$:

$$\bar{\varphi} \approx \frac{\int \varphi(r) W_I(r)\, d^3r}{\int W_I(r)\, d^3r} = 1 - \frac{Z_\infty}{\tilde{D}} \quad \text{at} \quad \tilde{D} \to \infty \quad (5.7)$$

where $\varphi(r)$ is given by expansion 3.5 in ref 21 valid for a single-channel recombination:

$$\varphi(r) = 1 - x\frac{1 + 2\lambda + 2\lambda^2 - \lambda(1 + \delta + 2\lambda)\, e^{-\delta/\lambda}}{1 + \delta} \quad (5.8)$$

Here

$$x = k_c/k_D, \quad \lambda = l_R/2\sigma, \quad \delta = (r - \sigma)/\sigma$$

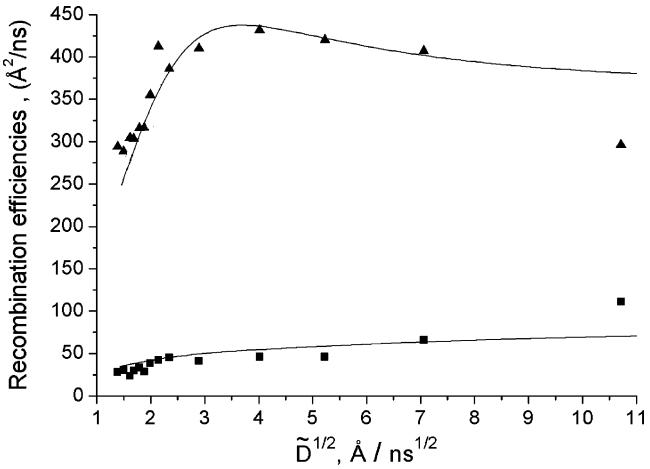

Figure 10. Fitting the theoretical efficiencies (—) to the real experimental data for total (▲) and triplet (■) recombination efficiencies, using the exponential models for both ionization and recombination rates. Parameters obtained from the best fit are the following: $W_i = 29.12\ ns^{-1}$, $W_s = 77\ ns^{-1} = 1.2W_t$, $l_l = 0.81$ Å, $l_R = 1.24$ Å, $k_s = 0.75\ ns^{-1}$, and $\sigma = 7.5$ Å. Analogous to Figure 3.75 in the ref 19.

where $k_c = \int W_S(r)\ d^3r$ is the singlet recombination constant, while the diffusional recombination constant $k_D = 4\pi\sigma\tilde{D}$, as usual. Although this expression was derived for only the singlet recombination at fast diffusion, it is applicable to our double channel model as well, since as $\tilde{D} \to \infty$ the triplet recombination being under spin-conversion control is finally switched off. As follows from eqs 5.7 and 5.8

$$Z_\infty = \frac{W_s\sigma^2 l_R}{(1 + 2\lambda_I + 2\lambda_I^2)l_I}\int_0^\infty [1 + 2\lambda + 2\lambda^2 - \lambda(1 + \delta + 2\lambda)\, e^{-\delta/\lambda}]\, e^{-\delta/\lambda_I}(1 + \delta)\, d\delta \quad (5.9)$$

where $\lambda_I = l_l/(2\sigma)$. Z_∞ is the height of the red plateau, which is really a bit lower than the blue one, appearing in the contact approximation: $\lim_{D\to\infty} Z = k_c/(4\pi\bar{r}_{min})$.

However, the principle difference between remote and contact recombination is seen only in the slow diffusion limit. There the high peak in Z and related increase in Z_T makes it more flat near the maximum. Since this diffusion region is the same as in real systems, it is worthy of special attention. In Figure 10, we see these very features first subjected to experimental and theoretical study in ref 8 but given preliminary noncontact interpretation only in ref 19, For better fitting, we did not assume W_s equal to W_t but took $W_s = 1.2W_t$. Only at the greatest diffusion, the experimental points deviate a bit from the theoretical curves, but all the rest are fitted quite well.

VI. Conclusions

Such an excellent fitting does not prove that the theory is actually the best. There are two essential weaknesses that we hope to eliminate in the near future.

- The exponential models for the ionization and recombination rates should be substituted by the Marcus formulas for these rates, which relate them to the true free energies of the reactions, as well as to the reorganization energy in a particular solvent.
- The true hyperfine interaction mechanism of spin conversion should be substituted for the phenomenological rate model of spin transitions in the RIP.
- The difference in size and encounter diffusion coefficients of ions and their neutral precursors should be taken into account especially in polar solvents.

Hopefully these improvements will enable the theory to correspond better with the fast diffusion experiments and relate the spin-conversion rate to the true values of the hyperfine interaction in particular radicals. However, this will not change our main conclusions:

- The contact reaction approximation can be reasonable for only heavy particles and proton transfer in liquids, whereas the electron transfer either forward or backward is not contact.
- The shape and width of the remote transfer rates strongly affect the yields of reaction products, changing essentially their diffusional dependence.

The unified encounter theory is the universal instrument for investigation of any transfer at any diffusion rate.

References and Notes

(1) Schulten, K.; Staerk, H.; Weller, A.; Werner, H.-J.; Nickel, B. *Z. Phys. Chem. (Frankfurt/Main)* **1976**, *101*, 371.
(2) Schulten, Z.; Schulten, K. *J. Chem. Phys.* **1977**, *66*, 4616.
(3) Werner, H.-J.; Staerk, H.; Weller, A. *J. Chem. Phys.* **1978**, *68*, 2419.
(4) Weller, A.; Nolting, F.; Staerk, H. *Chem. Phys. Lett.* **1983**, *96*, 24.
(5) Weller, A.; Staerk, H.; Treichel, R. *Faraday Discuss. Chem. Soc.* **1984**, *78*, 271.
(6) Michel-Beyerle, M. E.; Haberkorn, R.; Bube, W.; Steffens, E.; Schrëder, H.; Neusser, H. J.; Schlag, E. W. *Chem. Phys.* **1976**, *17*, 139.
(7) Brocklehurst, B. *Chem. Phys. Lett.* **1974**, *28*, 357.
(8) Gladkikh V. S.; Burshtein A. I.; Angulo G.; Grampp G. *Phys. Chem. Chem. Phys.* **2003**, *5*, 2581.
(9) Steiner, U. E.; Ulrich, Th. *Chem. Rev.* **1989**, *89*, 51.
(10) Burshtein A. I. *Adv. Chem. Phys.* **2000**, *114*, 419.
(11) Burshtein, A. I.; Neufeld, A. A. *J. Phys. Chem. B* **2001**, *105*, 12364.
(12) Neufeld, A. A.; Burshtein, A. I.; Angulo, G.; Grampp, G. *J. Chem. Phys.* **2002**, *116*, 2472.
(13) Angulo, G.; Grampp, G.; Neifeld, A.; Burshtein A. I. *J. Phys. Chem. A* **2003**, *107*, 6913.
(14) Burshtein, A. I.; Krissinel, E. *J. Phys. Chem. A* **1988**, *102*, 516.
(15) Burshtein, A. I. *Chem. Phys. Lett.* **1992**, *194*, 247.
(16) Dorfman, R. C.; Fayer, M. D. *J. Chem. Phys.* **1992**, *96*, 7410.
(17) Kilin, S. F.; Mikhelashvili, M. S.; Rozman I. M. *Opt. Spectrosc.* **1964**, *16*, 576.
(18) Steinberg, I. Z.; Katchalsky E. *J. Chem. Phys.* **1968**, *48*, 2404.
(19) Burshtein, A. I. *Adv. Chem. Phys.* **2004**, *129*, 105.
(20) Krissinel, E. B.; Agmon, N. *J. Comput. Chem.* **1996**, *17*, 1085.
(21) Burshtein, A. I.; Zharikov, A. A.; Shokhirev, N. V. *J. Chem. Phys.* **1992**, *96*, 1951.

Available online at www.sciencedirect.com
SCIENCE DIRECT
Chemical Physics 323 (2006) 351–357
Chemical Physics
www.elsevier.com/locate/chemphys

Double-channel recombination of the radical pairs via incoherent Δg-mechanism of spin-conversion

V.S. Gladkikh, A.I. Burshtein *

Weizmann Institute of Science, Chemical Physics, Rehovot 76100, Israel

Received 17 May 2005; accepted 23 September 2005
Available online 19 October 2005

Abstract

The recombination/separation of the radical pair from its singlet and triplet state is studied. The spin conversion in a pair is considered as a stochastic (incoherent) process, assuming that the recombination of both singlet and triplet radical pairs is contact. The quantum yields of recombination products and free radical production are calculated for any initial separation of radicals in a pair.

1. Introduction

The pair of radicals created in either of its singlet or triplet states can recombine from there in the singlet or triplet products or be separated with quantum yield φ:

Scheme I

$$D + {}^3A^* \leftarrow {}^3[\dot{D}\cdots\dot{A}] \rightarrow \dot{D} + \dot{A} \tag{1.1a}$$

$$\downarrow\uparrow \qquad\qquad \varphi$$

$$D + A \leftarrow {}^1[\dot{D}\cdots\dot{A}] \rightarrow \dot{D} + \dot{A}. \tag{1.1b}$$

The quantum yield of recombination through either the singlet or triplet channels (or through them both) is $1-\varphi$ where the quantum yield of free radicals

$$\varphi = \frac{1}{1+Z/D}. \tag{1.2}$$

Generally, the recombination efficiency $Z = Z_S + Z_T$ but it coincides with that for a single channel, Z_S or Z_T, if another channel is switched off [1]. The spin conversion in the radical pair allows the recombination to proceed in whatever channel is switched on. The conversion is carried out by spin relaxation with transversal and longitudinal times T_2 and T_1 as well as by mixing of the S and T_0 states, with a frequency

$$\Omega = \frac{\omega_A - \omega_B}{2}. \tag{1.3}$$

Here, $\omega = g\beta H/\hbar$ is the Zeeman frequency in the magnetic field H, which is different for the two radicals in a pair, A and B, provided they have different g-factors ($\Delta g = g_A - g_B \neq 0$). If $T_1 = \infty$, only two states, S and T_0, are worthy of consideration because the other two, T_+ and T_-, remain out of the game.

This particular case of a two-level system is equally good as a model of spin conversion induced by the hyperfine interaction (HFI) in high magnetic fields [2]. This model was the subject of a detailed investigation in our recent work [3] where the pair was assumed to be initially separated by distance $r = r_0$ but recombines only at contact (at $r = \sigma$) with the rate constants k_c^S and k_c^T for alternative channels. If the start is also from contact ($r_0 = \sigma$) and from the singlet state of a pair the recombination efficiency was shown to be [3]

$$Z = \begin{cases} \frac{z_s}{2}\frac{2+\alpha}{1+\alpha} = Z_S & \text{at } k_c^T = 0, \\ z = \frac{k_c}{4\pi\sigma} & \text{at } k_c^T = k_c^S = k_c, \\ \frac{z_t}{2}\frac{\alpha}{1+\alpha+z_t/D} = Z_T & \text{at } k_c^S = 0, \end{cases} \tag{1.4}$$

where $z_s = k_c^S/4\pi\sigma$, $z_t = k_c^T/4\pi\sigma$ and D is the coefficient of the encounter diffusion of radicals in a pair. The results obtained for the contact recombination through single channel in [2], as well as in earlier work [4], were shown to be identical with that presented in Eq. (1.4) [3].

* Corresponding author. Tel.: +972 8934 3708; fax: +972 8934 4123.
E-mail address: cfbursh@wisemail.weizmann.ac.il (A.I. Burshtein).

0301-0104/$ - see front matter © 2005 Elsevier B.V. All rights reserved.
doi:10.1016/j.chemphys.2005.09.030

Generally, the important parameter α is a complex function of diffusion, the recombination constant and conversion frequency. The latter is responsible for the magnetic field effect in the case of the Δg-mechanism of spin conversion [5]. Only in the limit of stochastic (incoherent) conversion the expression for α becomes rather simple and does not depend on recombination

$$\alpha = \sqrt{2\frac{\tau_d}{T_2}(1+\Omega^2 T_2^2)} = \sqrt{2\tau_d\left(\frac{1}{T_2}+k_0\right)} \quad \text{provided } \Omega T_2 \ll 1. \tag{1.5}$$

Here, $\tau_d = \sigma^2/D$ is the encounter time while

$$k_0 = \Omega^2 T_2 \tag{1.6}$$

is the rate of stochastic spin conversion. This very rate has to be used further on because the present work is also confined to the incoherent spin conversion. However, this time we will consider the general four-level spin system which represent the radical pair with arbitrary T_1. This pair, subjected to double channel recombination ($k_c^S \neq 0 \neq k_c^T$), starts from singlet spin state and any initial separation of the radicals in a pair ($r_0 \geqslant \sigma$).

2. Diffusional kinetic equations

The basic set of four equations relates the singlet state population, ρ_S, and the three populations of the triplet sub-levels ρ_0, ρ_+ and ρ_- [3,4]

$$\dot\rho_S = \left(k_0+\frac{1}{T_2}-\frac{1}{2T_1}\right)\rho_0 - \left(k_0+\frac{1}{T_2}+\frac{1}{2T_1}\right)\rho_S + \frac{\rho_+ + \rho_-}{2T_1} + \mathbf{L}\rho_S, \tag{2.1a}$$

$$\dot\rho_0 = \left(k_0+\frac{1}{T_2}-\frac{1}{2T_1}\right)\rho_S - \left(k_0+\frac{1}{T_2}+\frac{1}{2T_1}\right)\rho_0 + \frac{\rho_+ + \rho_-}{2T_1} + \mathbf{L}\rho_0, \tag{2.1b}$$

$$\dot\rho_+ = \frac{\rho_S+\rho_0}{2T_1} - \frac{\rho_+}{T_1} + \mathbf{L}\rho_+ \quad \text{and} \quad \dot\rho_- = \frac{\rho_S+\rho_0}{2T_1} - \frac{\rho_-}{T_1} + \mathbf{L}\rho_-, \tag{2.1c}$$

where

$$\mathbf{L} = \tilde D \frac{1}{r^2}\frac{\partial}{\partial r} r^2 e^{-U(r)/k_B T}\frac{\partial}{\partial r} e^{U(r)/k_B T} \tag{2.2}$$

is an operator of the encounter diffusion in the inter-particle potential $U(r)$. For an ion–radical pair this is the Coulomb interaction $U(r) = -r_c/r$, with Onsager radius $r_c = e^2/\varepsilon k_B T$ (at temperature T and dielectric constant ε).

The set of equations (2.1) should be solved with radiation boundary conditions at contact

$$\mathbf{j}\rho_S|_{r=\sigma} = k_c^S \rho_S(\sigma, r_0, t), \qquad \mathbf{j}\rho_i|_{r=\sigma} = k_c^T \rho_i(\sigma, r_0, t), \quad i = +, 0, -, \tag{2.3}$$

where $\mathbf{j}(r) = 4\pi r^2 \tilde D \frac{\partial}{\partial r} e^{U(r)/k_B T}$ is an operator of flux at distance r. The initial conditions select the spin state where the radical pair was born at $t = 0$

$$\rho_S(r, r_0, 0) = \frac{\delta(r-r_0)}{4\pi r^2}; \qquad \rho_i(r, r_0, 0) = 0, \quad i = +, 0, -. \tag{2.4}$$

Neglecting the Coulomb and any other interactions between radicals, we set $U(r) = 0$ and turn the diffusional operator (2.2) to the simplest form: $\mathbf{L}\rho = D\Delta\rho = D(\rho'' + \frac{2}{r}\rho')$. Then making the Laplace transformation of equations (2.1) with initial conditions (2.4) we obtain the set of uncoupled equations for the r-dependent quantities $\tilde\rho_k = \int \rho_k(r, r_0, t)\exp(-st)\,dt$

$$\tilde\rho'' + \frac{2}{r}\tilde\rho' - \frac{s}{D}\tilde\rho = -\frac{\delta(r-r_0)}{4\pi r^2 D}, \tag{2.5a}$$

$$\tilde\rho''_\Delta + \frac{2}{r}\tilde\rho'_\Delta - \frac{s+2(k_0+1/T_2)}{D}\tilde\rho_\Delta = -\frac{\delta(r-r_0)}{4\pi r^2 D}, \tag{2.5b}$$

$$\tilde\rho''_\alpha + \frac{2}{r}\tilde\rho'_\alpha - \frac{s+2/T_1}{D}\tilde\rho_\alpha = -\frac{\delta(r-r_0)}{4\pi r^2 D}, \tag{2.5c}$$

$$\tilde\rho''_\beta + \frac{2}{r}\tilde\rho'_\beta - \frac{s+1/T_1}{D}\tilde\rho_\beta = 0, \tag{2.5d}$$

where

$$\rho = \rho_S + \rho_0 + \rho_+ + \rho_-, \quad \rho_\Delta = \rho_S - \rho_0,$$
$$\rho_\alpha = \rho_S + \rho_0 - \rho_+ - \rho_-, \quad \rho_\beta = \rho_+ - \rho_-.$$

On the other hand, these variables relate to each other through the boundary conditions

$$4\pi D r^2 \frac{\partial\rho}{\partial r}\bigg|_{r=\sigma} = \frac{k_c^S + 3k_c^T}{4}\rho(\sigma, r_0, t) + \frac{k_c^S - k_c^T}{2}\rho_\Delta(\sigma, r_0, t) + \frac{k_c^S - k_c^T}{4}\rho_{\alpha(\sigma, r_0, t)}, \tag{2.6a}$$

$$4\pi D r^2 \frac{\partial\rho_\Delta}{\partial r}\bigg|_{r=\sigma} = \frac{k_c^S - k_c^T}{4}\rho(\sigma, r_0, t) + \frac{k_c^S + k_c^T}{2}\rho_\Delta(\sigma, r_0, t) + \frac{k_c^S - k_c^T}{4}\rho_{\alpha(\sigma, r_0, t)}, \tag{2.6b}$$

$$4\pi D r^2 \frac{\partial\rho_\alpha}{\partial r}\bigg|_{r=\sigma} = \frac{k_c^S - k_c^T}{4}\rho(\sigma, r_0, t) + \frac{k_c^S - k_c^T}{2}\rho_\Delta(\sigma, r_0, t) + \frac{k_c^S + 3k_c^T}{4}\rho_{\alpha(\sigma, r_0, t)}, \tag{2.6c}$$

$$4\pi D r^2 \frac{\partial\rho_\beta}{\partial r}\bigg|_{r=\sigma} = k_c^T \rho_\beta(\sigma, r_0, t). \tag{2.6d}$$

The last equation is separated from the others and can be omitted because the quantum yields we have to calculate do not depend on ρ_β but are expressed only through the other three variables.

The triplet products are truly determined by only the triplet sub-level populations integrated over time

$$\varphi_t(r_0) = k_c^T[\tilde\rho_0(\sigma, r_0, 0) + \tilde\rho_+(\sigma, r_0, 0) + \tilde\rho_-(\sigma, r_0, 0)] = k_c^T\left[\frac{3}{4}\tilde\rho(\sigma, r_0, 0) - \frac{1}{2}\tilde\rho_\Delta(\sigma, r_0, 0) - \frac{1}{4}\tilde\rho_\alpha(\sigma, r_0, 0)\right]. \tag{2.7}$$

As to the free radicals, their yield is actually $\rho(r, r_0, \infty)$ integrated over space

$$\varphi(r_0) = \int \lim_{s\to 0} s\tilde{\rho}(r, r_0, s)\, \mathrm{d}^3 r = 1 - k_D\left\{\left[\kappa' - \frac{\kappa}{2}\right]\tilde{\rho}(\sigma, r_0, 0) + \kappa\tilde{\rho}_\Delta(\sigma, r_0, 0) + \frac{\kappa}{2}\tilde{\rho}_\alpha(\sigma, r_0, 0)\right\}, \tag{2.8}$$

where

$$\kappa = \frac{k_c^S - k_c^T}{2k_D}, \quad \kappa' = \frac{k_c^S + k_c^T}{2k_D}. \tag{2.9}$$

As to the last quantum yield, for singlet products, it can be obtained from the first two and the conservation law [1]

$$\varphi_s(r_0) = 1 - \varphi_t(r_0) - \varphi(r_0). \tag{2.10}$$

It is common and useful to represent all the quantum yields as follows [1,6]:

$$\varphi = \frac{D}{D+Z}, \quad \varphi_t = \frac{Z_T}{D+Z}, \quad \varphi_s = \frac{Z_S}{D+Z}, \tag{2.11}$$

where Z_T and Z_S are the efficiencies of recombination from the triplet and singlet states of a pair and $Z = Z_T + Z_S$ is the total recombination efficiency.

3. Solution of the problem

From the structure of equations (2.5a)–(2.5c) we see that their solutions are the generalized functions [7] continuous in the whole r-domain, but their derivatives have discontinuities at $r = r_0$. At any $r \neq r_0$ the equations are homogeneous and their solutions take into account that any $\tilde{\rho}(r = \infty) = 0$. They are displayed in Table 1,

Table 1
General solution for the set (2.5)

	$r < r_0$	$r > r_0$
$\tilde{\rho}$	$(a_1/r)\exp\{-r\alpha_0/\sigma\} + (a_2/r)\exp\{r\alpha_0/\sigma\}$	$(a_3/r)\exp\{-r\alpha_0/\sigma\}$
$\tilde{\rho}_\Delta$	$(b_-/r)\exp\{-r\alpha_\Delta/\sigma\} + (b_2/r)\exp\{r\alpha_\Delta/\sigma\}$	$(b_3/r)\exp\{-r\alpha_\Delta/\sigma\}$
$\tilde{\rho}_\alpha$	$(c_1/r)\exp\{-r\alpha_\alpha/\sigma\} + (c_2/r)\exp\{r\alpha_\alpha/\sigma\}$	$(c_3/r)\exp\{-r\alpha_\alpha/\sigma\}$

where

$$\alpha_0 = \sigma\sqrt{s/D}, \quad \alpha_\Delta = \sigma\sqrt{(s + 2(k_0 + 1/T_2))/D}, \quad \alpha_\alpha = \sigma\sqrt{(s + 2/T_1)/D}. \tag{3.1}$$

The numerical constants $a_{1,2,3}$, $b_{1,2,3}$ and $c_{1,2,3}$ have to be found from the boundary conditions (2.6a)–(2.6c), taking into account that at $r = r_0$ all the functions defined at $r < r_0$ must be sewed together with their prolongations at $r > r_0$. With these nine constants one can get the exact values of $\tilde{\rho}(r, r_0, s)$, $\tilde{\rho}_\Delta(r, r_0, s)$ and $\tilde{\rho}_\alpha(r, r_0, s)$ which are the very complex expression given in Appendix A. Making inverse Laplace transformation of them one can recover the kinetics of geminate recombination.

Fortunately for the calculations of quantum yields from Eqs. (2.7) and (2.8) we need only the densities $\tilde{\rho}(\sigma, r_0, 0)$, $\tilde{\rho}_\Delta(\sigma, r_0, 0)$, $\tilde{\rho}_\alpha(\sigma, r_0, 0)$ that can be easily obtained from Eqs. (A.1)–(A.3) setting $r = \sigma$ and $s = 0$. In this particular case only two parameters characterizing the spin conversion remain non-zero:

$$\alpha_0 = 0, \quad \alpha_\Delta = \sqrt{2\frac{\tau_d}{T_2}(1 + k_0 T_2)} = \alpha, \quad \alpha_\alpha = \sqrt{2\frac{\tau_d}{T_1}} = \beta. \tag{3.2}$$

The first, α, coincides with that in Eq. (1.5) although the latter was introduced in the two-level theory assuming $T_1 = \infty$. In the present four-level theory the longitudinal relaxation is taken into account by a newly introduced parameter $\beta \neq 0$, but all the magnetic field effects are still accounted for by α, through k_0 defined in Eq. (1.6)

$$\tilde{\rho} = -\frac{1}{4\pi D r_0}\frac{\left[\beta\frac{k_c^S - k_c^T}{k_c^T + k_D} + \frac{k_c^S - k_c^T}{k_D}\right]e^{\alpha(1-r_0/\sigma)} + \left[\alpha\frac{k_c^S - k_c^T}{2(k_c^T + k_D)} + \frac{k_c^S - k_c^T}{2k_D}\right]e^{\beta(1-r_0/\sigma)} + P}{\alpha\left[\beta\frac{2k_D + \frac{3}{2}k_c^T + \frac{1}{2}k_c^S}{k_c^T + k_D} + 2 + \frac{k_c^S + k_c^T}{k_D}\right] + \beta\left(2 + \frac{3k_c^S + k_c^T}{2k_D}\right) + 2\left[1 + \frac{k_c^S + k_c^T}{k_D} + \frac{k_c^S k_c^T}{k_D^2}\right]},$$

$$\tilde{\rho}_\Delta = -\frac{1}{4\pi D r_0}\frac{\frac{k_c^S - k_c^T}{2k_D}e^{\beta(1-r_0/\sigma)} + \beta\frac{k_c^S - k_c^T}{2(k_c^T + k_D)} + \frac{k_c^S - k_c^T}{2k_D} - \left[\beta\frac{3k_c^T + k_c^S + 4k_D}{2(k_c^T + k_D)} + 2 + \frac{k_c^T + k_c^S}{k_D}\right]e^{\alpha(1-r_0/\sigma)}}{\alpha\left[\beta\frac{2k_D + \frac{3}{2}k_c^T + \frac{1}{2}k_c^S}{k_c^T + k_D} + 2 + \frac{k_c^S + k_c^T}{k_D}\right] + \beta\left(2 + \frac{3k_c^S + k_c^T}{2k_D}\right) + 2\left[1 + \frac{k_c^S + k_c^T}{k_D} + \frac{k_c^S k_c^T}{k_D^2}\right]},$$

$$\tilde{\rho}_\alpha = -\frac{1}{4\pi D r_0}\frac{\frac{k_c^S - k_c^T}{k_D}e^{\alpha(1-r_0/\sigma)} + \alpha\frac{k_c^S - k_c^T}{2(k_c^T + k_D)} + \frac{k_c^S - k_c^T}{2k_D} - \left[\alpha\frac{3k_c^T + k_c^S + 4k_D}{2(k_c^T + k_D)} + \frac{k_c^T + 3k_c^S + 4k_D}{2k_D}\right]e^{\beta(1-r_0/\sigma)}}{\alpha\left[\beta\frac{2k_D + \frac{3}{2}k_c^T + \frac{1}{2}k_c^S}{k_c^T + k_D} + 2 + \frac{k_c^S + k_c^T}{k_D}\right] + \beta\left(2 + \frac{3k_c^S + k_c^T}{2k_D}\right) + 2\left[1 + \frac{k_c^S + k_c^T}{k_D} + \frac{k_c^S k_c^T}{k_D^2}\right]},$$

where

$$P = -\alpha\frac{2k_D(\beta+1) + \frac{3}{2}k_c^T + \frac{1}{2}k_c^S}{k_c^T + k_D} - \beta\frac{k_c^S + k_c^T + 2k_D}{k_D + k_c^T} - \frac{3k_c^S + k_c^T + 4k_D}{2k_D}.$$

Substituting these results at $\beta = 0$ into the general definitions (2.7) and (2.8), we reproduced the expressions for $\varphi_t(r_0)$ and $\varphi(r_0)$ that have been derived for the two-level

system in [3], by a completely different method: see Eqs. (4.3) and (4.4) in this work.

4. Contact start

In the vast majority of analytical studies of the phenomenon, it was assumed for simplicity that the radicals are created at contact distance σ [1,2,4]. To compare with them we have to do the same, setting $r_0 = \sigma$. In this particular case, the last formulae truly become much more simple:

$$\tilde{\rho} = \frac{2}{k_D}\frac{\alpha\frac{k_c^T+k_D(1+\beta)}{k_c^T+k_D}+\beta+\frac{k_c^T+k_D}{k_D}}{\alpha\left[\beta\frac{2k_D+\frac{3}{2}k_c^T+\frac{1}{2}k_c^S}{k_c^T+k_D}+2+\frac{k_c^S+k_c^T}{k_D}\right]+\beta\left(2+\frac{3k_c^S+k_c^T}{2k_D}\right)+2\left[1+\frac{k_c^S+k_c^T}{k_D}+\frac{k_c^Sk_c^T}{k_D^2}\right]}, \tag{4.1a}$$

$$\tilde{\rho}_{\Delta} = \frac{2}{k_D}\frac{\beta+\frac{k_c^T+k_D}{k_D}}{\alpha\left[\beta\frac{2k_D+\frac{3}{2}k_c^T+\frac{1}{2}k_c^S}{k_c^T+k_D}+2+\frac{k_c^S+k_c^T}{k_D}\right]+\beta\left(2+\frac{3k_c^S+k_c^T}{2k_D}\right)+2\left[1+\frac{k_c^S+k_c^T}{k_D}+\frac{k_c^Sk_c^T}{k_D^2}\right]}, \tag{4.1b}$$

$$\tilde{\rho}_{\alpha} = \frac{2}{k_D}\frac{\alpha+\frac{k_c^T+k_D}{k_D}}{\alpha\left[\beta\frac{2k_D+\frac{3}{2}k_c^T+\frac{1}{2}k_c^S}{k_c^T+k_D}+2+\frac{k_c^S+k_c^T}{k_D}\right]+\beta\left(2+\frac{3k_c^S+k_c^T}{2k_D}\right)+2\left[1+\frac{k_c^S+k_c^T}{k_D}+\frac{k_c^Sk_c^T}{k_D^2}\right]}. \tag{4.1c}$$

Using them in Eqs. (2.7) and (2.8) we calculated the quantum yields and deduced from them the recombination efficiencies. The expressions for any of them are always much simpler than for the corresponding yields

$$Z/D = \frac{1}{k_D}\left[k_c^S + \frac{\frac{1}{2}\alpha(k_c^T-k_c^S)}{1+\alpha+k_c^T/k_D} + \frac{\frac{1}{4}\beta(k_c^T-k_c^S)}{1+\beta+k_c^T/k_D}\right]. \tag{4.2}$$

In the particular case of a two-level system ($\beta = 0$), the general expression (4.2) reduces to the following simpler formula:

$$Z/D = \frac{k_c^S}{k_D}\left[1+\frac{\alpha(k_c^T-k_c^S)}{2k_c^S(\alpha+1+k_c^T/k_D)}\right], \tag{4.3}$$

found in [3].

In the pioneering work of Schulten and Schulten [8] the spin-conversion was assumed to be separated from the inter-particle dynamics due to the equality of the recombination constants

$$k_c^S = k_c^T = k_c. \tag{4.4}$$

In this particular case, the total recombination efficiency (4.2) does not depend on the spin-conversion at all and is equal to the conventional parameter z of the simplest exponential model, as in Eq. (1.4) [5,6]. That is

$$Z = z \quad \text{and} \quad \varphi = \frac{1}{1+z/D} \tag{4.5}$$

at any k_0, that is at any magnetic field.

At the same time, the recombination to the triplet product is always spin dependent. As follows from Eqs. (2.7) and (2.11):

$$Z_T/D = \frac{k_c^T}{2k_D}\left[\frac{\alpha}{1+\alpha+k_c^T/k_D}+\frac{\beta}{2(1+\beta+k_c^T/k_D)}\right]. \tag{4.6}$$

The efficiency of recombination to the singlet one, following from Eqs. (2.11) and (2.8), is also spin-dependent:

$$Z_S/D = \frac{k_c^S}{2k_D}\left[\frac{\alpha+2(1+k_c^T/k_D)}{1+\alpha+k_c^T/k_D}-\frac{\beta}{2(1+\beta+k_c^T/k_D)}\right]. \tag{4.7}$$

As always $Z = Z_T + Z_S$, and each of the components is diffusion dependent.

5. Relation to other theories

In the particular case of a two-level system ($\beta = 0$) the result (4.6) reduces to that obtained in [3]

$$Z_T/D = \frac{k_c^T}{k_D}\frac{\alpha/2}{(1+\alpha+k_c^T/k_D)} \quad \text{at} \quad T_1 = \infty. \tag{5.1}$$

On the other hand, rather different result was found earlier in [1]

$$Z_T/D = \frac{k_c^T}{k_D}\frac{3\alpha_0/4}{(1+\alpha_0+k_c^T/k_D)} \quad \text{at} \quad T_1 = T_2 = T_0, \tag{5.2}$$

where α_0 is expressed through the spin-conversion rate k_s defined in [6]

$$\alpha_0 = \sqrt{4k_s\tau_d} = \sqrt{2\tau_d\left(\frac{1}{T_0}+\frac{2\Omega^2T_0}{3}\right)}. \tag{5.3}$$

The last results were derived within the simplified model of spin conversion used in a number of previous works [5,9–12]

$$\begin{array}{ccc} {}^1[\dot{A}\cdots\dot{D}] & \underset{k_s}{\overset{3k_s}{\rightleftarrows}} & {}^3[\dot{A}\cdots\dot{D}] \\ \Downarrow k_c^S & & \Downarrow k_c^T \\ [A\cdots D] & & [{}^3A^*\cdots D] \end{array} \tag{5.4}$$

According to this model the spin conversion equally mixes the singlet state with all three sub-levels of the triplet one. That is the reason why the last result differs from the

previous one. The simple analysis shows that this result follows from the general formula (4.6) provided that:

$$\Omega = H = 0 \quad \text{and} \quad \alpha = \beta = \sqrt{2\tau_d/T_0}. \tag{5.5}$$

Hence, in the extreme case of equal relaxation times (usually presumed), the model (5.4) is exact in the zero magnetic fields provided the recombination rates through different channels are equal as in Eq. (4.4). Under this condition the total yield φ from Eq. (4.5) can be used as an argument (instead of diffusion) to study the other yields as functions of φ changing in the finite limits, $0 \leqslant \varphi \leqslant 1$ [8,3]. In Fig. 1, the diffusional dependence of the yields presented in such a way demonstrates the non-monotonous behavior of φ_T unlike φ_S, decreasing monotonously with diffusion. The latter is the difference between the diagonal and the curves which represent φ_T. One of them (at $\alpha = \beta$ coincides with that resulting from the model calculations of φ_T, while another ($\beta = 0$) is the same quantity exactly calculated for the two-level system and shown in Fig. 2 of [3].

In moderate fields the spin-conversion parameters, α and α_0 can be expanded in $\Omega T_0 \ll 1$

$$\alpha \approx \beta(1 + \Omega^2 T_0^2/2), \tag{5.6a}$$

$$\alpha_0 \approx \beta(1 + \Omega^2 T_0^2/3). \tag{5.6b}$$

In the first-order approximation with respect to $\Omega^2 T_0^2$, we have from the exact expression (4.6) as well as from its model analog, Eq. (5.2), one and the same result

$$Z_T/D = \frac{k_c^T}{k_D}\frac{3\beta/4}{1+\beta+k_c^T/k_D}\left(1+\frac{\Omega^2 T_0^2}{3}\frac{1+k_c^T/k_D}{1+\beta+k_c^T/k_D}\right),$$

$$\text{where } \beta = \sqrt{2\frac{\tau_d}{T_0}}. \tag{5.7}$$

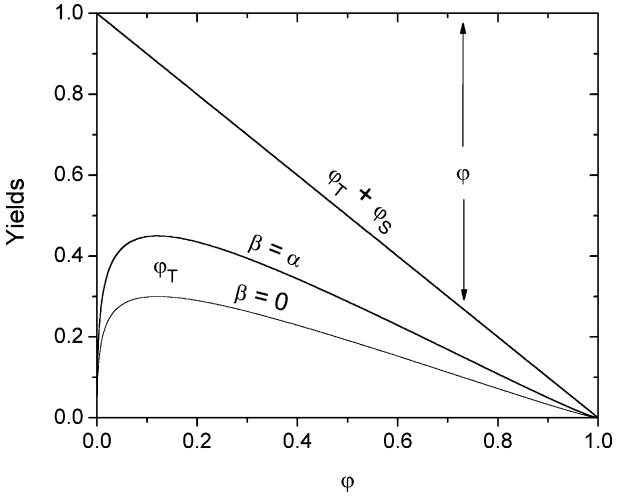

Fig. 1. The partition of all the products of double-channel recombination with equal rates into three components: the free radicals quantum yield φ, the yield of triplets φ_T, and that of singlets, $\varphi_S = 1 - \varphi - \varphi_T$. At $\beta = \alpha$ and zero field the present theory confirms the results following from the model (5.4) while at $\beta = 0$ it reproduces the situation when only two interacting levels remain in the system [3].

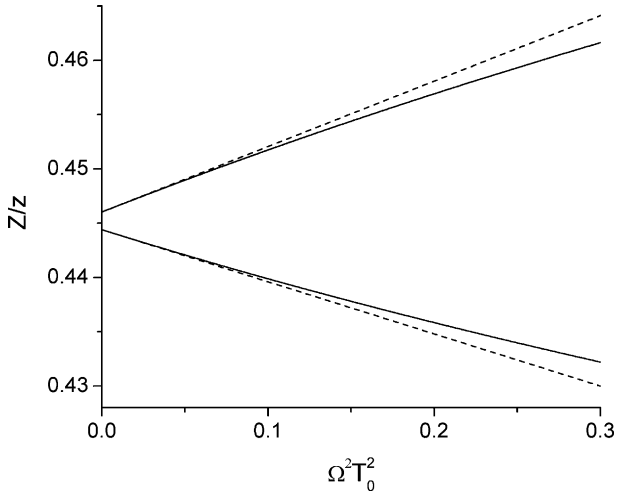

Fig. 2. The single-channel recombination efficiencies, from the triplet (above) and singlet (below), as functions of the magnetic field in square ($\Omega^2 \sim H^2$) at $D = 1.2 \times 10^{-5}$ cm^2/s, $\sigma = 7$ Å, $T_0 = 0.1$ ns and $z = 1.14 \times 10^{-5}$ cm^2/s. The exact results given by Eqs. (4.6) and (5.8) are represented by the solid lines and their linear interpolations, Eqs. (5.7) and (5.11), by dashed lines.

Hence, in the lowest-order approximation the simple model (5.4) describes the magnetic field effect as accurate as the present theory. This approximation is quasi-linear in $\Omega^2 \sim H^2$ until $\Omega^2 T_0^2 \ll 1$ (Fig. 2).

Another situation appears if the triplet channel is switched off. When $k_c^T = 0$ the recombination proceeds through the singlet channel alone and the general formula (4.2) reduces to the particular one

$$Z = \frac{z}{2}\left[\frac{2+\alpha}{1+\alpha} - \frac{\beta}{2(1+\beta)}\right] = Z_S \quad z = \frac{k_c^S}{4\pi\sigma}. \tag{5.8}$$

This is exactly what was obtained in the first single-channel theory of Mints and Pukhov [4]. The efficiency of recombination in the two-level system [3] follows from here at $\beta = 0$

$$Z_s = z\frac{1+\alpha/2}{1+\alpha}, \quad \beta = 0. \tag{5.9}$$

A similar result was obtained for the four-level model in [1]

$$Z_S = z\frac{1+\alpha_0/4}{1+\alpha_0}. \tag{5.10}$$

In the zero field (when $\Omega = 0$), the latter result coincides with that following from the general Eq. (5.8) at $\alpha = \alpha_0 = \beta$. In moderate fields, the exact and model results are also identical but in the lowest-order in $\Omega^2 T_0^2$ (see Fig. 2)

$$Z = z\left[\frac{1+\beta/4}{1+\beta} - \frac{\Omega^2 T_0^2}{4}\frac{\beta}{(1+\beta)^2}\right]. \tag{5.11}$$

This provides evidence that the simple model (5.4) is practically sufficient for studying the radical reactions assisted by an incoherent spin conversion.

It should be stressed that Z_T from Eq. (4.6) remains the same at any k_c^S. However, this is not true regarding the triplet

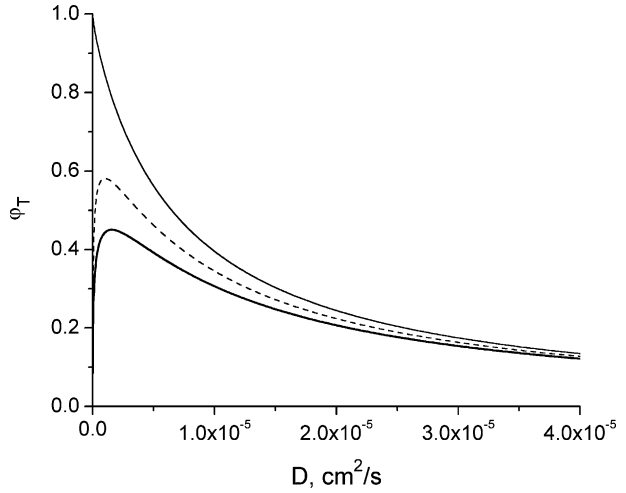

Fig. 3. The diffusional dependence of the triplet quantum yield at $k_c^S = 0$, $k_c^S = 0.5k_c^T$, $k_c^S = k_c^T$ (from top to bottom) at $\Omega T_0 = 0.14$ and $k_c^T = 10^4$ Å^3/ns. The rest of the parameters are the same as in the previous figure.

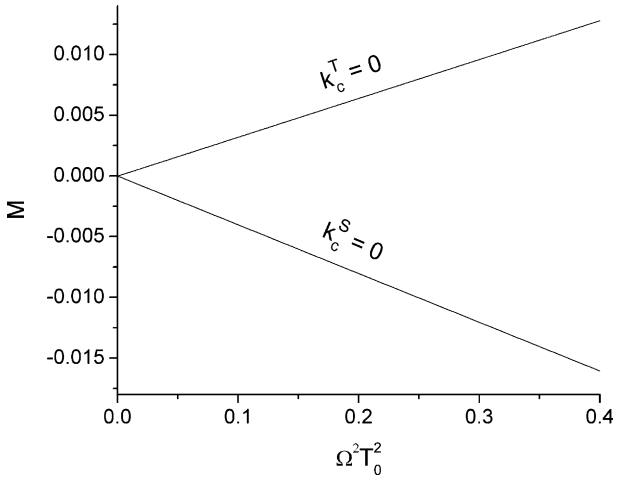

Fig. 4. The magnetic field effect for single-channel recombination through either the triplet (below) or singlet (above) states in the linear approximation regarding $\Omega^2 \sim H^2$ shown by the dashed lines in Fig. 2.

quantum yield $\varphi_t = Z_T/(D+Z)$. In particular, $\varphi_t = Z_T/(D+z)$ if the recombination rates are equal ($k_c^S = k_c^T$; $Z = z = \text{const}$). In this case the diffusional dependence $\varphi_t(D)$ duplicates the bell shape of Z_T. On the contrary, at $k_c^S = Z_s = 0$, when the singlet recombination channel is switched off, $Z = Z_T$, and the triplet yield $\varphi_t = Z_T/(D+Z_T)$ falls monotonously with D, from 1 to 0. Fig. 3 shows how the latter transforms to the former when k_c^S increases.

6. Magnetic field effects

Both recombination efficiencies (4.6) and (4.7), depend on magnetic field through the single parameter α containing $\Omega \sim H$. Therefore, the magnetic field affects also the quantum yields (2.11) but only the H-dependence of the free radicals quantum yield was studied experimentally until now. The conventional measure of the magnetic field effect (MFE) can be represented as follows:

$$M = \frac{\varphi(H) - \varphi(0)}{\varphi(0)} = \frac{Z(0) - Z(H)}{D + Z(H)}. \tag{6.1}$$

The incoherent description of the field induced spin-conversion is valid at rather low or moderate magnetic fields when

$$\Omega^2 T_0^2 = \left(\frac{\Delta g \beta H T_0}{\hbar}\right)^2 \ll 1. \tag{6.2}$$

Under this condition, we can use the lowest-order expansion of Z in this parameter.

For the particular case of single-channel recombination from the triplet state, $Z = Z_T$ is given by expression (5.7) linear in $\Omega^2 T_0^2$. The corresponding MFE is also linear with the same accuracy

$$M = -\frac{k_c^T}{k_D}\frac{\beta(1 + k_c^T/k_D)}{4(1+\beta+k_c^T/k_D)}\frac{\Omega^2 T_0^2}{1 + k_c^T/k_D + \beta\left(1 + \frac{3}{4}k_c^T/k_D\right)} \quad \text{at} \quad k_c^S = 0. \tag{6.3}$$

In the opposite case of recombination via only a singlet channel, the linearized function (5.11) should be used instead in Eq. (6.1) to get the following:

$$M = \frac{k_c^S}{k_D}\frac{\beta}{4(1+\beta)}\frac{\Omega^2 T_0^2}{1 + k_c^S/k_D + \beta\left(1 + \frac{1}{4}k_c^S/k_D\right)} \quad \text{at} \quad k_c^T = 0. \tag{6.4}$$

As can be seen from Fig. 4 the MFE has the opposite signs for the considered alternative limits. Being linear in $\Omega^2 T_0^2$ it is quadratic in the magnetic field H. However, the scale of MFE is limited to a 1–2% within the field interval (6.2) covered by the incoherent theory. In reality much stronger fields are available and the MFE can reach 25% [18]. For a quantitative description of such large effects, the general coherent theory must be used instead as has been done in [11]. The present theory is exact for spin conversion in a zero field but only an approximation for the non-zero field of low and moderate strength.

7. Conclusions

We present here a general solution for the problem of singlet radical pair recombination at contact through one or two parallel channels, assuming that it is assisted by incoherent spin conversion executed by spin relaxation and the Δg-mechanism. It reproduces all the efficiencies of contact recombination obtained earlier within the rate description of spin conversion as well as their diffusional and field dependencies. It was shown that the exact and model treatment of the problem lead to the results which are identical in the lowest-order approximation in the magnetic field. Our general results, valid at any initial separation of radicals in a pair, r_0, can be averaged over the initial distribution of these distances $f(r_0)$ if it is known.

The main restriction of the theory is the stochastic (rate) description of spin conversion in a non-zero magnetic field. It is justified if spin relaxation in radicals is much faster

than the difference between their resonance frequencies. This condition is met in a number of transition metal complexes with strong spin–orbital coupling [13–15], where $T_2 \approx T_1 \sim 10$ ps. Quite the opposite is the situation with organic radicals whose spin relaxation is about a few μs while the frequency of the hyperfine interaction responsible for spin conversion is higher than the relaxation rates. This is the coherent conversion that was widely studied, as well as the magnetic field effects resulting from it. However, to the best of our knowledge all these studies were confined to single channel recombination. The double-channel recombination assisted by coherent conversion is still open for discussion.

Another restriction is the contact approximation of recombination. In fact, the latter is distant at least for electron tunnelling in radical–ion pairs, at high exergonicity of their recombination [16,6]. This limitation can be overcome with a numerical solution of the problem, as it was done in [17,6] for the particular tunnelling rate, $W(r-\sigma)$.

It also should be mentioned that the most of the authors confined themselves to a single channel recombination of singlet born radical pair, whereas Mints and Pukhov took also into consideration the radical pair born in either of the triplet sub-states. Such an initial condition, as well as the start from the equally populated triplet sub-states, is worthy of separate study which is now in progress.

Appendix A

After long and cumbersome calculations, we obtained the following results:

$$\tilde{\rho} = \frac{\sigma}{8\pi D\alpha_0 r r_0}\left(e^{-|r-r_0|\alpha_0/\sigma} + \frac{4\kappa\alpha_0(\kappa+d_-)e^{\alpha_0(1-r/\sigma)+\alpha_\Delta(1-r_0/\sigma)} + 2\kappa\alpha_0(\kappa+b_-)e^{\alpha_0(1-r/\sigma)+\alpha_\alpha(1-r_0/\sigma)} + P_1 e^{\alpha_0(2-(r+r_0)/\sigma)}}{2\kappa[\kappa^2 - b_-(c_-+d_-)/2] + \kappa^2(c_-+d_-) - 2b_-c_-d_-}\right), \tag{A.1}$$

$$\tilde{\rho}_\Delta = \frac{\sigma}{8\pi D\alpha_\Delta r r_0}\left(e^{-|r-r_0|\alpha_\Delta/\sigma} + \frac{2\kappa\alpha_\Delta(\kappa+c_-)e^{\alpha_\Delta(1-r/\sigma)+\alpha_\alpha(1-r_0/\sigma)} + 2\kappa\alpha_\Delta(\kappa+d_-)e^{\alpha_\Delta(1-r/\sigma)+\alpha_0(1-r_0/\sigma)} + P_2 e^{\alpha_\Delta(2-(r+r_0)/\sigma)}}{2\kappa[\kappa^2 - b_-(c_-+d_-)/2] + \kappa^2(c_-+d_-) - 2b_-c_-d_-}\right), \tag{A.2}$$

$$\tilde{\rho}_\alpha = \frac{\sigma}{8\pi D\alpha_\alpha r r_0}\left(e^{-|r-r_0|\alpha_\alpha/\sigma} + \frac{4\kappa\alpha_\alpha(\kappa+c_-)e^{\alpha_\alpha(1-r/\sigma)+\alpha_\Delta(1-r_0/\sigma)} + 2\kappa\alpha_\alpha(\kappa+b_-)e^{\alpha_\alpha(1-r/\sigma)+\alpha_0(1-r_0/\sigma)} + P_3 e^{\alpha_\alpha(2-(r+r_0)/\sigma)}}{2\kappa[\kappa^2 - b_-(c_-+d_-)/2] + \kappa^2(c_-+d_-) - 2b_-c_-d_-}\right), \tag{A.3}$$

where κ and κ' were defined in Eq. (2.9),

$$P_1 = 2b_-c_+d_- + \kappa(c_+ + d_-)(b_- - \kappa) - 2\kappa^3,$$
$$P_2 = 2b_+c_-d_- + \kappa(c_- + d_-)(b_+ - \kappa) - 2\kappa^3,$$
$$P_3 = 2b_-c_-d_+ + \kappa(c_- + d_+)(b_- - \kappa) - 2\kappa^3$$

and

$$c_\pm = -1 \pm \alpha_0 - \kappa',$$
$$b_\pm = -1 \pm \alpha_\Delta - \kappa',$$
$$d_\pm = -1 \pm \alpha_\alpha - \kappa'.$$

If there is no recombination $k_c^S = k_c^T = 0$, $\kappa = \kappa' = 0$ and all $\tilde{\rho}(r, r_0, s)$, $\tilde{\rho}_\Delta(r, r_0, s)$, $\tilde{\rho}_\alpha(r, r_0, s)$ reduce to the corresponding Green-functions

$$\tilde{\rho} = \frac{\sigma}{8\pi D\alpha_0 r r_0}\left(e^{-|r-r_0|\alpha_0/\sigma} - \frac{1-\alpha_0}{1+\alpha_0}e^{\alpha_0(2-(r+r_0)/\sigma)}\right),$$
$$\tilde{\rho}_\Delta = \frac{\sigma}{8\pi D\alpha_\Delta r r_0}\left(e^{-|r-r_0|\alpha_\Delta/\sigma} - \frac{1-\alpha_\Delta}{1+\alpha_\Delta}e^{\alpha_\Delta(2-(r+r_0)/\sigma)}\right),$$
$$\tilde{\rho}_\alpha = \frac{\sigma}{8\pi D\alpha_\alpha r r_0}\left(e^{-|r-r_0|\alpha_\alpha/\sigma} - \frac{1-\alpha_\alpha}{1+\alpha_\alpha}e^{\alpha_\alpha(2-(r+r_0)/\sigma)}\right).$$

References

[1] V.S. Gladkikh, A.I. Burshtein, G. Angulo, G. Grampp, Phys. Chem. Chem. Phys. 5 (2003) 2581.
[2] M.J. Hansen, A.A. Neufeld, J.B. Pedersen, Chem. Phys. 260 (2000) 125.
[3] A.I. Burshtein, J. Chem. Phys. (in press).
[4] R.G. Mints, A.A. Pukhov, Chem. Phys. 87 (1984) 467.
[5] A.I. Burshtein, Adv. Chem. Phys. 114 (2000) 419.
[6] A.I. Burshtein, Adv. Chem. Phys. 129 (2004) 105.
[7] I.M. Gel'fand, G.E. ShilovGeneralized Functions, vol. 1, Academic Press, New York, 1964, p. 22 (Chapter I.2).
[8] Z. Schulten, K. Schulten, J. Chem. Phys. 66 (1977) 4616.
[9] A.I. Burshtein, E.B. Krissinel, J. Phys. Chem. A 102 (1998) 7541.
[10] A.I. Burshtein, E. Krissinel, J. Phys. Chem. A 102 (1998) 816.
[11] E. Krissinel, A.I. Burshtein, N. Lukzen, U. Steiner, Mol. Phys. 96 (1999) 1083.
[12] A.I. Burshtein, E. Krissinel, J. Phys. Chem. 100 (1996) 3005.
[13] U.E. Steiner, Th. Ulrich, Chem. Rev. 89 (1989) 51.
[14] E.B. Krissinel, A.I. Burshtein, N.N. Lukzen, U.E. Steiner, Mol. Phys. 96 (1999) 1083.
[15] A.I. Burshtein, E. Krissinel, U.E. Steiner, Phys. Chem. Chem. Phys. 3 (2001) 198.
[16] A.I. Burshtein, A.A. Neufeld, J. Phys. Chem. B 105 (2001) 12364.
[17] A.A. Neufeld, A.I. Burshtein, G. Angulo, G. Grampp, J. Chem. Phys. 116 (2002) 2472.
[18] H.-J. Wolff, D. Bürßner, U. Steiner, Pure Appl. Chem. 67 (1) (1995) 167.

Double-Channel Contact Recombination of Radical Pairs Subjected to Spin Conversion via the Δg Mechanism

V. S. Gladkikh and A. I. Burshtein*

Weizmann Institute of Science, Rehovot 76100, Israel

Received: September 5, 2005; In Final Form: December 21, 2005

The contact recombination from both singlet and triplet states of a radical pair is studied assuming that the spin conversion is carried out by the fast transversal relaxation and Δg mechanism. The alternative HFI mechanism is neglected as being much weaker in rather large magnetic fields. The magnetic-field-dependent quantum yields of the singlet and triplet recombination products, as well as of the free radical production, are calculated for any initial spin state and arbitrary separation of radicals in a pair. The magnetic field effect is traced and its diffusional (viscosity) dependence is specified.

1. Introduction

The most general diffusional theory of contact but spinless geminate recombination of an ion pair was developed by Hong and Noolandi.[1] Later on, the theory was developed further in a few works[2,3] and extended for the noncontact recombination from any starting distance between reactants[4,5] (see also section VIIB in the review[6]).

However, as was recognized long ago, in pairs of radicals or ion radicals the recombination is affected by spin conversion between initially populated and other spin states. Such a conversion is carried out by the spin relaxation and/or some mechanisms acting in a magnetic field. These are the Δg mechanism of spin conversion in pairs of radicals having different g factors and the mechanism of the hyperfine interaction (HFI) between the electron and nuclear spins if any. The HFI mechanism alone was studied a number of times assuming that the radical recombination proceeds via a single channel (either singlet or triplet).[7] This is a situation typical for the radical pairs with such long spin relaxation times T_2 and T_1 that the corresponding rates $1/T_2$ and $1/T_1$ are negligible in comparison with a rather large HFI constant A. Just recently, HFI theory was extended for the double-channel recombination which proceeds into both singlet and triplet products though in a zero magnetic field.[8] Here, we are going to do quite the opposite: neglecting HFI in comparison with the fast transversal spin relaxation $1/T_2$, we will study the magnetic field effect (MFE) produced by the Δg mechanism of spin conversion. The spin relaxation really dominates over HFI in transition metal complexes with strong spin−orbital coupling.[9−11] The exact solution of this problem will be obtained analytically assuming that recombination from the singlet and triplet states of the radical pair proceeds only at contact, with the constants k_c^S and k_c^T, respectively. Provided $AT_2 \ll 1$ is really negligible, the theory is valid at arbitrary magnetic fields though it takes into account only the Δg mechanism of spin conversion.

The pair of radicals created in either of its singlet or triplet states can recombine from there in the singlet or triplet products or be separated with the quantum yield φ.

* To whom correspondence should be addressed. E-mail: anatoly.burshtein@weizmann.ac.il.

$$\varphi_t \qquad D + {}^3A^* \overset{k_c^T}{\longleftarrow} {}^3[\dot{D} \ldots \dot{A}] \longrightarrow \dot{D} + \dot{A} \tag{1.1a}$$

$$T_2^{-1} \updownarrow \Omega \qquad\qquad \varphi$$

$$\varphi_s \qquad D + A \underset{k_c^S}{\longleftarrow} {}^1[\dot{D} \ldots \dot{A}] \longrightarrow \dot{D} + \dot{A} \tag{1.1b}$$

Here, T_2 is the transversal relaxation time assumed to be the same in both radicals and

$$\Omega = \frac{1}{2\hbar} \Delta g \beta_0 H \tag{1.2}$$

Here, β_0 is the Bohr magneton, $\Delta g = g_+ - g_-$ where g_+ and g_- are g factors of radical ions in a pair and H is the external magnetic field.

Unlike the majority of our previous works reviewed in refs 6 and 12, here, we do not assume that $\Omega T_2 \ll 1$, allowing the spin conversion to be coherent in a large field. The best analytical solution of this problem valid at any Ω was obtained by Mints and Pukhov[13] but only for a single-channel recombination of a radical pair (RP)—just from its singlet state to the ground state of the product. Unfortunately, the authors did not present the evaluation of their results, and to generalize them for the double-channel recombination, we have to derive everything from the very beginning.

This goal will be reached with a method disclosed in the next section.

II. General Formalism

The density matrix of the radical pair depending on the interradical distance r and time t obeys the following evolution equation[15,16]

$$\frac{\partial \rho(r,t)}{\partial t} = \hat{L}\rho(r,t) + \hat{\mathcal{K}}\rho(r,t) - \hat{W}(r)\rho(r,t) \tag{2.1}$$

with a reflective boundary condition at the contact of radicals $r = \sigma$

$$\hat{j}\rho(r,t)|_{r=\sigma} = 0 \tag{2.2}$$

Here, $\hat{L}$ is the operator diagonal in the Liouville space which

10.1021/jp0550107 CCC: $33.50
Published on Web 02/23/2006

describes the relative stochastic motion of the radicals, while $\hat{j}$ is a flux operator. As to $\hat{\mathscr{L}}$, this is the Liouville operator which consists of the rates of the paramagnetic relaxation and the spin transitions induced by the magnetic field. The rate operator $\hat{W}(r)$ represents the radical recombination depending on the distance between the radicals, r. The recombination occurs from either the singlet or triplet state of the radical ion pair (RIP) or from both of them.

One can represent the Laplace transformation of the solution of eq 2.1 as

$$\tilde{\rho}(r,r_0,s) = \tilde{\hat{G}}_0(r,r_0,s)\rho_0 - \int \tilde{\hat{G}}_0(r,r',s)\hat{W}(r')\tilde{\rho}(r',r_0,s)\,\mathrm{d}^3r' \tag{2.3}$$

where $\rho_0 = \rho(r,r_0,0)$ and $\hat{G}_0(r,r_0,t)$ is the Green function obeying the following equation

$$\frac{\partial \hat{G}_0(r,r_0,t)}{\partial t} = \hat{L}\hat{G}_0(r,r_0,t) + \hat{\mathscr{L}}\hat{G}_0(r,r_0,t),$$

$$\hat{G}_0(r,r_0,0) = \frac{\delta(r-r_0)}{4\pi r^2}\hat{E} \tag{2.4}$$

where $\hat{E}$ is an identity operator. It is convenient to represent the operator Green function

$$\hat{G}_0(r,r_0,t) = \mathrm{e}^{\hat{\mathscr{L}}t}\phi(r,r_0,t) \tag{2.5}$$

via the scalar analogue $\phi(r,r_0,t)$, which obeys the conventional diffusional equation with evident initial and boundary conditions

$$\frac{\partial \phi(r,r_0,t)}{\partial t} = \hat{L}\phi(r,r_0,t),\ \phi(r,r_0,0) = \frac{\delta(r-r_0)}{4\pi r^2},\ \left.\frac{\partial \phi}{\partial r}\right|_{r=\sigma} = 0 \tag{2.6}$$

The sole restriction of the present theory is the assumption that the recombination takes place only at contact, that is, that the rate operator $\hat{W}(r)$ is

$$\hat{W}(r) = \hat{Q}\,\frac{\delta(r-\sigma)}{4\pi\sigma^2} \tag{2.7}$$

where $\hat{Q}$ depends only on the rate constants k_c^S and k_c^T. Substituting this expression into eq 2.3, we have

$$\tilde{\rho}(r,r_0,s) = \tilde{\hat{G}}_0(r,r_0,s)\rho_0 - \tilde{\hat{G}}_0(r,\sigma,s)\hat{Q}\tilde{\rho}(\sigma,r_0,s) \tag{2.8}$$

This is a closed expression for the contact density matrix, $\tilde{\rho}(\sigma,r_0,s)$. Resolving it we obtain

$$\tilde{\rho}(\sigma,r_0,s) = [\hat{E} + \tilde{\hat{G}}_0(\sigma,\sigma,s)\hat{Q}]^{-1}\tilde{\hat{G}}_0(\sigma,r_0,s)\rho_0 \tag{2.9}$$

This important result was obtained by Purtov and Doktorov[14] and efficiently used in a recent investigation of the spin conversion induced by the HFI mechanism.[8]

The quantum yields of the singlet and triplet products of geminate recombination are defined through the components of the matrix 2.9

$$\varphi_s(r_0) = k_c^S\tilde{\rho}_{SS}(\sigma,r_0,0) \tag{2.10}$$

$$\varphi_t(r_0) = k_c^T[\tilde{\rho}_{T_0T_0}(\sigma,r_0,0) + \tilde{\rho}_{T_-T_-}(\sigma,r_0,0) + \tilde{\rho}_{T_+T_+}(\sigma,r_0,0)] \tag{2.11}$$

In the Liouville space basis (ρ_{SS}, $\rho_{T_0T_0}$, $\mathscr{R}\rho_{ST0}$, $\mathscr{J}\rho_{ST0}$, $\rho_{T_-T_-}$, $\rho_{T_+T_+}$), chosen by Mints and Pukhov,[13] we have

$$\hat{\mathscr{L}} = \begin{pmatrix} -\left(\frac{1}{2T_1}+\frac{1}{T_2}\right) & \frac{1}{T_2}-\frac{1}{2T_1} & 0 & -2\Omega & \frac{1}{2T_1} & \frac{1}{2T_1} \\ \frac{1}{T_2}-\frac{1}{2T_1} & -\left(\frac{1}{2T_1}+\frac{1}{T_2}\right) & 0 & 2\Omega & \frac{1}{2T_1} & \frac{1}{2T_1} \\ 0 & 0 & -\frac{1}{T_1} & 0 & 0 & 0 \\ \Omega & -\Omega & 0 & -\frac{2}{T_2} & 0 & 0 \\ \frac{1}{2T_1} & \frac{1}{2T_1} & 0 & 0 & -\frac{1}{T_1} & 0 \\ \frac{1}{2T_1} & \frac{1}{2T_1} & 0 & 0 & 0 & -\frac{1}{T_1} \end{pmatrix} \tag{2.12}$$

where T_1 and T_2 are the longitudinal and transversal times of paramagnetic relaxation, while the mixing of the S and T_0 states occurs with a frequency Ω from eq 1.2. The recombination operator $\hat{Q}$ in the same basis takes the form

$$\hat{Q} = \begin{pmatrix} k_c^S & 0 & 0 & 0 & 0 & 0 \\ 0 & k_c^T & 0 & 0 & 0 & 0 \\ 0 & 0 & \frac{k_c^S+k_c^T}{2} & 0 & 0 & 0 \\ 0 & 0 & 0 & \frac{k_c^S+k_c^T}{2} & 0 & 0 \\ 0 & 0 & 0 & 0 & k_c^T & 0 \\ 0 & 0 & 0 & 0 & 0 & k_c^T \end{pmatrix} \tag{2.13}$$

By finding $\hat{G}_0(r,r_0,t)$ from eqs 2.5 and 2.6 and substituting its Laplace transformation into eq 2.9, one can solve this matrix equation using $\hat{Q}$ from eq 2.13. The elements of the matrix obtained determine not only the partial yields of the recombination products from eqs 2.10 and 2.11 but also the yield of the separated radicals which escape recombination and become free

$$\varphi(r_0) = 1 - \varphi_s(r_0) - \varphi_t(r_0) \tag{2.14}$$

We usually represent all the yields as follows[17,6]

$$\varphi = \frac{D}{D+Z}$$

$$\varphi_t = \frac{Z_t}{D+Z}$$

$$\varphi_s = \frac{Z_s}{D+Z} \tag{2.15}$$

where Z_s and Z_t are the efficiencies of recombination through the singlet and triplet channels, respectively, while

$$Z = Z_s + Z_t$$

is the total efficiency of geminate recombination.

III. Exact Solution of the Problem

In our previous article, we solved the double-channel problem of geminate recombination assuming that the spin conversion

is incoherent which is the case at $\Omega T_2 \ll 1$.[18] This limitation was obviated by Mints and Pukhov,[13] who solved the problem exactly (i.e., generally, for coherent spin conversion) but for a single (singlet) recombination channel, when $Z_t = 0$ while $Z_s = Z \neq 0$. Here, we have to do the same but for the double-channel recombination when both Z_t and Z_s are not zero.

As the first step, one has to specify the exponent operator $e^{\hat{\mathcal{H}}t}$ in eq 2.5 that was found to be the following

$$e^{\hat{\mathcal{H}}t} = \begin{pmatrix} A_+ & A_- & 0 & -\sin(2\Omega t)e^{-2t/T_2} & B & B \\ A_- & A_+ & 0 & \sin(2\Omega t)e^{-2t/T_2} & B & B \\ 0 & 0 & e^{-t/T_1} & 0 & 0 & 0 \\ \frac{\sin(2\Omega t)}{2}e^{-2t/T_2} & -\frac{\sin(2\Omega t)}{2}e^{-2t/T_2} & 0 & \cos(2\Omega t)e^{-2t/T_2} & 0 & 0 \\ B & B & 0 & 0 & C_+ & C_- \\ B & B & 0 & 0 & C_- & C_+ \end{pmatrix} \tag{3.1}$$

where

$$A_\pm = \frac{1}{4} + \frac{1}{4}e^{-2t/T_1} \pm \frac{\cos(2\Omega t)}{2}e^{-2t/T_2}$$

$$B = \frac{1}{4} - \frac{1}{4}e^{-2t/T_1}$$

$$C_\pm = \frac{1}{4} + \frac{1}{4}e^{-2t/T_1} \pm \frac{1}{2}e^{-t/T_1}$$

In the particular case $T_2 \ll T_1 = \infty$, we have $B = C_\pm = 0$ and the rank of the problem reduces to 4×4 and becomes formally identical to the case of spin conversion via the HFI mechanism at the highest fields,[19] provided the exchange splitting of the singlet and triplet is negligible. For the particular case of incoherent spin conversion, the same problem was solved recently in refs 20 and 21.

Solving eq 2.6 and using the result in eq 2.5, we calculated exactly the Laplace transformation of the Green operator

$$\tilde{\tilde{G}}_0(\sigma,r_0,0) = \begin{pmatrix} \frac{F}{4}+\frac{P_2}{4}+\frac{Q_1}{4} & \frac{F}{4}+\frac{P_2}{4}-\frac{Q_1}{4} & 0 & -\frac{Q_2}{2} & \frac{F}{4}-\frac{P_2}{4} & \frac{F}{4}-\frac{P_2}{4} \\ \frac{F}{4}+\frac{P_2}{4}-\frac{Q_1}{4} & \frac{F}{4}+\frac{P_2}{4}+\frac{Q_1}{4} & 0 & \frac{Q_2}{2} & \frac{F}{4}-\frac{P_2}{4} & \frac{F}{4}-\frac{P_2}{4} \\ 0 & 0 & P_1 & 0 & 0 & 0 \\ \frac{Q_2}{4} & -\frac{Q_2}{4} & 0 & \frac{Q_1}{2} & 0 & 0 \\ \frac{F}{4}-\frac{P_2}{4} & \frac{F}{4}-\frac{P_2}{4} & 0 & 0 & \frac{F}{4}+\frac{P_2}{4}+\frac{P_1}{2} & \frac{F}{4}+\frac{P_2}{4}-\frac{P_1}{2} \\ \frac{F}{4}-\frac{P_2}{4} & \frac{F}{4}-\frac{P_2}{4} & 0 & 0 & \frac{F}{4}+\frac{P_2}{4}-\frac{P_1}{2} & \frac{F}{4}+\frac{P_2}{4}+\frac{P_1}{2} \end{pmatrix} \tag{3.2}$$

where

$$F = \tilde{\phi}(\sigma,r_0,0)$$

$$P_n = \tilde{\phi}(\sigma,r_0,n/T_1) \quad n = 1, 2 \tag{3.3}$$

and

$$Q_1 = 2\int_0^\infty e^{-2t/T_2}\cos(2\Omega t)\phi(\sigma,r_0,t)\,dt$$

$$Q_2 = 2\int_0^\infty e^{-2t/T_2}\sin(2\Omega t)\phi(\sigma,r_0,t)\,dt \tag{3.4}$$

IV. Highly Polar Solvents

In solvents with a large dielectric constant ϵ, one can neglect the Coulombic interactions between the counterions, setting the Onsager radius $r_c = 0$. For this particular case, $\tilde{\phi}(\sigma,r_0,s)$ is known to be

$$\tilde{\phi}(\sigma,r_0,s) = \frac{1}{4\pi r_0 D}\frac{\exp\{-(r_0-\sigma)\sqrt{s/D}\}}{1+\sigma\sqrt{s/D}} \tag{4.1}$$

so that the expressions in eq 3.3 become

$$F = \frac{1}{4\pi r_0 D}$$

$$P_n = \frac{\sigma}{r_0}\frac{e^{(1-r_0/\sigma)\sqrt{(n\tau_d/T_1)}}}{k_D(1+\sqrt{n\tau_d/T_1})} \quad n = 1, 2 \tag{4.2}$$

where $k_D = 4\pi\sigma D$ is the diffusional rate constant, while $\tau_d = \sigma^2/D$ is the so-called encounter time.

Taking the integrals in eq 3.4, one finds that the results can be expressed via $\tilde{\phi}(\sigma,r_0,s)$ given in eq 4.1. Using the latter, we obtain for highly polar solvents

$$Q_1 = \frac{2\sigma e^{(1-r_0/\sigma)\alpha_R}}{k_D r_0}\frac{(1+\alpha_R)\cos[\alpha_I(r_0/\sigma-1)] - \alpha_I\sin[\alpha_I(r_0/\sigma-1)]}{(1+\alpha_R)^2+\alpha_I^2} \tag{4.3a}$$

$$Q_2 = \frac{2\sigma e^{(1-r_0/\sigma)\alpha_R}}{k_D r_0}\frac{(1+\alpha_R)\sin[\alpha_I(r_0/\sigma-1)] + \alpha_I\cos[\alpha_I(r_0/\sigma-1)]}{(1+\alpha_R)^2+\alpha_I^2} \tag{4.3b}$$

where

$$\alpha_R = \sqrt{\frac{\tau_d}{T_2}}\sqrt{\sqrt{\Omega^2 T_2^{\,2}+1}+1}$$

$$\alpha_I = \sqrt{\frac{\tau_d}{T_2}}\sqrt{\sqrt{\Omega^2 T_2^{\,2}+1}-1} \tag{4.4}$$

are the most important parameters responsible for the spin conversion due to transversal relaxation ($1/T_2$) and field-induced coherent transitions with a frequency Ω.

In the limit of the low field, $\Omega^2 T_2^2 \ll 1$, the expressions in eq 4.4 reduce to the following

$$\text{At } \Omega \to 0$$

$$\alpha_R \to \sqrt{\frac{2\tau_d}{T_2}} = \gamma \quad \alpha_I \to 0 \tag{4.5}$$

Most of the experimental works studying electron-transfer reactions by optical and electrochemical methods are performed in the natural magnetic field of the Earth which is rather low. This is why this particular case is of exceptional importance.

V. Recombination only through the Singlet Channel

To illustrate the general theory, let us start from the simplest example of the triplet RIP irreversibly created by electron transfer from a triplet precursor.[9−11] Such a triplet RIP has to recombine through the singlet channel to the ground state because recombination from this triplet state is prohibited, $k_c^T = 0$, that is

$$Z_t = 0, \quad Z \equiv Z_s \tag{5.1}$$

Cumbersome but straightforward calculations show that the result depends on what spin level of a pair was initially populated. If this is S, T_0, or $T_\pm$, then

$$
\begin{aligned}
{}^{S}\varphi_s &= \frac{{}^{S}Z_s}{D + {}^{S}Z_s} \\
{}^{T_0}\varphi_s &= \frac{{}^{T_0}Z_s}{D + {}^{T_0}Z_s} \\
{}^{T_\pm}\varphi_s &= \frac{{}^{T_\pm}Z_s}{D + {}^{T_\pm}Z_s}
\end{aligned}
\tag{5.2}
$$

where the corresponding recombination efficiencies are

$$
\frac{{}^{S}Z_s}{D} = \frac{k_c^S((4 + k_c^S q_1)(F + P_2 + Q_1) + k_c^S q_2 Q_2)}{16 + k_c^S((4 + k_c^S q_1)(f - F + p_2 - P_2 + q_1 - Q_1) + 4q_1 + k_c^S q_2(q_2 - Q_2))} \tag{5.3}
$$

$$
\frac{{}^{T_0}Z_s}{D} = \frac{k_c^S((4 + k_c^S q_1)(F + P_2 - Q_1) - k_c^S q_2 Q_2)}{16 + k_c^S((4 + k_c^S q_1)(f - F + p_2 - P_2 + q_1 + Q_1) + 4q_1 + k_c^S q_2(q_2 + Q_2))} \tag{5.4}
$$

$$
\frac{{}^{T_\pm}Z_s}{D} = \frac{k_c^S(4 + k_c^S q_1)(F - P_2)}{(4 + k_c^S q_1)(4 + k_c^S(f - F + p_2 + P_2 + q_1)) + (k_c^S q_2)^2} \tag{5.5}
$$

where

$$
\begin{aligned}
p_2 &= P_2(r_0 = \sigma) \\
q_i &= Q_i(r_0 = \sigma) \\
f &= F(r_0 = \sigma) = 1/k_D
\end{aligned}
$$

are the contact values of the corresponding r_0-dependent quantities. For the particular case of contact start ($r_0 = \sigma$), all these results are identical to those obtained earlier by Mints and Pukhov.[13]

However, the most reasonable situation, presumed in the majority of earlier works, is the start from the equilibrated triplet state (T-pair) whose sublevels, T_0, T_+, T_-, are equally populated with the weights ($^1/_3$,$^1/_3$,$^1/_3$).

Summing the above efficiencies with these weights, we obtain for this case

$$
{}^{T}\varphi_s = \frac{1}{3}\,{}^{T_0}\varphi_s + \frac{2}{3}\,{}^{T_\pm}\varphi_s = \frac{{}^{T}Z_s}{D + {}^{T}Z_s} \tag{5.6}
$$

where

$$
\frac{{}^{T}Z_s}{D} = \frac{k_c^S[(4 + k_c^S q_1)(3F - P_2 - Q_1) - k_c^S q_2 Q_2]}{48 + k_c^S[(4 + k_c^S q_1)(3f - 3F + 3p_2 + P_2 + 3q_1 + Q_1) + 12q_1 + k_c^S q_2(3q_2 + Q_2)]} \tag{5.7}
$$

is the efficiency of a singlet recombination from the initially equilibrated triplet indicated as T.

A. Recombination of a Contact Born Pair. At contact start, $r_0 = \sigma$ and therefore it follows from eqs 4.3 and 4.2 that

$$
Q_1 = \frac{2}{k_D}\frac{1 + \alpha_R}{(1 + \alpha_R)^2 + \alpha_I^2} = q_1 \tag{5.8a}
$$

$$
Q_2 = \frac{2}{k_D}\frac{\alpha_I}{(1 + \alpha_R)^2 + \alpha_I^2} = q_2 \tag{5.8b}
$$

$$
P_2 = \frac{1}{k_D(1 + \beta)} = p_2 \tag{5.8c}
$$

while α_R and α_I are defined in eq 4.4 and

$$
\beta = \sqrt{\frac{2\tau_d}{T_1}} \tag{5.9}
$$

1. Recombination of the S-Pair. Using the results in eq 5.3, we obtain from there the recombination efficiency of the contact born radical pair initially created in the singlet state (S-pair)

$$
\frac{{}^{S}Z_s}{D} = \frac{k_c^S}{16 + 4k_c^S q_1}\left[\frac{4 + k_c^S q_1}{k_D}\left(\frac{2 + \beta}{1 + \beta} + k_D q_1\right) + k_c^S {q_2}^2\right] \tag{5.10}
$$

Such a complex result expressed via $q_i(\alpha_R,\alpha_I)$ from eq 5.8 is identical to that found by Mints and Pukhov.[13] Fortunately, it can be represented in a much more simple and transparent form found in ref 20

$$
\frac{{}^{S}Z_s}{D} = \frac{k_c^S}{2k_D}\left[\frac{\alpha + 2}{\alpha + 1} - \frac{\beta}{2(\beta + 1)}\right] \tag{5.11}
$$

where

$$
\alpha = \alpha_R + \frac{{\alpha_I}^2}{1 + \alpha_R + k_c^S/2k_D} \tag{5.12}
$$

is the only conversion-dependent parameter.

2. Recombination of the T-Pair. The same simplification is presented here for the efficiency of the singlet recombination from the equilibrated triplet state

$$
{}^{T}Z_s/D = \frac{k_c^S}{2k_D}\frac{2\alpha + \beta(1 + 3\alpha)}{2\left[3(1 + \beta)(1 + \alpha) + (3 + 2\beta + \alpha)\dfrac{k_c^S}{k_D}\right]} \tag{5.13}
$$

In the limits of kinetic and diffusional recombination, it takes the alternative forms

$$
{}^{T}Z_s/D = \begin{cases} \dfrac{k_c^S}{2k_D}\left[\dfrac{\alpha}{3(1 + \alpha)} + \dfrac{\beta}{6(1 + \beta)}\right] & \text{at } \dfrac{k_c^S}{k_D} \ll 1 \text{ kinetic} \\ \dfrac{2\alpha + \beta(1 + 3\alpha)}{4(3 + 2\beta + \alpha)} & \text{at } \dfrac{k_c^S}{k_D} \gg 1 \text{ kinetic} \end{cases} \tag{5.14}
$$

It must be noted that the general relationship between ${}^{S}\varphi_s$ and ${}^{T}\varphi_s$ reported in section 3.2.1 of ref 7 holds true. The product yields of the S-pair and T-pair recombination relate to each other as follows

$$
{}^{S}\varphi_s = \lambda - 3(1 - \lambda)\,{}^{T}\varphi_s, \quad \text{where } \lambda = \frac{k_c^S}{k_D + k_c^S}
$$

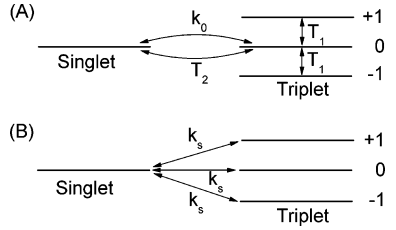

Figure 1. Scheme of spin transitions in the radical pair induced by transversal and longitudinal relaxation as well as by a Δg mechanism of incoherent spin conversion (A) and the elementary spin model of the same at equal relaxation times (B).

It is the straightforward consequence of the detailed balance principle and can be easily verified here using ${}^{S}\varphi_s$ from eq 5.2 and ${}^{T}\varphi_s$ from eq 5.6.

VI. Incoherent Spin-Conversion

In a rather low field (at $\Omega T_2 \ll 1$)

$$\alpha_R \approx \sqrt{\frac{2\tau_d}{T_2}\left(1+\frac{\Omega^2 T_2^{\,2}}{4}\right)} \quad \alpha_I \approx \Omega\sqrt{\tau_d T_2/2} \tag{6.1}$$

Obviously that in such a case the conversion proceeds with the rate $\Omega^2 T_2$ which is a parameter of the incoherent process. Using the results of eq 6.1 in the formulas in eq 5.12, we obtain the value of α for the incoherent spin conversion

$$\alpha = \sqrt{\frac{2\tau_d}{T_2}\left(1+\frac{\Omega^2 T_2^{\,2}}{4}\right)} + \frac{1}{2}\frac{\Omega^2\tau_d T_2}{1+\frac{k_c^S}{2k_D}+\sqrt{\frac{2\tau_d}{T_2}\left(1+\frac{\Omega^2 T_2^{\,2}}{4}\right)}} \tag{6.2}$$

This parameter depends on recombination only through the ratio $k_c^S/2k_D$, that is, small in the kinetic limit and large in the diffusional one. Correspondingly, we obtain in these limits

$$\alpha = \begin{cases} \sqrt{\frac{2\tau_d}{T_2}\left(1+\frac{3\Omega^2 T_2^{\,2}}{4}\right)} & \text{at } \frac{k_c^S}{2k_D} \le 1 \ll \sqrt{\frac{\tau_d}{T_2}} \\ \sqrt{\frac{2\tau_d}{T_2}\left(1+\frac{\Omega^2 T_2^{\,2}}{4}\right)} & \text{at } \frac{k_c^S}{2k_D} \gg 1, \sqrt{\frac{\tau_d}{T_2}} \end{cases} \tag{6.3}$$

These are exactly the same results that were found in appendix B of ref 20.

In the case of a low field

$$\alpha = \gamma = \sigma\sqrt{\frac{2}{DT_2}} \qquad \Omega^2 T_2^{\,2} \ll 1 \tag{6.4}$$

depends on a single variable parameter, encounter diffusion, changing with viscosity.

A. Rate Models. In a number of our and other works, the spin conversion was presumed to be incoherent and was considered from the beginning as a stochastic process occurring with some rate, k_0.[6,9,12,22−25] In general, when the nonreacting radical pair is immobile, its density matrix obeys the equation following from eq 2.1

$$\dot{\rho} = \hat{\mathcal{Y}}\rho \tag{6.5}$$

However, under the condition of incoherent conversion, $\Omega T_2 \ll 1$, the latter can be conventionally reduced to a set of four master equations for only diagonal elements of the density matrix, that is, populations of a singlet level, $\rho_S \equiv p_S$, and three sublevels of the triplet state, ρ_-, ρ_0, and ρ_+ (see Figure 1A)[12,20]

$$\dot{\rho}_S = \left(k_0+\frac{1}{T_2}-\frac{1}{2T_1}\right)\rho_0 - \left(k_0+\frac{1}{T_2}-\frac{1}{2T_1}\right)\rho_S + \frac{\rho_+ + \rho_-}{2T_1} \tag{6.6a}$$

$$\dot{\rho}_0 = \left(k_0+\frac{1}{T_2}-\frac{1}{2T_1}\right)\rho_S - \left(k_0+\frac{1}{T_2}+\frac{1}{2T_1}\right)\rho_0 + \frac{\rho_+ + \rho_-}{2T_1} \tag{6.6b}$$

$$\dot{\rho}_+ = \frac{\rho_+ + \rho_-}{2T_1} - \frac{\rho_+}{T_1}$$

and

$$\dot{\rho}_- = \frac{\rho_+ + \rho_0}{2T_1} - \frac{\rho_-}{T_1} \tag{6.6c}$$

Here

$$k_0 = \Omega^2 T_2 \tag{6.7}$$

is the rate of incoherent spin conversion in a stable radical pair proceeding via a Δg mechanism.

1. Two-Level Model. For the extreme case $T_1 = \infty$ ($\beta = 0$), only two levels out of four are involved in the spin conversion and the set (eq 6.6) is reduced to the following

$$\dot{\rho}_S = k_s(\rho_0 - \rho_S) \tag{6.8a}$$

$$\dot{\rho}_0 = k_s(\rho_S - \rho_0) \tag{6.8b}$$

while $\rho_+(t) = \rho_+(0)$, $\rho_-(t) = \rho_-(0)$ and

$$k_s = k_0 + \frac{1}{T_2} \tag{6.9}$$

The single-channel contact recombination assisted by the incoherent spin conversion in the two-level system was the subject of a separate exhaustive investigation in ref 20.

The comparison of the incoherent and coherent spin conversion assisting a single-channel contact recombination in a two-level system was continued in ref 21. It was confined only to the RIP starting from contact ($r_0 = \sigma$) when all the results are much simpler. If, in addition, $\beta = 0$, then the recombination efficiencies in eqs 5.11 and 5.13 gain the following form

$${}^{S}Z_s = \frac{z_s}{2}\left[\frac{\alpha+2}{\alpha+1}\right]$$

$${}^{T}Z_s = \frac{z_s}{2}\frac{\alpha}{3(1+\alpha)+(3+\alpha)\frac{z_s}{D}} \tag{6.10}$$

Here, $z_s = k_c^S/4\pi\sigma$ is the usual constant of the conventional (spinless) "exponential model".[12,6] Exactly the same result has been obtained in ref 20 solving the rate equations for the two-

level problem, eq 6.8, except that

$$\alpha = \sqrt{2\frac{\tau_d}{T_2}(1 + \Omega^2 T_2^2)} \tag{6.11}$$

does not depend on k_c^S at all, unlike its coherent analogue 6.2. Moreover, α from eq 6.11 does not coincide with either of the expressions in eq 6.3.

This is because the rate eqs 6.6 were obtained from their coherent analogue, eq 6.5, when the motion of radicals was switched off, together with the boundary conditions accounting for the recombination. When the motion of radicals is accounted for afterward, their recombination is affected by the spin conversion but the recombination itself no longer affects the spin conversion. This is a main weakness of rate theories first reducing the coherent spin conversion to incoherent and only then accounting for the encounter diffusion and recombination of radicals. Here, in section III, we did quite the opposite: we first solved the problem by simultaneously taking into account the relative motion and conversion and only then turned to the particular case (eq 6.1) where the latter is incoherent. Therefore, our α for coherent spin conversion is given by eq 5.12 and for the incoherent limit by eq 6.2, but the rate estimate (eq 6.11) does not follow from either of them.[20]

However, there is an exceptional case of zero field ($\Omega = 0$) when the transfer is carried out by only spin relaxation. This stochastic process, incoherent by its nature, is executed with the rate $k_s = 1/T_2$. Hence, the results (eq 6.10) with $\alpha = \gamma$ are exact for the zero field.

According to eq 6.4, γ increases with viscosity. On the other hand, the ratio ${}^S Z_s/z_s$ monotonically decreases with $(1/D)^{1/2}$ from 1 to $^1/_2$ (upper dashed line in Figure 2(A) At fast diffusion, the spin conversion does not have time to affect the recombination and ${}^S Z_s/z_s = 1$. On the contrary, for small values of D, the equipartition between S and T_0 is completed during the encounter time, reducing the recombination efficiency by one-half.

As for ${}^T Z_s$, it is zero at fast and slow diffusion passing through a maximum between (lower dashed line in Figure 2A). At fast diffusion, it is zero because no transition from T_0 to the reacting S state occurs before separation of the radicals. On the contrary, at slow diffusion, the encounter time is long enough for transfer to be completed

$$\left.\frac{{}^T Z_s}{D}\right|_{D \ll z_s} = \frac{1}{2}\frac{\alpha}{3+\alpha} \to \frac{1}{2} \quad \text{at } \alpha \gg 1$$

so that

$$\lim_{D\to 0} {}^T\varphi_s = \frac{{}^T Z_s/D}{1 + {}^T Z_s/D} = \frac{1}{3} \tag{6.12}$$

After T_0 is completely exhausted, the share of triplets that have reacted is only $^1/_3$ of the initial triplet population. The remaining $^2/_3$ that were in the other triplet states, $T_\pm$, were not involved in the reaction.

A similar picture develops when the system recombines only through the triplet channel except that ${}^S Z$ and ${}^T Z$ are interchanged (dashed lines in Figure 2B). The former passes through a maximum, while the latter monotonically decreases to another value, $^3/_4$, which needs a special explanation. In fact, the efficiency of recombination from T_0 reduces by one-half when $D \to 0$ while that from $T_\pm$ remains $z_t = k_c^T/4\pi\sigma$ at any D value. Therefore, eq 5.6 at slow D takes the following form

$${}^T\varphi_t = \frac{1}{3}\frac{z_t/2}{D + z_t/2} + \frac{2}{3}\frac{z_t}{D + z_t} = \frac{{}^T Z_t}{D + {}^T Z_t} \tag{6.13}$$

where

$$\text{At } D \to 0$$

$${}^T Z_t = \frac{5z_t D + 3z_t^2}{6D + 4z_t} \to \frac{3}{4} z_t$$

This is the very same limit for ${}^T Z_t$ as in the case $T_1 = T_2$ considered below and represented by solid lines in Figure 2.

2. Equal Spin Relaxation Times. If T_1 is finite, then all four states in eq 6.6 are involved in the reaction but the result (eq 5.11) first obtained for the incoherent spin conversion in ref 18 holds true provided that the parameter α is given by the expression 6.11. For the particular case of equal times

$$\alpha = \gamma\sqrt{(1 + k_0 T)} \tag{6.14}$$

where $T = T_1 = T_2$

$$\gamma = \sqrt{2\tau_d/T} = \sqrt{x/D}$$

and

$$x = 2\sigma^2/T \tag{6.15}$$

In this case, it follows from eq 5.11 that

$$\frac{{}^S Z_s}{D} = \frac{k_c^S}{2k_D}\left[\frac{\gamma\sqrt{1 + k_0 T} + 2}{\gamma\sqrt{1 + k_0 T} + 1} - \frac{\gamma}{2(\gamma + 1)}\right] \tag{6.16}$$

Similarly, from eq 5.13, one gets

$$\frac{{}^T Z_s}{D} = \frac{k_c^S}{4k_D} \times \frac{\gamma[1 + (2 + 3\gamma)\sqrt{1 + k_0 T}]}{3(1+\gamma)(1 + \gamma\sqrt{1 + k_0 T}) + (3 + 2\gamma + \gamma\sqrt{1 + k_0 T})\dfrac{k_c^S}{k_D}} \tag{6.17}$$

When the magnetic field is zero ($k_0 = \Omega = 0$), we obtain from eqs 6.16 and 6.17

$${}^S Z_s = \frac{z_s}{4}\frac{\gamma + 4}{\gamma + 1}$$

$${}^T Z_s = \frac{z_s}{4}\frac{\gamma}{1 + \gamma + \dfrac{k_c^S}{k_D}} \tag{6.18}$$

At very fast diffusion when $\tau_d = \sigma^2/D \to 0$, the spin conversion has no time to occur and $\gamma = 0$. In this limit, ${}^S Z_s$ reaches its maximal value, z_s, which is the efficiency of the singlet recombination in the absence of the spin conversion. As soon as the spin conversion is switched on, ${}^S Z_s$ falls down with decreasing diffusion and reaches the minimal value $z_s/4$ at $D = 0$. In this limit, all spin states are equally populated and the share of the singlet one is $^1/_4$.

Although the diffusional dependence of the singlet recombination from the equilibrated triplet state (the lower solid line

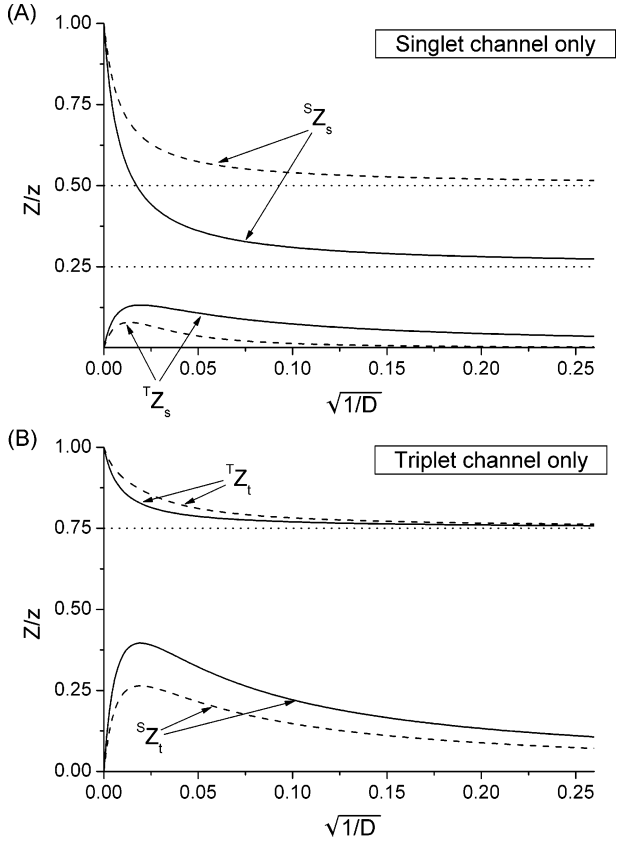

Figure 2. Zero field recombination efficiencies for a single-channel recombination through either singlet (A) or triplet (B) channels (z_s and z_t were taken equal, $z = 2.63 \times 10^{-4}$ cm^2/s). Dashed and solid lines relate to the cases $T_1 = \infty$ and $T_1 = T_2 = 15$ ps, respectively. The upper curves in (A) and (B) are for the efficiencies of allowed recombination from initially populated states, while the lower ones are for the recombination initially forbidden but switched on by spin conversion to the reacting state. The contact distance is $\sigma = 10$ Å everywhere.

in Figure 2A) is qualitatively the same as for the two-level model, the result appearing in the slow diffusion limit is different

$$\lim_{D\to 0} {}^{T}Z_s = \frac{z_s}{4}$$

so that

$$\lim_{D\to 0} {}^{T}\varphi_s = \frac{z_s/4D}{1 + z_s/4D} = 1 \tag{6.19}$$

In contrast to eq 6.12, in this case, the whole triplet is completely exhausted due to the longitudinal relaxation between its sublevels (see Figure 1A) which is as fast as the transversal one.

B. Elementary Spin Model (ESM). The simplest, but most widely used and rather successful, rate model follows from the set (eq 6.6) phenomenologically reduced to only two equations at $T_1 = T_2 = T$. These equations relate to each other the population of the singlet, $m_S \equiv \rho_S$, and the total population of the triplet, $m_T = \rho_0 + \rho_+ + \rho_-$. How these equations were obtained one can see in section VIIIA of ref 12. For the case of equal relaxation times, we have

$$\dot{m}_S = -3k_s m_S + k_s m_T \tag{6.20a}$$

$$\dot{m}_T = 3k_s m_S - k_s m_T \tag{6.20b}$$

with a microscopically defined spin conversion rate

$$k_s = \frac{1}{2T} + \frac{\Omega^2 T}{3} \tag{6.21}$$

As seen from Figure 1B, the conversion rate is $3k_s$ for the transition from singlet to triplet, while from any triplet substate as well as from all of them this is only k_s. Due to the spin conversion, the population of the singlet and triplet at $t \gg k_s^{-1}$ relate to each other as $^1/_4$:$^3/_4$, whatever was the initial state.

The elementary spin model (ESM) used in ref 17 enables us to calculate the efficiency of singlet-channel recombination from the singlet

$${}^{S}Z_s = \frac{z_s}{4}\frac{\alpha + 4}{\alpha + 1} \tag{6.22}$$

Being very similar to the double-level expression for $^{S}Z_s$ in eq 6.10, it is distinguished by

$$\alpha = \sqrt{4k_s\tau_d} = \sqrt{\frac{2\tau_d}{T}\left(1 + \frac{2\Omega^2 T^2}{3}\right)} \tag{6.23}$$

The latter differs noticeably from eq 6.11 in the weight of Ω^2. Although in this respect the α values from eqs 6.2 and 6.3 are also different at $\Omega = 0$ all of them turn to γ.

VII. Double-Channel Recombination after Contact Start

Let us now turn to the most general case when recombination is possible from either the singlet or triplet state of the pair. The triplet products are excited triplet molecules whose yield can be detected spectroscopically immediately after geminate recombination. Both triplet and singlet yields depend on the initial state of the pair given by ρ_0. Using the corresponding ρ_0 in eq 2.9 as well as the general $\hat{Q}$ from eq 2.13 and $\hat{G}_0$ from eq 3.2, with parameters from eq 5.8, we calculated from eqs 2.10 and 2.11 the yields $\varphi_s(\sigma)$ and $\varphi_t(\sigma)$. Only from them can one obtain the recombination efficiencies defined in eq 2.15: Z_s, Z_t, and $Z = Z_s + Z_t$, which are discussed below.

A. Start from the Singlet State. If initially only the singlet state is populated, then the efficiency of recombination through the singlet channel is

$${}^{S}Z_s/D = \frac{k_c^S}{2k_D}\left[\frac{\alpha + 2(1 + k_c^T/k_D)}{\alpha + 1 + k_c^T/k_D} - \frac{\beta}{2(\beta + 1 + k_c^T/k_D)}\right] \tag{7.1}$$

and that for the triplet channel is

$${}^{S}Z_t/D = \frac{k_c^T}{2k_D}\left[\frac{\alpha}{1 + \alpha + k_c^T/k_D} + \frac{\beta}{2(1 + \beta + k_c^T/k_D)}\right] \tag{7.2}$$

At $k_c^T = 0$, eq 7.1 reduces to eq 5.11 for $^{S}Z_s = {}^{S}Z$, while $^{S}Z_t$ becomes zero as in eq 5.1.

B. Start from the Individual Sublevels of the Triplet State. If initially one populates only the T_0 state, then the results are different

$${}^{T_0}Z_s/D = \frac{k_c^S}{2k_D(1 + \alpha + k_c^S/k_D)}\left[\alpha - \frac{\beta(1 + \alpha + k_c^T/k_D)}{2(1 + \beta + k_c^T/k_D)}\right] \tag{7.3}$$

$$ {}^{T_0}Z_t/D = \frac{k_c^T}{2k_D(1+\alpha+k_c^S/k_D)}\left[\alpha + 2\left(1+\frac{k_c^S}{k_D}\right) + \frac{\beta(1+\alpha+k_c^T/k_D)}{2(1+\beta+k_c^T/k_D)}\right] \quad (7.4) $$

Equation 7.3 is the contact analogue of eq 5.4 for the double-channel reaction, but it is greatly simplified in the same way as eq 5.11 when compared to eq 5.10.

Subject to similar simplification and generalization, eq 5.5 takes the form

$$ {}^{T_\pm}Z_s/D = \frac{k_c^S}{2k_D}\frac{\beta(1+\alpha+k_c^T/k_D)}{2(1+\beta)(1+\alpha)+2k_c^Sk_c^T/k_D{}^2+(2+\beta+\alpha)(k_c^S+k_c^T)/k_D} \quad (7.5) $$

and its triplet analogue, which is not zero anymore (since $k_c^T \neq 0$), is equal to

$$ {}^{T_\pm}Z_t/D = \frac{k_c^T}{2k_D}\left[2 - \frac{\beta(1+\alpha+k_c^T/k_D)}{2(1+\beta)(1+\alpha)+2k_c^Sk_c^T/k_D{}^2+(2+\beta+\alpha)(k_c^S+k_c^T)/k_D}\right] \quad (7.6) $$

The definition of the spin conversion parameter β remains the same as in eq 5.8c, while for eq 5.12, α should be substituted for the more general one

$$ \alpha = \alpha_R + \frac{\alpha_I^2}{1+\alpha_R+(k_c^S+k_c^T)/2k_D} \quad (7.7) $$

valid for the double-channel recombination ($k_c^T \neq 0$).

C. Start from the Equipopulated Triplet States. Having all the efficiencies, one can calculate any yield including the total yield of recombination from the equipopulated triplet states, through either the singlet or triplet channels. Analogous to eq 5.6 we have

$$ {}^T\varphi_s = \frac{1}{3}{}^{T_0}\varphi_s + \frac{2}{3}{}^{T_\pm}\varphi_s = \frac{{}^TZ_s}{D+{}^TZ} $$

$$ {}^T\varphi_t = \frac{1}{3}{}^{T_0}\varphi_t + \frac{2}{3}{}^{T_\pm}\varphi_t = \frac{{}^TZ_t}{D+{}^TZ} \quad (7.8) $$

where

$$ \varphi = 1 - {}^T\varphi_s - {}^T\varphi_t = \frac{D}{D+{}^TZ} $$

and

$$ {}^TZ = {}^TZ_s + {}^TZ_t \quad (7.9) $$

Using, in these formulas, the above obtained results, we get for the efficiencies of the singlet and triplet channels in the case under consideration

$$ {}^TZ_s/D = \frac{k_c^S}{2k_D}\times \frac{2\alpha(1+k_c^T/k_D)+\beta(1+3\alpha+k_c^T/k_D)}{2\left(3(1+\beta)(1+\alpha)+3\frac{k_c^Sk_c^T}{k_D{}^2}+\alpha\frac{k_c^T}{k_D}+\beta\frac{k_c^S}{k_D}+(3+\beta+\alpha)\frac{k_c^S+k_c^T}{k_D}\right)} \quad (7.10) $$

$$ {}^TZ_t/D = \frac{k_c^T}{2k_D}\times \left[2 - \frac{2\alpha(1+k_c^T/k_D)+\beta(1+3\alpha+k_c^T/k_D)}{2\left(3(1+\beta)(1+\alpha)+3\frac{k_c^Sk_c^T}{k_D{}^2}+\alpha\frac{k_c^T}{k_D}+\beta\frac{k_c^S}{k_D}+(3+\beta+\alpha)\frac{k_c^S+k_c^T}{k_D}\right)}\right] \quad (7.11) $$

D. General Presentation of the Main Results. Later on we will consider only the efficiencies of recombination from either the singlet or equilibrated triplet state, ${}^SZ$ and ${}^TZ$. They both can be represented uniformly in a very compact form

$$ {}^SZ_s = z_s(1-{}^S\Pi) \quad {}^SZ_t = z_t{}^S\Pi \quad (7.12a) $$

$$ {}^TZ_s = z_s{}^T\Pi \quad {}^TZ_t = z_t(1-{}^T\Pi) \quad (7.12b) $$

where

$$ {}^S\Pi = \frac{\alpha/2}{(1+\alpha z_t/D)} + \frac{\beta/4}{(1+\beta+z_t/D)} \quad (7.13a) $$

$$ {}^T\Pi = \frac{(1+z_t/D)\alpha/2 + (1+3\alpha+z_t/D)\beta/4}{3(1+\alpha)(1+\beta)+(\alpha z_t+3z_sz_t/D+\beta z_s)/D+(3+\alpha+\beta)(z_s+z_t)/D} \quad (7.13b) $$

E. Double-Channel Recombination in ESM. If the start was made from the singlet, then the efficiencies of the different channels in the ESM are the same as in the exact theory, eq 7.12a, but

$$ {}^S\Pi = \frac{3\alpha}{4(1+\alpha+z_t/D)} \quad (7.14) $$

where α is given in eq 6.23. At $z_t = 0$, the double-channel expression in eq 7.14 substituted to eq 7.12a reduces ${}^SZ_s$ to its previously obtained single-channel analogue 6.22.[17]

The start made from the equilibrated triplet, treated the same way, leads to another formula, an alternative to eq 7.13b

$$ {}^T\Pi = \frac{\alpha}{4(1+\alpha+z_s/D)} \quad (7.15) $$

It is remarkable that the efficiencies at which the recombination is switched on by the spin conversion, ${}^SZ_t$ and ${}^TZ_s$, depend on a single recombination parameter, z_t or z_s, respectively, while two other efficiencies depend on both of them.

1. Recombination in a Zero Magnetic Field. In the case of a zero field when $\alpha = \gamma$, the results following from eqs 7.12 after substituting the expressions from eqs 7.14 and 7.15 coincide with those that can be deduced from the exact eqs 7.1, and 7.2 and 7.10 and 7.11, respectively, provided

$$ \alpha = \beta = \gamma = \sqrt{x/D} \quad (7.16) $$

that is, $T_1 = T_2 = T$ in addition to $\Omega = 0$. This is because

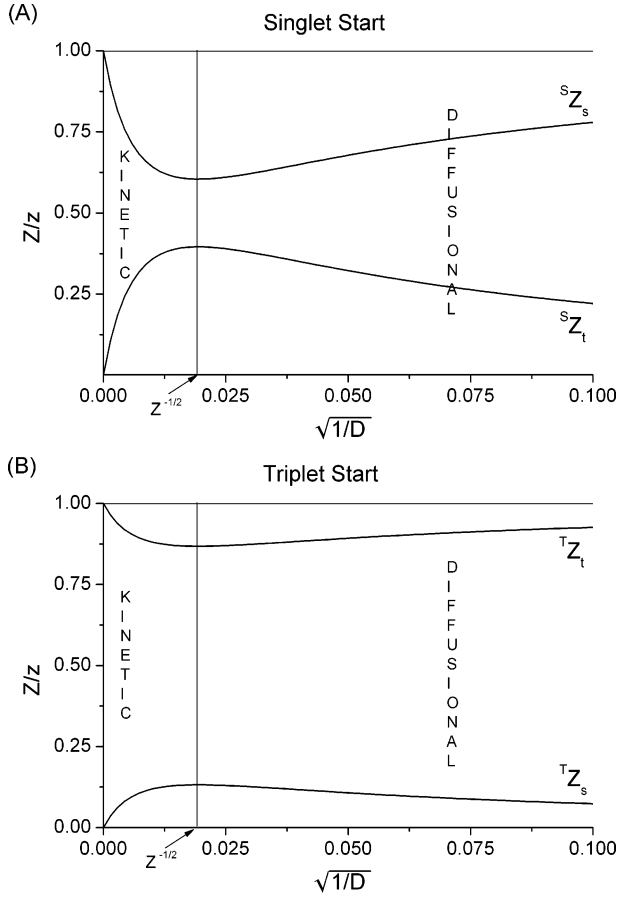

Figure 3. Diffusional dependence of the efficiencies of the zero field double-channel recombination at contact start and equal reaction constants of both channels ($z_s = z_t = z$). Spin conversion efficiency $x = 2\sigma^2/T = 5 \times 10^{-4}$ cm^2/s where $T = T_1 = T_2 = 15$ ps. (A) The start from the singlet state of contact radical pair. (B) The start from the equipopulated triplet states of the pair.

under these conditions the set of eqs 6.6 rigorously reduces to the ESM eqs 6.20 with $k_s = 1/2T$.

Figure 3 shows the viscosity dependence of all the recombination efficiencies at the contact start under condition 7.16. Unlike Figure 2, where they have been shown for the opposite cases of either the singlet channel ($k_c^S \neq 0 = k_c^T$) or triplet channel ($k_c^S = 0 \neq k_c^T$) recombination, here we are dealing with an intermediate case of "spin-independent recombination" first considered in ref 26. This is an exceptional case when the reactions from the singlet and triplet proceed with equal rates: $k_c^S = k_c^T$ ($z_s = z_t = z$). Under such conditions, the spin conversion does not modulate the recombination and cannot affect its total efficiency

$$\text{At } z_s = z_t = z$$
$$Z = Z_S + Z_T = z \tag{7.17}$$

However, Z_S and Z_T change with diffusion as shown in Figure 3. Under conditions 7.16 and 7.17, they obey the simple formulas

$$^{S}Z_s = z\left[1 - \frac{3\sqrt{x/D}}{4(1 + \sqrt{x/D} + z/D)}\right]$$
$$^{T}Z_s = z\frac{\sqrt{x/D}}{4(1 + \sqrt{x/D} + z/D)} \tag{7.18a}$$

$$^{S}Z_t = z\frac{3\sqrt{x/D}}{4(1 + \sqrt{x/D} + z/D)}$$
$$^{T}Z_t = z\left[1 - \frac{3\sqrt{x/D}}{4(1 + \sqrt{x/D} + z/D)}\right] \tag{7.18b}$$

All of them pass through an extremum at a common point

$$z = D$$

that is at

$$k_c = k_D$$

The vertical line at this point in Figure 3 separates the kinetic control, $D \gg z$, from the regime of diffusion control, $D \ll z$ (left and right branches of the curves).

2. Kinetic/Diffisional Reactions of Radicals Started from Contact. Far to the right, at the slowest diffusion, we obtain from eqs 7.18

$$\text{At } \frac{z}{D} \gg \gamma \gg 1$$
$$^{S}Z_s = z - \frac{3}{4}\gamma D = z - {}^{S}Z_t$$
and
$$^{T}Z_t = z - \frac{1}{4}\gamma D = z - {}^{T}Z_s \tag{7.19}$$

These formulae indicate that the rate constants $4\pi\sigma^{S}Z_t = {}^{3}/_{4}\gamma k_D$ and $4\pi\sigma^{T}Z_s = {}^{1}/_{4}\gamma k_D$ are proportional to the diffusional constant $k_D = 4\pi\sigma D$, multiplied by the spin conversion factor $\gamma = \sqrt{x/D}$. Therefore, they are proportional to $(D)^{1/2}$. When the radical pair starts from the singlet, the recombination constant is three times larger than in the case of the triplet start.

This is a very interesting peculiarity of a spin-selective theory compared to a spinless one. The latter may be diffusional only in the case of a noncontact start,[12,6] while the former is subdivided into kinetic and diffusional regimes, even if the radicals start to move being in contact. Immediately after the start they become separated; the reaction is switched off and the spin conversion is on. The recombination is now limited by diffusion of radicals from where they find themselves to the contact.

Its rate constant is diffusional when diffusion is slow and the reaction is accomplished at the very first recontact but the singlet and triplet products appear with the weights of these states in the radical pair after spin conversion is accomplished: ${}^{1}/_{4}$ and ${}^{3}/_{4}$.

Under kinetic control, the results are different

$$\text{At } \frac{z}{D} \ll 1 + \gamma$$
$$^{S}Z_s = \frac{4 + \gamma}{4(1 + \gamma)}z$$
$$^{S}Z_t = \frac{3\gamma\, z}{4(1 + \gamma)} = 3\,{}^{T}Z_s$$
$$^{T}Z_t = \frac{4 + 3\gamma}{4(1 + \gamma)}z \tag{7.20}$$

However, as $D \to \infty$, the spin conversion rate $\gamma \to 0$ and $^{S}Z_s =$

${}^{T}Z_t = z$ while ${}^{S}Z_t = {}^{T}Z_s = 0$. The same result follows from eq 7.19 for the opposite diffusional limit, $D \to 0$ ($\gamma \to \infty$).

This means that ${}^{S}Z_s$ and ${}^{T}Z_t$ vary with diffusion from z to z while ${}^{S}Z_t$ and ${}^{T}Z_s$ change from 0 to 0, but between the deviations from the z and 0, horizontal lines are three times larger for the singlet start (A) than for triplet (B). The maximal values of these deviations reached at $z = D$ are

$$\max {}^{S}Z_t = z - {}^{S}Z_s = \frac{3}{4} z \frac{\sqrt{x/z}}{2 + \sqrt{x/z}} \qquad (7.21a)$$

$$\max {}^{T}Z_s = z - {}^{T}Z_t = \frac{1}{4} z \frac{\sqrt{x/z}}{2 + \sqrt{x/z}} \qquad (7.21b)$$

The efficiency of recombination from the singlet state through the triplet channel is three times larger than the vice versa.

As for the spin conversion, it is either weak or strong depending on whether $x = 2\sigma^2/T$ is less or greater than z. If $x = 1/T = 0$ is zero, then the expressions in eq 7.21 also turn to zero and recombination proceeds only from the initial states: ${}^{S}Z_s = {}^{T}Z_t = z$. In the opposite case ($x \to \infty$), these expressions reach their maximal values which are $^3/_4 z$ for the singlet start (A) and $^1/_4 z$ for the triplet one (B).

VIII. Magnetic Field Effect

In the present theory, the frequency of spin conversion (eq 1.2) is proportional to the magnetic field H. Affecting conversion, the magnetic field changes the free ion quantum yield, averaged over the distribution of initial separations, $f(r)$

$$\bar{\varphi}(H) = \int \varphi(r,H) f(r)\, d^3r = \frac{1}{1 + Z(H)/D} \qquad (8.1)$$

The quantitative measure of the magnetic field effect (MFE) is conventionally defined as

$$M = \frac{\bar{\varphi}(H) - \bar{\varphi}(0)}{\bar{\varphi}(0)} = \frac{Z(0) - Z(H)}{D + Z(H)} \qquad (8.2)$$

As far as we know, until now, it has been studied experimentally only with systems subjected to a single-channel recombination. In particular, this was done in a wide range of fields with the reaction of photoexcited Ru-trisbipyridine with methyl viologen as an electron acceptor.[27,28] This reaction starts from the equilibrated triplet state of a pair that can recombine only through a singlet channel after the field-dependent spin conversion.

A. Singlet Recombination from the Triplet. In this particular case, $Z \equiv {}^{T}Z_s$. It depends on the starting point r_0 if $f(r) = \delta(r - r_0)/4\pi r^2$. The partial recombination efficiency

$$Z(H) = {}^{T}Z_s(\Omega, r_0) \qquad (8.3)$$

is given by expression 5.7, which is too complex for analytic investigations.

1. Contact Start. The situation becomes much simpler if we first focus our attention on the pair starting from contact when

$$Z(H) = {}^{T}Z_s(\Omega, \sigma) \qquad (8.4)$$

where the latter is given by expression 5.13 with β and α defined in eqs 5.9 and 5.12, respectively.

Low Fields. When the magnetic field is so small that $\Omega^2 T_2^2 \ll 1$, then using the approximate expressions (eq 6.1) in eq 5.12, we obtain in the lowest order approximation with respect to $\Omega^2 T_2^2$

$$\alpha \approx \gamma\left[1 + \frac{\Omega^2 T_2^{\,2}}{8}\left(1 + \frac{2\gamma}{1 + \gamma + z_s/2D}\right)\right] \qquad (8.5)$$

Under this condition, the MFE is linear in $\Omega^2 T_2^2$

$${}^{T}M_s \approx -\Phi \frac{\Omega^2 T_2^{\,2}}{8}\left(1 + \frac{2\gamma}{1 + \gamma + z_s/2D}\right) \qquad (8.6)$$

where

$$\Phi = (z_s/D)\,\{\gamma(1+\beta)^2(1 + z_s/D)\}/ \left\{\left[3(1+\gamma)(1+\beta) + \frac{z_s}{D}(3 + 2\beta + \gamma)\right]\left[2(1+\gamma)(1+\beta) + \frac{z_s}{D}\left(2 + \frac{3}{2}\beta + \gamma(1 + \beta/2)\right)\right]\right\}$$

The solution of the rate eqs 6.6 leads to a different result

$${}^{T}M_s \approx -\Phi \frac{\Omega^2 T_2^{\,2}}{2} \qquad (8.7)$$

because α has to be taken from eq 6.11

$$\alpha = \sqrt{\frac{\tau_d}{T_2} 2(1 + \Omega^2 T_2^{\,2})} \approx \gamma\left[1 + \frac{\Omega^2 T_2^{\,2}}{2}\right] \qquad (8.8)$$

As can be seen at slow conversion, ${}^{T}M_s$ is always linear in $\Omega^2 T_2^2$, but the slope of this linearity in the exact formula (eq 8.6) varies from $^1/_8$ at $\gamma \ll 1$ up to $^3/_8$ at $\gamma \gg 1$, $z_s/2D$, while in the analogous rate relationship, eq 8.7, it is always larger, $^1/_2$. Therefore, the parabolic Ω dependence of MFE at slow conversion is much sharper in the approximate rate theory than in the exact one.

This conclusion is also valid for the ESM, where T_1 is equal to T_2 and α is given by eq 6.23. The MFE estimated with ESM obeys exactly the same quadratic dependence (eq 8.7) provided one sets $\gamma = \beta$ in $\Phi(\gamma,\beta)$

$$\Phi_{ESM} = \Phi|_{\gamma=\beta} = \frac{z_s}{D} \frac{\gamma(1+\gamma)(1 + z_s/D)}{3\left[1 + \gamma + \frac{z_s}{D}\right]\left[2(1+\gamma)^2 + \frac{z_s}{D}\left(2 + \frac{5}{2}\gamma + \gamma^2/2\right)\right]}$$

However, the region where ${}^{T}M_s$ is quadratic in Ω holds in such a narrow strip (see Figure 4) that all the experimental points are usually obtained out of it.

High Magnetic Fields. In high magnetic fields, the MFE decreases with retardation approaching the constant negative value

$$\text{At } \Omega \to \infty \qquad {}^{T}M_s \approx -\Gamma + \frac{\Lambda}{\sqrt{\Omega T_2}} \qquad (8.9)$$

where

$$\Gamma = \frac{2 z_s (z_s + D)(1+\beta)^2}{[4(1+\beta)D + z_s(2+\beta)][3(1+\beta)(1+\gamma)D + z_s(3 + 2\beta + \gamma)]}$$

and Λ is also some function of z_s, β, and γ. It is useful to know

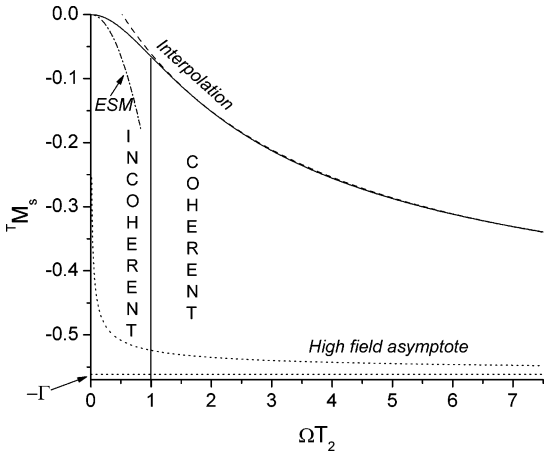

Figure 4. Field dependence of the MFE at contact start in the exact theory (solid line) and in the elementary spin model (dashed−dotted parabolic line). The vertical line separates the low field (incoherent) Ω dependence from the high field MFE, originating from the coherent spin conversion. The latter is well interpolated by the empirical formula 8.10 with $\xi = 0.91$, $\zeta = 3$, and $\Theta = 1.8$ shown as the dashed curve approaching the exact result from above. The highest field asymptotic behavior (eq 8.9) and its limit, $-\Gamma$, are shown by the dotted lines below. The rates of contact recombination, z_s, and other parameters are the same as in the previous figure while $D = 10^{-6}$ cm^2/s.

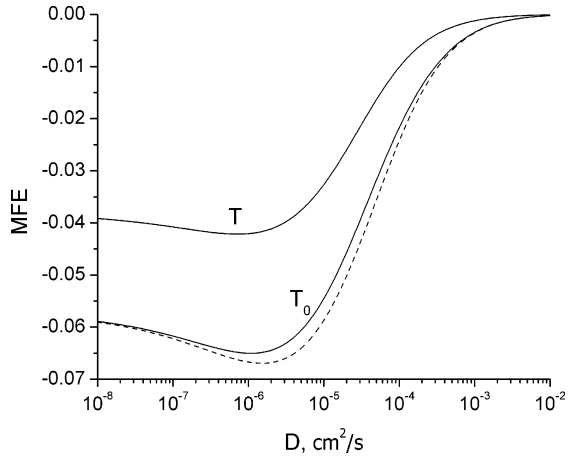

Figure 5. Diffusional dependence of the MFE at $T_1 = \infty$ and start from T_0 (dashed line), for $T_1 = T_2 = 15$ ps, and the same start (T_0), at equal times but starting from the equilibrated triplet (T). The contact rate constant $k_c^S = 3.31 \times 10^5$ Å^3/ns, $\Omega T_2 = 0.75$.

Γ which is actually an upper limit of the absolute value of MFE: $0 \le |^{T}M_s| \le \Gamma$. However, the asymptotic dependence (eq 8.9) shown by the dotted line in Figure 4 is not achievable because it holds at too high a magnetic field ($\Omega T_2 \gg 1000$), while the experimentally studied interval is around $\Omega T_2 \sim {}^1/_2$.

Moderate Magnetic Fields. Within this intermediate interval, the descending branch of the solid curve should be better interpolated with the following formula

$$^{T}M_s \approx -\xi\Gamma + \frac{\Theta}{\Omega T_2 + \zeta} \qquad (8.10)$$

With a proper choice of ξ, ζ, and Θ, this interpolation is as good as that shown in Figure 4 by the dashed line. This is the actual observed magnetic field dependence,[27,28,10] while the alternative (incoherent) parabolic dependence (eq 8.6) is hardly detectable and is described by ESM only qualitatively.

In Figure 5, the nonmonotonic diffusional dependence of the MFE is used to compare a few different approaches to the problem. It was exhaustively studied in the frame of "a two-state (S,T$_0$)" model in ref 10, presuming that the system starts from T$_0$ having $\beta = 1/T_1 = 0$. The solution to such a problem at contact recombination and contact start can also be obtained from our theory (dashed line in Figure 5). Nothing changes significantly if we take into account all four spin states, setting $T_1 = T_2$ (lower solid line in Figure 5). But if the start under these conditions is taken from the equilibrated triplet state (upper solid line in Figure 5), then the difference is much more pronounced. This means that the two-level model is too rough for fitting the real experimental data and even more so its incoherent analogue 6.8. On the other hand, it should be noted that the results are rather insensitive to the particular value of T_1 in the whole interval $\infty \ge T_1 \ge T_2$, if the starting state is the same.

2. Noncontact Start. It should be stressed that the results are very sensitive to the starting point especially if it is close to the contact. This peculiarity has been mentioned already in refs 4−6 and 17 where it was shown to result from the contact description of the recombination. In this approximation, the region of too low diffusion is not properly covered especially

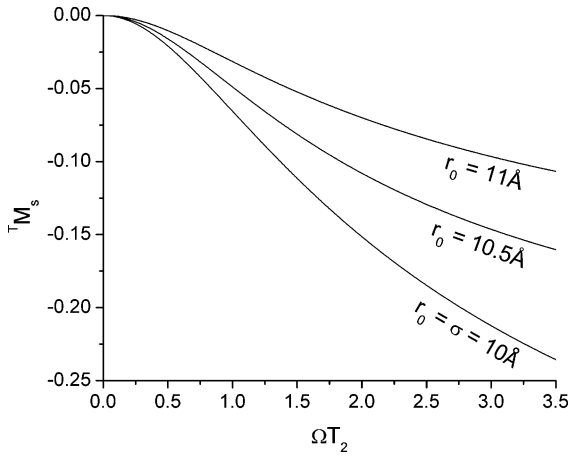

Figure 6. Field dependence of the single-channel MFE at different starting distances. The rest of the parameters are the same as in Figure 4.

when the initial particle separation $r_0 - \sigma$ is comparable or less than the tunneling length. However, it is instructive to recognize the general tendency of the MFE to change with r_0.

As shown in Figure 6, the MFE monotonically decreases with r_0 at any Ω and the sharper the larger it is.

However, the space-dependent recombination rate $W(r)$ is not actually the contact one, as in eq 2.7. Usually it is not narrower than the tunneling length $L \sim 1$ Å, that is, at so close starts, the recombination is for sure not contact. If nevertheless the contact approximation (eq 2.7) is used, then the diffusional dependence of the MFE at the contact start is questionable at slow diffusion (the lowest curve in Figure 7 at $D < 10^{-6}$). However, the curves for large separation are free of this weakness in the fast diffusion region, where the effect is the most pronounced (Figure 7).

Very similar curves with clearly expressed minima were obtained experimentally by Steiner et al.[28] They were fitted in ref 10 within the two-level model with an exponential (non-contact) recombination rate. The calculations include the averaging (eq 8.1) over the realistic distribution $f(r_0)$ which is different for any D values. Unfortunately, all diffusional dependencies were studied by the Steiner group varying D values (viscosity) by changing the solvent composition. This is accompanied by a significant variation of the static and optical dielectric constants changing the outer sphere reorganization energy λ, parallel to diffusion. It was shown later that such a

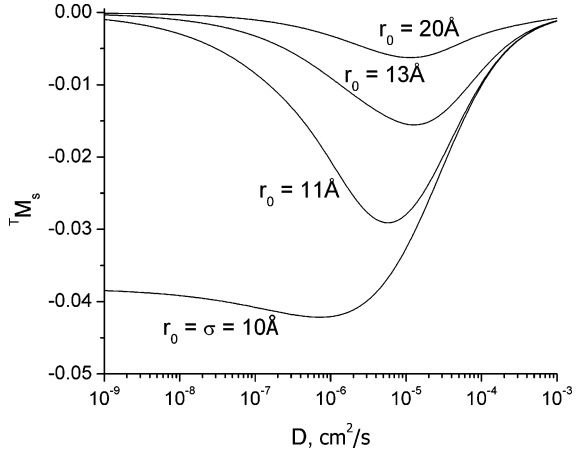

Figure 7. Diffusional dependence of the single-channel MFE at different starting points r_0. All the parameters are the same as in Figure 4..

TABLE 1

D, cm^2/s	T_2, ps	r_0, Å
6.67×10^{-7}	47.6	11.2
1.16×10^{-6}	40.8	10.8
2.30×10^{-6}	37	10.6

variation of λ affects significantly the space-dependent transfer rate and changes qualitatively the interpretation of the quantum yield diffusional dependence.[4−6] This is not the place to go into the details of fitting the real diffusional dependencies. Instead, it is better to concentrate on fitting the field dependence of the MFE when nothing is changed except Ω.

3. Fitting the Field Dependence of the MFE. The expected field dependence is exhibited in Figure 6. The different starting distances, r_0, represent the difference in diffusion. The faster the latter is the closer to the contact the actual initial distribution, $f(r_0)$, is. Instead of the whole distribution, $f(r_0)$, we take a single r_0, close to its average value, which shifts to contact when diffusion becomes faster. However, not only the starting distance changes with D but also T_2 is subjected to some changes indicated in the original experimental work (Table 1 in ref 28). We used these values to fit the related curves $^{\mathrm{T}}M_{\mathrm{s}}$ using r_0 as a single variable parameter and borrowing the value for $k_{\mathrm{c}}^{\mathrm{S}} = 3.31 \times 10^5$ Å^3/ns from ref 10 (see the caption to Figure 7 therein).

The results of our fitting are shown in Figure 8 and Table 1. They cannot be expected to be better because the contact approximation for recombination (eq 2.7) is employed instead of the true $W(r)$ and the single starting distance is used instead of $f(r_0)$.

The monotonic decreasing of r_0 with D confirms the nature of the forward electron transfer (ionization) that should be diffusional at such a small D value. The effective radius of the diffusional ionization is known to go down when the diffusion accelerated.[12,6] Of course, the variation of λ simultaneously with diffusion can imitate the same effect as it did already in another respect.[4−6] Nonetheless, the spin conversion responsible for the really observable MFE is an undoubtedly coherent process contrary to what was expected in previous works.[29,30]

B. Double-Channel Recombination. When both reaction channels are switched on, the yield of free radicals (eq 8.1) is also field dependent, though $Z(H) = Z_{\mathrm{s}} + Z_{\mathrm{t}}$ depends on both $k_{\mathrm{c}}^{\mathrm{S}}$ and $k_{\mathrm{c}}^{\mathrm{T}}$. Until now, there was only one system where Z and Z_{t} were measured simultaneously.[17] However, the MFE was not detected there. Besides, the spin conversion there was carried out by another (HFI) mechanism that was considered separately.[8]

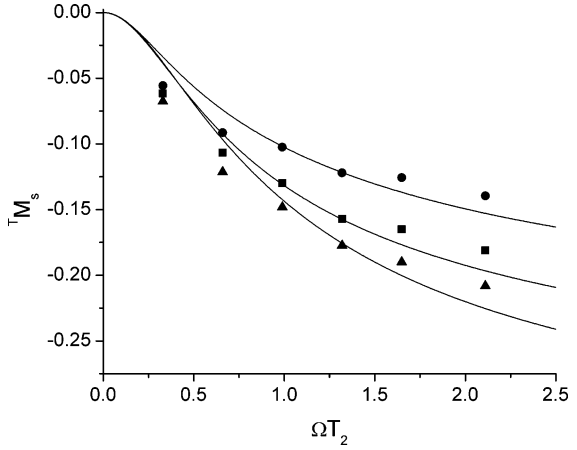

Figure 8. Fitting of the field dependence of MFE at various values of the diffusion coefficient, increasing from top to bottom (Table 1). The points are taken from experimental work.[28]

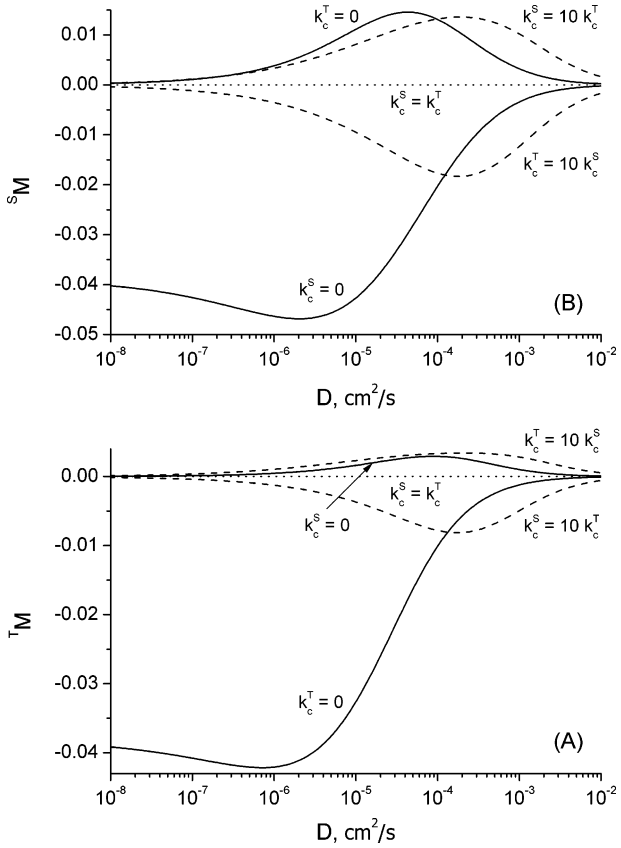

Figure 9. Diffusional dependence of the MFE for triplet (A) and singlet (B) radical pairs, starting from contact. Single-channel recombination is given by solid lines, double-channel recombination by dashed lines, and the spin-independent border case by a dotted one. The relative efficiencies of the singlet and triplet recombination channels are pointed out by the relative $k_{\mathrm{c}}^{\mathrm{S}}$ and $k_{\mathrm{c}}^{\mathrm{T}}$ values.

Therefore, we restrict our attention to only the contact start using $\varphi(\sigma,H)$ in eq 8.2 instead of $\bar{\varphi}(H)$. This is only a demonstration of the qualitatively different diffusional dependence of the MFE, which is very sensitive to the interrelationship between $k_{\mathrm{c}}^{\mathrm{S}}$ and $k_{\mathrm{c}}^{\mathrm{T}}$ at any starting state (Figure 9).

For triplet recombination through the singlet channel, $^{\mathrm{T}}M_{\mathrm{s}}$, we have in (A) the lowest curve ($k_{\mathrm{c}}^{\mathrm{T}} = 0$) which is the same as in Figures 7 and 5. An alternative recombination of the same pair, via the triplet channel only, $^{\mathrm{T}}M_{\mathrm{t}}$, takes place at $k_{\mathrm{c}}^{\mathrm{S}} = 0$ and has an opposite, positive sign of the MFE. A border case of the

double channel but "spin-independent recombination" ($k_c^T = k_c^S$) is a horizontal dotted line ${}^TM = 0$. At comparable but not equal rate constants $k_c^S = 10k_c^T$ and $k_c^T = 10k_c^S$, the signs of the effect are also the opposite as for the single-channel limits.

For recombination from the singlet initial state (B), the picture is qualitatively the same, except that the signs of the MFE when the singlet or triplet channel dominates are interchanged. Since the initial state of the photoinduced pair is usually known, the diffusional dependence of MFE allows one to find easily what channel is more efficient and by how much.

IX. Conclusions

The yields of singlet and triplet products of the double-channel recombination from either of these states and any initial separation of radicals are exactly calculated assuming the spin conversion is due to a Δg mechanism. The results for the recombination through the singlet channel, only obtained previously for the contact start from the singlet, are reproduced and extended for the start from the equipopulated triplet states. In the latter case, the MFE arising from the coherent spin conversion is estimated and well fitted to the available experimental data. The popular model considering the spin conversion as an incoherent rate process is not appropriate in a high field but becomes exact in a zero field, provided the spin relaxation times are equal. In this particular case, the diffusional dependence of all the yields coincides with the exact one and may be used for discrimination between the channels.

The only limitation of the theory is the contact approximation for distant recombination rates. It can be overcome by numerical calculations provided that the distance dependence of the rate is known.

Acknowledgment. The authors are thankful to Professor N. Lukzen for greatly appreciated help.

References and Notes

(1) Hong, K. M.; Noolandi, J. *J. Chem. Phys.* **1978**, *68*, 5163.

(2) Burshtein, A. I.; Zharikov, A. A.; Shokhirev, N. V.; Spirina, O. B.; Krissinel, E. B. *J. Chem. Phys.* **1991**, *95*, 8013.

(3) Zharikov, A. A.; Shokhirev, N. V. *Chem. Phys. Lett.* **1991**, *186*, 253.

(4) Neufeld, A. A.; Burshtein, A. I.; Angulo, G.;. Grampp, G *J. Chem. Phys.* **2002**, *116*, 2472.

(5) Burshtein, A. I.; Neufeld, A. A. *J. Phys. Chem. B* **2001**, *105*, 12364.

(6) Burshtein, A. I. *Adv. Chem. Phys.* **2004**, *129*, 105.

(7) Salikhov, K. M.; Molin, Yu. N.; Sagdeev, R. Z.; Buchachenko A. L. *Spin polarization and magnetic effects in radical reactions*; Molin, Yu., N., Ed.; Elsiever: Amsterdam, The Netherlands, 1984.

(8) Lukzen, N. N.; Pedersen, J. B.; Burshtein, A. I. *J. Phys. Chem. A* **2005**, *109*, 11914.

(9) Steiner, U. E.; Ulrich, Th. *Chem. Rev.* **1989**, *89*, 51.

(10) Krissinel, E. B.; Burshtein, A. I.; Lukzen, N. N.; Steiner, U. E. *Mol. Phys.* **1999**, *96*, 1083.

(11) Burshtein, A. I.; Krissinel, E.; Steiner, U. E. *Phys. Chem. Chem. Phys.* **2001**, *3*, 198.

(12) Burshtein, A. I. *Adv. Chem. Phys.* **2000**, *114*, 419.

(13) Mints, R. G.; Pukhov, A. A. *Chem. Phys.* **1984**, *87*, 467.

(14) Purtov, P. A.; Doktorov, A. B. *Chem. Phys.* **1993**, *178*, 47.

(15) Korst, N. N.; Lazarev, A. V. *Physica* **1969**, *42*, 31.

(16) Pedersen, J. B.; Freed, J. H. *J. Chem. Phys.* **1973**, *58*, 2746.

(17) Gladkikh, V. S.; Burshtein, A. I.; Angulo, G.; Grampp, G. *Phys. Chem. Chem. Phys.* **2003**, *5*, 2581.

(18) Gladkikh, V. S.; Burshtein, A. I. *Chem. Phys.*, in press.

(19) Hansen, M. J.; Neufeld, A. A.; Pedersen, J. B. *Chem. Phys.* **2000**, *260*, 125.

(20) Burshtein, A. I. *Chem. Phys.*, in press.

(21) Burshtein, A. I. *Chem. Phys. Lett.* **2005**, *411*, 66.

(22) Tomkiewicz, M.; Cocivera, M. *Chem. Phys. Lett.* **1971**, *8*, 595.

(23) Bube, W.; Haberkorn, R.; Michel-Beyerle, M. E. *J. Am. Chem. Soc.* **1978**, *100*, 5993.

(24) Sterna, L.; Ronis, D.; Wolfe, S.; Pines, A. *J. Chem. Phys.* **1980**, *73*, 5493.

(25) Hayashi, H.; Nagakura, S. *Bull. Chem. Soc. Jpn.* **1984**, *57*, 322.

(26) Schulten, Z.; Schulten, K. *J. Chem. Phys.* **1977**, *66*, 4616.

(27) Bürβner, D.; Wolff, H.-J.; Steiner, U. *Z. Phys. Chem. Board* **1993** *182* 297; *Angew. Chem., Int. Ed. Engl.* **1994**, *33*, 1772.

(28) Wolff, H.-J.; Bürβner, D.; Steiner U. *Pure Appl. Chem.* **1995**, *67* (1), 167.

(29) Burshtein, A. I.; Krissinel, E. *J. Phys. Chem. A* **1998**, *102*, 816.

(30) Burshtein, A. I.; Krissinel, E.; Steiner, U. E. *Phys. Chem. Chem. Phys.* **2001**, *3*, 198.

ARTICLES

Variation of the Resonant Transfer Rate When Passing from Nonadiabatic to Adiabatic Electron Transfer

V. Gladkikh and A. I. Burshtein*

Chemical Physics Department, Weizmann Institute of Science, Rehovot 76100, Israel

I. Rips

Department of Sciences, Holon Academic Institute of Technology, Holon 58102, Israel

Received: December 14, 2004; In Final Form: April 11, 2005

Two competing theories are used for bridging the gap between the nonadiabatic and the deeply adiabatic electron transfer between symmetric parabolic wells. For the high friction limit, a simple analytic interpolation is proposed as a reasonable alternative to them, well-fitted to the results of numerical simulations. It provides a continuous description of the electron transfer rate in the whole range of variation of the nonadiabatic coupling between the diabatic states. For lower friction, the original theories are used for the same goal. With an increase in coupling, the cusped barrier transforms into the parabolic one. Correspondingly, the pre-exponent of the Arrhenius transfer rate first increases with coupling, then levels off approaching the "dynamic solvent effect" plateau but finally reduces reaching the limit of the adiabatic Kramers theory for the parabolic barrier. These changes proceeding with a reduction in the particle separation affect significantly the spatial dependence of the total transfer rate. When approaching the contact distance, the exact rate becomes smaller than in the theory of dynamical solvent effects and much smaller than predicted by perturbation theory (golden rule), conventionally used in photochemistry and electrochemistry.

I. Introduction

The electron transfer rate is a fundamental property used in the theories of intramolecular and intermolecular reactions in dense media.[1−4] At high temperatures, the system motion is adiabatic everywhere except at the crossing point of the intersecting energy levels where the electron tunneling occurs. For electron exchange reactions, the potential surface consists of the two symmetric diabatic energy levels, which are commonly assumed to be parabolic (Figure 1). The free energy gap for electron transfer in both directions is zero, and the transfer rate is given by the conventional Arrhenius equation:

$$W = k\, e^{-(U-V)/T},\ U = \lambda/4 \tag{1.1}$$

Here, U is the energetic height of the crossing point, $2V$ is the nonadiabatic splitting of the energy levels 1 and 2 at this point, λ is the reorganization energy of transfer, and $k_B = 1$.

The preexponential factor, k, depends on the nonadiabatic coupling and the dynamic of motion along the reaction coordinate. The evaluation of this factor constitutes a complex problem that cannot be solved universally within a single theory. A number of theories have to be used to cover the whole domain of $k(V,\gamma)$ where γ is a friction along the reaction coordinate. This two-dimensional domain was used in a few works[5−7] to indicate the results of different theories and their mutual borders as shown in Figure 2, taken from ref 7. This figure establishes all of the results and their regions of applicability but does not provide bridging between them. Particularly, the variation of the prefactor k with the nonadiabatic coupling V at a fixed dissipation strength γ (in the vertical cross-section of the domain from bottom to top) is due to the monotonic increase of the coupling,

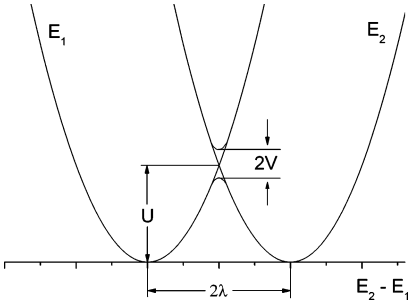

Figure 1. Energetic scheme of resonant electron transfer.

$$V(r) = V_0 e^{-(r-\sigma)/L} \tag{1.2}$$

with reduction of the inter-reactant separation (up to their closest approach at $r = \sigma$). Passing this way at high friction, one starts from the nonadiabatic perturbation theory subregion, where transfer is limited by tunneling, crosses the intermediate subregion of the dynamical solvent effect (DSE), but finishes in the adiabatic subregion where the reaction is controlled by

10.1021/jp044311y CCC: $30.25
Published on Web 05/18/2005

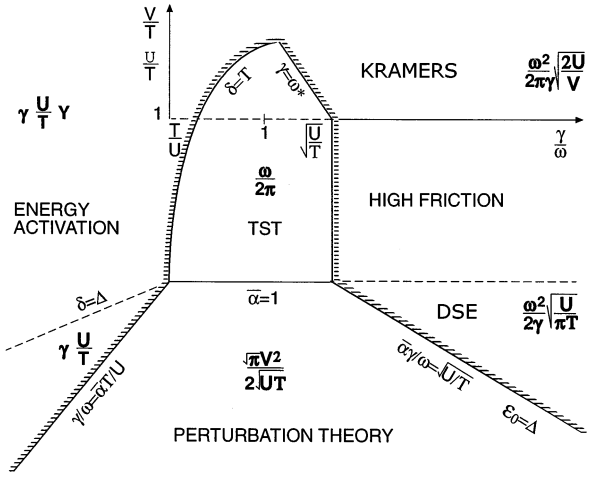

Figure 2. Entire domain of theoretical definitions of electron transfer pre-exponent $k(V,\gamma)$ given in ref 7. The vertical dashed line corresponds to the value $\lambda = 40T$ used further on.

diffusion to the crossing point. In each subregion, there are expressions for k, which differ from one another. The dependence of the preexponential factor $k[V(r)]$ is an essential part of the spatial dependence of $W(r)$ given in eq 1.1. As an input data used in the theories of intermolecular transfer,[3,4] it has to be continuous in r and not composed from a few pieces related to different theories valid at different distances. The main goal of the present work is to bridge these two pieces together to get a single continuous formula for the required $k(V)$ and $W(r)$ dependencies. It should be stressed that the urgent necessity to match the Fermi Golden Rule and Kramers high friction theory, including DSE, which separates them, was recognized long ago. At first, it was realized in the well-known Calef and Wolynes work[8] and then by means of the Pollak "variational transition state theory" (VTST).[9−12] In what follows, we will rely upon these two alternative approaches to the problem at hand.

Although the transfer is assisted by the system delivery to the crossing point, at sufficiently small V, it is limited everywhere not by this motion but by slow tunneling with the rate k_{PT}. The latter is given by the Fermi Golden Rule (second-order perturbation theory developed in ref 13; see also eqs 2.37 in ref 1 and 1.7 in ref 5):

$$k_{PT} = \frac{V^2}{\hbar}\sqrt{\frac{\pi}{\lambda T}} \tag{1.3}$$

However, at larger V, the tunneling ceases to control the reaction giving way to either energy activation at low friction ($\gamma \ll \omega$) or free vibrations at moderate friction (with the well frequency $\omega/2\pi$). At even larger values of the friction, the reaction is controlled by diffusion to the crossing point along the reaction coordinate. The last phenomenon was discovered independently in two simultaneously published papers, refs 14 and 15. The latter is addressed rather to the inner sphere low frequency vibrations such as in H-bonded complexes in water, studied later by pump−probe spectroscopy.[16−19] The former addressed more specifically the outer sphere electron transfer in Debye polar solvents where

$$\gamma = \omega^2 \tau_L \tag{1.4}$$

Here $\tau_L = \tau_D\, \epsilon_0/\epsilon$ is the longitudinal relaxation time of dielectric polarization related to the Debye relaxation time τ_D, through the ratio of the optical (ϵ_0) and static (ϵ) dielectric constants. Later on, the phenomenon of diffusional control in the reaction space, which became known as the dynamical solvent effect, was reproduced in a number of publications and observed experimentally.[20] However, with an increase in V, DSE gives way to the well-known Kramers result for the parabolic barrier. The latter is slightly different from DSE, which is actually its analogue for the cusped barrier:

$$k_{DSE} = 1/\tau_L\sqrt{\frac{\lambda}{16\pi T}} \text{ for the cusped barrier} \tag{1.5a}$$

$$k_{Kram} \simeq \frac{1}{\tau_L}\sqrt{\frac{\lambda}{8\pi^2 V}} \text{ for the parabolic one} \tag{1.5b}$$

In the present work, we focus mainly on the large friction (strong dissipation) region where the alternating formulas k_{PT}, k_{DSE}, and k_{Kram} follow one another with increasing V. There is also the more general expression derived by Zusman bridging between the first two:

$$k_{non} = \frac{k_{PT}\, k_{DSE}}{k_{PT} + k_{DSE}} = \begin{cases} k_{PT} & \text{weak nonadiabatic} \\ k_{DSE} & \text{strong nonadiabatic} \end{cases} \tag{1.6}$$

This is an exact solution of the sudden modulation equations used in refs 5, 14, and 15. There, the transfer was considered as nonadiabatic but weak where the perturbation theory holds and strong where it gives way to DSE. Later on, the two expressions (1.5) were also bridged by considering both of them as adiabatic transfer (along a quasi-ballistic mode) over either the cusped barrier or the parabolic one. The former transforms to the latter with an increase of the level splitting $2V$. This matching resulting in the general expression for the diffusion-assisted reaction k_{DAR} was first made by Calef and Wolynes[8] and later by Starobinets, Rips, and Pollak.[11] These approximations will be considered in the next section, and the simple interpolation formulas will be introduced for the large friction limit. In section III, these formulas will be bridged with that for perturbation theory for getting the final $k(V)$ and corresponding $W(r)$ dependencies. In section IV, we will do the same but will account for the spatial dependence of the reorganization energy peculiar for highly polar solvents. In the conclusions, we will summarize all of the results and outline the remaining problems.

It should be emphasized that in this paper we focus on high temperature, high barrier electron exchange reactions in Debye polar solvents. This implies that the reaction is thermally activated with electron tunneling proceeding in the vicinity of the crossing point of the diabatic potential surfaces. The solvent modes can be treated classically (nuclear tunneling is negligible). Furthermore, the effect of the high frequency quantum solvent modes is neglected.

II. Diffusion-Assisted Reaction

The matching alternative adiabatic results (1.5) allows covering the whole domain of diffusion-assisted transfer. An important generalization of this kind made by Calef and Wolynes[8] results in the following equation for the pre-exponent:

$$k_{CW} = \frac{\omega}{2\pi}\left\{\sqrt{1 + \frac{J^2}{2\pi\alpha}} - \frac{J}{\sqrt{2\pi\alpha}}\right\} \tag{2.1}$$

where

$$J(V,\lambda) = e^{V/T}\int_0^{\lambda/2T} dy\, \exp\left[\frac{y^2}{\lambda/T} - \sqrt{y^2 + (V/T)^2}\right] \tag{2.2}$$

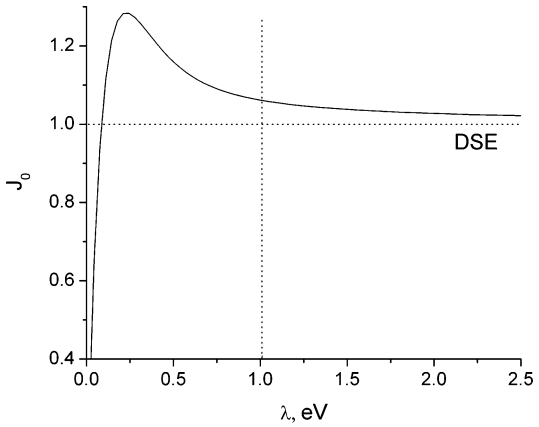

Figure 3. Correction factor for a cusped barrier rate, J_0, as a function of the reorganization energy.

and the dimensionless dissipative parameter

$$\alpha = \frac{\lambda}{2T}\left(\frac{\omega}{\gamma}\right)^2 \tag{2.3}$$

In general, the theory of Calef and Wolynes is valid from the intermediate (TST) to high friction (DSE) region (see Figure 2), so that

$$k_{\mathrm{CW}} = \begin{cases} \dfrac{\omega}{2\pi} = k_{\mathrm{TST}} & \gamma/\omega \ll \sqrt{\lambda/4T} \quad (\alpha \gg 2) \\ \dfrac{k_{\mathrm{DSE}}}{J(V,\lambda)} = k_\infty & \gamma \to \infty \qquad\qquad (\alpha \to 0) \end{cases} \tag{2.4}$$

but it is the best for the highest available friction (at $\alpha \to 0$). This is actually the case in which we are mainly interested.

In this particular case, the motion along the reaction coordinate to the crossing point is diffusional but it delivers the system to either a cusped or a quasi-parabolic barrier depending on whether the level splitting at the point is small or large, respectively. In the cusped barrier limit ($V \to 0$), the expression (2.2) reduces to the following one:

$$J(0, \lambda) = -\pi i \sqrt{\lambda/4T}\, e^{-\lambda/4T}\, \mathrm{erf}(i\sqrt{\lambda/4T}) = J_0(\lambda) \tag{2.5}$$

Although J_0 is real and positive, it is not equal to 1 at any finite barrier height $\lambda/4$, that is in general $k_\infty \neq k_{\mathrm{DSE}}$ even at $V \to 0$. As seen from Figure 3, J_0 approaches unity only as $\lambda \to \infty$. Otherwise

$$k_\infty = \begin{cases} k_{\mathrm{DSE}}/J_0(\lambda) = k_{\mathrm{CUSP}} & V \to 0 \\ \dfrac{1}{2\pi\tau L}\sqrt{\dfrac{\lambda}{2V} - 1} = k_{\mathrm{PAR}} & V \to \infty \end{cases} \tag{2.6}$$

The latter result is the more precise Kramers formula for a parabolic barrier. It differs slightly from its simplified version (1.5b) obtained for $2V \ll \lambda$. If V is not negligible (although smaller than $\lambda/2 = 2U$), then k_{PAR} should be used instead of eq 1.5b. Unlike the latter, it is nonlinear in the $\sqrt{T/V}$ coordinate of Figure 4.

It is easy to interpolate between the opposite limits represented in eq 2.6 to get a simple analytic alternative to the Calef and Wolynes k_∞ from eq 2.4:

$$k_{\mathrm{DAR}} = \frac{1}{\tau_{\mathrm{L}}}\sqrt{\frac{\lambda - 2V}{8\pi(2TJ_0^{\,2} + \pi V)}} = \begin{cases} k_{\mathrm{CUSP}} & \text{at } V \ll T \\ k_{\mathrm{PAR}} & \text{at } V \gg T \end{cases} \tag{2.7}$$

This is the pre-exponent of the diffusion-assisted rate of electron transfer over the barrier of arbitrary shape: from a cusped to a parabolic one. As can be seen in Figure 4, this interpolation not only approaches both these limits as expected but between goes through four points numerically calculated in ref 11.

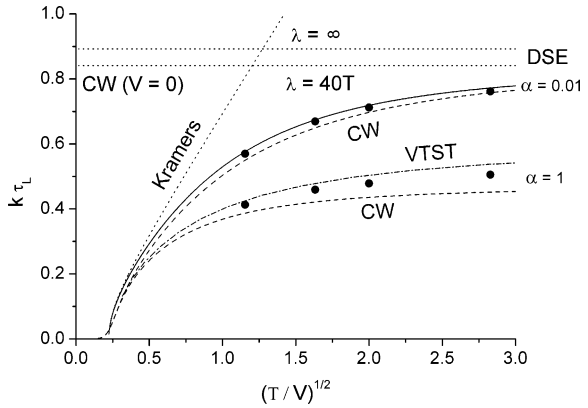

Figure 4. Pre-exponent k of diffusion-assisted electron transfer between the limits of cusped ($T/V \gg 1$) and parabolic ($T/V \ll 1$) barriers. The Kramers result for the latter is shown by the inclined dotted line while the horizontal dotted and dashed−dotted lines represent the DSE results for $\lambda = \infty$ and $\lambda = 40T$, respectively. All other curves are the following: our interpolation (solid line), Calef and Wolynes k_∞ for high and moderate friction (dashed lines), and VTST theory for the latter one (dash-dotted). The points represent the exact results obtained in ref 11 by numerical simulations for large ($\alpha = 0.01$) and moderate friction ($\alpha = 1.0$).

In the relatively low friction region, the better alternative to the Calef and Wolynes approximation is provided by VTST, which represents the pre-exponent in the following form:

$$k_{\mathrm{VTST}} = \frac{P}{2\pi\tau_{\mathrm{L}}}\sqrt{\frac{\lambda}{2\alpha T}} \tag{2.8}$$

and $P \equiv P(\alpha, V)$ has to be determined by solving the optimization problem as described in ref 11. Making this numerically, we found that the VTST curve $k(V)$ is very close to the four green points obtained for lower friction by numerical simulations made in ref 11. There, the reactive flux method[21] was employed for the integration of the Langevin equation of motion using the velocity Verlet algorithm.[22]

The black points in Figure 4 were calculated for $\alpha = 0.01$, that is for $\gamma/\omega \approx 45$ at $\lambda/T = 40$. This friction is large enough to be well-approximated by the Calef and Wolynes (CW) expression for k_∞. As for the green points, they were obtained in the same way and for the same λ/T but for $\alpha = 1$ when $\gamma/\omega \approx 4.5$. Here, we are very close to the boundary of the high friction region. As seen from Figure 2 in our case ($\lambda/T = 40$), this border is located at $\gamma/\omega = \sqrt{\lambda/4T} = \sqrt{10}$, that is far to the left from the cross-section $\gamma/\omega = 45$ to which we mainly address. The green points for the modest friction are somewhat better approximated by VTST than by the CW theory, while the black points for the higher friction are equally well-approximated by the original CW theory and our interpolation (2.7). However, the latter will be solely used further on just because of its relative simplicity.

III. General Interpolation

As a matter of fact, the cusp limit of either approximation (2.6) or interpolation (2.7) is never achieved in reality because at small V the limited stage of the transfer becomes not a

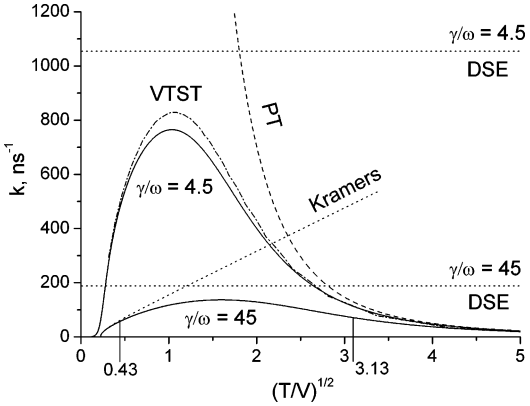

Figure 5. Solid curves are our interpolation (3.1) between the weak tunneling and the diffusion-assisted transfer. The former is given by the perturbation theory (PT, dashed line) while the latter is given by the Kramers and DSE approximation (dotted lines). The lowest solid line is our interpolation at high friction ($\alpha = 0.01$, $\gamma/\omega = 45$) while the upper dotted horizontal line over it represents the DSE approximation. Above them there are the similar lines for the lower friction ($\alpha = 1.0$, $\gamma/\omega = 4$, 5). The bottom vertical lines indicate the lower limits for the argument (3.13 and 0.43) accessible in two systems studied in refs 23 and 24, respectively.

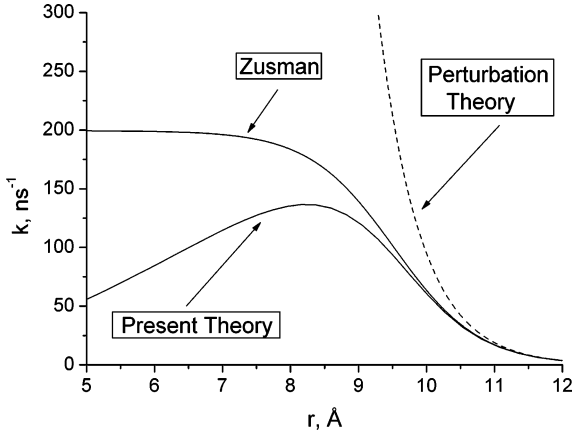

Figure 6. Pre-exponent k in different theories as a function of the interparticle distance at large friction ($\gamma/\omega = 45$) and $V_0 = 0.138$ eV, $L = 1.24$ Å.

diffusion to the crossing point but an electron tunneling. This means that the adiabatic theory should give way to the perturbation one as DSE does in the Zusman formula (1.6). Hence, to get the interpolation valid at any V, we just have to substitute k_{DSE} in this formula for k_{DAR} from eq 2.7:

$$k = \frac{k_{PT}\, k_{DAR}}{k_{PT} + k_{DAR}} \tag{3.1}$$

At small V, this constant is equal to k_{PT}, which is independent of friction unlike the longitudinal relaxation time τ_L, which increases with γ. At given $\omega = 10^{13}$, we obtain from the definition (1.4):

$$\frac{1}{\tau_L} = \omega\frac{\omega}{\gamma} = \begin{cases} 0.022\omega = 2.2 \times 10^{11}\ \mathrm{s}^{-1} & \text{at } \gamma/\omega = 45\ (\alpha = 0.01) \\ 0.22\omega = 2.2 \times 10^{12}\ \mathrm{s}^{-1} & \text{at } \gamma/\omega = 4.5\ (\alpha = 1) \end{cases} \tag{3.2}$$

Correspondingly, the height of the DSE plateau is higher the smaller is the friction (see Figure 5), but this plateau is never achieved by $k(V)$, which lowers with increasing V approaching the Kramers limit for the parabolic barrier. As a result, k is never as high as its DSE value but the very existence of this plateau as well as Kramers limit greatly reduces the actual k as compared with PT. However, the real deviation from the letter is not too large if $V \leq V_0 \ll T$, which is usually the case. For instance, T/V_0 calculated from the contact transfer rate obtained in ref 23 is equal to 3.13. As seen from Figure 5 at this point (in contact), k is only half of the perturbation theory value and this difference reduces quickly with increasing intermolecular distance. Only recently the system was encountered (perylene + TCNE) where the contact coupling is larger than T, namely, $T/V_0 = 0.43$.[24] There instead of the perturbation theory rate W_{PT} the Zusman formula (1.6) was used to account for DSE. However, at the highest $V = V_0$, even this correction is not enough. As seen from Figure 5 at this point, the Kramers high friction region is actually reached where the true k is twice smaller than its DSE alternative, not speaking about a much larger perturbation theory value.

To get an impression of what happens for lower friction, we used the same approach substituting k_{DSE} in the Zusman formula (1.6) by either k_{CW} from eq 2.4 or k_{VTST} from eq 2.8:

$$k = \frac{k_{PT}\, k_{CW}}{k_{PT} + k_{CW}} \text{ or } k = \frac{k_{PT}\, k_{VTST}}{k_{PT} + k_{VTST}} \tag{3.3}$$

Both of these results are also shown in Figure 5. The discrepancy between them is within the limits of accuracy of both approximations. The electron transfer rate increases with decreasing friction due to acceleration of the motion along the reaction coordinate. At a further decrease of friction, this motion becomes ballistic, and the transfer rate reaches its upper limit established by a plateau $k = k_{TST} = \omega/2\pi$. This plateau is not shown in Figure 5 because it is too high. Furthermore, we are interested in quite the opposite limit of the large friction available, where our interpolation (2.7) is the best.

In general, the importance of the diffusion control of the transfer increases with the increasing nonadiabatic coupling at contact. This effect is very impressive, especially if considered in real space. Using expression 1.2, we transformed into this space (Figure 6) the result obtained for the large friction $\gamma/\omega = 45$. It should be noted that in the vast majority of papers on intermolecular electron transfer, only the perturbation theory was so far used.[3,4] This is reasonable if either the electron coupling is much weaker than in the present example or the closest approach distance is much larger ($\omega > 10$ Å). In ref 24, for the first time, these conditions were shown to be broken in the system studied experimentally. There, only the use of the Zusman eq 1.6 instead of the perturbation theory allowed us to obtain a reasonable fit to the experimental data. However, Figure 6 shows that being better than perturbation theory, the Zusman approximation still overestimates the transfer rate at short distances where the barrier becomes parabolic. For attainment of the highest reliability of the fitting, the use of the present theory is essential. In the following section, we will see how it changes the real rate of transfer $W(r)$ given by eq 1.1.

IV. Transfer Rate in Polar Solvents

The reorganization energy employed in the foregoing analysis was considered as a distance-independent parameter. This is true only for in nonpolar solvents where the inner sphere contribution to the reorganization energy is the dominant one: $\lambda \equiv \lambda_{in} = \text{const}$. In highly polar solvents, the situation is the opposite: the inner sphere contribution can be neglected as

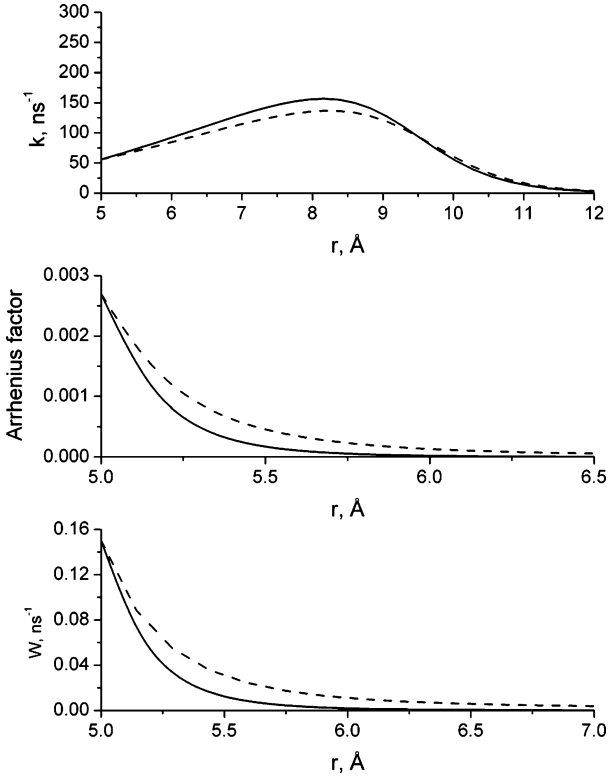

Figure 7. Pre-exponent, exponent, and their product W as functions of interparticle distance with (solid lines) and without (dashed lines) accounting for the space dependence of the reorganization energy.

compared with the outer sphere reorganization energy, which changes with distance between reactants according to the well-known law:[3,4]

$$\lambda(r) = \lambda_0(2 - \sigma/r) \tag{4.1}$$

In acetonitrile, the contact reorganization energy $\lambda_0 = 1.15$ eV and the average distance between contacting reactants is $\sigma = 5$ Å, if these are perylene and tetracyanoethylene (TCNE) as in ref 24.

Take into account that the $\lambda(r)$ dependence makes the pre-exponent k slightly larger in the adiabatic near contact region but smaller at larger separations, where the transfer is nonadiabatic (Figure 7). In parallel, $\lambda(r)$ dependence is responsible for the increase of $U(r) = \lambda(r)/4$ whose contact value is $U(\sigma) = \lambda_0/4$, while at infinite separation it is twice as large: $U(\infty) = \lambda_0/2$. As a result, the transfer rate

$$W(r) = k(r) \exp\left\{-\left[\frac{\lambda(r)}{4} - V(r)\right]/T\right\} \tag{4.2}$$

decreases with distance not only due to the pre-exponent but to increasing the activation energy as well.

Another important factor that affects the activation energy is the nonadiabatic coupling $V(r)$, which increases when approaching contact. As a result, the contact Arrhenius factor is significantly enhanced if $V_0 > T$, although it reduces sharply with increasing the inter-reactant distance. This effect is dominant at short distances where $V > T$, while at larger separation, the increase of $\lambda(r)$ contributes mainly to reduction of the Arrhenius factor.

The same tendency manifests itself in the reduction of $W(r)$, which is the product of $k(r)$ and the r-dependent Arrhenius factor (Figure 7). The spatial dependence of the transfer rate is

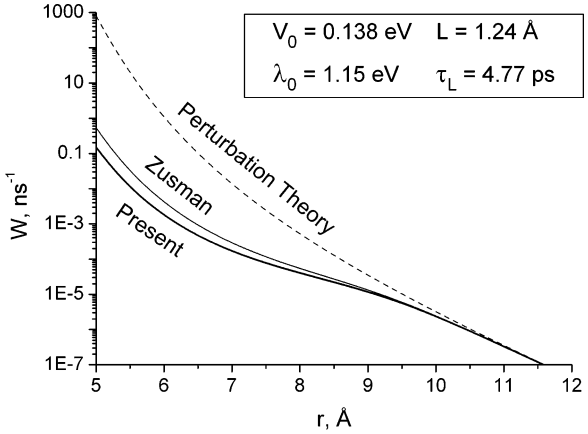

Figure 8. Space dependence of the transfer rates calculated with perturbation and Zusman theories and present interpolation.

significantly distorted, if the barrier reduction by $V(r)$ or $\lambda(r)$ dependence is ignored. In such a case, the kinetic rate constant

$$k_0 = \int W(r) d^3r$$

can be also overestimated as well as V_0 obtained by fitting the theory to the experimental data. Fortunately, the dispersion of reorganization energy is usually taken into account[3,4] and the lowering of the activation barrier was also accounted for when necessary.[25]

The diffusional control of the tunneling so far was considered only with the Zusman theory.[24,25] Now, we can estimate what is the difference between this and the present theory. In Figure 8, the present $W(r)$ is exhibited in the larger spatial interval than in Figure 7 and compared with the Zusman rate and that obtained using the Golden Rule (perturbation theory). Both our and the Zusman theories, which account for the diffusional control of the tunneling, and the rates of transfer at $r < 10$ Å are systematically lower than predicted by the perturbation theory. This difference ranges up to 3 orders of magnitude at the closest approach distance. The difference between the Zusman and our results is less pronounced but still runs as high as $3 \div 4$ times at $r < 6$ Å.

Special attention should be paid to the deviation of the true $W(r)$ dependence from its popular exponential approximation:

$$W(r) = W_0 e^{-(r-\sigma)/l} \tag{4.3}$$

In the limited range of distances, this simplification leads to a different and sometimes nonphysical value for W_0 and l. In particular, near the contact, l could be smaller than L, but in the medium larger than it and only as $r \rightarrow \infty$, the identity $l = L$ is reached. Too large values of l sometimes reported[26−29] are usually identified with L but associated with electron superexchange, which dominates the direct exchange of an electron.[30] However, it also may be an indication of too strong coupling, resulting in diffusional control of the transfer at short distances, making the dependence of the rate $W(r)$ on the distance less pronounced and leading to a natural excess of l over L. For instance, the "local" $l = -2\,(\mathrm{d}\ln W/\mathrm{d}r)^{-1}$ reaches in our case 1.67 Å (at $r = 8.4$ Å) as compared to the true tunneling distance $L = 1.24$ Å (at $r \rightarrow \infty$).

V. Conclusions

On a particular example of the resonant electron transfer, we have demonstrated that the Zusman account for the dynamical solvent effect is insufficient for determination of the transfer

rate if electron coupling at contact is too strong. Zusman's expression was generalized using the original interpolation between DSE and the adiabatic Kramers limit for high friction. The same was done for moderate values of the friction using two theories of diffusion-controlled electron transfer.[8,11] The present theory allows specifying the continuous distance dependence of the transfer rate from the infinite reactant separation and up to their closest approach where the maximal electron coupling is reached.

Although our analysis is quantitative only for the resonant transfer (with energy gap $\Delta G = 0$), it is qualitatively valid in the normal region ($-\Delta G < \lambda$) provided the transfer barrier

$$U = \frac{(\Delta G + \lambda)^2}{4\lambda} \tag{5.1}$$

does not differ significantly from $\lambda/4$. The situation changes qualitatively only in the inverted Marcus region ($-\Delta G > \lambda$). There, the dynamical solvent effect gives way to the sharp adiabatic cutoff of the transfer rate when electron coupling becomes too large. This situation was quantitatively described in ref 31 by eqs 53 and 28, which constitute an analogue of our eqs 3.1 or 3.3. A more complex situation arises at the boundary between the normal and the inverted region (at $-\Delta G = \lambda$), where the electron transfer is activationless ($U \approx 0$) and nonexponential.[32] The latter case deserves special consideration as well as the phonon-assisted electron transfer in the inverted region, which lowers the barriers, making one of the channels activationless.[3,4]

As already mentioned, our treatment of the nuclear motion of the solvent is classical, which is appropriate at high temperatures. At lower temperatures, nuclear tunneling has important physical effects on the electron transfer rate and should be taken into account.[33,34]

References and Notes

(1) Kuznetsov, A. M. *Charge Transfer in Physics, Chemistry and Biology*; Gordon & Breach: Amsterdam, 1995.
(2) May, V.; Kühn, O. *Charge and Energy Transfer Dynamics in Molecular Systems*; Wiley-VCH: Berlin, 2000.
(3) Burshtein, A. I. *Adv. Chem. Phys.* **2000**, *114*, 419.
(4) Burshtein, A. I. *Adv. Chem. Phys.* **2004**, *129*, 105.
(5) Burshtein, A. I.; Yakobson, B. I. *High Energy Chem.* **1981**, *14*, 211 (*Khim. Vysok. Energ.* **1980**, *14*, 291).
(6) Burshtein, A. I.; Zharikov, A. A. *Chem. Phys.* **1991**, *152*, 23.
(7) Burshtein, A. I.; Georgievskii, Yu. *J. Chem. Phys.* **1994**, *100*, 7319.
(8) Calef, D. F.; Wolynes, P. G. *J. Phys. Chem.* **1983**, *87*, 3387.
(9) Pollak, E. *J. Chem. Phys.* **1990**, *93*, 1116.
(10) Rips, I.; Pollak, E. *J. Chem. Phys.* **1995**, *103*, 7912.
(11) Starobinets, A.; Rips, I.; Pollak, E. *J. Chem. Phys.* **1996**, *104*, 6547.
(12) Pollak, E. In *Theoretical Methods in Condensed Phase Chemistry*; Schwartz, S. D., Ed.; Kluwer Academic Publishers: Dordrecht, 2000; pp 1−46.
(13) Levich, V. G. *Adv. Electrochem. Eng.* **1965**, *4*, 249.
(14) Zusman, L. D. *Chem. Phys.* **1980**, *49*, 295.
(15) Yakobson, B. I.; Burshtein, A. I. *Chem. Phys.* **1980**, *49*, 385.
(16) Burshtein, A. I.; Chernobrod, B. M.; Sivachenko, A. Yu. *J. Chem. Phys.* **1998**, *108*, 9796.
(17) Burshtein, A. I.; Chernobrod, B. M.; Sivachenko, A. Yu. *J. Chem. Phys.* **1999**, *110*, 1931.
(18) Burshtein, A. I.; Sivachenko, A. Yu. *J. Chem. Phys.* **2000**, *112*, 4699.
(19) Burshtein, A. I.; Sivachenko, A. Yu. *J. Phys.: Condens. Matter* **2000**, *12*, 173.
(20) Zusman, L. D. *Zeits. Phys. Chem.* **1994**, *186*, 1.
(21) Hänggi, P.; Talkner, P.; Borkovec, M. *Rev. Mod. Phys.* **1990**, *62*, 251.
(22) Allen, M. P.; Tildesley, D. J. *Computer Simulation of Liquids*; Oxford University Press: New York, 1987.
(23) Gladkikh, V. S.; Tavernier, H. L.; Fayer, M. D. *J. Phys. Chem. A* **2002**, *106*, 6982.
(24) Gladkikh, V. S.; Burshtein, A. I.; Angulo, G.; Pagès, S.; Lang, B.; Vauthey, E. *J. Phys. Chem. A* **2004**, *108*, 6667.
(25) Gladkikh, V. S.; Burshtein, A. I.; Feskov, S. V.; Ivanov, A. I.; Vauthey, E. In press.
(26) Killesreiter, H.; Baessler, H. *Chem. Phys. Lett.* **1971**, *11*, 411.
(27) Kuhn, H. *J. Photochem.* **1979**, *10*, 111.
(28) Bazhin, N. M.; Gritsan, N. P.; Korolev, V. V.; Kamyshan, S. V. *J. Lumin.* **1987**, *37*, 87.
(29) Paddon-Row, M. N. *Acc. Chem. Res.* **1994**, *27*, 18.
(30) Newton, M. *Chem. Rev.* **1991**, *91*, 767.
(31) Georgievskii, Yu.; Burshtein, A. I.; Chernobrod, B. *J. Chem. Phys.* **1996**, *105*, 3108.
(32) Burshtein, A. I.; Kofman, A. G. *Chem. Phys.* **1979**, *40*, 289.
(33) (a) Cao, J.; Minichino, C.; Voth, G. A. *J. Chem. Phys.* **1995**, *103*, 1391. (b) Cao, J.; Voth, G. A. *J. Chem. Phys.* **1997**, *106*, 1769. (c) Cao, J.; Jung, Y. *J. Chem. Phys.* **2000**, *112*, 4716.
(34) Topaller, M.; Makri, N. *J. Chem. Phys.* **1995**, *102*, 460.

Available online at www.sciencedirect.com
SCIENCE DIRECT
Chemical Physics 325 (2006) 359–364
Chemical Physics
www.elsevier.com/locate/chemphys

Near-contact adiabatic suppression of electron transfer in the inverted region

A.I. Burshtein *, V. Gladkikh

Chemical Physics Department, Weizmann Institute of Science, Rehovot 76100, Israel

Received 27 October 2005; accepted 3 January 2006
Available online 3 February 2006

Abstract

A few theories of activated electron transfer in inverted Marcus region are used for bridging the non-adiabatic, solvent controlled and deeply adiabatic transfer. The simple analytical interpolation between dynamic and stochastic theories provides a continuous description of the electron transfer rate at any non-adiabatic coupling between the diabatic states. When coupling increases with shortening of inter-particle distance the pre-exponent of the Arrhenius transfer rate first increases being quadratic in coupling, then levels off approaching the "dynamic solvent effect" (DSE) region and finally is cut off exponentially due to adiabaticity of the transfer.

These changes affect significantly the spatial dependence of the transfer rate near the contact provided the coupling there is strong. The rate tends to zero at contact distance being strongly suppressed nearby adiabatically. It is much smaller then the perturbation (golden rule) and even DSE results. The latter is actually unattainable anywhere if contact tunneling is really strong. The transfer rate is a bell-shaped curve adiabatic and non-adiabatic on the opposite sides and sensitive to the friction (DSE damping) only in between, near the maximum.

Keywords: Electron transfer; Inverted region; Transfer rate

1. Introduction

The electron transfer rate is a fundamental property used in the theories of intra-molecular and inter-molecular reactions in dense media [1–4]. For electron transfer reactions the potential surface consists of the two diabatic energy levels 1 and 2 which are commonly assumed to be parabolic and even identical but shifted relative to one another. Recently, we studied the resonant electron transfer when the free energy of the reaction $\Delta G = 0$ [5]. Here, we turn to the opposite case when the transfer $1 \to 2$ is irreversible and proceeds in Marcus inverted region (Fig. 1), where the free energy is negative and large:

$$-\Delta G > \lambda \gg k_B T, \tag{1.1}$$

where λ is the reorganization energy of electron transfer and k_B is the Boltzmann constant. This is for instance the highly exergonic ionization turning the neutral reactants to the pair of the counter-ions:

$$D + A \to D^+ + A^-.$$

In general the distant dependent rate of electron transfer

$$W = W_0 e^{-U/T} \tag{1.2}$$

is a product of exponential Arrhenius factor (from now on $k_B = 1$) and the pre-exponent W_0 whose r-dependence is very specific for different inter-reactant distances r. The activation energy

$$U = \frac{(\Delta G + \lambda)^2}{4\lambda} \tag{1.3}$$

is also r-dependent through both $\Delta G(r)$ and $\lambda(r)$ [3,4].

The free energy contains the Coulomb contribution which in case of electrostatic attraction between counter-ions reduces its value:

* Corresponding author. Tel.: +972 8934 3708; fax: +972 8934 4123.
E-mail address: cfbursh@wisemail.weizmann.ac.il (A.I. Burshtein).

0301-0104/$ - see front matter © 2006 Elsevier B.V. All rights reserved.
doi:10.1016/j.chemphys.2006.01.001

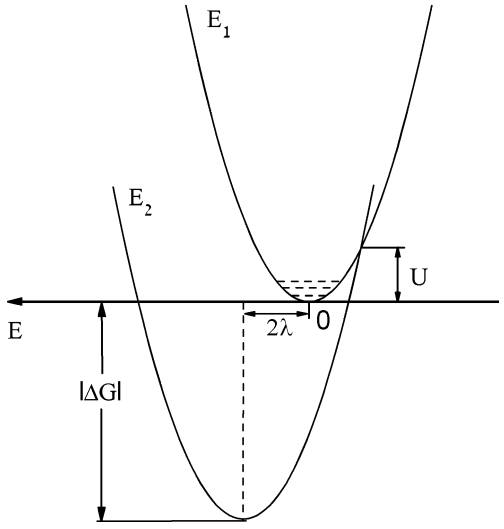

Fig. 1. The intersection of the parabolic diabatic energy levels in the inverted Marcus region.

$$\Delta G(r) = \Delta G_0 - \frac{e^2}{\epsilon r}, \tag{1.4}$$

where $\Delta\ G_0 = \Delta G(\infty)$ and ϵ is the static dielectric constant of the solvent. The polar surrounding of the ions affects also the reorganization energy making it distance dependent:

$$\lambda(r) = \lambda_i + \lambda_0(2 - \sigma/r), \tag{1.5}$$

where λ_i is the so-called inner-sphere reorganization energy and

$$\lambda_0 = \left(\frac{1}{\epsilon_0} - \frac{1}{\epsilon}\right)\frac{e^2}{\sigma}$$

is the outer-sphere reorganization energy (of polar surrounding with optical dielectric constant ϵ_0) at contact distance σ. In highly polar solvents considered here the Coulomb interaction is negligible, that is the free energy is actually constant ($\Delta G(r) = \Delta G_0 = \text{const.}$) and the reorganization energy is large compared to the small inner-sphere contribution neglected further on ($\lambda_i = 0$).

The r-dependence of $W_0(r)$ results mainly from the distance dependence on the non-adiabatic coupling which increases exponentially with reduction of distance:

$$V(r) = V_0\,\mathrm{e}^{-\frac{r-\sigma}{L}}, \tag{1.6}$$

where L is the tunnelling length. The tunneling determines the level splitting $2V$ at the crossing point of the diabatic energy levels. The transfer is non-adiabatic at large distances where the splitting is small but becomes adiabatic at contact if the coupling there is strong enough. In between it passes through the so-called dynamic solvent effect (DSE), when the transfer is limited by diffusion along the reaction coordinate to the crossing point [6,7]. Moreover, Zusman proposed the formula that sewed together the perturbation theory and DSE [6]. The latter becomes the upper limit of the transfer rate achieved at the largest $V \sim V_0$.

The DSE was obtained and studied a lot of times in the intramolecular transfer and in the solid state [8–15]. However, it was common until recently to use mainly the perturbation theory in the theories of electron transfer in liquids presuming that V_0 is small enough [3,4]. However, the precise fitting of transfer kinetics showed us that the true V_0 is as large that the DSE should be taken into account [16]. Now we think that this is not enough. We are going to show here that even at more reliable, much smaller $V_0 \sim 20$ meV the transfer becomes adiabatically suppressed at contact making DSE limit unattainable.

2. Pre-exponent dependence on distance

To cover the whole range of inter-particle distances one has to use a number of theories valid at different coupling, V, and the damping parameter γ, which is actually a friction along the reaction coordinate. The relationship between all these theories and their results was studied earlier [17] and presented in two-dimensional domain (V, γ). The latter is reproduced in Fig. 2 in slightly different notations and used further on to reconstruct the space dependence of $W_0(r)$ and $W(r)$ at high collision frequency γ. However, the value of the latter should not exceed the borders shown by the double line in Fig. 2. Within these limits the crossing region is passed by a single free pass. It is also presumed that $V \ll T$. Under these conditions the velocity of passing conserves during the crossing allowing the classical Landau–Zener formula to be employed [17].

It should be also noted that in Ref. [17] a bit different presentation of the transfer rate (1.2) was used:

$$W(r) = A\Gamma_{\mathrm{TST}} = A\frac{\omega}{2\pi}\mathrm{e}^{-U/T}, \tag{2.1}$$

where Γ_{TST} is the canonical expression of the transition state theory (TST) rate through the linear frequency of the free vibrations in parabolic potential well, $\omega/2\pi$. We see from the comparison that

$$W_0(r) = \frac{\omega}{2\pi}A(r) \tag{2.2}$$

has the same r-dependence as $A(r)$.

In particular, within the second order perturbation theory $W_0(r)$ has the commonly used form [3,4,17–21]:

$$W_0^{\mathrm{PT}} = \frac{V^2}{\hbar}\sqrt{\frac{\pi}{\lambda T}} = \frac{\omega}{2\pi}A_{\mathrm{PT}}, \tag{2.3}$$

where

$$A_{\mathrm{PT}} = 2\sqrt{\pi\Delta} \quad \text{and} \quad \Delta = \frac{\pi^2 V^4}{\hbar^2\omega^2\lambda T} = \alpha^2. \tag{2.4}$$

Parameter

$$\alpha = \sqrt{\Delta} = \frac{\pi V^2}{\hbar\omega\sqrt{\lambda T}} \tag{2.5}$$

is space dependent due to exponential decrease of coupling (tunnelling) strength with inter-particle distance according to Eq. (1.6). Parameter α chosen as an ordinate in Fig. 2

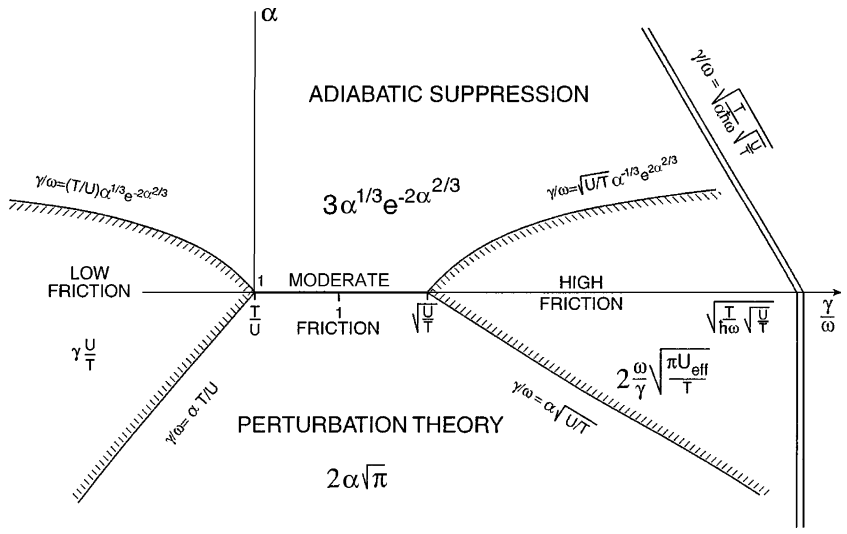

Fig. 2. Different theoretical results for $A(\alpha, \gamma/\omega)$ dependence and the borders between them established in Ref. [17].

grows when the distance between the reactants reduces. Correspondingly the transfer rate as well as its pre-exponent increase from the bottom to top in the vertical cross-section of the plane (α, γ) starting from the perturbation theory which is essentially non-adiabatic. The latter holds at high particle separation, within the borders indicated in Fig. 2. Above them (at $\alpha > 1$) the transfer becomes adiabatic and sharply reduces with increasing of $V(r)$ at further reduction of inter-reactants distance.

An adiabatic alternative to the perturbation theory result, (2.4), is given by the following formula [22]:

$$A_{\mathrm{AD}} \simeq 3\alpha^{1/3}\,\mathrm{e}^{-2\alpha^{2/3}}. \tag{2.6}$$

Since at small interaction A increases but decreases at large one there should be a maximum at $\alpha \approx 1$. This is really the fact following from the numerical calculation of thermally averaged prefactor A for moderate (intermediate) friction region [17]:

$$A_{\mathrm{MF}} = 2\int_0^\infty \mathrm{e}^{-\alpha/\sqrt{\epsilon}}\left(1-\mathrm{e}^{-\alpha/\sqrt{\epsilon}}\right)\mathrm{e}^{-\epsilon}\,\mathrm{d}\epsilon, \quad \frac{T}{U} < \frac{\gamma}{\omega} < \frac{U}{T}. \tag{2.7}$$

The results (2.3) and (2.6) for weak and strong inter-level interaction follow from this general formula at $\alpha \ll 1$ and $\alpha \gg 1$, respectively. The comparison of these limits with the result of exact calculation of $A_{\mathrm{MF}}(\alpha)$ from Eq. (2.7) are shown in Fig. 3. Taking into account Eq. (2.5) as well as $\lambda(r)$ dependence from Eq. (1.5) and $V(r)$ dependence from Eq. (1.6) we obtain the space dependence of A_{MF} for highly polar solvents (Fig. 4) which demonstrates the adiabatic suppression of electron transfer at short distances.

The same effect is present at higher friction. However, between the adiabatic and non-adiabatic regions there is a peninsula where the famous dynamic solvent effect (DSE) [6,7,23] takes place (Fig. 2). There A does not

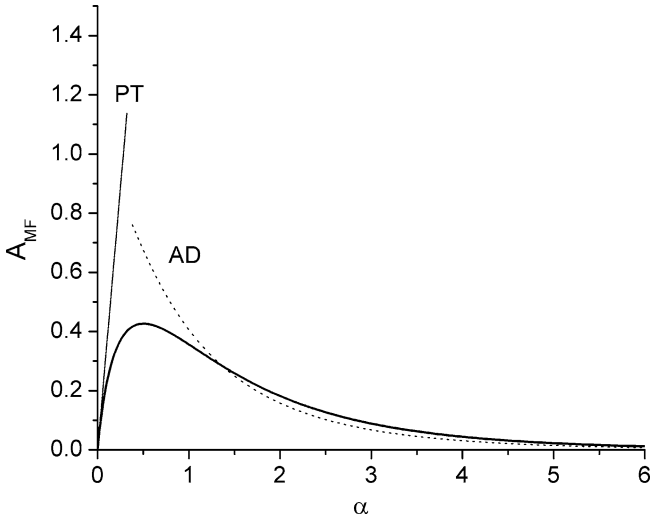

Fig. 3. The exact $A(\alpha)$ in moderate friction region in comparison with perturbation theory (PT) and adiabatic (AD) limits.

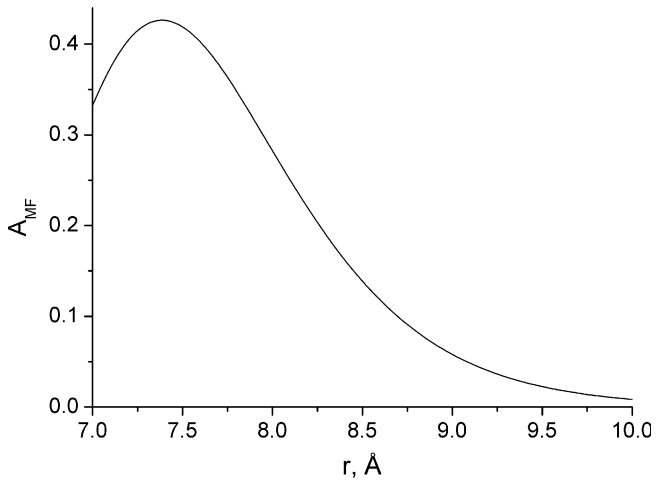

Fig. 4. The space dependence, $A_{\mathrm{MF}}(r)$, in highly polar solvent at $\lambda_0 = 1.15$ eV, $L = 1$ Å, $\sigma = 7$ Å, $V_0 = 0.02$ eV.

depend on the interaction in the crossing point, but is limited by a diffusion to this point along the reaction coordinate. As was shown in Ref. [17]:

$$A_{\mathrm{DSE}} = \frac{2\omega}{\gamma}\sqrt{\frac{\pi U_{\mathrm{eff}}}{T}}, \quad \text{where } U_{\mathrm{eff}} = \frac{U}{\left(1+\sqrt{U/U'}\right)^2}, \tag{2.8}$$

where U is the activation energy for the transition $1 \to 2$ as before, while U' is the activation energy for the reverse transition, $2 \to 1$. In inverted region the latter is always much larger than the former (see Fig. 1), so that $U_{\mathrm{eff}} \approx U$. In this case the weak r-dependence of A_{DSE} comes from only $U(r)$ dependence, that is from $\Delta G(r)$ or $\lambda(r)$. As to γ, it is simply related in polar solvents to the longitudinal relaxation time of dielectric polarization, τ_{L}: $\gamma = \omega^2\tau_{\mathrm{L}}$ [17]. Therefore one can easily get from Eqs. (2.8) and (2.2) the following result:

$$W_0^{\mathrm{DSE}} = \frac{\omega^2}{\gamma}\sqrt{\frac{U_{\mathrm{eff}}}{\pi T}} \approx \frac{1}{\tau_{\mathrm{L}}}\sqrt{\frac{U}{\pi T}}, \tag{2.9}$$

which is twice as much as the famous Zusman analog for reversible DSE. The difference is objective because we consider irreversible transfer ($U' \gg U$) while the resonant transfer is reversible in principle ($U' = U$).

The exact expressions for the high and low coupling obtained in Ref. [17] can be used for making a good interpolation between these limits which is valid approximately at any α:

$$\frac{1}{A} = \frac{1}{A_{\mathrm{MF}}} + \frac{1}{A_{\mathrm{DSE}}}. \tag{2.10}$$

It follows from this formula that $A = A_{\mathrm{MF}}$ at small and large α while $A = A_{\mathrm{DSE}}$ in between. At the highest friction the latter is almost a plateau which cuts off the top of $A_{\mathrm{MF}}(\alpha)$ dependence (Fig. 5). The same is true for $W_0(r) = \frac{\omega}{2\pi}A(r)$ dependencies which are greatly reduced near the contact comparing to perturbation theory valid at large distances (Fig. 6). Of course, the finite σ put an upper limit to V making deep adiabatic region seen in Fig. 5 unattainable if V_0 is not sufficiently large.

The comparison of different theories over an unrestricted range of $V(r)$ variation is given in Fig. 7 by example of the high friction curve 4 from Figs. 5 and 6. The result following from Eq. (2.10) is compared there with that of perturbation theory as well as with Zusman-like formula for irreversible electron transfer, accounting for DSE only:

$$W_{\mathrm{Zus}} = \frac{\omega}{2\pi}\frac{A_{\mathrm{PT}}A_{\mathrm{DSE}}}{A_{\mathrm{PT}}+A_{\mathrm{DSE}}} = \frac{W_0^{\mathrm{PT}}}{1+W_0^{\mathrm{PT}}/W_0^{\mathrm{DSE}}}. \tag{2.11}$$

As well as in the case of the resonant electron transfer, studied recently in Ref. [5] (Fig. 6), Zusman approximation

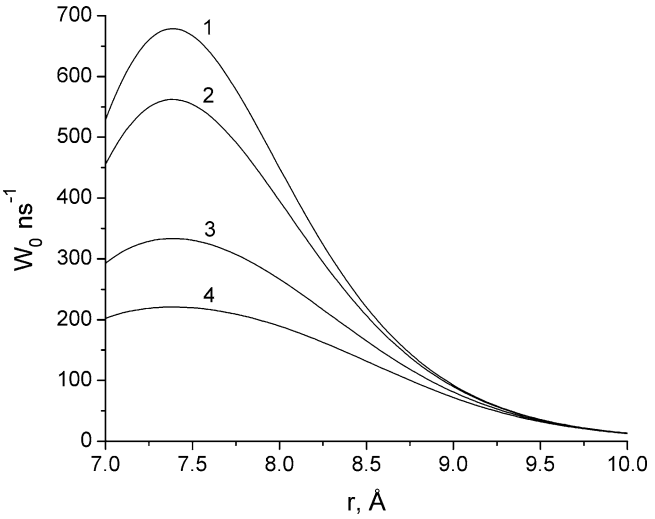

Fig. 6. Distance dependence of $W_0(r) = \frac{\omega}{2\pi}A$ at the same parameters as in previous figure.

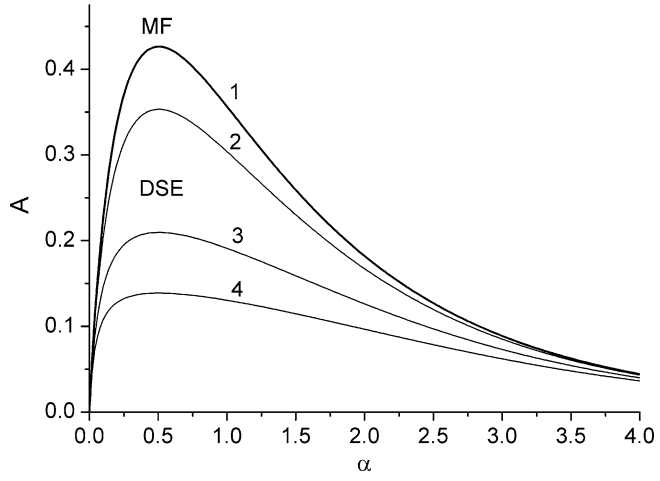

Fig. 5. The general $A(\alpha)$ dependence for moderate friction (1) and higher $\gamma = 5\times10^{13}$ s^{-1} (2); 2.5×10^{14} s^{-1} (3); 10^{15} s^{-1} (4) in highly polar solvent at $\Delta G = 2.14$ eV and $\omega = 10^{13}$ s^{-1}. The rest of the parameters are the same as in previous figure.

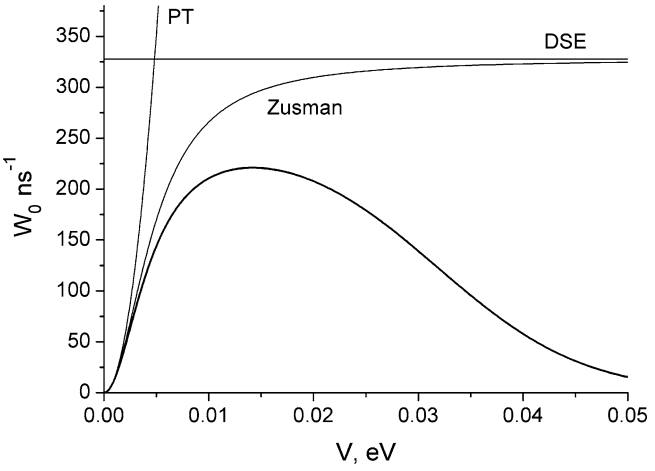

Fig. 7. The lowest curve from Figs. 5 and 6 as a function of coupling, V, compared to the perturbation theory result and Zusman approximation for W_0.

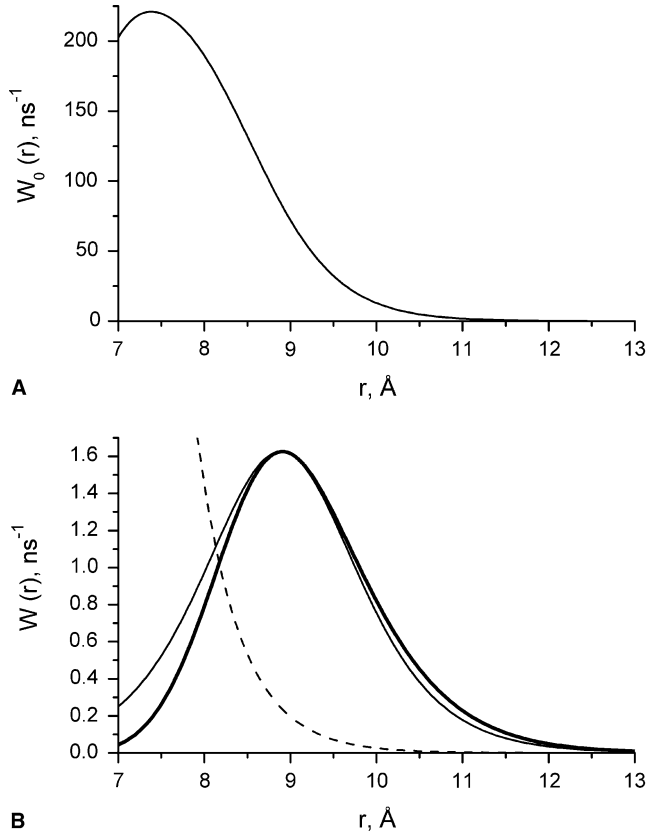

Fig. 8. (A) Distance dependence of the pre-exponent $W_0(r)$ and (B) the total transfer rate $W(r)$ in highly polar solvent (thick line). The thin line in (B) is the bell-shaped approximation to $W(r)$, (2.13), normalized to the same maximal value of W, while the dashed line is the perturbation theory estimate: $W(r) = W_0^{\mathrm{PT}} \exp(-U/T)$.

corrects essentially the perturbation theory but is not enough to approximate well the exact behavior of the pre-exponent W_0, especially at large electron coupling (short inter-particle distance) where the transfer becomes adiabatic.

Now we are ready to turn back to the space dependence of the total transfer rate (1.2) which is a product of W_0 and the Arrhenius factor which increases with distance due to space dependence of $U(r)$. It is this factor that shifts significantly the maximum of $W(r)$ to larger distance than that of $W_0(r)$ (Fig. 8). Such a bell shaped distance dependence of the transfer rate makes very problematic not only the popular contact approximation ($W(r) = k_0\delta(r-\sigma)$) but even the more reasonable exponential model,

$$W(r) = W_{\mathrm{c}}\, \mathrm{e}^{-2\frac{r-\sigma}{l}}. \tag{2.12}$$

Much better approximation is provided by a model proposed in Ref. [27]

$$W(r) = \frac{W_{\mathrm{m}}}{\mathrm{ch}^2\left(\frac{r-R}{\Lambda}\right)}. \tag{2.13}$$

Moreover, the latter allows the analytical solution of auxiliary diffusional equation of differential encounter theory (DET). It provides the rate constant of bimolecular electron transfer in Marcus inverted region at any encounter diffusion. Restricting discussion here to only kinetic limit we have for the corresponding rate constant:

$$k_0 = \int_{\sigma}^{\infty} W(r)\, \mathrm{d}^3 r. \tag{2.14}$$

Equalizing the results of k_0 calculation with either exact or bell shaped model of $W(r)$ we obtain $\Lambda = 1.19$ Å instead of $L = 1$ Å provided the maximal values are the same. As for exponential model it provides qualitatively different $W(r)$ dependence but with the same k_0 if $L = 1$ Å and $W_{\mathrm{c}} = 10.7\ \mathrm{ns}^{-1}$. If for some reasons the contact rate, W_{c}, is taken lower, then it appears that $l > L$ [24]. This may be a reason for often overestimation of the model tunnelling length when fitting of bimolecular (forward) electron transfer.

The exponential model of $W(r)$ was shown to be inapplicable in the inverted Marcus case for not only forward transfer but even more for the backward electron transfer in geminate ion pair. It fails to explain the experimentally observed non-monotonous viscosity dependence of the efficiency of geminate ion recombination [25,26,4]. The latter is originated by the ion start from inside of the bell shaped recombination layer. In case of kinetic ionization they are born at contact and move out through the recombination zone. The faster they cross it the smaller is the recombination yield. This contrasts with outer start of ions generated under diffusion control, whose recombination is facilitated by diffusion [25,26,4].

3. Conclusions

The space dependence of electron transfer rate in deeply inverted Marcus region was calculated taking into account the adiabaticity of the process at strong coupling near the contact. The result is qualitatively different from that obtained earlier for resonant electron transfer [5]. The transfer rate is non-monotonous, bell-shaped with a maximum shifted far from the contact. The best approximation to it is a model given by Eq. (2.13), but neither contact nor the exponential rate models.

References

[1] A.M. Kuznetsov, Charge Transfer in Physics, Chemistry and Biology Gordon & Breach, Amsterdam, 1995.
[2] V. May, O. Kühn, Charge and Energy Transfer Dynamics in Molecular Systems, Wiley-VCH, Berlin, 2000.
[3] A.I. Burshtein, Adv. Chem. Phys. 114 (2000) 419.
[4] A.I. Burshtein, Adv. Chem. Phys. 129 (2004) 105.
[5] V. Gladkikh, A.I. Burshtein, I. Rips, J. Phys. Chem. A 109 (2005) 4983.
[6] L.D. Zusman, Chem. Phys. 49 (1980) 295.
[7] B.I. Yakobson, A.I. Burshtein, Chem. Phys. 49 (1980) 385.
[8] H. Sumi, R.A. Marcus, J. Chem. Phys. 84 (1986) 4894.
[9] G. Grampp, W. Jaenicke, W. Harrer, J. Electroanal. Chem. 209 (1986) 223.
[10] R.M. Nielson, G.E. McManis, M.N. Golovin, M.J. Weaver, J. Phys. Chem. 92 (1988) 3441.

[11] U. Rempel, B. von Maltzan, C. von Borczyskowski, Z. Phys. Chem. Bd. 170 (1991) 107.
[12] L.D. Zusman, Z. Phys. Chem. Bd. 186 (1994) 1.
[13] D.G. Evans, A. Nitzan, M.A. Ratner, J. Chem. Phys. 108 (1998) 6387.
[14] P.A. Frantsuzov, J. Chem. Phys. 111 (1999) 2075.
[15] I. Rips, J. Chem. Phys. 121 (2004) 5356.
[16] V. Gladkikh, A.I. Burshtein, G. Angulo, S. Pages, B. Lang, E. Vauthey, J. Phys. Chem. A 108 (2004) 6667.
[17] Yu. Georgievskii, A.I. Burshtein, B. Chernobrod, J. Chem. Phys. 105 (1996) 3108.
[18] M. Newton, Chem. Rev. 91 (1991) 767.
[19] E. Pollak, J. Chem. Phys. 93 (1990) 1116.
[20] D.F. Calef, P.G. Wolynes, J. Phys. Chem. 87 (1983) 3387.
[21] V.G. Levich, Adv. Electrochem. Eng. 4 (1965) 249.
[22] H. Sumi, J. Phys. Soc. Jpn. 106 (1980) 6858.
[23] A.I. Burshtein, B.I. Yakobson, High Energy Chem. 14 (1981) 211 (Khim. Vysok. Energ. 14 (1980) 291).
[24] A.V. Popov, V.S. Gladkikh, A.I. Burshtein, J. Phys. Chem. A 107 (2003) 8177.
[25] A.I. Burshtein, A.A. Neufeld, J. Phys. Chem. B 105 (2001) 12364.
[26] A.A. Neufeld, A.I. Burshtein, G. Angulo, G. Grampp, J. Phys. Chem. 116 (2002) 2472.
[27] A.I. Burshtein, P.A. Frantsuzov, J. Luminesc. 51 (1992) 215.